

Analysis of Multiprotein Complexes in the Mammalian Retina

Monika Viktoria Beer

Dissertation an der Fakultät für Biologie der
Ludwig-Maximilians-Universität München



HelmholtzZentrum münchen
German Research Center for Environmental Health

Vorgelegt von Monika Viktoria Beer
aus Fürstentfeldbruck

München, den 12. August 2008

Cover:

Immunohistochemistry of porcine
retina sections with anti-Rac1 antibody

Erklärung:

Hiermit erkläre ich, dass ich die vorliegende Dissertation selbständig und ohne unerlaubte Hilfe angefertigt habe.

München, 12. August 2008

Dissertation eingereicht: 12. August 2008

Tag der mündlichen Prüfung: 19. Dezember 2008

Erstgutachter: Prof. Dr. Lutz Eichacker

Zweitgutachter: Prof. Dr. Hugo Scheer

Sondergutachter: Dr. Marius Ueffing

TABLE OF CONTENTS

A. ABBREVIATIONS.....	1
B. SUMMARY.....	5
C. ZUSAMMENFASSUNG.....	8
D. INTRODUCTION.....	12
1. THE MAMMALIAN RETINA.....	12
1.1 Structure and function.....	12
1.1.1 The retinal pigment epithelium.....	13
1.1.2 The photoreceptors.....	14
1.1.3 The other retinal cell types.....	15
<i>1.1.3.1 Other neurons.....</i>	<i>15</i>
<i>1.1.3.1.1 Bipolar cells.....</i>	<i>15</i>
<i>1.1.3.1.2 Horizontal cells.....</i>	<i>16</i>
<i>1.1.3.1.3 Amacrine cells.....</i>	<i>16</i>
<i>1.1.3.1.4 Ganglion cells.....</i>	<i>17</i>
<i>1.1.3.1.5 The interplexiform cells.....</i>	<i>17</i>
<i>1.1.3.2 Retinal glial cells.....</i>	<i>17</i>
<i>1.1.3.2.1 Müller glial cells (MC).....</i>	<i>17</i>
<i>1.1.3.2.2 Astrocytes.....</i>	<i>18</i>
1.1.4 Murine retina.....	18
1.1.5 Porcine retina.....	19
1.2 The G-protein-coupled receptor rhodopsin.....	19
1.2.1 Phototransduction.....	21
1.2.2 Light-regulated translocation of photoreceptor proteins.....	23
1.3 Cilia and ciliopathies.....	23
1.3.1 Cilia in vertebrate cells.....	23
<i>1.3.1.1 The photoreceptor connecting cilium.....</i>	<i>24</i>
1.3.2 Cilia-related disorders.....	26
<i>1.3.2.1 Leber congenital amaurosis.....</i>	<i>29</i>
<i>1.3.2.1.1 Lebercilin.....</i>	<i>30</i>

2. GTPASES.....	30
2.1 GTP binding proteins in signal transduction.....	30
2.2 Rho family GTPases.....	31
2.2.1 Cell morphology.....	32
2.2.2 Cell movement.....	33
2.2.3 Cell behaviour.....	35
2.2.4 Post-translational C-terminal modifications of Rho GTPases.....	35
2.2.5 Regulation of Rho family GTPases.....	36
2.2.6 Rho GTPases in the eye.....	38
2.2.6.1 <i>Rho GTPases in the retina</i>	39
2.3.Collapsin response mediator proteins (CRMP).....	40
2.3.1 CRMP2 switches RhoA and Rac1 morphology.....	40
3. PHOSPHODIESTERASES AND PDEδ.....	43
3.1 Phosphodiesterases.....	43
3.1.1 PDE6.....	45
3.2 PDEδ.....	45
3.2.1 PDE δ in the retina.....	46
3.2.2 Structure of PDE δ	46
3.2.3 PDE δ homologues.....	48
E. AIM OF THE STUDY	51
F. MATERIAL AND METHODS.....	54
1. MATERIAL.....	54
1.1 Chemicals.....	54
1.2 General equipment.....	54
1.3 Protein chemistry.....	55
1.3.1 Special equipment.....	55
1.3.2 Kits.....	55
1.4 Molecular biology.....	55
1.4.1 Special equipment.....	55
1.4.2 Kits.....	56
1.4.3 E. coli strains.....	56
1.4.4 Oligonucleotides.....	56
1.4.5 Plasmids and constructs.....	57

1.4.5.1 Plasmids.....	57
1.4.5.2 Constructs.....	57
1.5 Mammalian cell and tissue culture.....	57
1.5.1 Special equipment.....	57
1.5.2 Kits.....	57
1.5.3 Mammalian cell lines.....	58
1.5.4 Antibodies.....	58
1.6 Software and databases.....	60
1.6.1 Software.....	60
1.6.2 Databases.....	61
2. METHODS.....	62
2.1 Protein chemistry.....	62
2.1.1 Determination of protein concentration.....	62
2.1.2 Protein precipitation.....	62
2.1.3 Sodium dodecyl sulfate-polyacrylamide gel electrophoresis (SDS-PAGE).....	63
2.1.3.1 SDS-PAGE gradient gels.....	65
2.1.3.1.1 Casting of SDS gradient mini gels with a gradient maker.....	65
2.1.3.1.2 Sample preparation.....	65
2.1.4 Blue-native PAGE (BN-PAGE).....	65
2.1.5 Second-dimensional gel electrophoresis (2-DE).....	68
2.1.5.1 Sample preparation.....	69
2.1.5.2 Rehydration and sample loading.....	70
2.1.5.3 Isoelectric focusing (IEF).....	70
2.1.5.4 Equilibration and transfer of the IPG strips.....	70
2.1.5.5 Second dimension: SDS-PAGE.....	71
2.1.6 Staining of SDS gels.....	71
2.1.6.1 Silver staining.....	71
2.1.6.2 Coomassie staining.....	72
2.1.6.3 Digitalizing and drying of SDS gels.....	72
2.1.7 Western blot analysis.....	73
2.1.7.1 Semi dry blotting.....	73
2.1.8 Analysis of protein interactions.....	75

2.1.8.1 Immunoprecipitations from porcine retina.....	75
2.1.8.2 Immunoprecipitations from ROS.....	75
2.1.8.3 Rac1-GTP Pull Down.....	76
2.1.8.4 Tandem affinity purification (TAP).....	76
2.1.8.4.1 Transfection of HEK293 cells transiently expressing the SF-TAP fusion protein.....	77
2.1.8.4.2 SF-TAP purification protocol (Gloeckner in press).....	77
2.1.9 Mass spectrometry.....	78
2.1.9.1 In-gel proteolysis.....	79
2.1.9.1.1 In-gel proteolysis of silver-stained and Coomassie-stained gels.....	79
2.1.9.2 Matrix-assisted laser desorption/ionization mass spectrometry (MALDI-MS).....	79
2.1.9.3 Peptide mass finger printing (PMF) and tandem mass spectrometry (MS/MS).....	80
2.1.9.3.1 Mass measurement with the Applied Biosystems 4700 Proteomics Analyzer (AB4700).....	81
2.1.9.4 Electrospray ionization mass spectrometry (ESI-MS).....	82
2.1.9.4.1 Mass measurement with the Q-TOF II ESI mass spectrometer.....	82
2.1.9.4.2 Mass measurement with the LTQ OrbitrapXL mass spectrometer.....	83
2.1.9.5 Data processing and criteria for protein identification	84
2.2 Isolation of porcine rod outer segments.....	85
2.3 PDEδ subunit activity assay.....	86
2.4 Light- dependent methylation of Rac1 in ROS and autoradiography.....	87
2.4.1 Immunoprecipitation of methylated Rac1.....	87
2.4.2 Identification of methylated ROS proteins by mass spectrometry.....	88
2.5 Immunohistochemistry.....	88
2.6 Molecular biology.....	89
2.6.1 E. coli cultures.....	89
2.6.1.1 Liquid cultures.....	89
2.6.1.2 Plating cultures.....	89
2.6.1.3 Cryo cultures.....	89

2.6.1.4 Generation of chemically competent <i>E. coli</i>	89
2.6.2 Chemical transformation of <i>E. coli</i>	90
2.7.3 Plasmid DNA preparation.....	90
2.6.4 DNA sequencing.....	91
2.6.5 Agarose gel electrophoresis.....	92
2.6.6 Polymerase chain reaction (PCR).....	92
2.6.7 Gateway cloning.....	93
2.7 Establishment of an organotypical retinal explant system	
from murine retina	97
2.7.1 Culturing of retinal explants.....	97
2.7.2 Analysis of explant cultures.....	100
2.7.2.1 Tissue analysis.....	100
2.7.2.2 Test for apoptosis - TUNEL assay.....	100
2.8 Production of rat and mouse monoclonal	
CRMP2 specific antibodies	102
2.8.1 Peptide selection.....	103
2.8.2 Antibody validation by Western blot.....	106
2.8.3 Antibody validation by immunohistochemistry (IHC).....	107
2.8.4 Antibody validation by immunoprecipitation.....	107
G. RESULTS	108
1. ANALYSIS OF RHO GTPASES IN	
ROD OUTER SEGMENTS (ROS)	108
1.1 Identification of the Rac1 interactome in ROS	108
1.1.1 Establishment of the Rac1 IP from soluble	
and membranous ROS fractions.....	109
1.1.2 22 Rac1 specific interactors in ROS were identified	
by mass spectrometry.....	112
1.2 Co-immunoprecipitations reveal a light-dependent	
dynamic of the Rac1/RhoA/CRMP2/tubulin/Rock II	
multiprotein complex in ROS	114
1.2.1 CRMP2 and tubulin interact with the active, GTP-bound	
form of Rac1.....	115

2. DEVELOPMENT AND VALIDATION OF CRMP2-SPECIFIC MONOCLONAL ANTIBODIES.....	117
2.1 Antibody specificity and characterization of rat and mouse monoclonal antibodies against CRMP2.....	117
2.1.1 Production of monoclonal anti-CRMP2 antibodies using two different CRMP2-specific peptides.....	117
2.1.2 Immunization of rat and mice with two different CRMP2 antigens resulted in four CRMP2 specific stable monoclonal cell lines.....	120
2.1.3 Rat and mouse anti-CRMP2 antibodies recognize CRMP2 on IHC of porcine retina.....	121
2.1.4 Rat anti-CRMP2 antibodies from the stable monoclonal cell line Beer1-5D6 immunoprecipitate endogenous and recombinant CRMP2.....	124
3. MOUSE RETINAL EXPLANTS: AN ORGANOTYPICAL CULTURE SYSTEM FOR THE INVESTIGATION OF RETINAL DEVELOPMENT AND MAINTENANCE.....	127
3.1 Establishment of an organotypical retinal explant culture system.....	128
3.1.1 Retinal explants at div8 show limited apoptotic cell death.....	128
3.1.2 Validation of the correct cytoarchitecture of div8 retinal explants by immunohistochemistry with cell-type specific markers.....	129
3.1.3 Application of a Rock II-specific inhibitor on retinal explants affects distribution of RhoA in photoreceptors.....	131
4. OPTIMIZATION OF BN-PAGE FOR ISOLATION OF NATIVE PROTEIN COMPLEXES FROM ROS.....	135
5. PDEδ - A GDI FOR RAC1 IN PORCINE ROS?.....	137
5.1 Localization and expression of PDEδ and Rac1 in porcine retina.....	138
5.1.1 Colocalization of PDE δ and Rac1 in the retina.....	138
5.1.2 PDE δ is enriched in the membranes of dark-adapted porcine ROS.....	139
5.2 Interaction of PDEδ and Rac1 in ROS.....	140
5.2.1 PDE δ co-immunoprecipitates with Rac1 in ROS.....	140
5.2.2 Isolation and analysis of native protein complexes from ROS by BN-PAGE.....	142

5.2.2.1 <i>PDEδ</i> and <i>Rac1</i> colocalize in ROS in native protein complexes.....	143
5.3 Light-dependent carboxyl-methylation of <i>Rac1</i> in ROS.....	145
5.4 <i>PDEδ</i> dissociates <i>Rac1</i> from ROS membranes in vitro.....	149
6. IDENTIFICATION OF THE LEBERCILIN INTERACTOME.....	150
6.1 The lebercilin multiprotein complex in the retina.....	151
6.1.1 A lebercilin specific antibody immunoprecipitates lebercilin from porcine retina lysate.....	151
6.1.2 Analysis of the lebercilin interactome in the retina.....	151
H. DISCUSSION.....	154
1. RAC1 IN ROS: A LINK BETWEEN PHOTOTRANSDUCTION AND THE CYTOSKELETON?.....	154
2. <i>PDEδ</i> EXERTS GUANINE NUCLEOTIDE DISSOCIATION INHIBITOR FUNCTION FOR RAC1 IN PORCINE ROD OUTER SEGMENTS.....	161
2.1 Localization of <i>PDEδ</i> and <i>Rac1</i> in ROS.....	161
2.2 Light-dependent interaction of <i>PDEδ</i> and <i>Rac1</i> in ROS.....	161
2.3 In the manner of a GDI, <i>PDEδ</i> dissociates <i>Rac1</i> from ROS membranes.....	162
2.4 Light-dependent carboxyl-methylation of <i>Rac1</i> in ROS.....	163
I. PERSPECTIVE.....	166
J. REFERENCES.....	168
K. ANNEX.....	193
1. FIGURE INDEX.....	193
2. TABLE INDEX.....	194
3. PUBLICATIONS AND PRESENTATIONS.....	195
3.1 Journals.....	195
3.2 Poster and presentations.....	195
4. ACKNOWLEDGMENTS.....	196
5. CURRICULUM VITAE.....	198

FÜR TOMMY

A. ABBREVIATIONS

1-DE	One-dimensional gel electrophoresis
2-DE	Two-dimensional gel electrophoresis
AC	Astrocytes
APS	N,N,N,N'-Ammonium peroxodisulfate
Arr	Arrestin
ATP	Adenosine triphosphate
AX	Axoneme
BB	Basal body
BBS	Bardet-Biedl syndrome
BN	Blue native
bp	Base pair
BP	Bipolar cells
BSA	Bovine serum albumine
CC	Connecting cilium
Cdc42	Cell division cycle 42
cDNA	Coding DNA
CNG	Cyclic nucleotide-gated
CNS	Central nervous system
CKII α	Casein-KinaseII α
CKII β	Casein-KinaseII β
CR	Ciliary rootlet
CRMP	Collapsin response mediator protein
DAPI	4,6-diaminodiphenyl-2-phenylindole
dH ₂ O	Deionized water
ddH ₂ O	Ultra-pure water
DMEM	Dulbecco's modified Eagle's medium
DMSO	Dimethylsulfoxide
DNA	Deoxyribonucleic acid
dNTPs	Deoxynucleotide triphosphate
DPYSL2	Dihydropyrimidase-related protein 2
DTE	Dithioerythritol
DTT	Dithiothreitol
ECL	Enhanced chemiluminescence
EDTA	Ethylendiaminetetraacetate
ELISA	enzyme-linked immunosorbent assay
EM	Electron microscopy
ER	Endoplasmic reticulum
ERG	Electroretinogram

ESI-MS	Electrospray ionization mass spectrometry
EtOH	Ethanol
FCS	Fetal calf serum
FITC	Fluorescein isothiocyanate
GAP	GTPase-activating protein
GC	Guanylate cyclase
GCL	Ganglion cell layer
GDI	Guanine nucleotide dissociation inhibitor
GEF	Guanine nucleotide exchange factor
GFAP	Glia Fibrillary Acid Protein
GFP	Green-fluorescent protein
GPCR	G-protein coupled receptor
GS	Glutaminsynthetase
G _t	Photoreceptor-specific G protein transducin
HC	Horizontal cells
HRP	Horseradish peroxidase
IEF	Isoelectric focusing
IF	Immunofluorescence
IFA	Incomplete Freud's Adjuvants
IHC	Immunohistochemistry
INL	Inner nuclear layer
IP	Immunoprecipitation
IPG	Immobilized pH gradient
IPL	Inner plexiform layer
IS	Inner segment
kb	kilo base
kDa	kilo Dalton, molecular mass
KLH	Keyhole limpet hemocyanin
LB	Luria-Bertani
LC	Liquid chromatography
LCA	Leber congenital amaurosis
LC-MS/MS	Liquid chromatography coupled with tandem mass spectrometry
MALDI	Matrix-assisted laser desorption ionization
MALDI/TOF-MS	Matrix-assisted laser desorption ionization/Time-of-flight mass spectrometry
MC	Müller glia cells
MS	Mass spectrometry
MS/MS	Tandem mass spectrometry
N	Nucleus
NF200	Neurofilament 200

OD	Optical density
ONL	Outer nuclear layer
OPL	Outer plexiform layer
OS	Outer segment
OVA	ovalbumin
p.A.	pro analysis grade
PAF	Paraformaldehyde
PBS	Phosphate-buffered saline
PBST	PBS-Tween
pc	Post coitus
PCR	Polymerase chain reaction
PDC	Phosducin
PDE	Cyclic nucleotide phosphodiesterase
pI	Isoelectric point
PKC	Proteinkinase C
PN	postnatal
PR	Photoreceptor
PRL	Photoreceptor layer
pI	Isolelectric point
PMF	Peptide-mass fingerprinting
PMSF	Phenylmethylsulfonylfluorid
ppm	Parts per million
PVDF	Polyvinylidenedifluoride
R*	Photoactivated rhodopsin
Rac1	Ras-related C3 botulinum toxin substrate 1
Rec	Recoverin
RGC	Retinal ganglion cells
RhoA	Ras Homolog Gene Familiy, Member A
RK	Rhodopsin kinase
Rock II	RhoKinase II
ROS	Rod Outer Segments
RP	Retinits pigmentosa
RP3	Retinits pigmentosa type 3
RPE	Retinal pigment epithelia
RPGR	Retinitis Pigmentosa GTPase Regulator
RPGRIP	Retinitis Pigmentosa GTPase Regulator Interacting Protein
rpm	Rounds per minute
RT	Room temperature
SDS	Sodium dodecyl sulfate
SDS-PAGE	SDS-polyacrylamide gel electrophoresis
TAE	Tris-acetic acid-EDTA buffer
TAP	Tandem-affinity purification
TEMED	N',N',N',N'-tetraethylmethylenidiamine

TFA	Trifluoroacetic acid
TOF	Time-of-flight
Tris	Tris-(hydroxymethyl)-aminomethan
TUNEL	T4 terminal deoxynucleotidyl transferase-mediated dUTP nick end labeling
U	Unit
USH	Usher syndrome
UV	Ultra-violet radiation
UZ	Ultracentrifuge
WB	Western blot

B. SUMMARY

A large group of genetically inherited blinding diseases is associated with mutations in genes expressed in photoreceptors. Such mutations not only result in the impairment of the mutated protein, but also in a disruption of functional downstream protein networks, leading to alterations in the compositions of multiprotein complexes and in protein localization, with most severe physiological consequences. In the light-perceiving molecule rhodopsin alone, more than a hundred different mutations are described that may cause the retinal degenerative disease retinitis pigmentosa (<http://www.sph.uth.tmc.edu/RetNet/>). In sucrose-density gradient experiments by Dr. Magdalena Swiatek-deLange, which were preceding this study, rhodopsin was identified as part of a putative rhodopsin/Ras Homolog Gene Family Member A (RhoA)/Ras-related C3 botulinum toxin substrate 1 (Rac1)/RhoKinase II (Rock II)/Collapsin response mediator protein 2 (CRMP2) signaling multiprotein complex in rod photoreceptor outer segments (ROS). This complex was confirmed and further investigated in this study. A link between rhodopsin-induced photoreceptor degeneration and the regulation of the cytoskeleton via the Rho GTPase Rac1 was already established by Chang and colleagues (Chang and Ready, 2000), who demonstrated that expression of dominant active Rac1 in rhodopsin-null mutants of *Drosophila* rescued rhabdomere morphogenesis. Rac1, which acts as a molecular switch in cell signaling, alternates between an inactive, primarily cytosolic GDP-bound state and an active GTP-bound state, usually associated with membranes, and transduces receptor-mediated signals to the cytoskeleton. Although the role of Rac1 has been investigated in a wide variety of cells, only a few studies have addressed its role in retinal photoreceptors, where it was shown to be involved in the regulation of rhodopsin transport carrier fusion in photoreceptors of *Rana barlandieri* (Deretic et al., 2004), as well as in apoptosis in light-induced photoreceptor degeneration in mice (Belmonte et al., 2006). Despite these data supporting that Rac1 is an essential molecule for photoreceptor function, only limited knowledge is available to date about its function and regulation in photoreceptors.

In this study, the role of Rac1 in ROS was further investigated. The Rac1 interactome in ROS was analyzed and 22 Rac1-specific interactors were identified. Five of the identified Rac1 interactors have already been described in the literature, namely CRMP2, one of the main regulators of polarity development in neuronal cells, as well as the cytoskeletal proteins actin (α and γ) and tubulin (α and β). The other 17 interacting proteins represent putative new Rac1 interaction partners, among them the aryl hydrocarbon receptor-interacting protein like 1 (AIPL1), which is associated with Leber Congenital Amaurosis (LCA) and may be involved

in retinal protein trafficking (Sohocki et al., 2000), or a number of proteins that are part of the phototransduction cascade; like the 3', 5'-cyclic-GMP phosphodiesterase 6 subunit α , recoverin, arrestin and the α , β and γ subunits of transducin. This links light-perception through rhodopsin with a regulation of the cytoskeleton provided by Rac1 and suggests an interdependence of light-perception with proper cellular structure and function of photoreceptors.

In this study, the existence of the putative rhodopsin/RhoA/Rac1/Rock II/CRMP2 signaling multiprotein complex in ROS was confirmed, and a light-dependent dynamic of its complex members was demonstrated. In line with data from squid (Petrov et al., 1994) and bovine ((Wieland et al., 1990), (Balasubramanian and Slepak, 2003)) photoreceptors, a light-dependent activation of Rac1 in porcine ROS was substantiated. Light-activated GTP-bound Rac1 was shown to be predominantly associated with membranes, where effectors reside, while in dark-adapted ROS, only very little active Rac1 was present. This study provides also evidence that Rac1 and RhoA signaling is connected via CRMP2, while Rock II seems to be only part of the RhoA signaling complex. For CRMP2 function in ROS we propose a role as a physiological switch that coordinates the balance between Rac1- and RhoA driven signaling, as already suggested by Arimura and colleagues for CRMP2 signaling in neurons (Arimura et al., 2000). For a further investigation of CRMP2 signaling in ROS, CRMP2 antibodies, which were not commercial available at the beginning of this study, were required. In this study, the successful production and characterization of four stable lines of monoclonal, CRMP2-specific antibodies is reported. While all four antibodies were suitable for Western Blot and immunohistochemical analysis, one antibody was also able to precipitate the native CRMP2 protein from porcine retinal lysate, and therefore represents an excellent tool for a further characterization of CRMP2 function in ROS.

Three classes of regulatory proteins, all of which affect GDP/GTP exchange, tightly control Rac1 activity. One of these, the Rho GDP dissociation inhibitor (RhoGDI), controls the interaction of Rac1 with other regulatory proteins and effector targets as well as by binding of the prenyl tail of Rac1 the cycling between cytosol and membranes. But since RhoGDI could not be detected in ROS, this led to the assumption that another molecule must assume GDI function for Rac1 in ROS. The 17-kDa protein PDE δ , which has been considered a regulatory subunit of retinal rod cGMP phosphodiesterase 6, shares strong structural homology with RhoGDI. It interacts with a number of prenylated and unprenylated proteins and solubilizes a number of prenylated proteins from cellular membranes, reminiscent of the well characterized

action of RhoGDI on Rho family GTPases. This prompted us to test, if PDE δ exerts GDI function for Rac1 in ROS.

In this study a light-dependent interaction of Rac1 in complex with PDE δ in porcine ROS is demonstrated. Additionally it is shown that purified PDE δ solubilizes Rac1 from isolated ROS membranes in a dose dependent manner, a feature implicating its GDI-function for Rac1. The study also shows that the Rac1/PDE δ interaction correlates with light-dependent carboxyl-methylation of Rac1 in ROS, suggesting that the GDI function of PDE δ for Rac1 may be regulated via methylation of Rac1. Taken together, these data show that PDE δ functions as GDI for Rac1 in porcine ROS.

In this study, the identified Rac1-associated multiprotein complexes and their light-regulated dynamic provide evidence, that Rac1 links light perception through rhodopsin with signaling networks involved in structural integrity and polarity of photoreceptors. This suggests an interdependence of visual perception and proper cellular structure. With the delivery of high quality CRMP2-specific monoclonal antibodies, it provides a basis for further studies in this field of research.

Besides rhodopsin-associated complexes, a number of ciliary proteins are implicated in retinal degenerative diseases. In the novel ciliary protein lebercilin (den Hollander et al., 2007), mutations are associated with Leber congenital amaurosis (LCA), a most severe form of inherited retinal dystrophies ((Kaplan et al., 1990), (Perrault et al., 1999)).

By SF-TAP and LC/MS/MS analysis, 24 lebercilin interactors were identified in HEK cells (den Hollander et al., 2007). In this study, the putative lebercilin interactors were verified in porcine photoreceptors (published in (den Hollander et al., 2007). The identified interactors, which may represent potential candidate genes for LCA and other ciliopathies, implicate lebercilin as a ciliary and microtubules associated protein in the retina and emphasize the major role of disrupted ciliary processes in the molecular pathogenesis of LCA.

C. ZUSAMMENFASSUNG

Eine große Gruppe genetisch vererbter Erblindungskrankheiten steht im Zusammenhang mit Mutation in Genen, die in Photorezeptoren exprimiert sind. Diese Mutationen führen nicht nur zu einer Beeinträchtigung des mutierten Proteins selbst, sondern auch zu einer Störung von funktionell nachgeschalteten Proteinnetzwerken. In der Folge ändern sich die Zusammensetzung von Multiproteinkomplexen sowie die Proteinlokalisierung, was schwerwiegende physiologische Konsequenzen nach sich zieht. Alleine im lichtwahrnehmenden Molekül Rhodopsin sind mehr als hundert unterschiedliche Mutationen beschrieben worden, die vermutlich im Zusammenhang mit Retinitis pigmentosa, einer degenerativen Erkrankung der Retina, stehen (<http://www.sph.uth.tmc.edu/RetNet/>). In Saccharose-Dichte Gradienten Experimenten von Dr. Magdalena Swiatek-deLange, die dieser Studie vorangegangen sind, wurde Rhodopsin als Teil eines potentiellen Rhodopsin/Ras Homolog Gene Family, Member A (RhoA)/Ras-related C3 botulinum toxin substrate 1 (Rac1)/RhoKinase II (Rock II)/ Collapsin response mediator protein 2 (CRMP2) Signal-Multiproteinkomplexes in Außensegmenten von Stäbchen Photorezeptoren (ROS) identifiziert, welcher im Zuge dieser Studie bestätigt und eingehender untersucht wurde.

Ein Zusammenhang zwischen einer Rhodopsin-vermittelten Degeneration von Photorezeptoren und der Regulation des Cytoskeletts durch die kleine GTPase Rac1, wurde von Chang und Kollegen (Chang and Ready, 2000) hergestellt. Sie haben gezeigt, dass die Expression von dominant-aktivem Rac1 in Rhodopsin-Null Mutanten von *Drosophila* die Rhabdomer Morphogenese erhalten kann. In Zellen fungiert Rac1 durch den Wechsel zwischen einem inaktiven, vorwiegend cytosolischen und einem aktiven, überwiegend membranassoziierten Zustand, als molekularer Schalter in der Signaltransduktion und vermittelt Signale von Membranrezeptoren an das Cytoskelett. Obwohl die Rolle von Rac1 bereits in einer großen Zahl unteerschiedlicher Zellen untersucht worden ist, ist seine Funktion in Photorezeptoren noch immer weitgehend ungeklärt. Die wenigen vorhanden Studien, in denen beispielsweise gezeigt wurde, dass Rac1 an der Fusion von Rhodopsintransportcarriern in *Rana barlandieri* (Deretic et al., 2004) oder auch an der lichtinduzierten Degeneration von murinen Photorezeptoren beteiligt ist (Belmonte et al., 2006), machen aber deutlich, dass Rac1 ein für die Funktion und Regulation von Photorezeptoren wichtiges Molekül ist.

In dieser Studie wurde daher die Rolle von Rac1 in Photorezeptoren eingehender untersucht und ein Rac1-Interaktom in ROS, bestehend aus 22 Interaktoren, identifiziert. Von diesen 22 identifizierten Interaktoren sind fünf bereits als Interaktoren von Rac1 beschrieben worden,

darunter CRMP2, einer der Hauptregulatoren von Polarität in neuronalen Zellen, sowie die cytoskelettalen Proteine Aktin (α and γ) und Tubulin (α and β). Unter den 17 neuen potentiellen Rac1 Interaktoren befindet sich das Aryl Hydrocarbon Receptor-Interacting Protein Like 1 (AIPL1), das im Zusammenhang mit Leberscher kongenitaler Amaurose (LCA) sowie mit retinalem Proteintransport steht (Sohocki et al., 2000), sowie eine Reihe von Proteinen, die Teil der Phototransduktionskaskade sind, wie die α Untereinheit der 3', 5'-cyclic-GMP Phosphodiesterase 6, Recoverin, Arrestin sowie die α , β und γ Untereinheiten von Transducin. Rac1 verbindet damit die Lichtwahrnehmung durch Rhodopsin mit einer Regulation des Cytoskeletts und legt damit eine Interdependenz von Lichtwahrnehmung mit einer korrekten zellulären und funktionalen Struktur von Photorezeptoren nahe.

In dieser Studie wurde nicht nur die Existenz des potentiellen Rhodopsin/RhoA/Rac1/Rock II/CRMP2 Multiproteinkomplexes in ROS bestätigt, sondern auch eine lichtabhängige Dynamik und Interaktion der einzelnen Komplexbestandteile beschrieben. In Übereinstimmung mit Daten aus verschiedenen Organismen ((Wieland et al., 1990), (Petrov et al., 1994), (Balasubramanian and Slepak, 2003)) konnte eine lichtabhängige Aktivierung von Rac1 in ROS von Schweinen nachgewiesen werden. Während lichtaktiviertes, GTP-gebundenes Rac1 überwiegend membranassoziiert vorliegt, konnte in dunkeladaptierten ROS insgesamt nur eine sehr geringe Menge an aktivem Rac1 detektiert werden. Des Weiteren wurden in dieser Studie auch deutliche Hinweise geliefert, die auf eine CRMP2 vermittelte Verbindung von Rac1 und RhoA assoziierten Signalwegen hinweisen, wohingegen die Kinase Rock II nur Teil des RhoA assoziierten Signalkomplexes zu sein scheint. Als Funktion von CRMP2 liegt daher eine Rolle als physiologischer Schalter nahe, der die Balance zwischen Rac1 und RhoA vermittelter Signaltransduktion koordiniert. Eine solche Funktion für CRMP2 wurde von Arimura und Kollegen bereits für die Signaltransduktion in Neuronen vorgeschlagen (Arimura et al., 2000). Um die Signaltransduktion von CRMP2 in ROS eingehender untersuchen zu können, sind CRMP2 Antikörper unabdingbar, welche aber zu Beginn dieser Arbeit kommerziell nicht erhältlich waren. Daher war die Produktion und Charakterisierung von monoklonalen CRMP2 spezifischen Antikörpern ein wichtiger Teil dieser Studie. Von den vier erhaltenen stabilen Linien monoklonaler, CRMP2 spezifischer Antikörper waren alle für den Einsatz im Western Blot sowie in der Immunhistochemie geeignet, aber nur ein Antikörper erwies sich auch als geeignet für die Immunopräzipitation von nativem CRMP2 aus primärem retinalem Gewebe. Dieser Antikörper stellt damit ein exzellentes Werkzeug für die weitere Charakterisierung der Funktion von CRMP2 in ROS dar.

Drei Klassen von Proteinen regulieren die Aktivität von Rac1. Sie alle haben einen Einfluss auf den GTP/GDP-Austausch. Einer dieser Regulatoren ist der Rho GDP Dissociation Inhibitor (RhoGDI). Er kontrolliert die Interaktion von Rac1 mit weiteren regulatorischen Proteinen und Effektoren, sowie durch Interaktion mit dem Prenylrest von Rac1 das Pendeln zwischen Cytosol und Membran. Da aber der RhoGDI nicht in ROS nachgewiesen werden konnte (Balasubramanian and Slepak, 2003), legt dies den Schluss nahe, dass ein anderes Protein diese Funktion in ROS übernimmt. Das 17-kDa große Protein PDE δ , das lange Zeit als Untereinheit der retinalen cGMP Phosphodiesterase 6 aus Stäbchen galt, weist starke strukturelle Homologien zu RhoGDI auf. Es interagiert mit einer ganzen Reihe von prenylierten und unprenylierten Proteinen. Seine Fähigkeit, prenylierte Proteine von Zellmembranen zu lösen, erinnert stark an die Funktion, welche RhoGDI auf GTPasen der Rho Familie hat. Es wurde daher im Zuge dieser Studie untersucht, ob PDE δ in ROS GDI Funktion auf Rac1 ausübt.

In dieser Arbeit konnte eine lichtabhängige Interaktion von Rac1 mit PDE δ in ROS von Schweinen nachgewiesen werden. Des Weiteren wurde gezeigt, dass aufgereinigtes PDE δ Rac1 von isolierten ROS Membranen lösen kann, eine Eigenschaft, die deutlich auf eine GDI-Funktion von PDE δ für Rac1 hinweist. Zudem wurde gezeigt, dass die Interaktion von Rac1 mit PDE δ mit einer lichtabhängigen Carboxymethylierung von Rac1 in ROS korreliert, was ein Hinweis darauf sein kann, dass die die GDI Funktion von PDE δ durch die Methylierung von Rac1 reguliert wird. Alles in Allem zeigen diese Daten, dass PDE δ für Rac1 in ROS die Funktion eines GDIs ausübt.

In dieser Studie geben die identifizierten und mit Rac1 assoziierten Multiproteinkomplexe sowie deren lichtregulierte Dynamik einen deutlichen Hinweis darauf, dass Rac1 die Lichtwahrnehmung durch Rhodopsin mit Signalnetzwerken verbindet, die eine Rolle bei der strukturellen Integrität und Polarität von Photorezeptoren spielen. Dies deutet auf eine Abhängigkeit von Lichtwahrnehmung und funktioneller zellulärer Struktur hin. Mit der Bereitstellung von qualitativ sehr hochwertigen CRMP2 spezifischen Antikörpern liefert diese Studie zudem eine gute Basis für weiterführende Studien in diesem Forschungsfeld.

Neben Rhodopsin assoziierten Komplexen stehen auch eine ganze Reihe von ciliären Komplexen in Zusammenhang mit degenerativen Erkrankungen der Retina. Im kürzlich entdeckten ciliären Protein Lebercilin (den Hollander et al., 2007) wurden Mutationen mit Leberscher kongenitaler Amaurose (LCA) in Verbindung gebracht, einer sehr schweren Form einer erblichen retinalen Dystrophie ((Kaplan et al., 1990), (Perrault et al., 1999)).

Mit Hilfe von SF-TAP und LC/MS/MS Analysen konnten 24 Lebercilin Interaktoren in HEK Zellen identifiziert werden (den Hollander et al., 2007). Hier in dieser Studie wurden schließlich diese potentiellen Lebercilin Interaktoren auch in Photorezeptoren von Schweinen bestätigt (veröffentlicht in (den Hollander et al., 2007)). Die identifizierten Interaktoren stellen mögliche Kandidaten für Gene für LCA und andere Ciliopathien dar und weisen Lebercilin als ein ciliär und mikrotubulär assoziiertes Protein in der Retina aus. Dies betont den Stellenwert, welche gestörte ciliäre Prozesse in der molekularen Pathogenese von LCA besitzen.

D. INTRODUCTION

1. THE MAMMALIAN RETINA

1.1 Structure and function

The retina is a specialized light sensitive sensory organ that covers the inside of the eye (Figure 1). It transforms light into electric signals that are transmitted via the optic nerve to the visual centers of the brain. Here they are processed and integrated. During embryonic development, the retina is formed as a protrusion of the neuroectoderm, a specialized part of the ectoderm, which also develops into the central nervous system (CNS). The retina is therefore part of the CNS. Because of its well defined function, its highly organized structure and easy accessibility, it serves as a model system to study CNS function.

The mature mammalian retina consists of two distinct tissues: the neural retina and the retinal pigment epithelium of single layered epithelial cells.

The neural retina is composed of five classes of neurons (photoreceptors, bipolar-, horizontal-, amacrine- and ganglion cells), divided into at least 50 subtypes, and glial cells. All cells of the neural retina derive from multipotent progenitor cells, differentiating in a precise chronological order, conserved in many species (Cepko, 1993). The structure of the mature retina is highly organized. It consists of three somatic layers (cell bodies) and two plexiform layers (synapses) (Figure 1): the photoreceptor layer (PRL); containing the outer and inner segments of rod and cone photoreceptors; the outer nuclear layer (ONL), composed of the cell bodies of rod and cone photoreceptors, the outer plexiform layer (OPL), containing axons of rod and cones and the dendrites of horizontal and bipolar cells; the inner nuclear layer (INL), with the cell bodies of horizontal, bipolar, amacrine, Müller glia and interplexiform cells; the inner plexiform layer (IPL); containing axons of bipolar and amacrine cells as well as dendrites of ganglion cell; and the ganglion cell layer (GCL), with cell bodies of ganglion cells and displaced amacrine cells and astrocytes. The axons of the ganglion cells form the nerve fiber layer. They traverse the retina, collect in a bundle at the optic disc, and leave the eye to form the optic nerve.

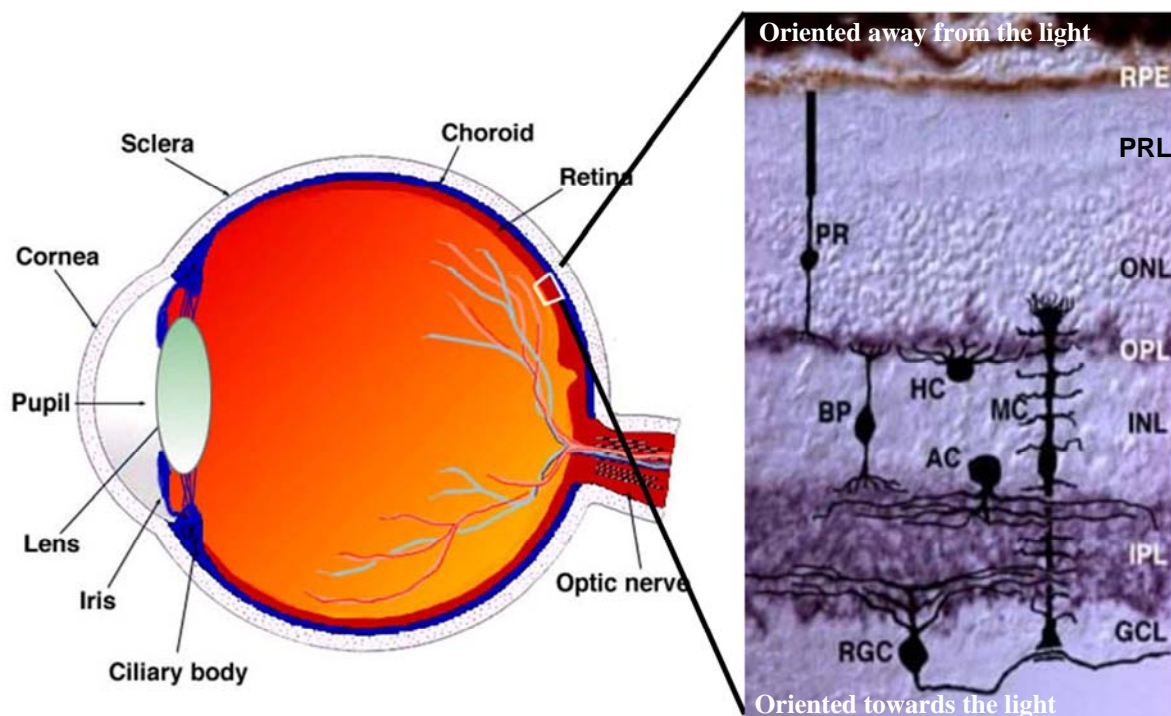


Figure 1: Section of the adult human eye (<http://webvision.med.utah.edu/>) and section through the retina with all important cell types of the retina depicted (<http://www.umr8080.u-psud.fr/Retinogenesis/retinogenesis-research.ht>). Abbreviations: PR, photoreceptor; HC, horizontal cells; BP, bipolar cells; MC, Müller glia cells; AC, astrocytes; RGC, retinal ganglion cells; RPE, retinal pigment epithelium; ONL, outer nuclear layer; OPL, outer plexiform layer; INL, inner nuclear layer; IPL, inner plexiform layer; GCL, ganglion cell layer.

1.1.1 The retinal pigment epithelium

The retinal pigment epithelium (RPE) consists of a single layer of post-mitotic pigmented epithelial cells. The apical membrane of the RPE faces the photoreceptor outer segments, surrounding them with long apical microvilli. The basolateral membrane of the RPE faces the Bruch's membrane, which separates the RPE from fenestrated endothelium of the choriocapillaris. The RPE plays an important role in the development and maintenance of the neural retina (Raymond and Jackson, 1995). It participates in the formation of the blood-retina barrier and it controls the transport of ions and metabolites that circle through the retina (Miller and Steinberg, 1979). RPE cells phagocytose continuously the shed discs of photoreceptor outer segments (Young, 1967) and recycle the visual pigments in the visual cycle of retinal ((Schadel et al., 2003), (Maeda et al., 2005)). As a layer of pigmented cells, it also protects the outer retina from excessive high-energy light and light-generated reactive oxygen species. A failure of these different functions can lead to degeneration of the retina and loss of visual function.

1.1.2 The photoreceptors

The visual process is initiated by the detection of a light signal by photoreceptor cells in the outer retina of the vertebrate eye. Photoreceptor cells absorb light (photons) and convert it into an electric neuronal signal through a process called phototransduction (see 1.2.1). Vertebrate rod and cone photoreceptor cells are highly specialized, polarized neurons with a unique morphology, consisting of morphologically and functionally distinct cellular compartments (Figure 2). The photoreceptor outer segment comprises the phototransduction machinery and is linked to the inner segment by a small intracellular bridge, the so-called connecting cilium (see 1.3.1.1), through which all intracellular intersegmental exchanges occur (Figure 2a) (Horst et al., 1990). The inner segment contains all organelles typical for the metabolism of a eukaryotic cell. It continues into the pericaryon and the synaptic region where electrical signals are transmitted from photoreceptor cells to horizontal and bipolar cells of the inner neuronal retina. Photoreceptors are the most abundant cell type in the retina. They are divided into two types, rods and cones, reflecting the form of their outer segments (Figure 2b). In the human retina, the total number of rods was determined as 110,000,000 – 125,000,000, and the total number of cones as 6,400,000 (<http://webvision.med.utah.edu/>). Rods are responsible for scotopic or nocturnal vision, while cones provide photopic or diurnal color vision.

The rod outer segments are densely filled with stacks of membranes, the discs, surrounded by the plasma membrane. The visual pigment rhodopsin is densely packed in the disc membranes, but is also found to a lesser degree in the plasma membrane. In contrast to the rod outer segments, the surface area of the cone outer segments is increased by repeated foldings of the plasma membrane. The cone outer segment is usually shorter than that of the rod and tapers in the distal direction. The outer segments are surrounded by a heterogeneous extracellular matrix, known as the interphotoreceptor matrix, where exchanges between the RPE and photoreceptors take place (Young, 1978).

The photoreceptor outer segment discs are continually renewed throughout lifetime. Newly synthesized disc membranes are added at the base of the outer segment by the expansion of the plasma membrane (Steinberg et al., 1980) or by incorporation of vesicular structures into nascent disc membranes (Obata and Usukura, 1992). At the distal tip of the outer segment, disc are shedded and phagocytosed by the cells of the RPE (see 1.1.1) (Young, 1967). The abundant membrane turnover of the photoreceptor outer segment implicates an efficient and massive vectorial transport of all disc components from the site of biogenesis, the ER and Golgi apparatus in the photoreceptor inner segment, to the base of the outer segment, the site

of disc neogenesis. In addition to these unidirectional constitutive translocations of outer segment molecules, massive light dependent bidirectional movements of visual signal cascade proteins, between the inner and outer segment, are in the focus of current research (see 1.2.2) (e.g.(Pulvermuller et al., 2002), (Sokolov et al., 2002), (Giessl et al., 2004), (Strissel et al., 2006)).

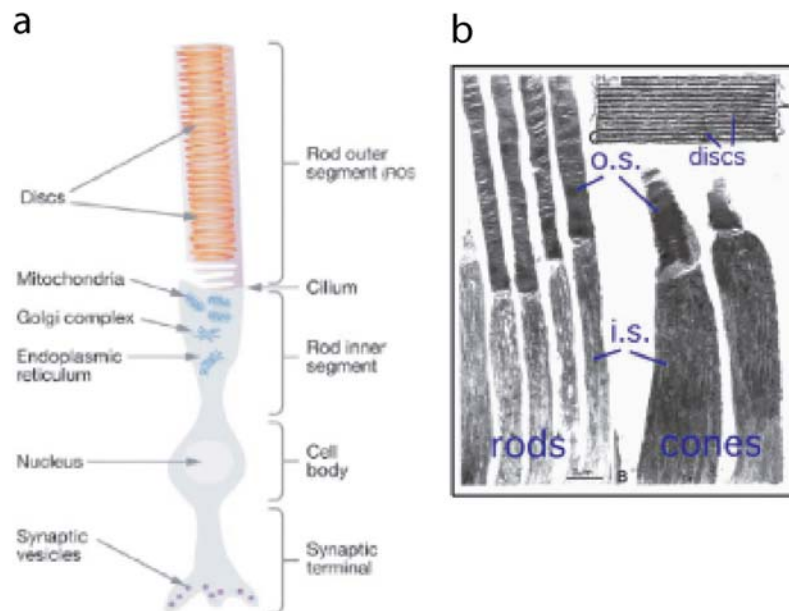


Figure 2: Vertebrate photoreceptors: a) from (Palczewski, 2006), b) from <http://webvision.med.utah.edu/>. **a)** Diagram depicting the rod cell. In ROS, hundreds of distinct, rhodopsin-loaded disk membranes are enveloped by the plasma membrane. In the inner segment the nucleus, mitochondria, endoplasmic reticulum and Golgi apparatus reside. **b)** Electron micrograph of rods and cones from human retina (Liang et al., 2003).

1.1.3 The other retinal cell types

1.1.3.1 Other neurons

The transmission and regulation of the visual signal within the retina is conducted via different functional classes of neurons. The information flow through the retina hereby can follow two paths: a direct path from photoreceptors to bipolar cells to ganglion cells, and an indirect path, in which horizontal cells may be interposed between photoreceptors and bipolars, and amacrine cells between bipolars and retinal ganglion cells.

1.1.3.1.1 Bipolar cells

Bipolar cells display the link between photoreceptors and ganglion cells. All the signals, originating in the photoreceptors and arriving at the ganglion cells, must pass through them.

All photoreceptor synapses release glutamate, but bipolar cells respond to glutamate differently. Some bipolar cells have ionotropic glutamate receptors, where glutamate opens a cation channel depolarizing the cell. Other bipolar cells have sign-inverting synapses that are mediated by metabotropic glutamate receptors and are hyperpolarizing in response to glutamate (Nawy and Jahr, 1991). When the retina is stimulated by light, one type of bipolar cell hyperpolarizes, leading to decreased neurotransmitter release and is therefore termed an OFF-center bipolar cell. The other type of bipolar cell depolarizes, causing increased neurotransmitter release from the cell terminal synapses and is called an ON-center bipolar cell. Rod photoreceptors transfer the signal only to ON-center bipolar cells, while cone photoreceptors signal to either ON-center or OFF-center bipolar cells. The distinction created at the first retinal synapse, is propagated throughout the visual system. ON-center bipolar cells supply ON-center ganglion cells, and OFF-center bipolar cells supply OFF-center ganglion cells (see 1.1.3.1.4).

1.1.3.1.2 Horizontal cells

Horizontal cells link photoreceptors and bipolar cells by relatively long connections that run parallel to the retinal layers. All rods and cones are supposed to receive feedback from horizontal cells. These cells represent a numerically small portion of the retinas interneurons, generally less than 6% of the cells of the inner nuclear layer. While in most mammals two morphologically distinct types of horizontal cells exist, mice and rats have only one. Horizontal cells adjust the system's response to the overall level of illumination. They measure the illumination across a broad region and subtract it from the signal that is transmitted to the inner retina about a local image (reviewed in (Masland, 2001)).

1.1.3.1.3 Amacrine cells

Retinal ganglion cells receive input from bipolar cells. Nevertheless, direct synapses from bipolar cells to ganglion cells represent a minority, as in most cases, amacrine cells link bipolar cells and ganglion cells by long connections parallel to the retinal layers. Twenty-nine types of amacrine cells exist in the mammalian retina (reviewed in (Masland, 2001)). They have distinct pre- and postsynaptic partners, contain a variety of different neurotransmitters and fulfill diverse functions. They globally adjust the retina's responsiveness to the characteristics of the visual environment, dim or bright light conditions, and they seem to account for correlated firing among ganglion cells.

1.1.3.1.4 Ganglion cells

Ten to fifteen types of ganglion cells exist in the mammalian retina, distinguished by their branching level, their receptive field and in many cases their directly recorded physiology, ON-center cells and OFF-center cells (reviewed in (Masland, 2001)). ON-center ganglion cells are activated and they discharge at markedly increased rates when a spot of light hits the center of their receptive field and are inactivated when light falls on the periphery of their receptive field. OFF-center ganglion cells react the opposite way. The two kinds of cells seem to be equally common in the retina. An OFF-center cell discharges at its highest rate in response to a dark spot on a white background, because then only the surrounding of its receptive field is illuminated. ON-center cells respond in the same way to bright spots as OFF-center cells to dark spots. The center-surround receptive field enables the cell to make comparisons between the amount of light hitting a certain spot on the retina with the average amount falling on the immediate surrounding. Not the absolute intensity of the illumination but the relative illumination of a spot and its surrounding (like letters on a piece of paper), are important.

1.1.3.1.5 The interplexiform cells

The interplexiform cells represent a rare cell type in the retina and modulate information in the inner nuclear layer. Interplexiform cells extend their neurites in the outer and inner plexiform layers or establish synaptic contacts with other neurons in the inner nuclear layer. In primates, two types have been described based on their neurotransmitter; GABA-positive interplexiform cells and tyrosine-hydroxylase-positive interplexiform cells.

1.1.3.2 Retinal glia cells

1.1.3.2.1 Müller glia cells (MC)

The MC are elongated cells, spanning radially throughout the entire neural retina. The terminations of the MC form the inner and outer limiting membrane, while their cell bodies are situated in the inner nuclear layer. The apical portions of the MC completely envelop the photoreceptor cell bodies within the outer nuclear layer, and secondary extensions envelop dendritic or axonal processes of other retinal neurons. MC derive from the same progenitor cells as neurons during retinal development, and they play a primordial role in the orientation, migration and movement of neurons (Rakic Lj et al., 1981). In the mature retina, MC act as support cells but also possess crucial metabolic functions, important for the survival of retinal neurons. They are responsible for the regulation of extracellular potassium ((Miller and

Dowling, 1970), (Newman, 1987)), and levels of the recapture and degradation of neurotransmitters such as glutamate, GABA ((Brew and Attwell, 1987), (Malchow et al., 1989)) or acetylcholine, and control pH through their elevated carbonic anhydrase activity ((Sarthy and Bunt, 1982), (Newman, 1985)).

1.1.3.2.2 Astrocytes

Astrocytes are a class of glia cells that appear in the mammalian retina late in development, because they are not intrinsic to the retina. During development, they migrate along the optic nerve and insert into the retina (Watanabe and Raff, 1988). The positioning of astrocytes in the retina depends on the co-migration of vascular endothelium cell precursors (Chan-Ling and Stone, 1991), explaining their absence in non-vascularized retinas. Astrocytes are absent from the peripheral avascular margin of the primate retina and from the foveal avascular area (Stone and Dreher, 1987). In the mature retina, astrocytes are found in the ganglion cell layer and optic fiber layer, where numerous blood vessels are situated (Bussow, 1980). Astrocytes play a role in the construction of the blood-retina barrier, provide important structural support to retinal vessels and are able to modulate the growth of endothelial cells (Jiang et al., 1993).

1.1.4 Murine retina

The murine retina is becoming an important source for studies of mammalian retinal organization, and natural mutant and transgenic mouse models have contributed significantly to understanding human eye disease, particularly various types of photoreceptor degenerations (Travis et al., 1989), (Bowes et al., 1990), (Redmond and Hamel, 2000). Mice have the advantage of rather easy handling, short generation time and lifespan with many offsprings. Although recent data indicate some differences in genetic control of photoreceptor differentiation between mice and humans (Bibb et al., 2001), no major morphologic or biochemical differences have been identified between mouse and human. However, mouse and human cones are both qualitatively and quantitatively different. While across the mouse retina cones constitute about 1% of the photoreceptors (Jeon et al., 1998), the photoreceptors of the human fovea are 100% cones, in the central 1 mm of human retina, cone represent 50% of the photoreceptors and over the entire human retina the cone average is 5% of total photoreceptors (Curcio et al., 1990). Besides these differences in cone content, there are also significant differences on the molecular level. Humans are normally trichomats and their cones are separated into three types, characterized by the presence of short (S)-, middle (M)-, or long (L)-wavelength sensitive opsin in the OS ((Nathans et al., 1986), (Jacobs, 1998)).

Mice on the other hand are dichromats expressing an M opsin and an ultraviolet (UV)-wavelength sensitive opsin (Jacobs et al., 1991).

1.1.5 Porcine retina

In recent years, the use of pigs (*Sus scrofa*) in research has gained more and more importance. One of the main advantages in the use of pigs is that eyes from domestic pigs are widely available from local slaughter houses. The eyes are large and the retina has a high cone density with two types of cones (Hendrickson and Hicks, 2002). Recent advantages in technology have also enabled the creation of transgenic pigs, which mimic common human retinal mutations, such as the rhodopsin P347L mutation that causes retinitis pigmentosa ((Tso et al., 1997), (Li et al., 1998)). Although the retina lacks a macula, it contains a structure that resembles the human macula to a certain degree, namely a broad band or visual streak above the optic disc with high cone density (Hendrickson and Hicks, 2002).

1.2 The G-protein-coupled receptor rhodopsin

The visual pigment of the rod photoreceptors has been intensively studied in recent decades. Because of its easy accessibility, it is the best characterized G-protein-coupled receptor (GPCR) so far (Menon et al., 2001). GPCRs are members of the most diverse class of cell-surface receptors that mediate the actions of various hormones, neurotransmitters and sensory stimuli by activating heterotrimeric G proteins (Oldham and Hamm, 2008). Nearly 800 different human genes encoding GPCRs have been identified so far. They are targets of ~30% of all pharmaceuticals on the market ((Bjarnadottir et al., 2006), (Hopkins and Groom, 2002)). Like rhodopsin, all GPCRs have seven transmembrane-spanning α -helices, an extracellular N-terminus and an intracellular C-terminus (see Figure 3A and 3B). Currently, the crystal structure of bovine rhodopsin provides the only high-resolution structural data on the transmembrane bundle of any GPCR ((Palczewski et al., 2000), (Teller et al., 2001), (Okada et al., 2004), (Li et al., 2004)). Rhodopsin is the only GPCR where the ground-state receptor is covalently bound to an inverse agonist, the vitamin A derivate 11-cis-retinal (Figure 3A and 3B), which holds the transmembrane region of the protein in the inactive conformation. Rhodopsin is activated by photoisomerization of its chromophore to all-trans-retinal in the disc membranes of ROS.

Synthesis of the seven-transmembrane apoprotein portion of rhodopsin, called opsin, begins in the inner segment of photoreceptors, where it undergoes maturation in the endoplasmic reticulum (ER) and Golgi membranes, before it is transported vectorially to the ROS. The C-

terminal region of the protein is essential for interactions with the transport machinery that delivers rhodopsin on membrane vesicles to the ROS ((Sung et al., 1994), (Tam et al., 2000), (Deretic, 2004)). Transport of rhodopsin mutants, lacking the C-terminal region, to the ROS does not occur *in vivo*, and the mutant is piggybacked to the ROS only in the presence of wt-rhodopsin ((Frederick et al., 2001), (Deretic et al., 2004)). The regeneration of rhodopsin from opsin and its chromophore 11-cis-retinal is not essential for vectorial transport to the ROS, as mice deficient in chromophore production still develop ROS ((Redmond et al., 1998), (Batten et al., 2004)), but because of the continuous coupling of rhodopsin with G proteins, these rods slowly degenerate ((Jin et al., 2003), (Woodruff et al., 2003; Lem and Fain, 2004)).

The rhodopsin gene was cloned in the 1980s (Nathans and Hogness, 1983) and the first mutation linked to disease was identified in 1990 (Dryja et al., 1990). To date, over 100 mutations in the human rhodopsin gene have been associated with recessive and dominant retinitis pigmentosa, as well as congenital stationary night blindness (see <http://www.sph.uth.tmc.edu/RetNet/>). Mutant mice and flies have been generated, in whom the rhodopsin gene has been knocked out. They are unable to form disc membranes, indicating a structural role for rhodopsin in addition to that of a light perceptive molecule (Chang and Ready, 2000).

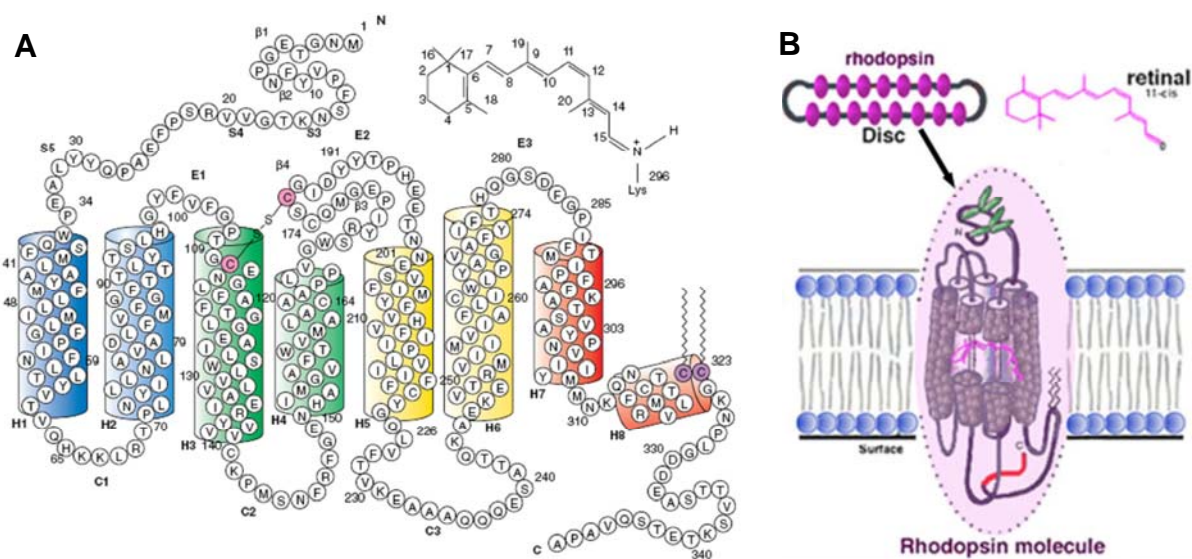


Figure 3: Rhodopsin. **A**) 2D model for the organization of bovine rhodopsin in the disk membrane. Amino acid residues are depicted in single letter code. Transmembrane α -helical segments (H1-H7) and the cationic amphiphathic helix H8 are shown as cylinders. An essential disulfide bond links Cys110 and Cys187 (pink). Cys322 and Cys323 (purple) are palmitoylated. Extracellular domains E1-E3, cytoplasmic loops C1-C3 and the amphiphathic helix H8 are shown. Insert: structure of the 11-cis-retinal chromophore. Carbon atoms are numbered 1-20 (Sakmar, 2002). **B**) Schematic diagram of rhodopsin in the outer segment disk (<http://webvision.med.utah.edu/photo1.ht>).

1.2.1 Phototransduction

Vision begins in the outer segments of rod (dim light) and cone (bright light) photoreceptor cells of the retina, where visual pigment molecules absorb photons and become activated. In a process called phototransduction (see Figure 4), the light energy is converted into an electrical signal. To generate a reliable signal, the initial photon-induced change in a single molecule is enormously amplified. The discs in the human outer segments of rods and in the plasma membrane enfoldings of human cones are constituted to a high degree of the photosensitive pigments, rhodopsin in rods, and red, green and blue opsin in cones. Most of the studies on phototransduction have been conducted on rods. Upon arrival of a light stimulus, absorption of a photon converts 11-cis-retinal to all-trans-retinal, inducing a conformational change in rhodopsin within about 35 femtoseconds. While 11-cis-retinal fits its surrounding perfectly, the steric shape of all-trans-retinal requires changes in the internal configuration of the tertiary opsin structure, until a final equilibrium is reached. These changes are identified by a series of precisely measurable changes in color of the molecule by light spectroscopy. Photoactivated rhodopsin (R^*) finally becomes colorless, that is why this whole process is called “bleaching”. The photoisomerized chromophore, all-trans-retinal, is released from the opsin, is reduced to all-trans-retinol and diffuses to the adjacent retinal pigment epithelium, where it undergoes enzymatic transformation back to 11-cis-retinal in a metabolic pathway known as the retinoid cycle. Opsin recombines with replenished 11-cis-retinal to form rhodopsin ((Schadel et al., 2003), (Maeda et al., 2005)). R^* activates thousands of molecules of photoreceptor-specific G protein transducin (Kohn et al.) that exists as a heterotrimeric complex composed of its three subunits α , β and γ , with GDP bound to the α subunit. Activation by R^* leads to an exchange of GDP to GTP and to dissociation of transducin α from the $\alpha\beta\gamma$ complex. The GTP-bound transducin α activates the catalytic α and β subunits of PDE6 (see 3.2) by displacing the inhibitory γ subunits from the active site of the enzyme, leading to cGMP hydrolysis. In the dark, high levels of cGMP maintain cyclic nucleotide-gated (CNG) cation channels open, allowing the influx of sodium and calcium into the photoreceptor, resulting in depolarization. The activated PDE6 hydrolyses cGMP to 5'GMP. The decrease in cGMP leads to closure of the CNG cation channels. The resulting decreased influx of sodium and calcium leads to hyperpolarization of the photoreceptor. Hyperpolarization decreases the release of the neurotransmitter glutamate at the photoreceptor synapses, which is constitutively released in the depolarized state. Onset of light is thus transduced by a reduction in chemical signaling, which is transmitted to second order neurons.

The deactivation of the phototransduction cascade involves several different steps and mechanisms: first, transducin is inactivated by GTP to GDP exchange in the outer segments, resulting in dissociation of the GDP-bound form of transducin α from the PDE6- $\alpha\beta$ subunit. Second, the inhibitory PDE6 γ subunits reassociate with PDE6 α and β , leading to their inactivation. Third, R^* is phosphorylated by rhodopsin kinase (RK), which is thought to diminish the ability of R^* to activate transducin. The rate of R^* phosphorylation by RK is regulated by recoverin (Rec). Finally, arrestin (Arr) interacts with R^* preventing interaction with transducin. The major players in restoration of cGMP levels are guanylate cyclase (GC), the enzyme producing cGMP, the Ca^{2+} -inhibited GC-activating proteins (GCAPs) and the $Na^+/Ca^{2+}/K^+$ exchanger. (for review see: (Ridge et al., 2003) and (Baehr, 2001)).

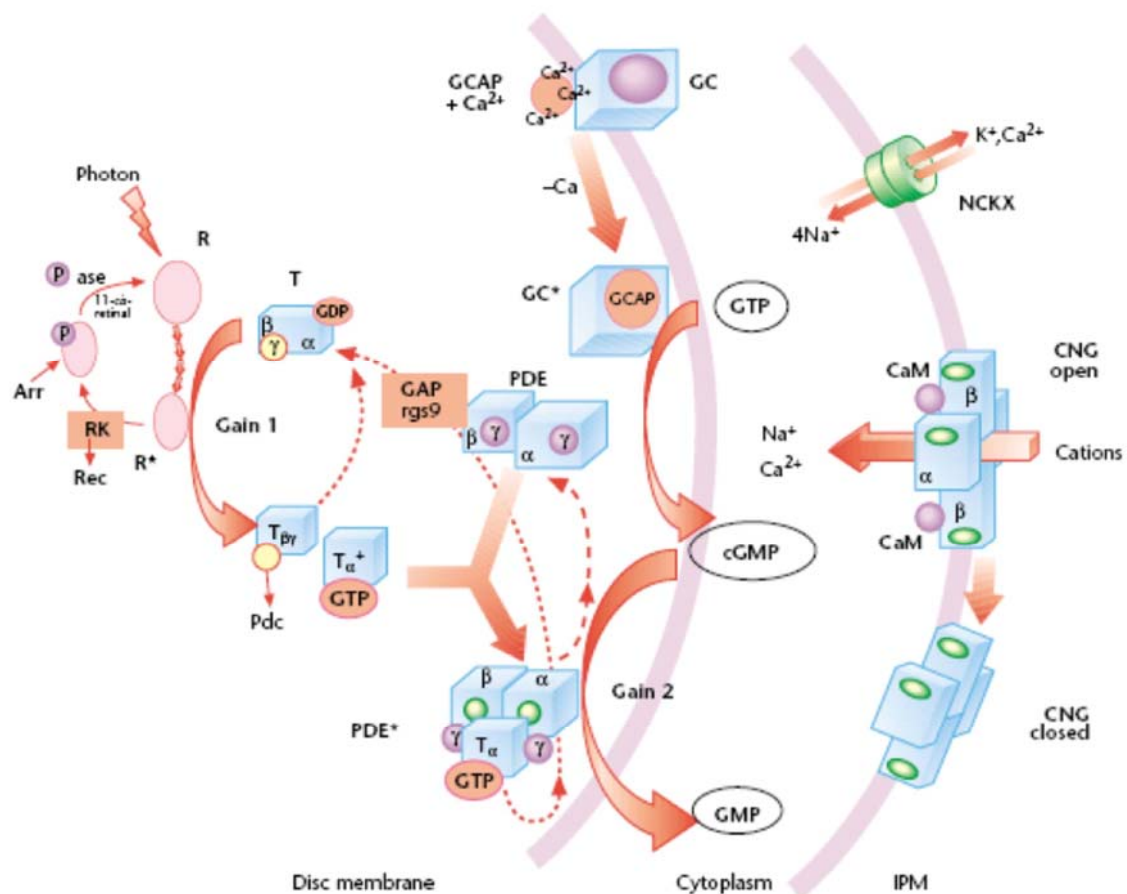


Figure 4: Model of rod phototransduction (Baehr, 2001). Rhodopsin serially activates many copies of G_t (gain 1). The α subunit of G_t in turn activates α PDE, which rapidly hydrolyses cytoplasmic cGMP (gain 2). The drop in cGMP concentration closes CNG cation channels in the plasma membrane, leading to hyperpolarization of the outer segment plasma membrane. Cytoplasmic Ca^{2+} concentration drops owing to its continued extrusion by the light-independent exchanger, also located in the plasma membrane. In a negative feedback loop, the drop in Ca^{2+} causes stimulation of a GC by one or several specific Ca^{2+} -binding proteins, the GCAPs. Sites where regulatory proteins (phosducin (PDC), Arr, Rec) interact with components of the cascade are indicated by arrows.

1.2.2 Light-regulated translocation of photoreceptor proteins

The dynamic localization of proteins within cells is often determined by environmental stimuli. In retinal photoreceptors, light exposure results in the massive translocation of three key signal transduction proteins, transducin, arrestin and recoverin, into and out of the outer segment. In response to bright light, transducin α of rods moves out of the outer segment and accumulates in the inner segment ((Philp et al., 1987), (Brann and Cohen, 1987), (Whelan and McGinnis, 1988)). Arrestin moves in the opposite direction (Broekhuysse et al., 1985), and recoverin shifts from the outer segment towards the synapse (Strissel et al., 2005). In cones, arrestin ((Mirshahi et al., 1994), (Zhu et al., 2002), (Zhang et al., 2003)) but not transducin moves in response to light ((Kennedy et al., 2004), (Elias et al., 2004), (Coleman and Semple-Rowland, 2005)). Recoverin translocation has not yet been analyzed in cones.

Photoreceptors can adjust their sensitivity over a broad range of ambient light intensities, and protein translocation is likely to contribute to this process. Recent quantitative measurements of the magnitude and rate of protein translocation, along with the first functional data on transducin translocation, argue that this phenomenon contributes to photoreceptor adaptation to bright continuous illumination, such as normally encountered during daylight hours (Sokolov et al., 2002). What remain unknown to date are functional contributions of the translocations of arrestin and recoverin and the role that protein translocation has in broader aspects of photoreceptor maintenance and survival. The current debate in the field is whether protein translocation is driven by diffusion or by active transport by molecular motors that carry proteins along cytoskeletal elements. Mechanistic studies favor the idea that light-induced protein translocation is set by an interplay between protein binding to compartment-specific sites and cytoplasmic diffusion (reviewed in (Calvert et al., 2006)).

1.3 Cilia and ciliopathies

1.3.1 Cilia in vertebrate cells

Humans experience their environment through cilia. Light, odorant, and sound perception depend on these complex organelles. Cilia and flagella are evolutionary conserved organelles that, besides their presence on cells in primary sensory tissues, are present on almost all human cells (Pan et al., 2005). They are microtubule-filled, cellular extensions, in which enclosing membrane is continuous with the cell plasma membrane. Although cilia and flagella are identical in structure and composition, the two names were originally chosen to indicate distinctive movement patterns and are still used (Pan et al., 2005). The most familiar

cilia are the multiple, motile cilia involved in cell motility (sperm) and transport of mucus and other fluids, but most of the cilia, which enable us to experience our environment, are primary, non-motile cilia, present just one per cell ((Wheatley, 1995), (Wheatley et al., 1996), (Praetorius et al., 2004)). In vertebrates, the light-perceptive molecule rhodopsin is housed in a modified non-motile cilium, the rod outer segment. Odorant receptors of olfactory epithelial cells are expressed on the tufts of long cilia that project from the olfactory knob. And the single kinocilium on the hair cells of the ear is intimately associated with the stereocilia (actin-filled microvilli), the movements of which with respect to each other lead to sound perception (Pan et al., 2005). A specialized motile form of the primary cilia is the nodal cilia in the blastocyst. It is responsible for the nodal flow, which is crucial for the development of left-right sidedness in the developing mouse embryo (Nonaka et al., 1998).

A prototypic motile cilium contains nine sets of doublet microtubules that surround a central pair of singlet microtubules ($9 \times 2 + 2$). The outer doublet microtubules contain motor complexes (dynein arms). They enable ATP driven movement that causes adjacent microtubule doublets to slide past each other. Spoke-like structures (the radial spokes) project from each of the outer microtubule doublets towards the central pair of singlet microtubules (Pan et al., 2005). The ciliary shaft originates from a basal body complex with a pair of centrioles (Rieder et al., 2001). The centriolar triplet arrangement of the microtubules in the basal body ($9 \times 3 + 0$) is converted in the transition zone, where the central pair of singlet microtubules is missing ($9 \times 2 + 0$ microtubular array), into the axonemal microtubular array ($9 \times 2 + 2$).

In contrast to motile cilia, non-motile cilia normally miss the central pair of microtubules ($9 \times 2 + 0$) and the radial spokes and the dynein arms (Pan et al., 2005).

1.3.1.1 The photoreceptor connecting cilium

The photoreceptor connecting cilium (CC), so called because it connects the inner and outer segment of photoreceptors, represents a specialized sensory non-motile cilia (Figure 5A). It is found in photoreceptor cells of the vertebrate retina, where the entire outer segment can be considered as the highly modified distal part of a primary non-motile cilium ((Rohlich, 1975), (Horst et al., 1990)). The CC originates from the basal body beneath the apical inner segment membrane (Figure 5B) and long striated ciliary rootlets project through the inner segment into the cell body ((Spira and Milman, 1979), (Yang and Li, 2006)). The CC of mammalian photoreceptors has a $9 \times 2 + 0$ microtubule configuration (Figure 5C) ((Rohlich, 1975), (Schmitt and Wolfrum, 2001)), and it appears to play an important role in photoreceptor organization,

development and maintenance ((Rohlich, 1975);(Horst et al., 1990);(Schmitt and Wolfrum, 2001)). At the base of the CC, the apical membrane of the photoreceptor inner segment is specialized into a so-called pericilliary ridge complex ((Papermaster et al., 1985), (Papermaster, 2002)), linking the inner segment membrane via extracellular fibers to the membrane of the CC (Horst et al., 1990). At this membrane specialization, transport vesicles dock and hand over their load to the ciliary transportation machinery (Deretic, 2004). The axonemal cytoskeleton of the outer segment loses the stereotypical $9 \times 2 + 0$ arrangement and is reduced to a small number of “axonemal” microtubules that continue from the connecting cilium and project through the outer segment, in some species for up to 80% of its length ((Kaplan et al., 1987), (Liu et al., 2002)).

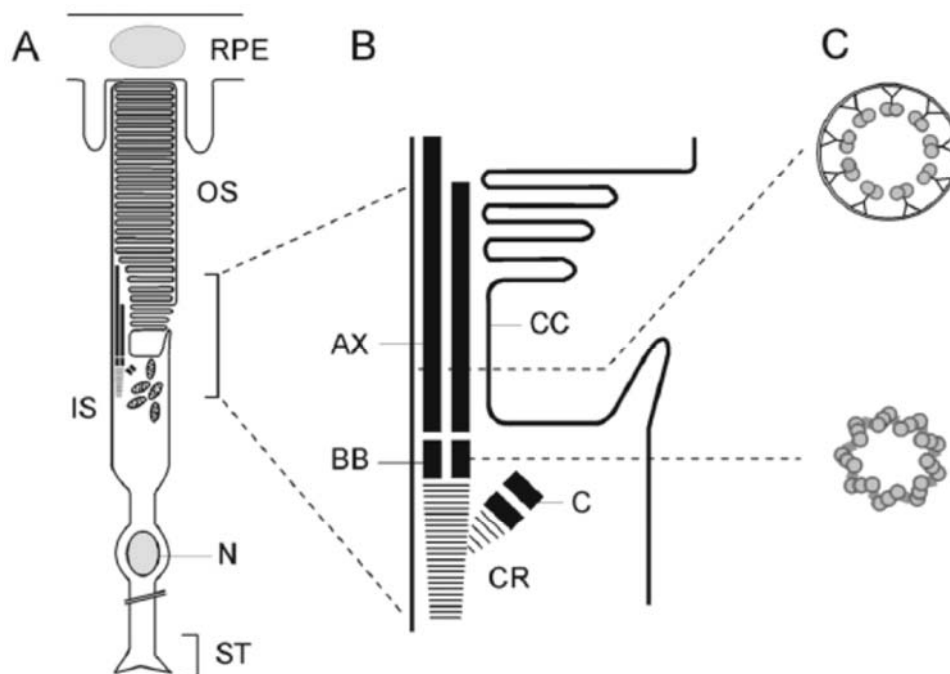


Figure 5: Diagram illustration of a rod photoreceptor and its ciliary apparatus. **A)** The rod photoreceptor consists of an outer segment (OS), linked to the inner segment (IS) via the connecting cilium (CC). The cell body contains the nucleus (N), the axon and synaptic termini (ST). RPE: retinal pigment epithelium. **B)** Detail of the ciliary apparatus. It consists of the microtubule based axoneme (AX), and the basal body-centriole complex with a ciliary rootlet (CR), which projects into the inner segment. BB: basal body, C: centriole. **C)** Schematic cross section of the basal body and the ciliary axoneme. The basal body shows the characteristic 9×3 -structure, the modified cilium a $9 \times 2 + 0$ structure (Schmitt and Wolfrum, 2001).

1.3.2 Cilia-related disorders

The sensory roles of cilia are essential for the normal functioning of many tissues, and the role of cilia is recognized in an emerging class of human genetic disorders (see Table 1 for an overview). Ciliary defects can cause a number of different phenotypes such as retinal degeneration, polycystic liver and kidney disease, situs inversus, hydrocephalus, anosmia, sinusitis, infertility and polydactyly. Many of these syndromes are often combined with global levels of cognitive impairment and developmental delay, indicating the importance of primary cilia in neurological function.

Location of cilia	Properties/functions	Phenotype	Ciliary defect
Embryonic node	9+0; motile and non-motile/non-motile cilia senses leftward nodal flow created by motile cilia	Situs inversus	Immotility
Ependymal cells in brain ventricles	9+2; motile/flow of cerebrospinal fluid	Hydrocephalus	Immotility
Photoreceptor cells in the retina	9+0; non-motile/light perception	Blindness	Intraflagellar transport
Apical knob on olfactory neurons	9+2 (at the base, microtubule singlets distally); non-motile	Anosmia	No cilia
Epithelium of the upper and lower airways	9+2; motile/mucus clearance	Respiratory tract infections, rhinitis, sinusitis	Immotility
Sperm	9+2; motile/sperm motility	Male infertility	Immotility
Oviduct epithelium	9+2; motile/egg transport	Female infertility	Immotility
Epithelium of the kidney, bile, and pancreatic ducts	9+0; non-motile/mechanical sensing	Cyst formation	Failure to signal
Unknown	9+0?; non-motile?/function in development and metabolism	Obesity, polydactyly, diabetes, cognitive impairment, other ailments	Failure to signal?

Table 1: Cilia-related disorders - overview of the locations and properties of cilia that are known to be associated with several human phenotypes (Pan et al., 2005).

Although the phenotypes of the various genetic diseases caused by ciliary defects are versatile, many of them belong to a group of retinal degenerations termed retinitis pigmentosa (RP). RP is a genetically heterogeneous form of blindness, with 33 known different gene loci that affects 1 out of 3,500 people worldwide (Berson, 1993). In a number of retinal degenerations, such as retinitis pigmentosa type 3 (RP3), Usher syndrome (USH), Bardet-Biedl syndrome (BBS) and Leber congenital amaurosis (LCA), protein complexes of the photoreceptor connecting cilium are involved.

RP3 is caused by mutations in the N-terminal domain of the X-linked gene retinitis pigmentosa GTPase regulator (RPGR) ((Roepman et al., 1996a), (Roepman et al., 1996b), (Meindl et al., 1996)). This domain shows significant homology to the regulator of chromosome condensation (RCC1) that functions as a guanine nucleotide exchange factor (GEF) for the small GTPase Ran ((Roepman et al., 1996b), (Meindl et al., 1996)). The RCC1 homologous domain has been identified to bind to PDE δ (Linari et al., 1999b) and to the RPGR interacting protein 1 (RPGRIP1) ((Boylan and Wright, 2000), (Roepman et al., 2000a), (Roepman et al., 2000b)). In photoreceptors, RPGR was shown to be localized to the axoneme and the basal body of connecting cilia via RPGRIP1 ((Hong et al., 2001), (Hong et al., 2004) (Khanna et al., 2005)).

Usher syndrome (USH) is the most frequent cause of combined deaf-blindness in humans. It is clinically and genetically heterogeneous and at least 11 genes are assigned to the three clinical USH types, namely *USH1B-G*, *USH2A-C*, *USH3A* ((Reiners et al., 2006), (Gerber et al., 2006)). Although the colocalization of all USH1 and USH2 proteins at the photoreceptor synapse suggests a synaptic localization of the USH protein network in photoreceptors, a subset of USH proteins is also present at the ciliary apparatus of photoreceptor cells indicating a USH network here (Reiners et al., 2006).

The Bardet Biedl Syndrome (BBS) is a rare polygenetic and pleiotropic disorder associated with basal body and ciliary defects (Beales, 2005). To date, 8 genes have been identified to be associated with BBS ((Kaplan et al., 1990), (Blacque and Leroux, 2006)). Patients with this multifaceted disease can suffer from a large number of symptoms, including retinal (rod-cone) degeneration, obesity, cystic kidneys, learning disabilities, hearing loss and anosmia (Green et al., 1989), ((Beales et al., 1999), (Moore et al., 2005)).

1.3.2.1 Leber congenital amaurosis

Leber congenital amaurosis (LCA), first described by Theodore Leber in the 19th century (Leber, 1869), is the earliest and most severe form of all inherited retinal dystrophies, characterized by blindness or severe visual impairment from birth or within a few months of birth. LCA, diagnosed as bilateral congenital blindness, accounts for at least 5% of all retinal dystrophies and it is the most common congenial blindness in infants and children (Kaplan et al., 1990), (Perrault et al., 1999). Visual difficulties are usually noticed before the age of six months and the electroretinogram (ERG) is usually extinguished before the age of one year. Most of the LCA patients show nystagmus, photophobia, eye poking and sluggish pupils ((Foxman et al., 1985), (Heckenlively et al., 1988)). LCA is generally inherited in an autosomal recessive manner, although some autosomal dominant families have been described ((Heckenlively et al., 1988), (Sohocki et al., 1998)). To date, mutations in eight genes and three chromosomal loci have been associated with autosomal recessive forms of LCA (MIM 204000; RetNet): 1) Aryl hydrocarbon receptor-interacting protein-like 1 (AIPL1) (Sohocki et al., 2000); 2) Crumbs homolog 1 (CRB1) (den Hollander et al., 2001); (Lotery et al., 2001); 3) cone-rod homeobox (CRX) (Freund et al., 1998); 4) guanylate cyclase 2D (GUCY2D) (Perrault et al., 1996); 5) RPE65 (Marlhens et al., 1997); 6) retinitis pigmentosa GTPase regulator-interacting protein 1 (RPGRIP1) (Dryja et al., 2001); 7) RD3 (Friedman et al., 2006); and 8) RDH12 (Perrault et al., 2004).

Although the exact roles in eye development and homeostasis are not yet known for all LCA-associated genes, it is clear that their protein products have very diverse functions. AIPL1 and RPGRIP1 may be involved in retinal protein trafficking ((Hollander et al., 1999), (Sohocki et al., 2000), (Roepman et al., 2000a), (Boylan and Wright, 2000)). GUCY2D is essential for the recovery of the dark state after photoexcitation of the photoreceptors by catalyzing the conversion of GTP to cGMP. RPE65 and RDH12 play a crucial role in the synthesis of 11-cis-retinal in the visual cycle ((Redmond et al., 1998), (Perrault et al., 2004)). CRB1 may be important for photoreceptor morphogenesis (Pellikka et al., 2002). RD3 is thought to be involved in transcription and splicing processes (Friedman et al., 2006) and CRX is a homeobox transcription factor required for the elongation of photoreceptor outer segments, and is essential for the phototransduction pathway (Furukawa et al., 1999).

1.3.2.1.1 Lebercilin

By homozygosity mapping the *LCA5* gene on chromosome 6q14 was identified, which encodes the novel ciliary protein, lebercilin (den Hollander et al., 2007). Homozygous nonsense and frameshift mutations in the *LCA5* gene were identified in five LCA families. In a sixth family the *LCA5* transcript was completely absent due to a homozygous 1598-bp deletion in the promoter region and the non-coding exon1. The patients presented a severe congenital retinal dystrophy consistent with LCA (congenital visual loss, nystagmus, high hyperopia, and a non-detectable electroretinogram) and showed normal neurological and renal function (Dharmaraj et al., 2000) or were documented with poor vision from early infancy, and were otherwise healthy as far as could be established without detailed clinical testing (Mohamed et al., 2003). All genes implicated in LCA are expressed exclusively or predominantly in the eye. An exception is *LCA5* that intriguingly shows a wide expression pattern throughout development, while the phenotype in patients is limited to the eye. Lebercilin localizes to the connecting cilia of photoreceptors and to the microtubules, centrioles and primary cilia of cultured mammalian cells. Truncation of lebercilin due to *LCA5*-associated null mutations abrogates the microtubule association (den Hollander et al., 2007).

2. GTPASES

2.1 GTP binding proteins in signal transduction

GTPases, together with their associated regulators and effectors, are central control elements in signal transduction pathways in nearly every aspect of cell biology. Most GTPases belong to the RAS superfamily of GTPases and share a basic biochemical activity, namely GTP binding and hydrolysis. By cycling between two conformational states, a GTP-bound, active state and a GDP-bound, inactive state, they act as molecular switches and control complex cellular processes. In the GTP-bound active state they interact with high affinity with downstream effector proteins and generate a response until GTP hydrolysis switches the GTPase off again. Most RAS proteins contain posttranslational lipid modification and are predominantly associated with membranes.

The RAS superfamily of GTPases can be further subclassified into Ras, Rho, Rab and Arf families, as well as the closely related G α family. Members of the Ras family of GTPases are involved in control of mitogenesis, differentiation, protein trafficking and cytoskeleton dynamics (Feig, 2003). They also play a role in oncogenesis. Elevated Ras activity due to mutationally activated forms of RAS proteins, especially K-Ras as well as H-Ras and N-Ras,

is found in a broad spectrum of tumors ((Mitsuuchi and Testa, 2002), (Grady and Markowitz, 2002), (Jaffee et al., 2002)). Other mechanisms leading to an elevated Ras activation in different tumors are enhanced amplification or overexpression of RAS genes (Vageli et al., 1996), mutations that affect the responsiveness to regulatory proteins (Zhang et al., 1990), increased signaling of upstream receptors (von Lintig et al., 2000), mutations in genes encoding negative regulators (Xu et al., 1990) or overexpression of positive regulators (Shinohara et al., 1997). Members of the Rho family GTPases are involved in multiple aspects of cytoskeletal remodeling and cell polarity (see chapter 2.2) ((Heo and Meyer, 2003), (Fransson et al., 2003)) and mounting evidence also supports their involvement in cancer (Sahai and Marshall, 2002). The Rab family of GTPases represents the largest Ras subfamily and members function in protein trafficking pathways, vesicle formation, movement and fusion ((Stenmark and Olkkonen, 2001), (Pereira-Leal and Seabra, 2001)). The Ran proteins, formerly considered a separate Ras subfamily, are a branch of the Rab family. They are implicated in nuclear import and export (Weis, 2003). Proteins of the Arf family of GTPases are regulators of trafficking of intracellular proteins and membranes and of cytoskeletal remodeling (Randazzo et al., 2000). Proteins of the G α family of GTPases were among the first well-characterized mammalian GTPases. Mutant G α proteins are associated with several diseases including cancer (Lyons et al., 1990). The functions of G α -type GTPases are inextricably linked to their association with $\beta\gamma$ heterotrimeric subunits and with GPCRs (see chapter 1.2.1). Downstream effectors of G α proteins include multiple adenyl cyclase isoforms, several ion channels and transporters, and various other cell regulatory components (Neves et al., 2002).

2.2 Rho family GTPases

Rho family GTPases comprise a main branch of the RAS superfamily and are found in all eukaryotic cells. They function as molecular switches, and they are known principally for their pivotal role in regulation of the actin cytoskeleton. They also regulate a variety of cellular processes including cell-cycle progression, gene transcription, development of cell morphology, cell polarity, microtubule dynamics, membrane transport pathways, cell migration, cell adhesion, phagocytosis, cytokinesis, neurite extension and retraction, as well as cell growth and survival (reviewed by (Etienne-Manneville and Hall, 2002)). Furthermore, aberrant regulation of Rho family GTPases promotes malignant transformation and is essential for the oncogenic properties of Ras and other oncogenes (Sahai and Marshall, 2002). The activation of Rho family GTPases is often mediated through various cell-surface

receptors, including the cytokine, tyrosine kinase and adhesion receptors, as well as GPCRs ((Kjoller and Hall, 1999), (Sah et al., 2000)). The cycling between GDP- and GTP-bound states is controlled by three classes of regulators (see chapter 2.4). Mammalian cells contain several hundred GTPases and 22 Rho GTPases have been described so far: Rho (three isoforms: A, B, C); Rac (1, 2, 3); Cdc42; TC10; TCL; Wrch1 and Chp/Wrch2; RhoG; Rnd (1, 2, 3); RhoBTB (1, 2, 3); RhoD; Rif; RhoH/TTF; and Miro (1, 2) (Wennerberg and Der, 2004). Although target proteins do not contain a single recognizable sequence motif useful for database searches, for Rac1 (*Ras-related C3 botulinum toxin substrate 1*), RhoA and Cdc42 (*cell division cycle 42*), the three best-characterized members of the Rho GTPase family, over 60 target molecules have been identified experimentally so far. This is consistent with the involvement of Rho GTPases in a huge variety of cellular processes that can be divided into three broad, often overlapping topics to all eukaryotic cells: Cell morphology, cell movement and cell behavior (reviewed by (Etienne-Manneville and Hall, 2002)).

2.2.1 Cell morphology

Cells adopt a huge diversity of shapes. They are highly dependent on the external environment, which also provides guidance cues that drive the establishment of intracellular polarity. The first evidence linking Cdc42 to cell polarity was provided by analysis of budding yeast, where the cell was not able to establish a defined site for daughter cell growth in the absence of this GTPase and the protrusion did not occur at the right place (Pruyne and Bretscher, 2000). In epithelial cells, Cdc42 and Rac1 were shown to be important for the establishment of cell morphology and cell polarity, which is driven by two types of intercellular adhesive junctions: Adherens junctions, which form a strong mechanical link between adjacent cells and tight junctions, which form a physical barrier and prevent the diffusion of lipids and proteins between the basolateral and apical membranes, required for establishing of the apical/basolateral asymmetry. Along with the assembly of these junctions, the actin and microtubule cytoskeletons are reorganized and the vesicular transport is polarized ((Raich et al., 1999), (Vasioukhin et al., 2000), (Jacinto et al., 2001)). The generation of intracellular asymmetry in response to environmental cues is required in most animal cell types to direct a morphogenetic program, but perhaps none is as complex as that in neurons. Neurons extend neurites, one of which differentiates into an axon while the others become dendrites (Figure 6A). Dendrites form small actin-rich projections along their length, the spines, which form synapses with axons of other neurons. The mechanism that determines which of the many neurites becomes the axon, is still not understood, but it seems to be a cue

coming from the environment. While Cdc42 and Rac1 are positive regulators of neurite outgrowth, RhoA inhibits neurite extension (Luo, 2000). The observations of opposing activities of these GTPases on the actin cytoskeleton in fibroblasts, where Cdc42 and Rac1 promote membrane protrusion (through actin filament assembly at the periphery), whereas RhoA promotes membrane retraction (through contractile actin and myosin filaments), have been used extensively to explain their effects observed in neurons. In *Drosophila*, Rac1 was shown to be required for nerve growth factor (NGF)-induced axon growth, while RhoA limits dendritic outgrowth ((Lee et al., 2000), (Ozdinler and Erzurumlu, 2001)). Similarly, Rac1 activation in neurons increases the number of dendritic spines, whereas RhoA activation has the opposite effect ((Li et al., 2000), (Wong et al., 2000)). But the idea that opposing Rac1 and RhoA activities control the neuronal shape through the actin cytoskeleton seems to be an oversimplification. It is still unclear what the relative contributions of the actin and microtubule cytoskeleton in dendrite and axon outgrowth are, and there is also evidence that Rho GTPases directly control microtubule dynamics (see 2.2.2).

2.2.2 Cell movement

Axon guidance can be thought of as a specialized form of directed migration, the cell body does not move, but the growth cone at the axon tip responds to attractive and repulsive extracellular cues as it extends to its target site (Figure 6B) (Liu and Strittmatter, 2001). Repulsion requires RhoA activation and is induced by the ephrin/Eph family of ligand/receptors. Growth cone outgrowth on the other hand is associated with activated Rac1 (Etienne-Manneville and Hall, 2002). These data fit well the mutually opposing retraction/extension model for Rac1 and RhoA, but another class of chemorepellents adds additional complexity. The semaphorins, axonal growth cone guidance molecules, acting through the plexin receptor family require Rac1 activity to induce growth cone collapse (see 2.3).

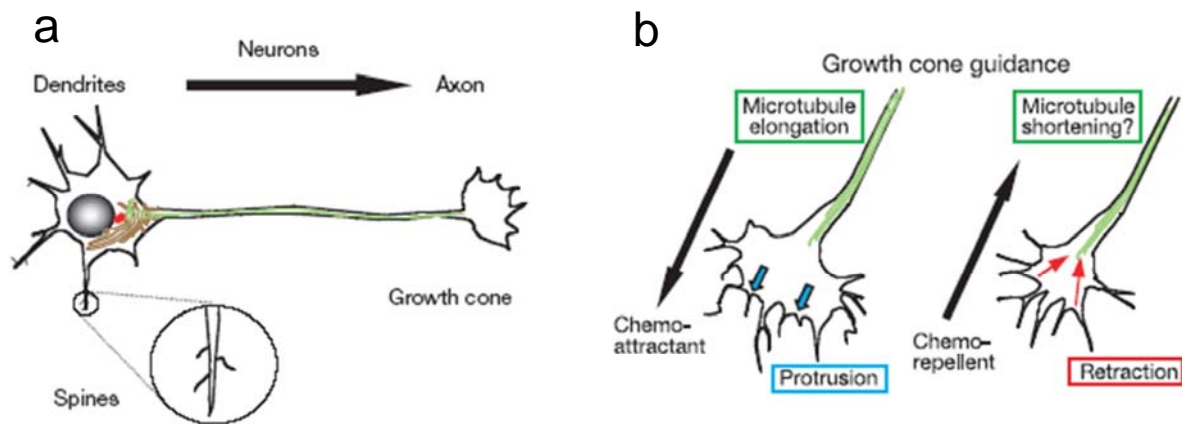


Figure 6 Morphology and polarity (Etienne-Manneville and Hall, 2002). **a)** Rho GTPases are involved in determining the morphology of neurons. They affect axon, dendrite and spine growth, as well as axon guidance. **b)** Growth cone guidance: Growth cone movement of an axon is governed by attractive or repulsive cues, leading to actin-dependent protrusion or retraction, respectively. Microtubule dynamics and vesicular transport pathways also have a role in facilitating directed cell migration.

The migration of cells, either as individuals or as groups, is a principal feature of metazoan embryonic development. In the adult, migration of cells is just as important and it is required to maintain tissue integrity and during immune surveillance. For movement, an asymmetric organization of cellular activities is required. The front of a migrating cell promotes a protrusive force (extension of a lamellipodium in the direction of migration), coupled with the development of new cell adhesions to the extracellular substrate and cell contraction allows the cell body to follow the extending front. Thereby, the actin cytoskeleton is believed to provide the driving force in cell migration. Rac1 induces actin polymerization and integrin adhesion complex assembly at the cell periphery, leading to membrane protrusion. Fluorescence resonance energy transfer (FRET) has revealed that Rac1 GTP levels are highest at the leading edge of a migrating cell (Kraynov et al., 2000), but a spatial distribution of RhoA activity during cell migration has yet to be demonstrated. Directional movement is normally directed by extracellular cues (chemotaxis), and is controlled by Cdc42. In a study by Allen and colleagues (Allen et al., 1998), macrophage cells were shown to move up a gradient of a chemotactic factor. When Cdc42 was inhibited, the macrophage showed a random, undirected movement, whereas inhibition of Rac1 blocked all cellular movement. Cdc42 therefore seems to direct and/or stabilize Rac1 activity at the cell front.

Although Rac1-induced actin polymerization is the driving force in cell migration, other cellular activities, like the microtubular cytoskeleton, seem to play an essential role, too. It was shown that at the leading edge of growth cones, detyrosinated microtubules accumulate and microtubule growth is increased. Migration is also accompanied by re-orientation of the

microtubule organizing centre (MTOC) with respect to the direction of migration (Wittmann and Waterman-Storer, 2001).

2.2.3 Cell behaviour

RhoA, Rac1 and Cdc42 are also involved in cell contraction, phagocytosis, proliferation and regulated secretion. Phagocytosis is driven by assembly and disassembly of peripheral actin filaments that promote localized changes in the structure of the plasma membrane. Two distinct phagocytic pathways have been uncovered in mammalian macrophages so far, type I (for example through the immunoglobulin receptor) requires both Rac1 and Cdc42, whereas type II (for example through the complement receptor) requires RhoA (Caron and Hall, 1998).

In addition to their effects on the cytoskeleton, Rho GTPases contribute to the regulation of cell cycle progression. In epithelial cells and fibroblasts *in vitro* RhoA, Rac1 and Cdc42 each contribute to G1 cell cycle progression. All three can promote entry into G1 and progression to S phase when expressed in quiescent fibroblasts, whereas inhibition of any of the three proteins blocks serum-induced G1 progression (Olson et al., 1995). The cell cycle is completed with cytokinesis. In animal cells this action is driven by an actin and myosin contractile ring, which constricts to form the two daughter cells. Not only inhibition but also expression of constitutively active RhoA or Cdc42 prevents the assembly of the contractile ring in a variety of mammalian cells, suggesting that cycling between the active and inactive forms is required for function (Etienne-Manneville and Hall, 2002).

2.2.4 Post-translational C-terminal modifications of Rho GTPases

Rho GTPase function is critically dependent on association of the GTPases with membranes and their subcellular locations. These properties are influenced by C-terminal lipid modifications, as well as by interaction of the GTPases with RhoGDIs (see 2.2.5). Following synthesis as soluble precursor proteins, Rho GTPases become associated with intracellular membrane compartments via post-translational modifications of their C-termini. The majority of Rho GTPases terminate with a CAAX motif (C = Cys; A = aliphatic amino acid, X = any amino acid) that targets them for their post-translational modification, the isoprenylation. Some Rho GTPases are farnesylated (C15) others are modified by the more hydrophobic geranylgeranyl (C20) modification. Rac1 has a Cys-A-A-Leu ((Didsbury et al., 1989)) structure in its C-terminal region. Small G-proteins having this C-terminal structure are post-translationally processed by: 1) geranylgeranylation of the cystein residue; 2)

removal of the A-A-Leu portion by peptidase cleavage; and 3) carboxyl methylation of the exposed cysteine residue. The geranylated cysteine becomes the carboxyl terminus and the free carboxyl group can be methylated by an S-adenosyl-L-methionine-dependent methyltransferase. Methylation is the only step in this modification pathway that is reversible under physiological conditions. Therefore it may be involved in the regulation of protein/protein interactions (Cook et al., 2000) and the control of the activity of prenylated proteins (Perez-Sala et al., 1991).

Other cellular proteins that carry a C-terminal CAAX sequence are processed by the same mechanism; this group comprises proteins of the nuclear envelope (lamins A and B), the γ subunit of heterotrimeric G proteins, as well as several proteins involved in phototransduction such as rhodopsin kinase, the α subunit of transducin and both α and β catalytic subunits of the cGMP phosphodiesterase from retinal rods and cones (Zhang and Casey, 1996).

2.2.5 Regulation of Rho family GTPases

Biochemical and genetic studies have led to the identification of three classes of regulatory proteins that control the nucleotide state of Rho family GTPases (see Figure 7): 1) guanine nucleotide exchange factors (GEFs), 2) GTPase-activating proteins (GAPs) and 3) guanine nucleotide dissociation inhibitors (GDIs) (reviewed by (DerMardirossian and Bokoch, 2005)). The different nucleotide bound states of GTPases are normally also associated with a different localization in the cell. While the inactive GDP-bound state is primarily cytosolic, the active GTP-bound state is usually associated with membranes, where effector targets reside. Because of the presence of high concentrations of Mg^{2+} that prevent spontaneous guanine nucleotide exchange, conversion of inactive GTPases to an active form requires the action of GEFs that catalyze the exchange of bound GDP for ambient GTP. GTPase inactivation involves the catalysis of GTP hydrolysis, which is intrinsically slow, through the action of GAPs that convert the GTPase to the inactive GDP-bound state (DerMardirossian and Bokoch, 2005). However, an additional level of regulation exists for GTPases of the Rho and Rab subfamilies owing to their association with a third class of proteins, the GDP dissociation inhibitors (GDIs).

Three human Rho GDIs have been identified so far: the ubiquitously expressed RhoGDI (or GDI α /GDI1) that was also described as GDI for Rac1 ((Ueda et al., 1990), (Fukumoto et al., 1990)), the hematopoietic cell-selective Ly/D4GDI (or GDI β /GDI2) (Scherle et al., 1993) and RhoGDI γ (or GDI3), specific for RhoB and RhoG and specifically expressed in lung, brain and testis ((Zalcman et al., 1996), (Adra et al., 1997)). Besides their function to inhibit

dissociation of bound GDP from their GTPases, two further biochemical activities have been described for RhoGDIs (DerMardirossian and Bokoch, 2005). First, they are able to interact with the GTP-bound form of the Rho GTPase to inhibit GTP hydrolysis, blocking both intrinsic and GAP-catalyzed GTPase activity and preventing interactions with effector targets. Compared to its binding strength with GDP-bound GTPases, RhoGDI binds to GTP-bound GTPases with weaker (Sasaki et al., 1993) or up to equal affinity ((Chuang et al., 1993), (Nomanbhoy et al., 1996)). The biological consequences of this interaction are still unclear, but it may serve to translocate active GTPases within the cell (DerMardirossian and Bokoch, 2005). Furthermore, GTPases have also been reported to bind to an effector molecule as GTPase(GDP)-RhoGDI complex (Takahashi et al., 1997), suggesting that RhoGDI may also have a role in directing the GTPase to the effector. The second activity of GDIs is to modulate the cycling of Rho GTPases between cytosol and membranes. GDIs maintain Rho GTPases as soluble, cytosolic proteins by forming high-affinity complexes, in which the geranylgeranyl membrane targeting moiety present at the C-terminus of the Rho GTPases (see 2.2.4) is shielded from the solvent by its insertion into the hydrophobic pocket at the immunoglobulin-like β sandwich of the GDI ((Gosser et al., 1997), (Hoffman et al., 2000), (Scheffzek et al., 2000), (Grizot et al., 2001)).

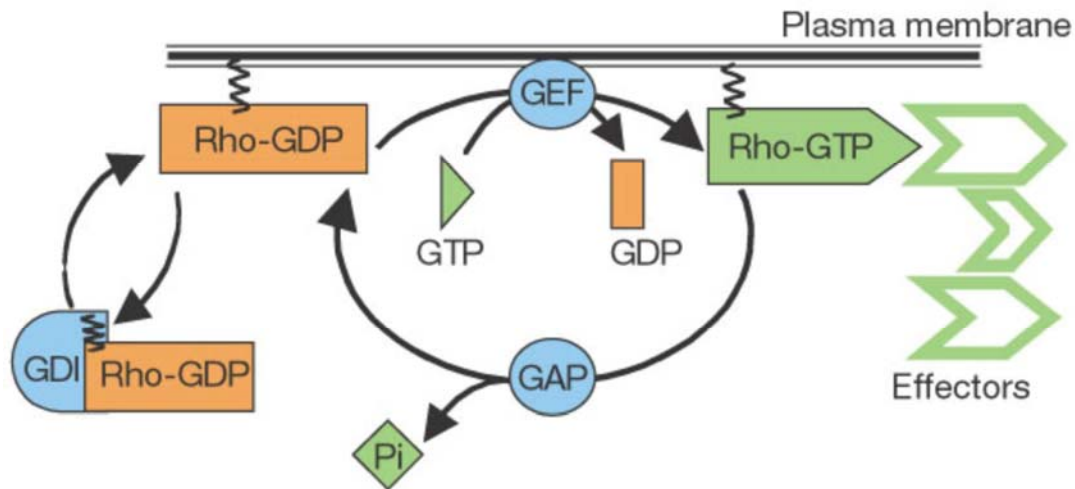


Figure 7: The Rho GTPase cycle (Etienne-Manneville and Hall, 2002). Rho GTPases cycle between an active, GTP-bound state and an inactive, GDP-bound state. The cycle is highly regulated by three classes of proteins: 1) guanine nucleotide exchange factors (GEFs), which catalyze the exchange of GDP to GTP, leading to GTPase activation 2) GTPase-activating proteins (GAPs), stimulating GTP hydrolysis and enzyme inactivation and 3) guanine nucleotide dissociation inhibitors (GDIs) that solubilize inactive GTPases from the membranes. All Rho GTPases are prenylated at their C-terminus and this posttranslational modification is required for function

2.2.6 Rho GTPases in the eye

Since Rho family GTPases play an important role in modulating cell differentiation and cytoskeletal changes, they are believed to play a crucial role during the morphogenesis of eye development. The expression pattern of the three major Rho GTPases, RhoA, Rac1 and Cdc42, in embryonic (11.5 post coitus (pc), 14.5 pc and 17.5 pc), postnatal (PN1) and adult (2 months) mouse eyes was recently investigated by Mitchell and co-workers (Mitchell et al., 2007). The authors showed that RhoA and Cdc42 expression were detectable in cornea, retina, lens epithelial and lens fiber cells at 11.5 pc, while Rac1 expression was only detectable in these compartments at 14.5 pc. The expression levels of all three GTPases were increased at embryonic 17.5 pc, suggesting an important function for the morphogenesis of the different compartments of the mouse eye. In the adult mouse eye, Rho GTPases seem to be involved in differentiation of corneal epithelial cells, ocular lens and retina, where they are expressed at different levels. In corneal endothelial cells, only RhoA expression was detected, which may be required for endothelial cell differentiation. In the lens, only Rac1 was expressed, which seems to play an important role supporting continuous lens growth and maintenance of lens transparency.

The role of Rho GTPases was also investigated in the eye of other species like *Drosophila*. Here, nuclear signaling by Rac1 and RhoA was shown to be required in the establishment of epithelial planar polarity in the *Drosophila* ommatidia (Fanto et al., 2000).

In *Xenopus* retinal ganglion cells (RGC), Rac1 was shown to be required for axon initiation and dendrite formation (Ruchhoeft et al., 1999). The importance of Rac1 in the eye was also demonstrated in a human RPE cell line, where Rac1 was reported to mediate H₂O₂-induced apoptosis through activation of downstream kinases such as p38 and JNK (Ho et al., 2006). Rac1 was also believed to play a role in corneal wound healing, because it was shown to be necessary for the promotion of human epithelial cell adhesion and motility (Kimura et al., 2006).

2.2.6.1 Rho GTPases in the retina

The role of Rho GTPases has been investigated in a wide variety of cells, but only few studies have addressed their role in retinal photoreceptors. For instance the Rho family GTPase Rac1 was shown to be involved in the regulation of rhodopsin transport carrier fusion in photoreceptors of *Rana barlandieri* conjointly with phosphoinositides, ezrin/moesin and Rab8 (Deretic et al., 2004) and therefore is believed to play an important role in the regulation of physiological processes in photoreceptors. Rac1 activity in photoreceptor rod outer segments (ROS) has been reported to be light-regulated by interaction with the GPCR rhodopsin. Up to now, the light-dependent interaction and activation of Rac1 with rhodopsin has been shown in squid (Petrov et al., 1994) and bovine ((Wieland et al., 1990), (Balasubramanian and Slepak, 2003)) photoreceptors, but no function could be assigned so far. The importance of Rac1 for the development and maintenance of photoreceptor morphology has been demonstrated by the rescue of the rhabdomere morphogenesis by expression of dominant active Drac1 in rhodopsin-null *Drosophila* mutants (Chang and Ready, 2000). In another study it was shown that Rac1 was involved in apoptosis during light-induced photoreceptor degeneration in mice (Belmonte et al., 2006).

2.3 Collapsin response mediator proteins (CRMP)

The collapsin response mediator protein (CRMP) family of phosphoproteins was first characterized on the basis of their requirement for Sema3A signaling. CRMPs, also known as TOAD (*turned on after division*), Ulip (*unc-33 like protein*) or DRP (*dihydropyrimidinase related protein*) and are highly expressed in the nervous system. CRMPs are homologues of *Caenorhabditis elegans unc-33*, whose mutations cause abnormal axon growth and guidance as well as uncoordinated movements (Li et al., 1992), demonstrating a role for these molecules in normal neuronal development and function. Currently there are five known members in the vertebrate CRMP family (CRMP1-4, and CRAM/CRMP5) (Fukada et al., 2000), of which CRMP2 is the most widely studied. Although CRMPs were initially reported to be expressed exclusively in the developing nervous system, subsequent analyses have revealed that they are also expressed in non-neuronal tissues, albeit at much lower levels (Shih et al., 2001).

2.3.1 CRMP2 switches RhoA and Rac1 morphology

Axon guidance is essential for the complexity of brain circuitry. Growth cones are thought to be a sensor for guidance molecules during development. They are localized at the tips of axons and dynamically change their morphology in response to attractive and repulsive guidance cues, thus determining the direction of growth (Dent and Gertler, 2003). The formation and directional guidance of neurites involves a dynamic and coordinated regulation of Rho family GTPases. Activation of Rac1 and Cdc42 promotes neurite outgrowth, whereas Rho activation causes neurite retraction. However, recent data have indicated that not activation itself, but the balance of Rho GTPase activities is the most important factor in the regulation of neurite outgrowth (Koh, 2006). By inhibition of Rac1, as well as by expression of dominant active Rac1, neurite outgrowth was reduced, showing that just the right amount of GTPase activity is required for neurite outgrowth (Koh, 2006). This coordinated activation of Rac1 and RhoA that is required for neurite outgrowth may be provided by CRMP2.

CRMP2 is implicated in axonal outgrowth and is a component of the semaphorin 3A (Sema 3A) pathway (Goshima et al., 1995). Sema3A leads to growth cone collapse by activation of the Neurophilin-1/Plexin-A1 receptor complex that stimulates phosphorylation of cofilin, a protein that regulates actin filament assembly (see Figure 9B) (Liu and Strittmatter, 2001). Rho kinase (Rock II), a serin-threonine kinase and probably the most important effector of RhoA in growth cones, binds to and is activated by the GTP-bound active form of RhoA ((Matsui et al., 1996), (Ishizaki et al., 1996), (Amano et al., 1997), (Arimura et al., 2000)). In

the brain, CRMP2 was found to be a prominent substrate of Rock II. It is phosphorylated by Rock II at Thr-555 in response to lysophosphatidic acid (LPA) signaling or by activation of Ephrin-5A ((Shamah et al., 2001), (Knoll and Drescher, 2004) (Sahin et al., 2005)), but not after Semaphorin 3A signaling (Arimura et al., 2000). In the case of Semaphorin 3A-induced growth cone collapse, phosphorylation of CRMP2 by Cdk5 (Ser-522) and GSK-3 β (Thr-514 and Ser-518) was reported ((Brown et al., 2004), (Cole et al., 2004), (Uchida et al., 2005), (Yoshimura et al., 2005)).

Arimura and colleagues (Arimura et al., 2000) therefore proposed that there may be Rock II-dependent and -independent pathways leading to growth cone collapse (Figure 8A). The role of CRMP2 in Semaphorin 3A-induced axonal outgrowth was investigated by Hall and colleagues in neuroblastoma cells (Hall et al., 2001). They showed that CRMP2 switches GTPase signaling when expressed in combination with either dominant active Rac1 or RhoA, respectively. Co-expression of CRMP2 with dominant active RhoA V14 induced Rac1 morphology (cell spreading and ruffling, formation of neurites) while co-expression with dominant active Rac1 V12 inhibited Rac1 morphology (cell rounding, neurite retraction). They also observed that Rock II is a pivotal regulator of CRMP2 in neuroblastoma cells. While CRMP2 phosphorylation was required for CRMP2/Rac1 V12 inhibition, it was not necessary for the induction of Rac1 morphology by CRMP2/RhoA V14. CRMP2, regulated by Rock II, thereby was shown to promote outgrowth and collapse in response to active RhoA and Rac1, respectively, reversing their usually observed morphological effects. As a reversible switch between RhoA and Rac1 signaling pathways, CRMP2 thereby provides a mechanism for dynamic modulation of growth cone guidance (Hall et al., 2001). Semaphorin 3A-induced growth cone collapse in sensory neurons is Rac1-dependent ((Jin and Strittmatter, 1997), (Vastrik et al., 1999)) and the results from Hall and colleagues suggest that CRMP2 can initiate growth cone collapse downstream of Rac1 activation (Hall et al., 2001).

While growth cone collapse and outgrowth is thought to be regulated via the actin cytoskeleton, CRMP2 was also identified as a regulator of another major cytoskeletal component, the microtubules (Fukata et al., 2002). CRMP2 is thought to function as a carrier of tubulin heterodimers to the plus end nucleating sites of growing microtubules. It was also shown to bind to tubulin dimers with higher affinity than to microtubules. Furthermore CRMP2 promotes microtubule assembly by copolymerizing together with tubulin dimers into microtubules.

Another element that is essential for axonal growth and maintenance is the transport of tubulin and microtubules in the growing axon. Although the molecular mechanism underlying

the linkage of tubulin and microtubules to motor proteins is not yet clear, it has been shown that a CRMP2/Kinesin-1 complex regulates soluble tubulin transport to the distal part of the growing axon (Kimura et al., 2005). Figure 8B shows the result of sucrose-density gradient centrifugation (sdgc) in order to isolate putative native protein complexes from porcine rod outer segments (ROS). This work by Magdalena Swiatek-de Lange in our lab, provided the first hint that the conserved signaling network RhoA/CRMP2/tubulin may also be existent in ROS. The occurrence of rhodopsin in the same sdgc fractions may indicate that rhodopsin is an integral part of this signaling network, suggesting a possible light-regulation of the RhoA/CRMP2/tubulin that was further investigated in this study.

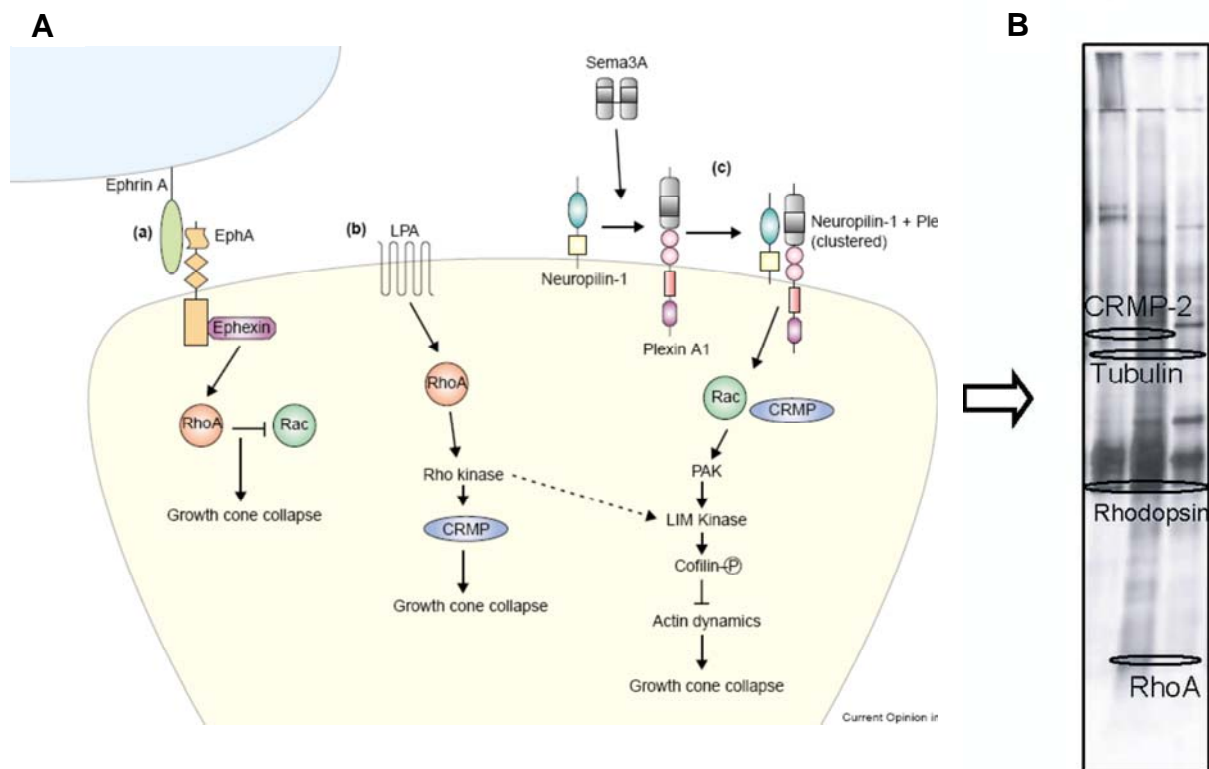


Figure 8: A) Schematic representation of signal transduction pathways involved in growth cone collapse (Liu and Strittmatter, 2001). a) Activation of the EphA receptor leads to RhoA activation through the GEF Ephexin, and concomitant downregulation of Rac1 activity. b) The serum factor lysophosphatidic acid (LPA) induces growth cone collapse and neurite retraction. LPA signals through a seven transmembrane receptor that triggers activation of RhoA, leading to activation of Rho kinase, phosphorylation of CRMP2 and growth cone collapse. c) Sema3A signaling initiates clustering of the receptors Plexin and Neurophilin. In a CRMP2-dependent process, this clustering leads to alterations of a Rac1-dependent pathway that modulates the actin filament assembly in the growth cone. **B)** SDS-PAGE of fractions from sucrose-density gradient centrifugation of porcine rod outer segments (ROS). Proteins were identified by mass spectrometry. All proteins co-segregating in one fraction may belong to a common protein complex. In ROS, CRMP2, tubulin and RhoA were found in a rhodopsin-associated complex (Swiatek-de Lange in Prep.). This links the light-perceiving molecule rhodopsin, a seven transmembrane receptor like the LPA-receptor, with known components responsible for neuronal structure, morphology and polarity

3. PHOSPHODIESTERASES AND PDE δ

3.1 Phosphodiesterases

Cyclic nucleotide second messengers (cAMP and cGMP) play a central role in signal transduction and regulation of physiologic responses (Essayan, 2001). Their intracellular levels are controlled by cyclic nucleotide phosphodiesterases (PDEs) that are ubiquitously distributed in mammalian tissues. They play a major role in cell signaling by hydrolyzing cAMP and cGMP (Lugnier, 2006). Twenty-one genes encoding PDEs have been identified in the human genome, and corresponding proteins have been characterized in terms of their physiochemical and regulatory properties ((Conti and Jin, 1999), (Soderling and Beavo, 2000), (Francis et al., 2001)). Based on their sequence relatedness, kinetics, modes of regulation, and pharmacological properties, they are divided into 11 families (PDE1-PDE11) (Beavo et al., 1994) (Table 2). Three of the 11 PDE families selectively hydrolyze cAMP (PDE 4, 7, and 8), three families are selective for cGMP (PDEs 5, 6, and 9), and five families hydrolyze both cyclic nucleotides with varying efficiency (PDEs 1, 2, 3, 10, and 11). Due to their diversity, which allows specific distribution at cellular and subcellular levels, PDEs are able to selectively regulate various cellular functions. Because of their important role in intracellular signaling, PDEs are designated as new therapeutic targets. New agents were developed to selectively inhibit PDE isozymes, notably Sildenafil (marketed as ViagraTM by Pfizer), which inhibits selectively PDE5 in human erectile dysfunction but also shows slight cross-reactivity on the structurally related PDE6, leading to neuroophthalmologic side effects with sometimes blue tinting of vision (Essayan, 2001). The social use of PDE inhibitors, such as caffeine dates back several millennia (Essayan, 2001).

Family	Substrate	Property	Primary tissue distribution	Examples of inhibitors
PDE1	cAMP, cGMP	Ca ²⁺ /calmodulin-activated	Heart, brain, lung, smooth muscle	KS-505a Vinpocetine
PDE2	cAMP, cGMP	cGMP-stimulated	Adrenal gland, heart, lung, liver, platelets	EHNA (MEP-1)
PDE3	cAMP, cGMP	cGMP-inhibited	Heart, lung, liver, platelets, adipose tissue, immunocytes	Cilostamide Enoxamone Milrinone Siguazodan
PDE4	cAMP	cGMP-insensitive	Sertoli cells, kidney, brain, liver, lung, immunocytes	CDP840 Rolipram SB 207499 Tibenelast
PDE5	cGMP	Protein kinase A and G-phosphorylated	Lung, platelets, smooth muscle	Dipyridamole MY-5445 Sildenafil Zaprinast
PDE6	cGMP	Transducin-activated	Photoreceptor	Dipyridamole Zaprinast
PDE7	cAMP	Rolipram-insensitive	Skeletal muscle, heart, kidney, brain, pancreas, T lymphocytes	Several in development
PDE8	cAMP	Rolipram-insensitive 3-isoutyl-1-methylxanthine-insensitive	Testes, eye, liver, skeletal muscle, heart, kidney, ovary, brain, T lymphocytes	None selective
PDE9	cGMP	3-isoutyl-1-methylxanthine-insensitive	Kidney, liver, lung, brain	None selective
PDE10	cAMP, cGMP	Unknown	Testes, brain	None selective
PDE11	cAMP, cGMP	Unknown	Skeletal muscle, prostate, kidney, liver, pituitary and salivary glands, testes	None selective

Table 2: Human cyclic nucleotide phosphodiesterase isozymes. After ((Essayan, 2001), (Lugnier 2006)).

3.1.1 PDE6

PDE6 is a key-component in phototransduction (see chapter 1.2.1) and it is exclusively expressed in photoreceptors, where it exists in a rod and a cone specific form. Rod specific PDE6 consists of two catalytic subunits, α and β , and two inhibitory γ -subunits (Hamilton et al., 1993). The catalytic subunits of PDE6, α and β , undergo posttranslational C-terminal prenylation and are attached to the ROS disc membranes via C-terminal farnesyl- and geranylgeranyl side chains, respectively ((Qin et al., 1992), (Anant et al., 1992)). The inhibitory γ -subunits are associated with the catalytic subunits and their binding is regulated allosterically by cGMP binding to a protein domain of the catalytic subunits, the so called GAF domain (Norton et al., 2000). A putative fourth 17 kDa subunit was copurified with bovine retinal phosphodiesterase (Hurwitz et al., 1985) and was later referred to as delta subunit, PDE δ . Proteolytic removal of the C-terminal region of PDE6 catalytic subunits resulted in loss of interaction between PDE δ and the catalytic subunits, suggesting an involvement of the prenyl side chains in the interaction (Florio et al., 1996). Cone-specific PDE6 consists of two catalytic α' -subunits and two inhibitory γ -subunits that are not identical to the rod inhibitory subunits (Lorenz et al., 1998). The structure of the membrane bound rod PDE6 holoenzyme is $\alpha\beta\gamma_2$, whereas it is $\alpha'\gamma_2$ for cone PDE6 (Artemyev et al., 1996).

A number of hereditary eye diseases are caused by mutation in PDE6 genes. A form of dysplasia (RDC, rod-cone dysplasia) in Irish Setter Terrier is caused by a point-mutation in codon 807 of PDE6 β , leading to C-terminal truncation of PDE β and to a total loss of catalytic activity in rods (Suber et al., 1993). The homozygous nonsense-mutation in *pdea* and *pdeb* leads in humans to a form of autosomal-recessive retinitis pigmentosa and a missense-mutation in *pdeb* causes an autosomal-dominant form of inhereditary congenital stationary night blindness (Lorenz et al., 1998).

3.2 PDE δ

The 17 kDa protein PDE δ was formerly considered to be a regulatory subunit of the retinal rod PDE6 (Polans et al., 1996). But in the course of the studies on PDE δ , numerous proteins were identified as PDE δ -interacting proteins. This, together with the broad expression pattern of PDE δ that, in contrast to the photoreceptor specific catalytic subunits of PDE6, is expressed in all mammalian tissues analyzed to date (Marzesco et al., 1998), (Florio et al., 1996), suggested that PDE δ may be a protein with various cellular functions. One of the most interesting properties of PDE δ is its ability to extract prenylated proteins from cellular

membranes. Purified PDE δ protein was shown to solubilize the two prenylated α and β catalytic subunits of PDE6 from purified ROS membranes (Florio et al., 1996). It was also able to solubilize Rab 13 GTPase (Marzesco et al., 1998), as well as the Ras family GTPases Rap1, Rap2, Ras from HeLa cell membranes *in vitro* (Nancy et al., 2002). As most of the identified PDE δ -interacting proteins are prenylated, including the small GTPases Rab13 (Marzesco et al., 1998), Ras and Rap proteins ((Nancy et al., 1999), (Ershova et al., 1997)), Rab8 (Norton et al., 2005), Rheb and Rho6 (Hanzal-Bayer et al., 2002), GRK1 and GRK7 (Zhang et al., 2004a) and a prenylated prostacyclin receptor (Wilson and Smyth, 2006), PDE δ was termed prenyl-binding protein (PrBP/ δ) (Zhang et al., 2006). The property of PDE δ to extract prenylated proteins from membranes is of particular interest, because it is reminiscent of the well characterized action of RhoGDI on Rho family GTPases.

However, PDE δ also interacts with several proteins in a prenylation-independent manner, like with the small GTPases Arl2 and Arl3 (Linari et al., 1999a) and with the non-prenylated protein retinitis pigmentosa GTPase regulator (RPGR) (Linari et al., 1999b).

3.2.1 PDE δ in the retina

To date several results have been published regarding localization of the ubiquitously expressed protein PDE δ in the retina leading to controversy. The first immunohistochemical data on PDE δ in bovine retina indicated that PDE δ is localized to the outer segments of rods, but not cones (Florio et al., 1996). Later PDE δ was shown to be distributed in mice throughout the whole retina, with a most prominent labeling of the inner segments of rod and cone photoreceptors ((Zhang et al., 2004a), (Zhang et al., 2007)). Norton and colleagues (Norton et al., 2005) demonstrated that PDE δ is localized in bovine retina primarily to the connecting cilium, a structure bridging the inner and the outer segment of photoreceptors.

3.2.2 Structure of PDE δ

While the overall sequence homology between PDE δ and RhoGDI is rather low, both proteins exhibit striking structural similarities. Sequence alignments of human PDE δ with human RhoGDI revealed 20% identity over 78 amino acids (Nancy et al., 2002). The crystal structure of RhoGDI in complex with Cdc42, a member of the Rho-family, has been solved ((Gosser et al., 1997), (Hoffman et al., 2000)), and was compared by structure based sequence alignment with PDE δ . In complex with RhoGDI, the geranylgeranyl tail of Cdc42 is bound in a hydrophobic cleft between two beta sheets in the immunoglobulin-like domain of RhoGDI.

This prenyl binding domain of RhoGDI is similar in size to, PDE δ , and there is 18% amino acid identity between the PDE δ and the prenyl binding domain of RhoGDI (Cook et al., 2000)). The structure-based sequence alignment shows that the residues lining the inner surface of this hydrophobic pocket are in identical or very similar positions in both proteins, suggesting that not only the fold but also the lipid binding pockets are common features of both PDE δ and RhoGDI. After superimposition of the protein backbones of RhoGDI and PDE δ , the geranylgeranyl moiety of Cdc42 fits surprisingly well over almost its complete length into the hydrophobic pocket of PDE δ (Linari et al., 1999a) (Figure 9). The crystal structure of the Rac1-RhoGDI complex was solved by Grizot and colleagues (Grizot et al., 2001). They showed that the overall structure of the Rac1-RhoGDI complex is globally similar to the structure of Cdc42-RhoGDI ((Gosser et al., 1997), (Hoffman et al., 2000)), which suggests that a complex between Rac1 and PDE δ as suggested for Cdc42 and PDE δ (Linari et al., 1999a) may be possible.

Hanzal-Bayer et al. ((Hanzal-Bayer et al., 2002)) presented the crystal structure of full-length Arl2-GTP in complex with its effector PDE δ solved in two crystal forms. Up to date, very little is known about the function of Arf-like (Arl) proteins, which are close relatives of the Arf-subfamily of GTPases. Arf proteins are regulators of vesicular transport in intracellular trafficking. The crystal structure of PDE δ (PDE δ was cocrystallized with Arl2/GTP) verified the presence of a hydrophobic domain packed by two opposite β -sheets. The overall β -sandwich fold is identical to that of RhoGDI ((Hanzal-Bayer et al., 2002)). The binding of Arl2 to PDE δ was found to be independent of lipids, suggesting that PDE δ can interact with proteins in two distinct ways: 1) through a lipid binding pocket and 2) β -sheet/ β -sheet interactions ((Hanzal-Bayer et al., 2002)). In terms of prenylated ligand specificity, PDE δ is more promiscuous than GDI. Although only GTPases of the Rho family have been shown to interact with RhoGDI, PDE δ interacts with various prenylated proteins including protein kinases, PDE subunits, and GTPases.

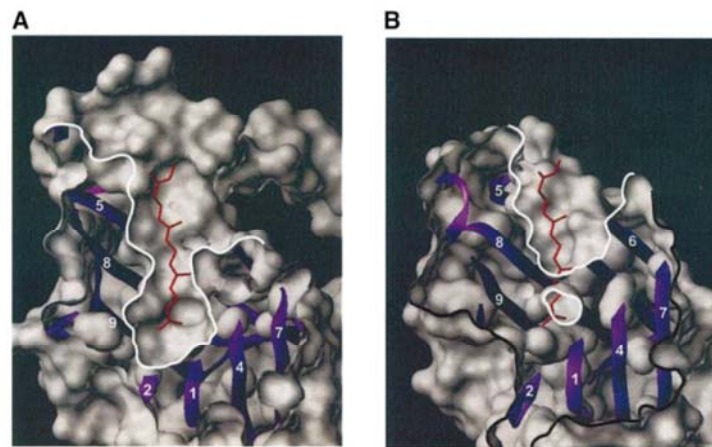


Figure 9 The hydrophobic pocket in PDE δ (Hanzal-Bayer et al., 2002). **A)** Cut through a surface representation of RhoGDI showing the deep hydrophobic pocket with the geranylgeranyl moiety (red) from Cdc42-GDP (violet ribbon). **B)** PDE δ has a similar but less deep hydrophobic pocket. The geranylgeranyl moiety of Cdc42 has been positioned by superimposition of the protein backbone of RhoGDI to PDE δ , followed by a small manual adjustment within the pocket.

3.2.3 PDE δ homologues

The PDE δ gene is located on human chromosome 2q35-36, and expresses a single mRNA species ((Florio et al., 1996), (Marzesco et al., 1998)). The sequence of PDE δ is highly conserved among mammals, since the bovine, canine, and murine proteins only differ from the human protein by one non-conservative (T68A) and zero to three conservative changes. In *Drosophila melanogaster* and the eyeless nematode *C. elegans*, orthologues exist sharing 61% and 69% identity with human PDE δ , respectively (Nancy et al., 2002). Subsequent research for proteins closely related to PDE δ revealed significant similarities with the UNC-119/RG4 group of proteins from mammals, zebrafish, *C. elegans*, and *D. melanogaster* (Figure 10A, lower panel). These proteins were identified on the basis of their high expression in the *C. elegans* nervous system as well as in mammalian photoreceptor cells (Ershova et al., 1997), but to date, still very little is known about their function. Besides an unrelated N-terminal region of 50-90 residues (depending on the species), the alignment of human PDE δ with human RG4 and RhoGDI proteins demonstrated that they exhibit 47% similarity and 22% identity for the human proteins, extending through to their C-termini. Alignment of UNC119/RG4, PDE δ and RhoGDI of human origin also revealed that the structural features, conserved between PDE δ and RhoGDI, are also conserved in UNC119/RG4 (Figure 10B). These structural features contain the elements responsible for their Ig-like fold as well as hydrophobic residues at conserved positions, which could line the surface of a prenyl-binding

pocket. Nancy et al. (Nancy et al., 2002) therefore proposed that UNC119/RG4, PDE δ and RhoGDI define a new family of proteins, conserved through evolution that interact with prenylated proteins and regulate their association with membranes. Such a high evolutionary conservation suggests that the function of PDE δ has been conserved as well. The C-terminus of PDE δ contains putative SRV and FYV sequence motifs described as necessary and sufficient for the interaction with PDZ domains present in many proteins of synaptic, septate and tight junctions (PSD95, Dlg, ZO-1) (Marzesco et al., 1998). PDZ domains are involved in submembranous protein networks and in the recruitment of proteins to specific plasma membrane microdomains ((Kornau et al., 1995), (Fanning and Anderson, 1996)).

A

CNRD_HUMAN	11	ILRGFKLNWNLRDAETGKILWQGTED(13)KKILCKAVSRELFSSAEQ-MEKFRLEOKVYFK	83
P17/HUMAN	11	ILRGFKLNWNLRDAETGKILWQGTED(13)KKILCKAVSRELFSSAEQ-MEKFRLEOKVYFK	83
CNRD_MOUSE	11	ILRGFKLNWNLRDAETGKILWQGTED(13)KKILCKAVSRELFSSAEQ-MEKFRLEOKVYFK	83
CNRD_BOVIN	11	ILRGFKLNWNLRDAETGKILWQGTED(13)KKILCKAVSRELFSSAEQ-MEKFRLEOKVYFK	83
CNRD_CANFA	11	ILRGFKLNWNLRDAETGKILWQGTED(13)KKILCKAVSRELFSSAEQ-MEKFRLEOKVYFK	83
YK91_CAEEL	20	ILAGFKLNWNLRDAETGKVLWQSTED(13)KNLLCKRTVSRELFSSSVK-IEKFRLEOKVYFK	92
CG9296/DROME	12	IQKGFQNYILLRDAETGKIIVWENKD(13)VKILDMRAVSRELFSTIES-MENFRLEOKVLFK	84
U119_HUMAN	82	NLYKIDVRFKIRDMDSGIVLFEIKKP(26)PAFLALRQVGATVFTVGDKPVNFRMIERHYFR	168
U119_MOUSE	82	NLYKIDVRFKIRDMDSGIVLFEIKKP(26)PAFLALRQVGATVFTVGDKPVNFRMIERHYFR	168
U119_RAT	82	NLYKIDVRFKIRDMDSGIVLFEIKKP(26)PAFLALRQVGATVFTVGDKPVNFRMIERHYFR	168
U119b/BRARE	83	NEYNIDETREKIRDMDSGIVLFEIKKP(24)PAFLALRQVGATVFTVGDIFINFRMIERHYFR	134
U119c/BRARE	50	NEYNIDETREKIRDMDSGIVLFEIAKP(28)PAFLALRQVGATVFTVGDQPVNFRMIERHYEQ	171
U119_CAEBR	65	NEYNIEETKQIRDMDTEQVLFIAKP(22)PNFLALRQVGATVFKVGDIPHHFRMIERHFFF	147
U119_CAEEL	66	NEYNIEETKQIRDMDTEHVLFIAKP(23)PNFLALRQVGATVFKVGDVPIHHFRMIERHFFK	149
U119_DROME	90	NWFEIDETREKIRDMDSGAVLFEIAKP(41)PAFLALRQVGATVFTVGSQPVNFRMIERHFFR	191
CNRD_HUMAN	84	GQCLEBWFDFGFVIPNSINTWOSLIAAPESMPASVLTGNVILIETK--FFDDLLVSTSRVRLFYV	150 (150)
P17/HUMAN	84	GQCLEBWFDFGFVIPNSINTWOSLIAAPESMPASVLTGNVILIETK--FFDDLLVSTSRVRLFYV	150 (150)
CNRD_MOUSE	84	GQCLEBWFDFGFVIPNSINTWOSLIAAPESMPASVLTGNVILIETK--FFDDLLVSTSRVRLFYV	150 (150)
CNRD_BOVIN	84	GQCLEBWFDFGFVIPNSINTWOSLIAAPESMPASVLTGNVILIETK--FFDDLLVSTSRVRLFYV	150 (150)
CNRD_CANFA	84	GQCLEBWFDFGFVIPNSINTWOSLIAAPESMPASVLTGNVILIETK--FFDDLLVSTSRVRLFYV	150 (150)
YK91_CAEEL	93	GTHIEDWYDFGFVIPNSINTWONMIAAPESMPFPPSVLSGNVIVVETL--FYDGDLLVSTSRVRLYYD	159 (159)
CG9296/DROME	85	GRIMEBWFDFMGFVIGANTINTWOSTIAAPESMPAKVFNNGNVIIQTS--FYDNTLLITKSVVRLYYI	151 (151)
U119_HUMAN	169	NQLLKSDFDFHGFQIPSSKNTCEHIYDFPPLSEELISEMIRHPYETSDSFYFVDDRLVMHMKADYSYS	237 (240)
U119_MOUSE	169	NQLLKSDFDFHGFQIPSSKNTCEHIYDFPPLSEELISEMIRHPYETSDSFYFVDDRLVMHMKADYSYS	237 (240)
U119_RAT	169	NQLLKSDFDFHGFQIPSSKNTCEHIYDFPPLSEELISEMIRHPYETSDSFYFVDDRLVMHMKADYSYS	237 (240)
U119b/BRARE	135	EQLLKSDFDFHGFQIPSSKNTCEHIYDFPPLSEELIREMILHPYETSDSFYFVDDRLVMHMKADYSYS	203 (206)
U119c/BRARE	172	DRLLKSDFDFHGFQIPSSKNTCEHIYDFPQLSEELIRLIMIEHPYETRSDFSFYFVDDRLVMHMKADYAYN	240 (243)
U119_CAEBR	148	DRLLKSDFDFHGFQIPSSRNNTCEHIYDFPQLSEELIMDDMINNPNETRSDFSFYFVDDRLVMHMKADYSYD	216 (217)
U119_CAEEL	150	DRLLKSDFDFHGFQIPSSRNNTCEHIYDFPQLSEELIMDDMINNPNETRSDFSFYFVDDRLVMHMKADYSYD	218 (219)
U119_DROME	192	DRLLKTEDFDFHGFQIPSSKNTCEHIYDFPNLPPDLVAEMISSPEETRSDFSFYFVDDRLVMHMKADYAYD	260 (265)

B

Human RG4	82	NLYKIDVRFKIRDMDSGIVLFEIKKPVSERLPIN(16)TPAFLALRQ
Human PDEδ	11	ILRGFKLNWNLRDAETGKILWQGTEDLSVPCVEHEARVERKILCKA
Human RhoGDI	84	NVVVTLITLVCSST----APGPLELDTLGDLESEK-----KQSEVLFK
Human RG4		---VGATVFTVGDKPVNFRMIERHYFNQLLKSDFDFHGFQIPSSKN
Human PDEδ		---VSRELFSSAEQ-MEKFRLEOKVYFKGQCLEBWFDFGFVIPNSIN
Human RhoGDI		GVEYRIKISERVNREIVSGMYYIQHTYRKGVKLDKTDYVGSYGERAE
Human RG4		TCCEHIYDFPPLSEELISEMIRHPYETSDSFYFVDDRLVMHMKADYSYS 237
Human PDEδ		ITWOSLIEAAPESMPASVLTGNVILIETK--FFDDLLVSTSRVRLFYV 150
Human RhoGDI		-----YEFLTPMEFAKQMLARGSYVTKS--FFDDDDRLDHLSEWENLTI 213

Figure 10 Alignments of PDEδ, RhoGDI and UNC119/RG4 proteins (Nancy et al., 2002): **A**) the alignment among PDEδ (upper part) and UNC119/RG4 proteins (lower part) from various species. Identities are shown as white on a black background; similarities are shaded gray (white and black letters for hydrophobic and non hydrophobic aminoacids, respectively). Sequences that could not be aligned are indicated by number of residues; The total length of each sequence is indicated within brackets. BRARE, *Danio rerio* (zebrafish); CAEEL, *Caenorhabditis elegans*; CAEBR, *Caenorhabditis briggsae*; CANFA, *Canis familiaris*; DROME, *Drosophila melanogaster*. **B**) Alignment of human RG4, PDEδ and RhoGDI proteins. Annotations are the same as in A.

E. AIM OF THE STUDY

A large group of genetically inherited blinding diseases is associated with mutations in genes expressed in photoreceptors. In the light-perceiving molecule rhodopsin, more than a hundred different mutations may cause the retinal degenerative disease retinitis pigmentosa (<http://www.sph.uth.tmc.edu/RetNet/>). Because most, if not all proteins require binding to other proteins to function in a regulated manner, mutations in a single protein, like in rhodopsin, not only result in an impairment of its function, but also in a disruption of functional protein networks downstream of the mutated protein. This leads to alterations in the compositions of multiprotein complexes as well as in protein localization with most severe physiological consequences. The identification of the composition and the dynamic of multiprotein complexes therefore is a premise to understand physiological processes and disease mechanisms.

In the beginning of this study, this work was based on preceding sucrose-density gradient experiments by Dr. Magdalena Swiatek-deLange, which suggested the presence of a rhodopsin/RhoA/Rac1/Rock II/CRMP2 signaling multiprotein complex in porcine ROS, but had not been validated or further characterized thus far. Rac1, which is supposed to be part of this putative rhodopsin multiprotein complex, was shown to be an important molecule for photoreceptor development and function. For example in *Drosophila*, where overexpression of constitutively active Rac1 was able to rescue retinal degeneration in rhodopsin-null mutants (Chang and Ready, 2000).

The aim of this study was the validation and further characterization of this new putative rhodopsin multiprotein complex and its interaction partners, for a detailed insight into the role of the small Rho family GTPases Rac1 and RhoA as well as CRMP2 in mammalian photoreceptors. Furthermore, the effect of light- versus dark-adaptation on the composition and dynamic of retinal multiprotein complexes was investigated in this study.

Objective 1: Establishment and optimization of methods for the isolation and investigation of native protein complexes from ROS.

For a validation and further characterization of the putative rhodopsin/RhoA/Rac1/Rock II/CRMP2 multiprotein complex and its interaction partners in ROS, the solubilization and isolation of native protein complexes from ROS by immunoprecipitation and BN-PAGE were important tools. Both methods were established and optimized in this study for the analysis of the composition and dynamic of native multiprotein complexes in ROS.

Objective 2: Identification of the Rac1 interactome in ROS.

Although Rac1, a member of the rhodopsin/RhoA/Rac1/Rock II/CRMP2 multiprotein complex in ROS, is one of the best investigated GTPases in various tissues and organisms, only sparse information is available concerning Rac1 function and regulation in ROS. To further investigate Rac1 function in ROS, the Rac1 interactome was identified by co-immunoprecipitation of Rac1 interaction partners from ROS and subsequent analysis by mass spectrometry.

Objective 3: Is the activity of Rac1 and its interactions with signaling molecules in porcine ROS regulated by light?

The reported light-activation of Rac1 in squid (Petrov et al., 1994) and bovine ((Wieland et al., 1990), (Balasubramanian and Slepak, 2003)) photoreceptors suggested that interactions of Rac1 with signaling molecules may also be regulated by light. Therefore, the effect of light on the signaling network of Rac1 and also RhoA in ROS was investigated. Rac1 and RhoA interactors were co-immunoprecipitated from light- and dark-adapted ROS and subsequently analyzed by Western blot for a light-dependence of their interaction. Furthermore, active, GTP-bound Rac1 was selectively captured using the GST fusion of the Rac1 binding domain of PAK1-kinase. Activation and distribution of active Rac1 in ROS were investigated as well as interactions, specific for the active form of Rac1.

Objective 4: Production and characterization of monoclonal CRMP2-specific antibodies. CRMP2 was detected as component of the putative rhodopsin/RhoA/Rac1/Rock II/CRMP2. Since no CRMP2 antibodies, which would enable a further investigation of this protein in ROS, were commercially available at the beginning of this study, the aim was the production of monoclonal CRMP2 antibodies as well as their characterization.

Objective 5: Establishment of an organotypical retinal explant system.

To study the physiological function of the putative rhodopsin/RhoA/Rac1/Rock II/CRMP2 complex in the retina, the establishment of a model system was necessary. Therefore an organotypical retinal explant system was established, which highly resembles the *in vivo* situation and enables the application of pharmacological agents for blocking of GTPase and Rock II signaling without unnecessary animal testing.

Objective 6: Does PDE δ act as GDI for Rac1 in porcine ROS?

The importance of Rac1 for development and maintenance of photoreceptor morphology has been demonstrated in several studies. Nevertheless, only limited knowledge is available on the molecular mechanism of its regulation. RhoGDI, one of the key regulators of Rac1 GTPase function, though present in the inner segments of photoreceptors was not detected in ROS, leading to the assumption that an other molecule must assume GDI function for Rac1 in ROS.

The 17 kDa protein PDE δ , which has been considered as a regulatory subunit of retinal rod cGMP phosphodiesterase 6 (PDE6), shares strong structural homology with RhoGDI. PDE δ has been shown to interact with a number of prenylated and unprenylated proteins, but one of its most interesting properties is its ability to extract prenylated proteins from cellular membranes, reminiscent of the well characterized action of RhoGDI on Rho family GTPases. This properties and the fact that PDE δ is expressed at highest levels in the retina compared to all tissues analyzed to date, prompted to test PDE δ as a candidate GDI for Rac1 in ROS in this study

F. MATERIAL AND METHODS

1. MATERIAL

1.1 Chemicals

All chemicals were purchased from Sigma-Aldrich (Sigma, Fluka, Aldrich; Taufkirchen, Germany) and VWR International (Darmstadt, Germany) if not otherwise stated.

1.2 General equipment

Autoclave Bioclav	Schütt Labortechnik, Göttingen, Germany
Autoclave Systec 5075 ELV	Systec, Wettenberg, Germany
Analysis scales BP221S	Sartorius, Göttingen, Germany
Precision scales Basic Plus BP2100	Sartorius, Göttingen, Germany
Optima TLX ultracentrifuge with TLA110 rotor	Beckman Coulter, Krefeld, Germany
Optima-Max ultracentrifuge with S50 rotor	Beckman Coulter, Krefeld, Germany
Ultracentrifuge L7-65 with SW41Ti rotor	Beckman Coulter, Krefeld, Germany
Sigma Laboratory Centrifuges 6K15 and 4K15C and rotors	Sigma Laborzentrifugen, Osterode, Germany
Table top centrifuge 5415D with standard rotor	Eppendorf, Hamburg, Germany
Shaker Duomax 1030	Heidolph Instruments, Schwabach, Germany
Shaker KS260 basic	IKA Labortechnik, Staufen, Germany
Magnetic stirrer RH basic	IKA Labortechnik, Staufen, Germany
Milli-Q Biocell	Millipore, Bedford, USA
SpeedVac SPD111V, freeze drying chamber for lyophilization and ValuPump VLP80	Savant, Fisher Scientific, Schwerte, Germany
Ultra-low temperature freezer (-80°C) VIP™ series	Sanyo Scientific, IL, USA
Ultrasonic bath Transsonic 310/H	Elma Ultrasonic, Singen, Germany
Ultraspec 3300 pro UV/Vis photometer	GE Healthcare, Freiburg, Germany
Vortex Genie 2	Scientific Industries, VWR
Water bath HRB 4 digital	IKA Labortechnik, Staufen, Germany
Zoom Stereomicroscop Nikon SMZ645	Nikon, Amstelveen, Netherlands
Surgical/Microsurgical instruments	FST, Heidelberg, Germany
Millicell Culture Plate Insert	Millipore, Bedford, USA
MILLEX GP; syringe driven filter unit, 0.22 µm	Millipore, Bedford, USA
Steritop-GP filter unit, 0.22 µm	Millipore, Bedford, USA
Cellculture plates 6-well/10cm/14cm	Nunc, Wiesbaden, Germany
Falcon conical tubes 15/50	BD Bioscience, Heidelberg, Germany
Safe lock reaction tubes 0.5/1.5/2.0	Eppendorf, Hamburg, Germany
Microspin columns	GE-Healthcare, Chalfont St. Giles, GB
Cryostat HM560	Microm AG, Walldorf, Germany

1.3 Protein chemistry

1.3.1 Special equipment

Power Supply Power Pac 3000	BioRad, Munich, Germany
Mini Protean III for SDS-PAGE	BioRad, Munich, Germany
Protean II for SDS-PAGE	BioRad, Munich, Germany
GelAir dryer	BioRad, Munich, Germany
GS-710 Calibrated Imaging Densitometer	BioRad, Munich, Germany
Fuji FLA-3000 scanner	Fuji, Düsseldorf, Germany
Trans-Blot SD semi-dry transfer blot	BioRad, Munich, Germany
Agfa Curix 60 Developer	Agfa, Cologne, Germany
Rehydration chamber for IPG strips	GSF workshop
Multiphor II for isoelectric focusing (IEF)	GE Healthcare, Chalfont St. Giles, GB
Equilibration chamber for IPG strips	GSF workshop
Ettan Dalt II Gel Caster System for 2-DE	GE Healthcare, Chalfont St. Giles, GB
Ettan Dalt II Electrophoresis Chamber for 2-DE	GE Healthcare, Chalfont St. Giles, GB
MALDI-TOF/TOF mass spectrometer ABI 4700 Proteomics Analyzer	Applied Biosystems, Foster City, USA
HPLC	Dionex, Sunnyvale, USA
Q-TOF	Waters, Milford, USA
FLAG peptide and FLAG elution buffer	Sigma-Aldrich

1.3.2 Kits

BioRad Protein Assay Kit	BioRad, Munich, Germany
Enhanced chemiluminescence kit, ECLplus	GE Healthcare, Chalfont St. Giles, GB

1.4 Molecular biology

1.4.1 Special equipment

SubCell GT chambers for agarose gel electrophoresis	BioRad, Munich, Germany
UV transilluminator UVT-40M	Herolab, Wiesloch, Germany
ABI Prism 3100 Genetic Analyzer for DNA sequencing	Applied Biosystems, Foster City, USA
PCR DNA Engine Tetrad Gradient Cycler PTC-225	MJ Research, BioRad
Incubator for <i>E. coli</i>	Memmert, Schwabach, Germany
GFL Incubator Shaker for <i>E. coli</i>	Burgwedel, Germany

1.4.2 Kits

Big Dye Terminator v3.1 Cycle Sequencing Kit	Applied Biosystems, Foster City, USA
PureYield Plasmid Midiprep System	Promega, Mannheim, Germany
QIAquick Gel Extraction Kit	Qiagen, Hilden, Germany
QIAquick PCR purification Kit	Qiagen, Hilden, Germany
QIAprep Spin Plasmid Miniprep Kit	Qiagen, Hilden, Germany
Gateway BP Clonase II enzyme mix	Invitrogen, Carlsbad, USA
Gateway LR Clonase II enzyme mix	Invitrogen, Carlsbad, USA
Phusion High-fidelity PCR Kit	New England Biolabs, Ipswich, USA

1.4.3 *E. coli* strains

DH5 α	Invitrogen, Carlsbad, USA
BL21	Invitrogen, Carlsbad, USA
TOP10	Invitrogen, Carlsbad, USA
T1 ^R	Invitrogen, Carlsbad, USA

1.4.4 Oligonucleotides

Primer for PCR and sequencing were ordered from a GSF-intern producer, whereas primer for Gateway-Cloning was purchased from Metabion (Martinsried, Germany).

Table 3: Primer for Gateway-Cloning

Primer name	Sequence
humanPDE δ -GWN-f	5'-AAAAAGCAGGCTTCTCAGCCAAGGACGAGCG-3'
humanPDE δ -GW-TAA-r	5'-AAGAAAGCTGGGTGTTAAACATAGAAAAGTCTCACTCTG-3'
humanCRMP2-GWN-f	5'-AAAAAGCAGGCTTCTCTTATCAGGGGAAGAAAATATTC-3'
humanCRMP2-GW-TAA-r	5'-AAGAAAGCTGGGTGCTAGCCCAGGCTGGTG-3'
humanRac1-GWN-f	5'-AAAAAGCAGGCTTCCAGGCCATCAAGTGTGTGG-3'
humanRac1-GW-TAA-r	5'-AAGAAAGCTGGGTGTTACAACAGCAGGCATTTTC-3'
attB1	5' GGGGACAAGTTTGTACAAAAAAGCAGGCT-3'
attB2	5'-GGGGACCACTTTGTACAAGAAAGCTGGGT-3'

Table 4: Sequencing and PCR primer

Primer name	Sequence
pcDNA3-fw	5'-GCGGTAGGCGTGACGGTGGG-3'
pcDNA3-rv	5'-GGGCAAACAACAGATGGCTGGC-3'

1.4.5 Plasmids and constructs

1.4.5.1 Plasmids

Table 5: Plasmids

Plasmid	Description	Resistance	Provider
pcDNA3.0	mammalian expression vector	Ampicillin (100 µg/mL)	UMR
pDONR201	Gateway-Donor Vector	Kanamycin (50 µg/mL)	Invitrogen
pDEST/N-SF-TAP	Gateway-Entry Vector	Ampicillin (100 µg/mL)	Invitrogen modified by Johannes Gloeckner (Gloeckner et al., 2007a)
N-SF-TAP	pcDNA3, N-terminal tandem Strep-Flag-tag	Ampicillin (100 µg/mL)	Johannes Gloeckner (Gloeckner et al., 2007a)

1.4.5.2 Constructs

Table 6: Constructs

Construct name	cDNA	Plasmid	Provider
PDE δ -pDONR201_1/2/3	PDE δ /HEK	pDONR201	this study
Rac1-pDONR201_1/3	Rac1/HEK	pDONR201	this study
CRMP2-pDONR201_1/3	CRMP2/HEK	pDONR201	this study
PDE δ -N-TAPe5_1/2/3	PDE δ /HEK	N-SF-TAP	this study
Rac1-N-TAPe5_1/3	Rac1/HEK	N-SF-TAP	this study
CRMP2-N-TAPe5_1/3	CRMP2/HEK	N-SF-TAP	this study
Rac1	Human	pcDNA3.1+	UMR

1.5 Mammalian cell and tissue culture

1.5.1 Special equipment

Leica inverse table top microscope DMIL	Leica Microsystems, Wetzlar, Germany
Leica inverse fluorescence microscope (DMIRE2, CTRMic) with camera DC250	Leica Microsystems
Zeiss ApoTome™ with AxioCam HRc	Zeiss, Jena, Germany
CO ₂ incubator	Sanyo, Munich, Germany
Laminar flow	BDK, Sonnenbühl-Genkingen, Germany
Liquid Nitrogen Tank Chronos, ADUR β	Messer, Sulzbach, Germany
Potter S	B. Biotech International, Melsungen, Germany

1.5.2 Kits

<i>In situ</i> cell death detection kit for TUNEL assay	Roche Applied Sciences, Mannheim, Germany
Effectene Transfection Reagent for lipofection	Qiagen

1.5.3 Mammalian cell lines

Table 7: Mammalian cell lines

Cell line	Description	Provider
HEK293	Human embryonic kidney, ACC 305	DSMZ, Braunschweig, Germany

1.5.4 Antibodies

Table 8: Antibodies against mammalian proteins

Antibodies	Species	Dilution	Provider
Anti-GAPDH	mouse, monoclonal	1:1000 WB	Chemicon, Hampshire, UK
Anti-Rhodopsin (4D2)	mouse, monoclonal	1:10000- 1:100000 WB 1:1000 IF	R. Molday, University of British Columbia, Canada
Anti-Rhodopsin (ABR)	rabbit, polyclonal	1:1000 WB 1:1000 IF	Dianova, Hamburg, Germany
Anti-Rhodopsin (1D4)	mouse, monoclonal	1:1000 WB	Sigma-Aldrich
Anti- β -Tubulin	mouse, monoclonal	1:1000 WB 1:500 IF	Sigma-Aldrich
Anti-Rac1	mouse, monoclonal	1:1000 WB 1:200-1:1000 IF	Upstate
Anti-Rac1	mouse, monoclonal	1:1000 WB 1:200-1:1000 IF	BD Transduction Laboratories
Anti-Rac1	goat, polyclonal	1:1000 WB 1:200 IF	Santa Cruz
Anti-Rac1	rabbit, polyclonal	1:1000 WB	Santa Cruz
Anti-RhoA	goat, polyclonal	1:1000 WB	Santa Cruz
Anti-RhoA	mouse, monoclonal	1:1000 WB	Cytoskeleton
Anti-RhoA	mouse, monoclonal	1:1000 WB	Santa Cruz
Anti-RhoABC	rabbit, polyclonal	1:1000 WB	Sigma-Aldrich
Anti-Rab3b	rabbit, polyclonal	1:1000 WB	Santa Cruz
Anti-Rab8a	rabbit, polyclonal	1:1000 WB	Santa Cruz
Anti-CRMP2	mouse, monoclonal	1:10000 WB 1:600 IF	Y. Ihara, University of Tokyo, Japan
Anti-CRMP2b	rabbit, polyclonal	1:1000 WB 1:600 IF	J. Kappler, University of Bonn, Germany
Anti-CRMP2-family	rabbit, polyclonal	1:1000 WB	J. Kappler, University of Bonn, Germany
Anti-Syntaxin	mouse, monoclonal	1:1000 IF	Sigma-Aldrich
Anti-GFAP	rabbit, polyclonal	1:800 IF	DAKO
Anti-PKC	mouse, monoclonal	1:50 IF	Santa Cruz
Anti-GS	mouse, monoclonal	1:500 IF	BD Transduction Laboratories
Anti-RPGR	goat, polyclonal	1:500 WB 1:100 IF	Santa Cruz
Anti-RPGR	rabbit, polyclonal	1:1000 WB 1:250 IF	Ronald Roepmann, University of Nijmegen, Netherlands
Anti-RockII	mouse, monoclonal	1:1000 WB 1:100-1:500 IF	BD Transduction Laboratories
Anti-PDE β	rabbit, polyclonal	1:1000 WB	ABR
Anti-PDE δ	rabbit, polyclonal	1:1000 WB 1:200 IF	Sigma-Aldrich

		IP	
Anti-PDE δ	rabbit, polyclonal	1:1000 WB 1:200 IF IP	ABR
Anti-PDE δ	chicken, polyclonal	1:1000 WB 1:200-1:1000 IF	GenWay
Anti-Rhodopsin Kinase 1a	mouse, monoclonal	1:1000WB	ABR
Anti-Arrestin	rabbit, polyclonal	1:1000 WB 1:50 IF	ABR
Anti-Transducin α	rabbit, polyclonal	1:1000 WB	ABR
Anti- β Actin	mouse, monoclonal	1:5000 WB 1:500 IF	Sigma-Aldrich
Anti- β Tubulin	mouse, monoclonal	1:1000 WB 1:250 IF	Sigma-Aldrich
Anti-Lebercilin	rabbit, polyclonal	1:1000 WB IP	Chris F. Inglehearn, University of Leeds, UK
Anti-FLAG-HRP	mouse, monoclonal	1:1000- 1:10000WB	Sigma-Aldrich
Anti-Nucleolin	rabbit, polyclonal	1:5000 WB	Sigma-Aldrich
Anti-Centrin3	rabbit, polyclonal	1:1000 IHC	Uwe Wolfrum/Mainz
Anti-Nucleophosmin	mouse, monoclonal	1:1000 WB	Sigma-Aldrich
Anti-Dynein/IgM	mouse, monoclonal	1:1000 WB	Sigma-Aldrich
Anti-HSP90	rabbit, polyclonal	1:1000 WB	Cell Signaling Techn.
Anti-14-3-3 γ	rabbit, polyclonal	1:500 WB	Santa Cruz
Anti-Dynaectin/p50	mouse, monoclonal	1:1000 WB	BD Transduction Laboratories
Anti-p150/glued	mouse, monoclonal	1:5000 WB	BD Transduction Laboratories
Anti-CKII α	rabbit, polyclonal	1:500 WB	Sigma-Aldrich
Anti-CKII β	rabbit, polyclonal	1:500 WB	Sigma-Aldrich

IF: Immunofluorescence, WB: Western blot, IP: Immunoprecipitation

Table 9: Secondary antibodies

Antibodies	Species	Dilution	Provider
Anti-Mouse IgG HRP-conjugated	goat, polyclonal	1:15000 WB	Jackson ImmunoResearch Laboratories, Dianova
Anti-Mouse IgG/IgM HRP-conjugated	goat, polyclonal	1:15000 WB	Jackson ImmunoResearch Laboratories, Dianova
Anti-Rabbit IgG HRP-conjugated	goat, polyclonal	1:15000 WB	Jackson ImmunoResearch Laboratories, Dianova
Anti-Rat IgG HRP-conjugated	goat, polyclonal	1:15000 WB	Jackson ImmunoResearch Laboratories, Dianova
Anti-Chicken IgY HRP-conjugated	donkey, polyclonal	1:15000 WB	Jackson ImmunoResearch Laboratories, Dianova
Anti-Goat IgG HRP-conjugated	donkey, polyclonal	1:15000 WB	Jackson ImmunoResearch Laboratories, Dianova
Anti-Mouse IgG Alexa Fluor 488-conjugated	goat, polyclonal	1:1000 IF	Molecular Probes, Invitrogen
Anti-Mouse IgG Alexa Fluor 568-conjugated	goat, polyclonal	1:1000 IF	Molecular Probes, Invitrogen
Anti-Rabbit IgG Alexa Fluor 488-conjugated	goat, polyclonal	1:1000 IF	Molecular Probes, Invitrogen
Anti-Rabbit IgG Alexa Fluor 568-conjugated	goat, polyclonal	1:1000 IF	Molecular Probes, Invitrogen
Anti-Goat IgG Alexa Fluor 488-conjugated	donkey, polyclonal	1:1000 IF	Molecular Probes, Invitrogen
Anti-Goat IgG Alexa Fluor 568-conjugated	donkey, polyclonal	1:1000 IF	Molecular Probes, Invitrogen
Anti-Chicken IgG Alexa Fluor 488-conjugated	goat, polyclonal	1:1000 IF	Molecular Probes, Invitrogen
Anti-Chicken IgG Alexa Fluor 568-conjugated	goat, polyclonal	1:1000 IF	Molecular Probes, Invitrogen

IF: Immunofluorescence, WB: Western blot

1.6 Software and databases

1.6.1 Software

Adobe Illustrator 10.0	Adobe Systems, Seattle WA, USA
Adobe Photoshop 7.0	Adobe
AxioVision LE 4.0-4.5 for fluorescence and electron microscopy	Zeiss
GPS Explorer 3.6 for analysis of MALDI-TOF/TOF MS	Applied Biosystems
Mascot 1.7 search engine	Matrix Science, London, UK
MS Office 2002 (Word, Excel, Powerpoint)	Microsoft, Redmond, WA, USA
Vector NTI Suite 9.0/10.0 for molecular biology	Invitrogen
Scaffold 2_00_06	Proteome software Inc.,m Portland

1.6.2 Databases

NCBI	http://www.ncbi.nlm.nih.gov/
PubMed	http://www.ncbi.nlm.nih.gov/entrez/query.fcgi
NCBI Protein	http://www.ncbi.nlm.nih.gov/entrez/query.fcgi?db=protein
NCBI Nucleotide	http://www.ncbi.nlm.nih.gov/entrez/query.fcgi?db=nucleotide
BLAST	http://blast.ncbi.nlm.nih.gov/Blast.cgi
Swiss-Prot	http://us.expasy.org/sprot/
RZPD	http://www.rzpd.de/
HPRD	http://www.hprd.org
Ensembl	http://www.ensembl.org
MINT	http://mint.bio.uniroma2.it/mint/Welcome.do
Webvision	http://webvision.med.utah.edu/

2. METHODS

2.1 Protein chemistry

2.1.1 Determination of protein concentration

Total protein concentration in a given solution was measured using the Bradford colorimetric assay (Bradford, 1976). This assay is based on the binding of Coomassie Brilliant Blue G-250 to proteins in acidic solution and subsequent absorbance shift of the dye from 465 nm to 595 nm. Unbound protonated forms of Coomassie are green and red while the dye in its bound anionic form is brilliant blue. The dye has been assumed to bind in its anionic form to proteins via electrostatic attractions of the dye's sulfonic acid groups. The increase in the absorbance at 595 nm is proportional to the amount of bound dye and therefore also to the amount of protein in the sample. Beer's law can be applied for accurate quantitation of protein by selecting an appropriate ratio of dye volume to sample concentration. The dye binds unspecifically to cationic and non-polar, hydrophobic side chains of proteins (mainly arginine and aromatic amino acids). The Bradford method shows a high sensitivity and is linear over a range from 1 µg-120 µg protein/mL. For the Bradford assay the BioRad Protein Assay Kit (BioRad) was used following manufacturer's instructions. The Dye Reagent Concentrate, consisting of Coomassie Brilliant Blue G-250 in phosphoric acid and methanol, was diluted 1:5 with dH₂O. 1 mL of the diluted reagent was mixed with an appropriate amount of protein sample and incubated for 5 min at room temperature (RT). Diluted reagent was used as a blank. Absorption was measured at a wavelength of 595 nm in a photometer (Ultraspec 3300 pro, GE Healthcare). Protein concentrations were calculated using a standard regression curve with bovine serum albumin (BSA) as the protein standard (2-10 µg BSA/mL).

2.1.2 Protein precipitation

For protein enrichment from diluted protein extracts or to remove disturbing components in the sample buffers, proteins were precipitated using a denaturing chloroform-methanol method (Wessel and Flügge, 1984). This precipitation method is relatively insensitive against lipids, salts, reducing agents and detergents. For precipitation, 0.1 mL of aqueous protein sample was vortexed with 0.4 mL methanol (p.A.). Following short centrifugation (30 sec, 9000 g, RT), 0.1 mL chloroform (p.A.) was added. Vortexing and centrifugation was repeated as described before. Addition of 0.3 mL ddH₂O, vortexing and centrifugation (1 min, 9000 g, RT) resulted in two distinct phases with precipitated proteins accumulated in the interphase. After removal of the upper (aqueous) phase, the remaining solution was mixed with 0.3 mL methanol. Following centrifugation (2 min, 9000 g, RT) the supernatant was discarded and

the pellet, containing the precipitated denaturated proteins, was air-dried, dissolved in Laemi-buffer (1% (w/v) SDS, 50 mM Tris-HCl pH 6.8, 10% (v/v) glycerol, 100 mM β -mercaptoethanol, 0.005% (w/v) bromophenol blue) and further analyzed by SDS-PAGE (see chapter 2.1.3).

2.1.3 Sodium dodecyl sulfate-polyacrylamide gel electrophoresis (SDS-PAGE)

For separation of protein mixtures under denaturing conditions, SDS-PAGE was used (Laemmli, 1970). In SDS-PAGE, proteins bind the denaturing detergent SDS and become completely covered by negatively charged SDS anions. The strong negative charge load of bound SDS masks the intrinsic charge of the proteins, thus leading to a nearly constant charge-to-mass ratio of the SDS-protein complexes. Electrophoresis of SDS-treated protein samples therefore results in a strict separation of SDS-protein complexes according to their molecular masses. To improve resolution a discontinuous gel system with multiphasic buffer systems was used. The 4% stacking gel with a pH value of 6.8 was polymerized on top of a higher percentage separating gel with a pH value of 8.8. The pH value of the stacking gel is in the range of the isoelectric point (pI) of glycine, a major component of the electrophoresis buffer. At this pH value, glycine exists nearly completely in its netto-uncharged zwitterionic form. Therefore, at the beginning of electrophoresis, the mobility of the chloride ions (leading ions) is greater than the mobility of the glycine ions (trailing ions). The mobility of the sample molecules is intermediate. As the ion front sweeps through the sample molecules, they are carried along and become “stacked” into a thin distinct layer. At the interphase between stacking and separating gel, the pH and pore size changes abruptly. At the pH of 8.8, glycine has stronger negative charge, leading to increased glycine mobility. While mobility of SDS-protein complexes is decreased by the sieving effect of the higher percentage gel matrix, glycine accelerates, passing the stacked layers of sample molecules and the process of unstacking in the separating gel begins.

For casting of the gels, Mini Protean III (BioRad) or Mighty-Small II (Hoefer) casting chambers for mini gels and Protean II (BioRad) casting chambers for 18 cm gels were used, respectively. Depending on the further application of the gels, spacers with 0.75, 1.0 or 1.5 mm thickness were selected. The casting chamber was filled with a separating gel solution that was overlaid with isopropanol. The percentage of the used acrylamide concentration was dependent on the size of the separated proteins of interest, ranging from 9-15% (Table 10). The radical polymerization reaction of the polyacrylamide matrix, containing the monomers acrylamide and bisacrylamide, was induced by the radical starter of the polymerization

ammonium peroxodisulfate (APS) and accelerated by addition of the catalyst N',N',N',N'-tetraethylmethylenediamine (TEMED). After polymerization, the isopropanol was removed completely by rinsing the top of the separating gel with ddH₂O. Residual water was removed with Whatman paper. On top of the separating gel a stacking gel was poured (Table 11) and suitable combs (10- or 15-well combs) were inserted.

Table 10: Gel solution for SDS separating gel (30 mL)

	9%	10%	12%	15%
Acrylamide:bisacrylamide (37.5:1)	9 mL	10 mL	12 mL	15 mL
1.0 M Tris-HCl pH 8.8	11.25 mL	11.25 mL	11.25 mL	11.25 mL
20% (w/v) SDS	0.15 mL	0.15 mL	0.15 mL	0.15 mL
ddH ₂ O	9.6 mL	8.6 mL	6.5 mL	3.5 mL
TEMED	18 µL	18 µL	18 µL	18 µL
10% (w/v) APS	180 µL	180 µL	180 µL	180 µL

Table 11: Gel solution for SDS stacking gel (10 mL)

	4%
Acrylamide:bisacrylamide (37.5:1)	2.7 mL
1.0 M Tris-HCl pH 6.8	1.25 mL
20% (w/v) SDS	0.05 mL
ddH ₂ O	6 mL
TEMED	17 µL
10% (w/v) APS	50 µL

For electrophoresis, gels were placed into the electrophoretic chambers (MiniProtean III, Mighty-Small II and Protean II, respectively) and the buffer chambers were filled with 1 x SDS electrophoresis buffer (25 mM Tris, 192 mM glycine, pH 8.6-8.8). Protein extracts were treated with Laemi-buffer, incubated at RT for 15 min and loaded onto the gel. For protein size determination, pre-stained protein standards were used as markers (PageRuler Prestained Protein Ladder, Fermentas). Electrophoresis was started with 60 V (MiniProtean III, Mighty-Small II) or 5 mA (Protean II) for 20 min and was then increased to 110 V or 9 mA, respectively. When the bromophenol blue front reached the end of the separating gel, electrophoresis process was stopped and the gels were either stained (see chapter 2.1.6) or used for Western blot analysis (Towbin et al.) (see chapter 2.1.7).

2.1.3.1. SDS-PAGE gradient gels

2.1.3.1.1 Casting of SDS gradient mini gels with a gradient maker

Unlike standard SDS-PAGE, where the separating gel has a constant acrylamide concentration, gradient gels have a acrylamide gradient with a high percentage (15%) of acrylamide at the bottom of the gel and a low percentage (9%) at the top (Table 12). Two solutions of different acrylamide concentrations were mixed by gravity flow using gradient maker (VWR) positioned above the gelpcassette.

Table 12: Gel solution for SDS gradient separating gel (30 mL)

	9%	15%
Acrylamide:bisacrylamide (37.5:1)	9 mL	15 mL
1.0 M Tris-HCl pH 8.8	11.25 mL	11.25 mL
20% (w/v) SDS	0.15 mL	0.15 mL
ddH ₂ O	9.6 mL	0.5 mL
80% glycerol	-	3 mL
TEMED	18 µL	18 µL
10% (w/v) APS	180 µL	180 µL

2.1.3.2 Sample preparation of rod outer segments (ROS)

For electrophoresis of total ROS lysates, isolated light- and dark-adapted ROS corresponding to 15 µg of protein were incubated in Laemi Buffer (1% (w/v) SDS, 50 mM Tris-HCl pH 6.8, 10% (v/v) glycerol, 100 mM β-mercaptoethanol, 0.005% (w/v) bromophenol blue) for 15 min at room temperature (RT) and separated on 12% gels using SDS-PAGE.

For preparation soluble and membranous ROS fractions, isolated light- and dark-adapted ROS corresponding to 15 µg protein were ruptured by freeze-thaw cycles in IP-buffer containing 20 mM Tris, 150 mM NaCl, 1 mM EDTA pH 7.4, protease inhibitors (Roche) and centrifuged for separation of membranous and soluble fractions at 4°C for 10 min at 16000 g. Both fractions were separated on 12% gels using SDS-PAGE.

2.1.4 Blue-native PAGE (BN-PAGE)

SDS-PAGE separates proteins due to the use of the strong ionic detergent SDS under denaturing conditions. However, proteins can also be solubilized by using comparatively mild non-ionic detergents, such as Triton X-100, dodecyl maltoside or digitonin ((le Maire et al., 2000), (Seddon et al., 2004)). These detergents allow the solubilization of native membrane proteins and native membrane protein complexes that can then be separated by native electrophoretic methods. Negative charges are provided by adding the negatively charged

protein-binding dye Coomassie Brilliant Blue G-250 ((Schagger and von Jagow, 1991), (Reisinger and Eichacker, 2006), (Wittig et al., 2006)). BN-PAGE was developed by Schagger and colleagues for the separation of mitochondrial membrane protein complexes ((Schagger and von Jagow, 1991), (Schagger et al., 1994), (Schagger, 2001)). The selection of the type and the concentration of detergents is critical for the isolation of membrane protein complexes and therefore has to be determined empirically for every type of membrane sample ((Reisinger and Eichacker, 2006), (Schagger, 2001)). Segregation of the solubilized protein complexes occurs in native, non-reducing polyacrylamide gradient gels according to their size. In these gradient gels, protein complexes migrate in these gradient gels with decreasing pore size until they reach their specific size-dependent pore-size limit.

For identification and characterization of the composition of native membrane protein complexes, a 2-DE approach, with native BN-PAGE as first dimension and denaturing SDS-PAGE as second dimension is applied (BN/SDS-PAGE) ((Schagger and von Jagow, 1991; Reisinger and Eichacker, 2006), (Wittig et al., 2006)). The first dimension separates membrane extracts in individual native membrane protein complexes according to their molecular mass ((Figure 11; (Braun et al., 2007)). The lane of the first dimension or individual protein bands are treated with SDS under reducing conditions, resulting in the denaturation of the native protein complexes. The gel strip or protein band is then placed on top of a SDS gel and SDS-PAGE is performed (Figure 11). All proteins released from one protein complex are separated along the electric field and positioned in a straight line one below the other according to their molecular mass (Figure 11). BN/SDS-PAGE represents an alternative method to immunoprecipitation if physiological protein-protein interactions and compositions of membrane protein complexes are to be determined ((Schagger and von Jagow, 1991), (Reisinger and Eichacker, 2006), (Wittig et al., 2006)). It has the advantage that no antibodies are necessary but the conditions are not as sensitive due to the failure to detect detergent-labile interactions partners (Wittig et al., 2006).

The significance of BN/SDS-PAGE for the separation of membrane protein complexes has noticeably increased during the last few years. Beside the systematic analysis of mitochondrial membrane protein complexes (*e.g.* (Reifschneider et al., 2006)), BN/SDS-PAGE has also been successfully applied for the analysis of protein complexes of various other membrane preparations. Examples are thylakoid membranes of chloroplasts (Granvogel et al., 2006), microsomal membranes (Chen et al., 2004), and rod photoreceptor outer segments (Suda et al., 2004). Thus, BN/SDS-PAGE is a gel-based 2D approach highly suitable for the systematic proteomic analysis of membrane protein complexes.

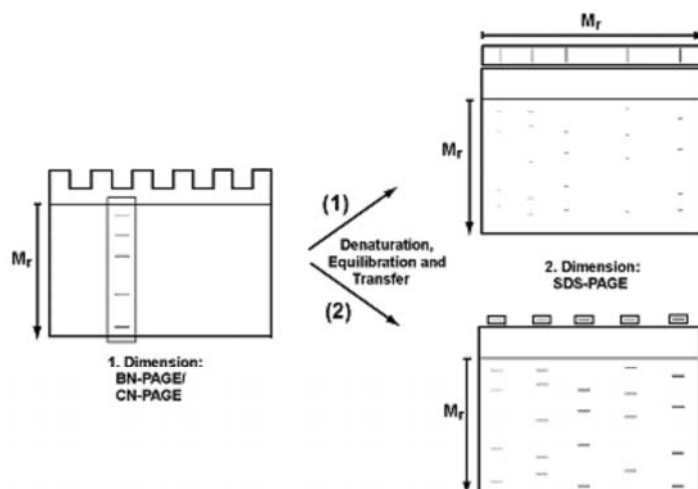


Figure 11: 2-DE electrophoresis of native protein complexes (Braun et al., 2007). Protein complexes are separated electrophoretically in a polyacrylamide gel under native conditions according to their molecular mass (BN-PAGE). Gel lanes (1) or individual BN bands (2) are cut out, equilibrated under denaturing conditions, and transferred to a SDS polyacrylamide gel. SDS-PAGE is performed, resulting in the separation of potential protein complex subunits.

BN PAGE was performed according to Schägger (Schagger, 2001). Membranes from ROS corresponding to 100 μg protein were suspended in 30 μL ACA buffer (500 mM ϵ -aminocaproic acid, 50 mM Imidazole, 0.5 mM EDTA pH 7.0) and solubilized for 30 min on ice with 7g β -dodecylmaltoside per g protein. Unsolubilized material was removed by ultracentrifugation at 4°C for 30 min at 100000 g (Beckman Optima ultracentrifuge). The supernatant containing the solubilized protein complexes was mixed with 3.5 μL loading buffer (5% (w/v) Coomassie Serva Blue G (Serva) in 500 mM ϵ -aminocaproic acid, corresponding to a Coomassie/detergent ratio of 1:4, and loaded onto a native 6-12% gradient gel (Table 13 and 14). The lanes of the first dimension were cut and incubated for 20 min in solubilization buffer (2% (w/v) SDS, 1% (w/v) mercaptoethanol, 66 mM Na_2CO_3 , 50 mM Tris pH 7.4, 150 mM NaCl, 2 mM EDTA), resulting in the denaturation of the multiprotein complexes. Individual lanes were blotted directly onto PVDF membranes (as described in chapter 2.1.7.1) or they were laid on top of denaturing 9-15% gradient gels and SDS-PAGE was performed. The second dimensional gels were used for WB analysis (see chapter 2.1.7) or subjected to silver staining (see chapter 2.1.6.1).

Table 13: Gel solutions for BN-PAGE separating gel (10.5 mL)

	4%	6%	12%
30% (w/v) Acrylamide:bisacrylamide (37.5:1, Serva)	1.4 mL	2.1 mL	4.2 mL
3 x Gel-Buffer (75 mM Imidazole, 1.5 M ϵ -aminocaproic acid pH 7.0)	3.5 mL	3.5 mL	3.5 mL
ddH ₂ O	5.6 mL	4.9 mL	1.25 mL
Glycerol p.A.	-	-	2.1 g
TEMED	9 μ L	9 μ L	9 μ L
10% (w/v) APS	27 μ L	27 μ L	27 μ L

Table 14: Gel solutions for BN-PAGE stacking gel (20 mL)

	4%
30% (w/v) Acrylamide:bisacrylamide (37.5:1, Serva)	2.66 mL
3 x Gel-Buffer (75 mM Imidazole, 1.5 M ϵ -aminocaproic acid pH 7.0)	6.66 mL
ddH ₂ O	10.48 mL
TEMED	20 μ L
10% (w/v) APS	200 μ L

2.1.5 Second-dimensional gel electrophoresis (2-DE)

2-DE is still the method of choice if complex protein mixtures are to be separated with high resolution, permitting the simultaneous analysis of hundreds or even thousands of gene products. The separation is based on the combination of two orthogonal separation principles. In the first dimension, proteins are separated due to their different isoelectric points and in the second dimension due to their molecular weight (Figure 12). 2-DE was performed using immobilized pH gradients (IPG-Dalt) based on the protocol of (Görg et al., 1988). In the first dimension, denaturated proteins were separated by isoelectric focusing (IEF) according to their intrinsic charge at a certain pH. Proteins have electrophoretic mobility as long as they reach the pH at which their intrinsic net charge becomes zero (isoelectric point, pI). Consequently they migrate in a stable pH gradient upon high voltage to the pH where they reach their isoelectric point. The pI of a specific protein depends on its content of basic and acidic amino acids. Commercially available IPG strips contain a pre-formed pH gradient immobilized in a homogeneous polyacrylamide gel.

In the second dimension the intrinsic charge of the proteins is shielded by the anionic detergent SDS and therefore separation of the proteins occurs due to their apparent molecular mass by gradient SDS-PAGE. Separated proteins can be visualized as protein spots by staining of the gel (see chapter 2.1.6).

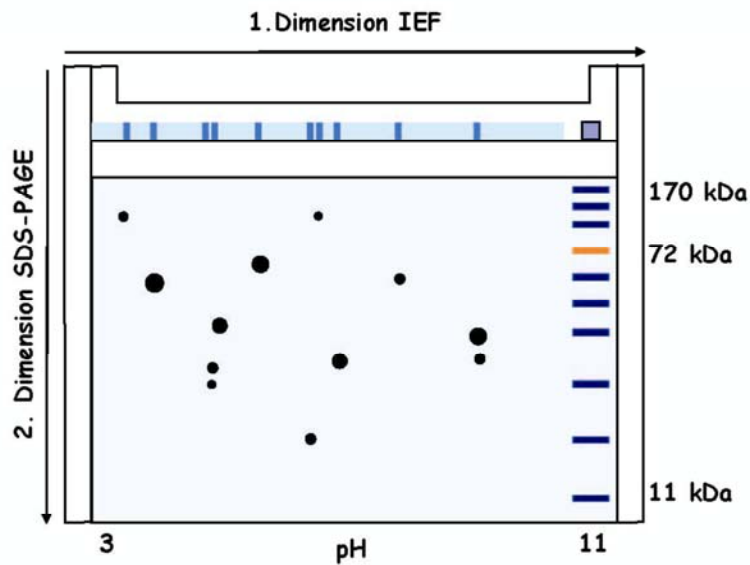


Figure 12: Separation principle of 2-DE gel electrophoresis. 1. dimension IEF: separation of the proteins due to their different isoelectric points. 2. dimension SDS-PAGE: separation of proteins according to their molecular weight.

2.1.5.1 Sample preparation

Pre-treatment of samples for 2-DE involves solubilization, denaturation and reduction to completely break up the interactions between the proteins (Rabilloud et al., 1997). Solubilization and denaturation of proteins was accomplished using 2-DE lysis buffer. It contains high molar concentrations of urea (9 M) and thiourea (2 M), as well as the zwitterionic detergent 3-[(3-cholamidopropyl)-dimethyl-ammonio]-1-propansulfonate (CHAPS; 4% (w/v)) and is supplemented with dithioerythritol (DTE; 65 mM). The 2-DE lysis buffer was stored at -80°C .

Soluble fractions of light- and dark-adapted ROS were immunoprecipitated with anti-Rac1 and anti-RhoA antibodies (see chapter 2.1.8.2) and proteins were eluted with 210 μL 2-DE lysis buffer in microspin columns (GE Healthcare). The eluate was supplemented with 2.2 μL Pharmalyte (carrier ampholytes pH 3-10 for IEF, 0.36 meq/mL, GE Healthcare) and 1.1 μL bromophenol blue (0.5% (w/v)) and centrifuged for 30 min at 22°C and 50000 g (Beckman Optima ultracentrifuge; TLA110 rotor).

2.1.5.2 Rehydration and sample loading

7 cm IPG strips with a non-linear pH gradient covering pH values from 3-11 with a flat pH gradient at neutral pH values were used (GE Healthcare) for IEF. The sample (prepared as described in chapter 2.1.5.1) was pipetted air bubble free into the rehydration tray and the IPG strip was placed, with the gel matrix side facing down, directly into the sample solution. IPG strips were completely overlaid with gas-free mineral oil (DryStrip Cover Fluid, GE Healthcare), in order to exclude drying and formation of urea crystals.

2.1.5.3 Isoelectric focusing (IEF)

IEF was performed using the Multiphor II apparatus (GE Healthcare) with a water cooling system. For uniform cooling, the Dry Strip Kit was laid air bubble free onto the cooling plate with 10 mL mineral oil to ensure equal contact. The focusing strip aligner was placed air bubble free into the Dry Strip Kit with 8 mL mineral oil in between. Surplus mineral oil, urea crystals and proteins that had not entered the gel matrix during the in-gel rehydration step were carefully removed from the IPG strips by dabbing with wet (ddH₂O) filter papers (Whatman). IPG strips were then laid gel-side-up into the grooves of the aligner. Wet (ddH₂O) electrode strips (GE Healthcare) were placed at the anodic and cathodic ends of the strips, respectively and electrodes were positioned upon the electrode strips. Subsequently, the IPG strips were overlaid with mineral oil. Isoelectric focusing was performed under cooling at 20 to 23°C. In the beginning, a low voltage step (150 V) was applied, in order to remove remaining salts from the strips. At higher voltages (up to 3500 V) proteins began to focus in the stable pH gradient. Focusing of the 7 cm stripes was continued until 10-15 kWh were reached (IEF-program: 30 V: slope/1 min, hold/16 h; 200 V: slope/1 min, hold/2 h; 3500 V: slope/2 h, hold/3 h). At this time point the steady state phase was reached, *i.e.* the time point at which all the proteins were focused. After isoelectric focusing, IPG strips were used immediately for the second dimension or were frozen at -20°C between two sheets of plastic film until further use.

2.1.5.4 Equilibration and transfer of the IPG strips

After IEF, the IPG strips were rinsed with ddH₂O and incubated in two steps in 2-DE equilibration solutions to prepare the stripes for the second dimension (SDS-PAGE). In order to prevent electroendosmotic effects during the protein transfer from the focusing strip into the SDS gel, 2-DE equilibration solutions contained urea and glycerol (50 mM Tris-HCl pH 6.8, 6 M urea, 30% (v/v) glycerol, 2% (w/v) SDS). In the first step, IPG strips were incubated

for 10 min at RT in reducing 2-DE equilibration solution containing 65 mM DTE (freshly prepared) resulting in cleavage of disulfide bonds between the sulfhydryl groups of the polypeptides. Subsequently the stripes were incubated for 10 min at RT in 2-DE equilibration solution supplemented with 260 mM 2-iodoacetamide and bromophenol blue. The resulting alkylation of free sulfhydryl groups, from excessive DTE and cystein residues, prevented the reformation of disulfide bonds. Following equilibration of the stripes in SDS electrophoresis buffer, they were transferred air bubble free on top of the stacking gel of a SDS-gradient gel (9-15%), with the gel side facing the smaller glass plate and with the acidic end of the strips oriented to the left side of the gel. For protein size determination a small piece of Whatman paper, soaked with 7 μ L of pre-stained protein ladder (PageRuler Prestained Protein Ladder, Fermentas), was carefully positioned next to the strip.

Excessive SDS electrophoresis buffer was gently removed with Whatman paper and IPG strips were embedded air bubble free in agarose solution (0.5% (w/v) agarose in SDS electrophoresis buffer).

2.1.5.5 Second dimension: SDS-PAGE

2DE Electrophoresis was performed in a mini Protean III (BioRad) electrophoresis chamber with a voltage of 60 V until the proteins reached the separating gel. The voltage was elevated to 110 V until the bromophenol blue front reached the end of the gels (about 1,5 h). Following electrophoresis gels were stained using the silver staining method (see chapter 2.1.6.1)

2.1.6 Staining of SDS gels

2.1.6.1 Silver staining

Silver staining of proteins in SDS gels was developed by Hubbell and colleges (Hubbell et al., 1979). The staining method is based on the reduction of silver ions to elemental silver by formaldehyde under alkaline conditions and was later advanced by Shevchenko and colleges to be compatible for mass spectrometry (Shevchenko et al., 1996). By destaining of the silver-stained proteins prior to enzymatic digestion, the detection of the peptides by mass spectrometry was further enhanced (Gharahdaghi et al., 1999).

Visualization of protein spots or bands is achieved by complex formation of the silver ions with proteins. Silver binds to the amino side chains, primarily the sulfhydryl and carboxyl groups of proteins.

After electrophoresis, SDS gels were incubated two times for 30 min in a fixation solution (50% (v/v) methanol, 12% (v/v) acetic acid, 500 $\mu\text{L/L}$ 37% formaldehyde). Formaldehyde serves here as a crosslinker and reduces loss of polypeptides. Incubation of the gels in 50% (v/v) ethanol (3 times; 10 min) was followed by rehydration of the gels in an aqueous 0.02% (w/v) sodium thiosulfate ($\text{Na}_2\text{S}_2\text{O}_3$) solution for 1 min and by two washing steps in dH_2O . By the shrinking and swelling of the gels, SDS was removed from the gel matrix, and the application of sodium thiosulfate removed oxidating groups and radicals within the gel in order to minimize background staining. Following incubation of the gels in silver nitrate (0.2% (w/v) AgNO_3 , 750 $\mu\text{L/L}$ 37% formaldehyde) for 30 min, the gels were incubated in developing solution (6% (w/v) sodium carbonate (Na_2CO_3), 0.005% (w/v) sodium thiosulfate, 500 $\mu\text{L/L}$ 37% formaldehyde), where the silver ions in complex with proteins were reduced to elementary silver. When the desired staining degree was accomplished, the staining was stopped with fixation solution. Gels were equilibrated in storage solution (20% (v/v) ethanol, 2% (v/v) glycerol) for at least 15 min.

2.1.6.2 Coomassie staining

Coomassie Brilliant Blue R-250 binds to proteins through ionic interactions between the dyes sulfonic acid groups and positive protein amine groups as well as through Van der Waals attractions.

Following electrophoresis, SDS gels were incubated in fixation solution (50% (v/v) methanol, 12% (v/v) acetic acid) for 30 min. Protein bands were visualized by incubation in Coomassie staining solution (50% (v/v) methanol, 12% (v/v) acetic acid, 0.4% (w/v) Coomassie Brilliant Blue R-250) for 1h at RT with gentle agitation. Gels were washed several times in fixation solution until background staining was removed and a clear protein pattern could be observed.

2.1.6.5 Digitalizing and drying of SDS gels

Stained SDS gels (silver or Coomassie) were digitalized using a GS-710 Calibrated Imaging Densitometer (BioRad) and Adobe Photoshop 7.0 software package. SDS gels were subsequently packed air bubble-free between two wet cellophane foils (BioRad) and dried in a gel drier (BioRad) at 50°C for 3h.

2.1.7 Western blot analysis

2.1.7.1 Semi dry blotting

Blotting (Figure 13) is the transfer of large molecules onto the surface of an immobilizing membrane. The molecules that are absorbed on the membrane surface are freely available to macromolecular ligands like specific antibodies.

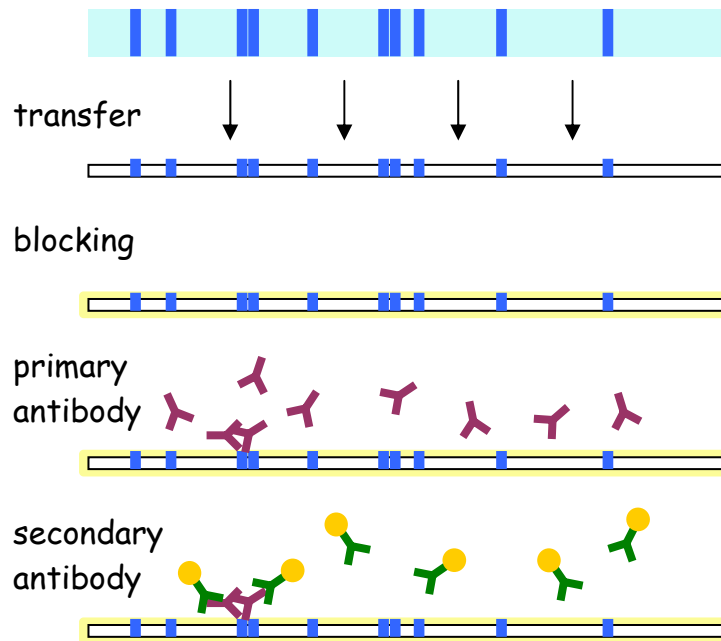


Figure 13: The most important steps during Western blotting:
Transfer: Proteins are blotted electrophoretically onto PVDF membranes.
Blocking: unspecific free binding sites were blocked with blocking-reagent.
Primary antibody: binds to its specific antigen on the membrane. *Secondary antibody:* HRP-conjugated; recognizes all antigens from a specific species.

SDS-protein complexes separated by SDS-PAGE can be transferred electrophoretically onto membranes for immunodetection of individual proteins using specific antibodies (Towbin et al., 1979). Proteins were blotted onto Polyvinylidenedifluoride (PVDF) transfer membranes (GE Healthcare) by a semi dry blotting apparatus (BioRad). Semi dry blotting has the advantage over tank blotting in that only a limited volume of buffer is necessary and a discontinuous buffer system can be used (Kyhse-Andersen, 1984).

Following electrophoresis, SDS gels were incubated in Anode-buffer II (0.3 M Tris) for 30 sec. PVDF membranes, cut in the size of the gel, were activated with methanol, rinsed in dH₂O and incubated in Anode buffer II. Filter papers (Whatman) in the size of the gel were soaked in three different blotting buffers (see Figure 14). Three filter papers were soaked in Anode-buffer I (0.025 M Tris), two in Anode-buffer II and three in Cathode-buffer (40 mM ϵ -

aminocaproic acid, 0.01 % SDS). Filter papers, Gel and membrane were positioned air bubble free onto a horizontal semi dry blotting apparatus as depicted in Figure 14. Up to four mini-gels could be blotted side by side simultaneously. Proteins were transferred with 0.8 mA per cm² of gel. After blotting, the membranes were stained for 10 min in Ponceau staining solution (0.5% (w/v) Ponceau S, 1% (v/v) acetic acid). Background staining was removed by incubation of the membranes in Ponceau destaining solution (3 x 10 min; 10% (v/v) acetic acid, 40% (v/v) ethanol). Protein band patterns on the membranes were digitalized using the GS-710 Calibrated Imaging Densitometer (BioRad) and Adobe Photoshop 7.0 software package. Membranes were destained in TBST (50 mM Tris pH 7.4, 150 mM NaCl, 2 mM EDTA, 0.1% Tween20). To block unspecific binding sites, the membranes were blocked for 30 min at RT in blocking-reagent (5% non-fat dry milk (BioRad) in TBST (50 mM Tris pH 7.4, 150 mM NaCl, 2 mM EDTA, 0.1% Tween20)). The blots were incubated over night at 4°C with primary antibodies (see Table 8). Following incubation with a secondary antibody in blocking reagent (1-2h, RT), immunoreactive signals were visualized using enhanced chemiluminescence (ECL+, GE Healthcare) on Hyperfilms (GE Healthcare) with a Agfa Curix 60 developer (Agfa). In some experiments, Western blots were stripped by incubation in 100mM Tris-HCl buffer, pH 6.8, containing 100mM β -mercaptoethanol and 2% SDS or alternatively in 0.2 M Glycine pH 2.5 for 30 min at 55°C with gentle agitation, to remove all bound antibodies. The stripped blots were washed in TBST, blocked with an appropriate Blocking reagent and re probed with antibodies as described above.

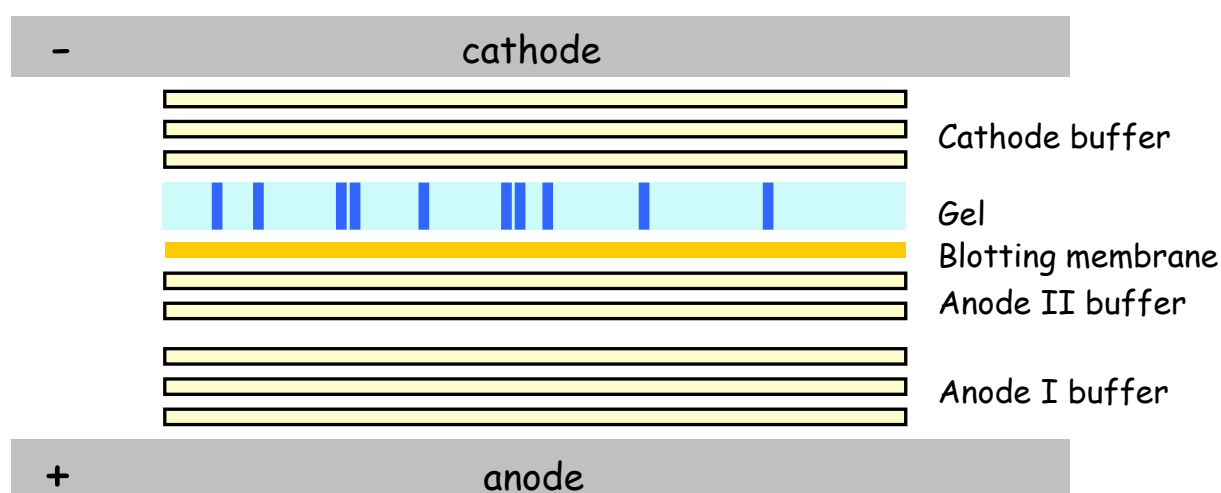


Figure 14: Diagram of a horizontal graphite blotter for semi dry blotting. Proteins are electrophoretically transferred from a SDS-gel to the blotting membrane. Filter papers soaked in a discontinuous buffer system are used to facilitate the transfer.

2.1.8 Analysis of protein interactions

Isolation of native protein complexes and the determination of functional relationships between proteins is one of the most important tasks in protein science. Several affinity based methods for the isolation of native protein complexes have been developed in recent years, which allow the analysis of the assembled proteins by Western blot or mass spectrometry. If suitable antibodies are available, immunoprecipitations of the protein of interest from cell or tissue lysates can be the method of choice. Here the success of the method depends strongly on the quality of the antibody and antibody IgGs may cause a high background. A pull-down assay with overexpressed recombinant proteins is an alternate method to discover protein-protein interaction in cellular system. Another method, the tandem-affinity purification (TAP) method, originally developed for the analysis of protein interactions in yeast, allows systematic protein-protein interactions analysis under near physiological conditions ((Rigaut et al., 1999), (Gavin et al., 2002)). Compared to purifications via single affinity tags or classical immunoprecipitations, a two step procedure results in marked reduction of the background that is caused by unspecific binding of proteins.

2.1.8.1 Immunoprecipitations (IP) from porcine retina

A porcine retina was isolated as described in chapter 2.2, and immediately placed in protease inhibitors (Roche). The retina was homogenized and solubilized for 30 min on ice with 1% β -dodecylmaltoside in IP-buffer (150 mM NaCl, 1 mM EDTA, 20 mM Tris pH 7.4, protease inhibitors (Roche)). Unsolubilized material was removed by centrifugation: 4°C, 1h, 57000 g, Beckman optima, TLA110.

500 μ g retina lysate was adjusted with IP-buffer to a protein concentration of 1 μ g/ μ L and precleared for 30 min at 4°C with 50 μ L Protein-G-PLUS-Agarose (Santa Cruz).

The precleared lysate was mixed with anti-lebercilin antibody (1.6 μ g per 100 μ g total protein) and incubated at 4°C overnight. 30 μ L Protein-G-Agarose was subsequently added for 1h. Proteins were eluted with Laemmli-buffer for 15 min at RT. Samples were resolved by SDS-PAGE and analysed by Western blot (see chapter 2.1.3 and 2.1.7, respectively).

2.1.8.2 Immunoprecipitations from ROS

Isolated light- and dark-adapted ROS corresponding to 500 μ g protein were employed as total lysates or separated into a soluble and a membranous fraction (as described in chapter 2.1.3.2). While the total lysates and the soluble fractions were subjected directly to IP, the pellets corresponding to the membranous fractions were resuspended in IP-buffer (150 mM

NaCl, 1 mM EDTA, 20 mM Tris pH 7.4 and protease inhibitors (Roche)) and solubilized for 10 min on ice with 1% β -dodecylmaltoside. Unsolubilized material was removed by centrifugation for at 4°C for 10 min at 16000 g. All fractions were precleared for 30 min at 4°C with 50 μ L Protein-G-PLUS-Agarose (Santa Cruz) under agitation.

The precleared lysates were mixed with mouse anti-Rac1 antibodies (Upstate), rabbit anti-PDE δ antibodies (Sigma) or mouse anti-RhoA antibodies (Santa Cruz) at a concentration of 1.4 μ g per 100 μ g protein and incubated for 3 h at 4°C under agitation. As a control for unspecific protein binding, a parallel experiment with mouse or rabbit IgG (1.4 μ g per 100 μ g protein) was performed. 30 Protein-G-Agarose was subsequently added for 1 h and proteins were eluted with Laemmli-buffer for 15 min at RT. Samples were resolved by SDS-PAGE and analysed by Western blot (see chapter 2.1.3 and 2.1.7, respectively).

2.1.8.3 Rac1-GTP Pull Down

Freshly isolated light- and dark-adapted ROS corresponding to 500 μ g protein were ruptured by osmotic shock in Mg-Lysisbuffer (20 mM Hepes, 150 mM NaCl, 10 mM MgCl₂, 1 mM EDTA, pH 8.0, protease inhibitors (Roche)) and centrifuged for separation of membranous and soluble fractions for 10 min at 16000 g and 4°C. While the soluble fraction was subjected directly to the pull-down experiment, the pellet corresponding to the membranous fraction was resuspended in Mg-Lysisbuffer and solubilized for 10 min on ice with 1% β -dodecylmaltoside. Unsolubilized material was removed by centrifugation for 10 min at 16000 g and 4°C. Both fractions were precleared for 30 min at 4°C with Glutathione-agarose (Santa Cruz).

The precleared lysates were mixed 20 μ L PAK1 PBD agarose conjugate (Upstate) and incubated for 3 h at 4°C. Proteins were eluted with Laemmli-buffer for 15 min at RT, separated by SDS-PAGE and analyzed by Western blot (see chapter 2.1.3 and 2.1.7, respectively).

2.1.8.4 Tandem affinity purification (TAP)

The SF-TAP tag (Figure 15C) has been developed in our lab by Johannes Gloeckner (Gloeckner et al., 2007a). The SF-TAP tag consists of a tandem Strep-tag II (Skerra and Schmidt, 2000) and a FLAG epitope (see figure 15C). SF-TAP constructs are expressed in mammalian cells under the control of the viral CMV promoter. The expression vectors have been generated on the basis of the pcDNA3.0 (Invitrogen) expression vector containing an N-

or C-terminal version of the SF-TAP tag and a gateway for recombination based cloning (Gloeckner et al., 2007a).

2.1.8.4.1 Transfection of HEK293 cells transiently expressing the SF-TAP fusion protein

For the transient expression of proteins tagged with the N-SF-TAP HEK293 cells were selected, because they provide a very high transfection efficiency, are fast growing and produce high amounts of protein (10-15 mg total protein per 14 cm dish corresponding to approx. 7×10^7 HEK293 cells). HEK293 cells were grown in DMEM supplemented with 10% heat inactivated fetal calf serum (FCS). Cells were transfected at 40-80% confluency. Transfection of the cells was performed with 4 μ g of plasmid DNA and Effectene transfection reagent (Qiagen) according to manufacturer's protocols. After 48h, cells were harvested for SF-TAP purification (see chapter 2.1.8.4.2).

2.1.8.4.2 SF-TAP purification protocol (Gloeckner, in press).

A flow chart of the SF-TAP purification procedure is shown in Figure 15B.

The medium was removed from 14 cm HEK293 plates transiently expressing the SF-TAP fusion protein and cells were scraped in 1 mL lysis buffer (30 mM Tris-HCL pH 7.4, 150 mM NaCl, 0.5% Nonidet-P40, protease inhibitors (Roche) and phosphatase inhibitor cocktails I and II (Sigma)) on ice using a cell scraper (Sarstedt). After cell lysis (20 min, 4°C under agitation), the cell debris was removed by centrifugation (10 min, 10000 g, 4°C, Beckman bench top centrifuge). The lysates were cleared by filtering through a syringe 0.22 μ m filter device (Millipore) and the cleared lysates were used for Western blot analysis or incubated with Strep-Tactin superflow resin (IBA; 50 μ L/plate) for 1h at 4°C under agitation. The mixture was transferred on a microspin column (GE-Healthcare) and the supernatant was removed by gentle centrifugation (5 sec, 100 g). The remaining beads were washed on the microspin column 3 x with 500 μ L wash buffer (30 mM Tris-HCL pH 7.4, 150 mM NaCl, 0.1% Nonidet-P40, protease inhibitors (Roche) and phosphatase inhibitor cocktails I and II (Sigma)). Bound protein was eluted with 500 μ L desthiobiotin elution buffer for 10 min on ice. The eluate was transferred to a fresh microspin column, mixed with anti-FLAG-M2-agarose (25 μ L/plate) and incubated under gentle agitation at 4°C for 1h. The supernatant was removed by centrifugation (5 sec, 100 g) and the beads were washed with 1 x 500 μ L wash buffer and 2 x 500 μ L TBS buffer (30 mM Tris-HCL pH 7.4, 150 mM NaCl). Bound proteins were eluted with 200 μ L FLAG elution buffer (200 μ g/mL Flag peptide in TBS) for 10 min on ice. Eluted proteins were analysed by Western blot or mass spectrometry.

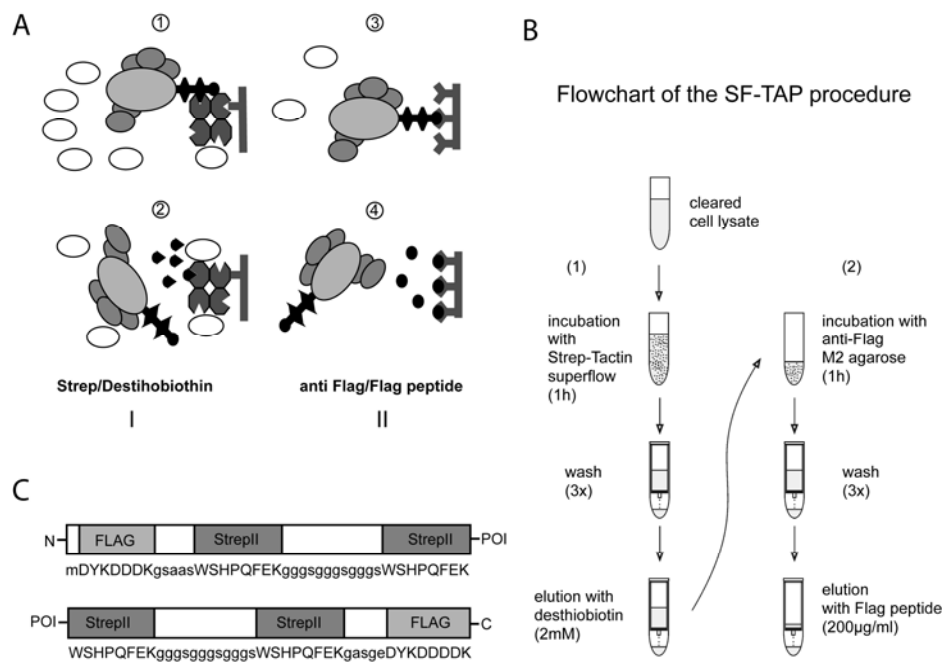


Figure 15: Overview of the SF-TAP procedure (Gloeckner, in press). **A**) First purification step (I): tandem Strep-tag II is bound by Strep-Tactin matrix (1) and eluted by desthiobiotin (2). Second purification step (II): FLAG moiety is bound to anti-FLAG M2 agarose and eluted with FLAG peptide. **B**) (1) Binding of SF-fusion protein by Strep/Strep-Tactin. (2) Second purification of the SF-fusion protein by the FLAG/anti-FLAG M2 system. (Gloeckner et al., 2007b) **C**) Sequences of the N- and C-terminal versions of the SF-TAP tag (POI = protein of interest) (Gloeckner et al., 2007b).

2.1.9 Mass spectrometry

Mass spectrometry measures the mass of molecules with very high sensitivity and is therefore used in a wide range of applications. Its beginning dates back to the early twentieth century, but it was not before the 1980s that it also started to play a significant role in biological science. Since that time it became a powerful tool in protein analysis and the key technology in the field of proteomics. Mass spectrometry based proteomics has become possible due to the development of softer ionization methods, enabling the ionization of large biomolecules, like the electrospray ionisation ((Pinter et al., 1998), (Fenn et al., 1989)) and the matrix-assisted laser desorption/ionisation (MALDI) (Hillenkamp et al., 1991). For the discovery and development of these methods, Fenn and Tanaka were awarded with the Nobel Prize for chemistry in 2002.

A mass spectrometer consists of an ion source that ionizes the sample, a mass analyzer that resolves the generated ions according to their mass-charge-ratio (m/z) and a mass detector.

2.1.9.1 In-gel proteolysis

Because the analysis of peptides has many advantages over the analysis of intact proteins, like a higher mass accuracy that leads to higher and more significant protein hits, it has become the preferred method in mass spectrometry.

After electrophoretical separation of protein samples, protein spots or bands are excised from the gel and the enzymatic digestion is carried out directly in the polyacrylamide gel matrix. Obtained peptides are eluted from the gel matrix and analyzed by mass spectrometry. A number of proteases can be used, but the most common one is the endoprotease trypsin. It cleaves the amide bond of proteins c-terminally to arginine and lysine (Olsen et al., 2004). The peptide-mixture from enzymatic cleavage is subjected directly to MALDI-MS.

2.1.9.1.1 In-gel proteolysis of silver-stained and Coomassie-stained gels

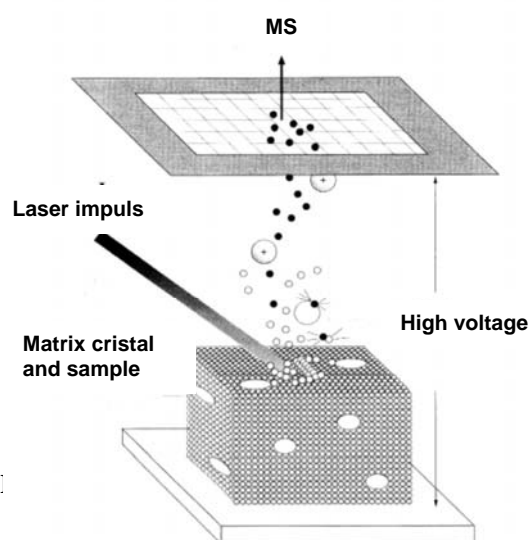
Protein spots and protein bands of interest were excised with a scalpel from dried or wet silver and Coomassie stained 2-DE or 1-DE gels. If bands were excised from dried gels, gel plugs were equilibrated three times for 15 min in 100 μ L ddH₂O in a 96-well plate (Nunc). Plugs were transferred into a fresh 96-well plate (Nunc) and equilibrated for 5 min with 100 μ L ddH₂O per gel plug. If wet bands were excised, this transfer step was not necessary. In order to destain the silver stained protein plugs, 100 μ L of freshly prepared destaining solution was added (30 mM K₃Fe(CN)₆ and 100 mM Na₂S₂O₃ in a 1:2 ratio). The plugs were incubated in destaining solution until they were completely destained. The supernatants were removed and the gel plugs were washed three times for 5 min with 100 μ L ddH₂O. Excised Coomassie bands were directly incubated in ddH₂O as described above. Then plugs were dehydrated by incubation with 100 μ L of a 40% acetonitril solution (three times for 15 min, respectively). Residual acetonitril was removed by evaporation. Subsequently the plugs were proteolyzed with trypsin in 10 μ L 1mM Tris-HCl pH 8.0 containing 0.01 μ g/ μ L trypsin (Sequencing Grade Modified Trypsin; Promega) overnight at 37°C.

2.1.9.2 Matrix-assisted laser desorption/ionization mass spectrometry (MALDI-MS)

MALDI sublimates and ionizes the samples out of a dry, crystalline matrix via laser pulses. The MALDI principle is depicted in Figure 16 (from (Lottspeich, 1998)). In a standard MALDI-MS preparation, the sample is mixed with matrix, mostly organic acids like α -cyano-4-hydroxycinnamic acid (CHCA), 2,5-dihydroxybenzoic acid (DHB), sinapinic acid (SA) or butanedioic acid (BA). These matrices exhibit strong absorption at the administered laser wavelength. After spotting the sample solution mixed with matrix, the solvent evaporates and

the analytes and matrix are co-crystallizing. The sample molecules are embedded into the crystal lattice of the matrix. Sample and matrix molecules are vaporized by several short intensive laser beams. In this process the matrix absorbs the laser energy and relays it to the sample molecules. Thus, a transfer of the matrix and the protein molecules into the gas phase and ionization of the sample molecules is achieved. Due to this soft ionization, the large, thermally labile protein or peptide molecules remain intact.

The formed ions enter the mass spectrometer where they are accelerated and separated in a time-of-flight (Saiki et al., 1988) analyzer. Since the time of flight at a given acceleration potential and flight path is dependent only upon the root of mass/charge (m/z), an accurate mass determination of the analyte molecule can be achieved by calibration with a peptide standard. To enhance the resolution, TOF analyzers are usually coupled with reflectors, where the ions are reflected before they hit the detector to compensate for small differences in kinetic energy.



2.1.9.3 Peptide mass fingerprinting (PMF) and tandem mass spectrometry (MS/MS)

Protein spots and protein bands of interest are excised from gels and subjected to in-gel proteolysis (see chapter 2.1.9.1.1). The peptide masses of the digested protein are analyzed and in order to identify the protein, compared to databases with known protein sequences. This method is referred to as peptide-mass fingerprinting (PMF) ((Cottrell, 1994), (Pappin, 1997)). To get sequence information of the peptides and to decrease the probability for false positive identifications, tandem mass spectrometry is used. After the recording of an MS spectrum, the most abundant peptide ions are selected for fragmentation. These selected ions

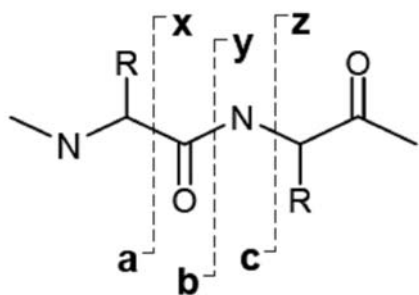


Figure 17: Fragmentation of peptides (Nomenclature after Roepstorff and Fohlmann).

are isolated, and the labile peptide-bondage is fragmented by collision with neutral gas in a predictable manner. The resulting fragment ions are referred to as a-, b- or c-ions, if they contain the n-terminal end of the former peptide, or x-, y or z-ions, if the fragment contains the c-terminal end (see Figure 17). The resulting fragment ion masses are used to search a sequence database.

The combination of PMF with MS/MS analysis increases the confidence in protein identification and enables the identification of proteins which may be represented by too few peptides for PMF to yield reliable results.

2.1.9.3.1 Mass measurement with the Applied Biosystems 4700 Proteomics Analyzer (AB4700)

For sample preparation, 0.5 μ L aliquots of sample digest were spotted on a steel target plate, mixed 1:1 with matrix consisting of 2 mg/mL α -cyano-4-hydroxycinnamic acid in 70% (v/v) acetonitril and 0.1% (v/v) TFA and dried.

MALDI-TOF peptide mass fingerprinting and MS/MS-analysis was performed on a MALDI-TOF/TOF tandem mass spectrometer (ABI 4700 Proteomics Analyzer, Applied Biosystems). Measurements were performed with a 355 nm Nb:YAG laser in positive reflector mode with a 20 kV acceleration voltage. For each MS and MS/MS spectrum, 4000 shots in a m/z window of 800-4000 were accumulated. To obtain a higher mass accuracy than 50 ppm, internal calibration using peptides resulting from autoprolysis of trypsin (2163.05 Da, 2211.10 Da) was used. In addition, an external calibration in the mass range from 800-3000 with a peptide mass standard of 8 peptides (Bruker) was used.

Peak labeling was automatically done by 4000 series explorer software Version 3.6 (Applied Biosystems) without smoothing of the peaks or baseline subtraction. In addition to peptide mass fingerprint spectra, the five most abundant precursor ions were chosen for MS/MS fragmentation which was performed using medium collision energy. Known ion masses of trypsin were excluded.

2.1.9.4 Electrospray ionization mass spectrometry (ESI-MS)

ESI-MS is an alternative soft ionization method. The sample is dissolved in an organic solvent, typically acetonitril or methanol. With a capillary, the solvent is continuously sprayed

into an electric field between the tip of the capillary and the orifice of the mass spectrometer. The formed uniform charged droplets lose their solvent very quickly, which results in a rapid increase of charge density on the droplet-surface. This leads repeatedly to spontaneous disintegration of the droplets (Coulomb-explosion) and formation of desolvated ions.

They enter the mass spectrometer, where they are normally analyzed with a quadrupole mass analyzer. This type of mass analyzer is a mass filter, which only allows ions with a defined mass/charge ratio to pass through. All other ions cannot pass the analyzer and are lost. Through continuous changes of the potential of the radio frequency between the quadrupole rods, ions of different masses are allowed to pass sequentially (scanning), and the intensity of the ion flow is recorded in relation to the m/z ratio by the detector. Electron spray ion sources can nowadays be coupled with different kinds of analyzers like ion-traps or TOF analyzers (Q-TOF).

2.1.9.4.1 Mass measurement with the Q-TOF II ESI mass spectrometer

For ESI LC-MS/MS analysis, protein samples were separated by SDS-PAGE. In-gel proteolysis of silver-stained and Coomassie-stained gels was performed as described above (see chapter 2.1.9.1). 10 μ L 0.5% formic acid was added to the peptides and the fractions were subsequently subjected to LC-ESI-MS/MS. LC separation on a CapLC system (Waters) was performed using a 120 min gradient (5-50% solution B in 89 min; solution A: 5% acetonitrile, 0.1% formic acid; solution B: 80% acetonitrile, 0.1% formic acid). The MS/MS analysis was performed online on a Q-TOF II mass spectrometer (Micromass).

Q-TOF data were processed using the proteinlynx globalserver (Waters/micromass). No background subtraction was performed on the collected MS/MS spectra. MS/MS ion database search was performed with MASCOT using the SWISSPROT database (release: 06/12/2005, 201594 entries, 13227 human sequences) selecting the enzyme trypsin and allowing one missed cleavage. The variable modifications were set to methionine oxidation, phosphoserine, phosphothreonine and phosphotyrosine. The peptide mass tolerance was set to ± 2 Da, and the fragment mass tolerance was set to ± 0.8 Da.

2.1.9.4.2 Mass measurement with the LTQ OrbitrapXL mass spectrometer

Bands corresponding to the radiolabelled proteins were excised from the dried coomassie-stained gels, washed 4 times for 15 min in 100 µl nanopure water under agitation and dehydrated in 100 µl of 40% acetonitrile (3 x 15 min) and airdried. Samples were subjected to tryptic proteolysis in 10 µl 1mM Tris-HCL pH 9.0 containing 0.01 µg/µL trypsin (Sequencing Grade Modified Trypsin; Promega) over night at 37°C. Peptide separation by nano HPLC was performed on an UltiMate3000 nano-LC system (Dionex Corporation, Sunnyvale, CA) equipped with a 75 µm C18 column. The mobile phases were 2% acetonitrile with 0.1% formic acid (solution A), and 80% acetonitrile with 0.1% formic acid (solution B). Peptides were separated by a gradient of 5–50% solution B over 30 min, followed by a gradient of 50–100% solution B over 5 min at a flow rate of 200 nL/min. Eluting peptides were identified online on an LTQ OrbitrapXL mass spectrometer (Thermo Scientific, Waltham, MA). One high resolution MS scan in the Orbitrap was followed by CID fragmentation and MS/MS analysis of the 5 most abundant peptides in the linear ion trap. For database-searching, tandem mass spectra were extracted, charge state deconvoluted and deisotoped by BioWorks version 3.3. All MS/MS samples were analyzed using Sequest (ThermoFinnigan, San Jose, CA; version SRF v. 5). Sequest was set up to search the uniprot/swissprot database (version 14, 392,667 entries) assuming the digestion enzyme trypsin. Sequest was searched with a fragment ion mass tolerance of 1.00 Da and a parent ion tolerance of 20 ppm. Oxidation of methionine and iodoacetamide derivative of cysteine were specified in Sequest as variable modifications.

2.1.9.5 Data processing and criteria for protein identification

The processing of spectra obtained with the 4700 Proteomics Analyzer was achieved with the software GPS Explorer™ Version 3.6 (Applied Biosystems). The combined MS and MS/MS spectra were searched against the Swiss-Prot and the NCBI nr database using an in-house version of Mascot (Version 2.0) search engine (Matrix Science Ltd.) with one miscleavage allowed. As taxon “mammalian” was chosen and as enzyme “trypsin”. Mass errors of 65 ppm for precursor ions and 0.3 Da for fragment ions were allowed. For MS/MS of peptides, further filtering criteria were applied; the maximum peptide rank was set at 3, and the minimum ion score was set at 30% confidence interval.

The GPS Explorer 3.6 software reports three different scores: 1) The mascot “best ion score”, i.e. the highest score of a single peptide; 2) a “total ion score”, i.e. the sum of all peptide scores of one protein; 3) and a “protein score” which includes a score for the peptide mass fingerprint in addition to the total ion score. Because different database search engines have different Mascot significance levels due to different database sizes and different numbers of masses submitted for search, MOWSE scores cannot be compared directly.

A protein was regarded as identified if the probability-based MOWSE protein score was above the 5% significance threshold for the respective database. To give an estimation statistically significant protein hits resulted in a “peptide score” for a given MS/MS spectra of > 20 and > 50 for a “protein score”.

The processing of spectra obtained with the LTQ OrbitrapXL mass spectrometer was achieved with the Scaffold (version Scaffold_2_00_06, Proteome Software Inc., Portland, OR) was used to validate MS/MS based peptide and protein identifications. Peptide identifications were accepted if they could be established at greater than 95.0% probability as specified by the Peptide Prophet algorithm (Keller et al., 2002). Protein identifications were accepted if they could be established at greater than 99.0% probability and contained at least 2 unique peptides. Protein probabilities were assigned by the Protein Prophet algorithm (Nesvizhskii et al., 2003).

2.2 Isolation of porcine rod outer segments.

For each preparation, 25 porcine eyes were obtained from a local slaughterhouse. In the case of dark-adapted retinæ, the eyes were immediately shielded from light by wrapping the flask in aluminium foil and all following steps were carried out under dim red light conditions (kinderman dukalux x-tronic 2580, 640 nm). The retinæ were dissected and ROS were isolated according to Molday with several modifications (Molday and Molday, 1987). The muscle tissue around the eyeball was removed and the eyeball was disinfected by subsequent incubation for 5 min on ice in 100% ethanol and mucasept disinfectant (Merz), respectively. The eyeballs were rinsed in CO₂-independent medium (Gibco) and cornea, lens and vitreous body were removed. The eyecup was immediately filled with cold CO₂-independent medium and the retina was dissected. The retinæ were collected in a 50 mL falcon tube containing 2 mL isolation medium (20% (w/v) sucrose, 20 mM Tris, 2 mM MgCl₂, 130 mM NaCl, pH 7.2) on ice. Retinæ were transferred to a 2 mL glass potter and ROS were detached from retinal tissue by gentle mechanical homogenization (7 strokes with a teflon pestle) and the homogenate was layered onto linear sucrose density gradients (27-50% sucrose in 5 mM Tris, 2 mM MgCl₂ and 130 mM NaCl, pH 7.2).

The linear sucrose density gradients were poured using 14 x 89 mm UZ tube (Beckman-Coulter) the day prior to the ROS isolation and stored at 4°C overnight. The gradient was formed using a gradient mixer (VWR). The two reservoirs of the gradient mixer were filled with 5.2 mL sucrose solution of 27% and 50% concentration, respectively and the gradient was poured by gravity flow under constant stirring. Air bubbles had to be carefully avoided.

After centrifugation in a Beckman SW41Ti-rotor for 1h at 180000 g and 4°C, purified ROS were collected from the sucrose gradient (see figure 18B), diluted with HBBS and pelleted by centrifugation (4500 g, 10 min, 4°C). Pellets were resuspended in cold isolation medium and protein content was determined by Bradford assay (see chapter 2.1.1). Samples were either used immediately for further experiments or snap-frozen with liquid nitrogen and stored at -80°C.

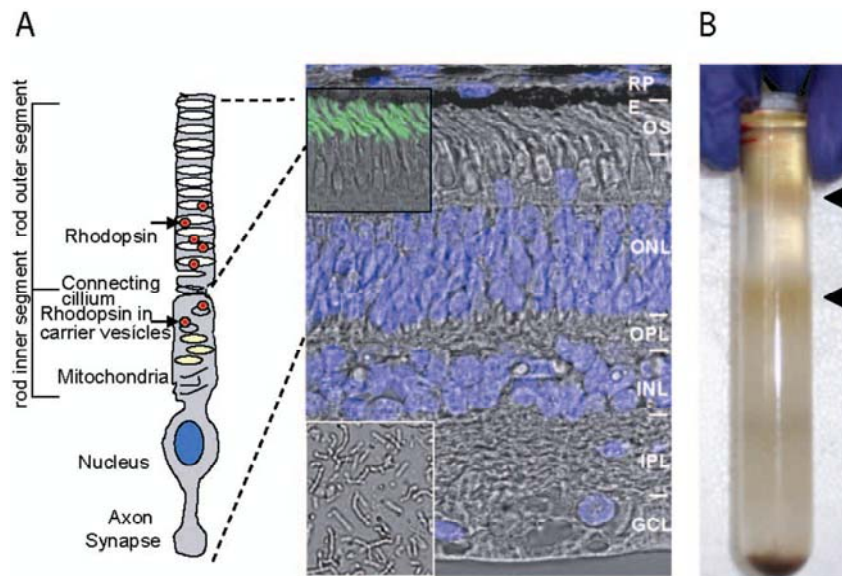


Figure 18: ROS isolation. **A)** left: schematic representation of rod photoreceptor. OS with stacks of discs membranes containing the visual pigment molecules; IS containing mitochondria, Golgi and ER membranes and vesicles where opsin molecules are assembled before they are transported to the OS; cell body with the nucleus and synaptic termini. Right: section of porcine retina (magnification 40X). Nuclei were labelled with DAPI (blue). Upper micrograph: immunolabelling of ROS with anti-rhodopsin (green). Lower micrograph: isolated ROS (magnification 40X). **B)** Sucrose gradient after ultracentrifugation with isolated ROS from light-adapted retina. Arrows indicate the two ROS containing bands that were collected.

2.3 PDE δ subunit activity assay

Recombinant PDE δ protein (rhPDE δ) was obtained from GenWay Biotech at a concentration of 0.7 $\mu\text{g}/\mu\text{L}$ in storage buffer (10 mM Tris, pH 8.0, 0.1% Triton X-100, 0.002% NaN_3 and 10 mM dithiothreitol). ROS (in isolation medium) corresponding to 100 μg protein were ruptured by three freeze-thaw-cycles with liquid nitrogen and centrifuged at 4°C for 30 min at 100000 g (Beckman Optima ultracentrifuge; Rotor TLA110). The resulting pellet, containing the membranous fraction, was resuspended in 100 μL incubation buffer (25 mM Hepes, 20 mM Tris-HCl, pH 7.5, 1 mM dithiothreitol, 1 mM MgCl_2 , 5 mM EDTA, 150 mM NaCl and protease inhibitor cocktail (Roche)) and incubated with different amounts (0, 0.5, 1, 2, 4, 6 and 8 μg) of rhPDE δ for 1h at 37°C in a horizontal shaker. To rule out any effect of Triton X-100 that was contained in the storage media of the recombinant PDE δ , all samples were adjusted to the same volume (volume of the sample with the highest PDE δ concentration used) with storage buffer. Samples were then separated into membrane and soluble fractions by centrifugation at 4°C for 30 min at 100000 g and analyzed by SDS-PAGE and Western blot using anti-Rac1 antibodies and anti-PDE β antibodies.

2.4 Light-dependent methylation of Rac1 in ROS and autoradiography

Two aliquots of light- and dark-adapted ROS (corresponding to 180 µg protein) were adjusted to a final volume of 100 µL with ROS-Buffer (20 mM MOPS, 2 mM MgCl₂, 60 mM KCl, 30 mM NaCl, pH 7.2 and protease inhibitors (Roche)). In the case of dark-adapted ROS, all following steps were carried out under dim red light conditions (see chapter 2.2). Following addition of 3 µL ³H -S-Adenosyl methionine (SAM) (GE Healthcare; 0.03 mCi/mL), the light-adapted sample was incubated for 1 h at 30°C in a horizontal shaker in the light. The dark-adapted sample was incubated accordingly in the dark. After centrifugation at 5000 g for 5 min the pelleted ROS were subjected to hypotonic lysis with 10 mM Tris pH 7.4 for 10 min on ice. The membranous fraction was separated from the soluble fraction by centrifugation at 16000 g for 10 min and resuspended in 60 µL of ROS-Buffer. Both fractions were incubated with Laemi-buffer for 15 min at RT, loaded onto 9-15% gels and resolved by SDS-PAGE (BioRad ProteanII). The gels were stained with Coomassie blue (see 2.1.6.2) and soaked in Amplify (GE Healthcare) for fluorography. Gels were dried and exposed to films (HyperfilmTM ECL; GE Healthcare) at -80°C for 7 days.

2.4.1 Immunoprecipitation of methylated Rac1.

Light-adapted ROS corresponding to 400 µg protein were subjected to *in vitro* methylation with 10 µL ³H-SAM as described above. After incubation of the sample for 1 h at 30°C in a horizontal shaker, ROS were pelleted by centrifugation at 5000 g for 5 min and subjected to hypotonic lysis with 10 mM Tris pH 7.4. Membranous and soluble fractions were obtained as described in chapter 2.1.3.2. Both fractions were adjusted to 400 µL with IP-buffer (150 mM NaCl, 1 mM EDTA, 20 mM Tris pH 7.4 and protease inhibitors (Roche)) and solubilized for 10 min on ice with 1% β-dodecylmaltoside. Unsolubilized material was removed by centrifugation for at 4°C for 10 min at 16000 g and methylated Rac1 was immunoprecipitated with anti-Rac1 antibodies (Upstate) at a concentration of 1.4 µg per 100 µg protein for 1 h at RT under agitation. Protein-G-Agarose was subsequently added for 30 min and proteins were eluted with Laemi-buffer. In parallel, 180 µg light adapted ROS were subjected to *in vitro* methylation as described before. Both Samples were resolved on 9-15% gels by SDS-PAGE, stained with Coomassie blue and soaked in Amplify (GE Healthcare) for fluorography. Gels were dried and exposed to film (HyperfilmTM ECL; GE Healthcare) at -80°C for 7 days.

2.4.2 Identification of methylated ROS proteins by mass spectrometry.

Bands corresponding to the methylated proteins on the radiography were excised from the dried coomassie-stained gels, digested (as described in 2.1.9.1.1) and subjected to analysis by mass spectrometry. LC-MS/MS-analysis was performed on a LTQ OrbitrapXL mass spectrometer as described in (chapter 2.1.9.4.2).

2.5 Immunohistochemistry

Light- and dark-adapted porcine eyes were cut along the median, cornea, lens and vitreous body were removed. The retina, still attached to the sclera, was cut in 0.5 x 0.5 cm pieces and immersion-fixed for 1 h at 4°C in 4% paraformaldehyde in PBS. The fixed retina was cryoprotected by consecutive incubation at 4°C in 5%, 10% (1h each) and 20% sucrose in PBS overnight. The cryoprotected retina was carefully removed from the sclera, embedded in tissue freezing media (Polyscience). Cut in 12 µm sections on a Cryostat HM560 (Microm AG) and transferred to glass slides. The sections were incubated with blocking reagent (3% goat serum (PAA Laboratories) in PBS with 0.1% Tween20) for 30 min and primary antibodies were applied in a humidified chamber overnight at 4°C. The sections were incubated with anti-PDEδ (Sigma) and anti-Rac1 (BD) primary antibodies overnight. Alexa-coupled secondary antibodies were applied at RT for 1 h along with DAPI in a 1:500 dilution (for dilutions of the antibodies see chapter 1.5.4). The sections were mounted with FluorSafe (Calbiochem) and examined by using a Zeiss ApoTome™ with AxioCam HRc.

2.6 Molecular biology

2.6.1 *E. coli* cultures

2.6.1.1 Liquid cultures

LB medium (Luria-Bertani; 1% (w/v) tryptone, 0.5% (w/v) yeast extract, 1% (w/v) NaCl, pH 7.0) was supplemented with appropriate antibiotics and inoculated either with an *E. coli* colony (grown overnight on LB plates) or with small amounts of an *E. coli* cryo culture. Inoculated cultures were grown overnight at 37°C under shaking with 130 rpm in baffled flasks or with 225 rpm in 14 mL Falcon tubes.

2.6.1.2 Plating cultures

Plating cultures were plated out from cryo cultures onto LB plates (LB medium with 1.5 (w/v) agar supplemented with the appropriate antibiotics). Plates were incubated overnight at 37°C and stored at 4°C.

2.6.1.3 Cryo cultures

500 µL of an overnight *E. coli* culture was mixed with 500 µL 80% (v/v) glycerol. Cryo cultures were stored at -80°C.

2.6.1.4 Generation of chemically competent *E. coli*

E. coli competent for chemical transformation according to the rubidium chloride (RbCl₂) method were generated from the *E. coli* strains BL21 (Invitrogen) and TOP10 (Invitrogen). BL21 and TOP10 cryo cultures were plated out on LB plates without antibiotics and incubated overnight at 37°C. A single colony was expanded in 2.5 mL LB medium overnight at 37°C in a 14 mL Falcon tube under shaking with 225 rpm. The overnight culture was diluted 1:100 in LB medium supplemented with 20 mM MgSO₄. The culture was grown to an optical density (OD₆₀₀) of 0.4 to 0.6 and centrifuged (5 min, 10000 g, 4°C). The cell pellet was then gently resuspended in 100 µL ice-cold TFB1 buffer (30 mM potassium acetate, 100 mM RbCl₂, 10 mM CaCl₂, 50 mM MnCl₂, 15% (v/v) glycerol, pH 5.8) and incubated on ice for 5 min. The suspension was centrifuged (5 min, 10000 g, 4°C), and the cell pellet was gently resuspended in 10 mL TFB2 buffer (10 mM MOPS [3-(*N*-morpholino)propanesulfonic acid], 75 mM CaCl₂, 10 mM RbCl₂, 15% (v/v) glycerol, pH 6.5). The suspension was incubated on ice for 15 to 60 min, portioned in 100 µL aliquots and then shock frozen with liquid nitrogen. Competent bacteria were stored at -80°C.

2.6.2 Chemical transformation of *E. coli*

Chemically competent *E. coli* were slowly thawed on ice. 10 ng of plasmid DNA (see chapter 2.6.3) were gently mixed with a 100 μ L aliquot of competent *E. coli*. Incubation for 60 min on ice was followed by a heat shock treatment at 42°C for 45 sec and a short incubation on ice. The heat shock initiated the incorporation of DNA-salt complexes into the bacteria. 600 μ L SOC medium without antibiotics (2% (w/v) tryptone, 0.5% (w/v) yeast extract, 0.05% (w/v) NaCl, 20 mM glucose) was added and the *E. coli* were grown for 1h at 37°C under shaking with 225 rpm. The *E. coli* were sedimented (1 min, 16000 g, RT). 400 μ L of the supernatant were discarded and the pellet was gently resuspended in the remaining supernatant and plated onto a LB plate supplemented with appropriate antibiotics. The LB plate was incubated overnight at 37°C. Single colonies were expanded in LB medium supplemented with the appropriate antibiotic. Cultures were subsequently used for plasmid preparation (see chapter 2.6.3) and cryo cultures (see chapter 2.6.1.3).

2.6.3 Plasmid DNA preparation

Single transformed *E. coli* colonies (see chapter 2.6.2) were expanded in LB medium supplemented with appropriate antibiotics. When applying the QIAprep Spin Plasmid Miniprep Kit (Qiagen), 2-5 mL of an overnight culture were sedimented (10 min, 10000 g, RT) and the pellets were used for plasmid DNA preparation according to manufacturer's protocol. For preparative purposes, the QIAprep Spin Plasmid Midiprep Kit (Qiagen) was used. 50-200 mL of an overnight culture was sedimented (10 min, 10000 g, RT) and the pellets were used for preparation of plasmid DNA as described in the manufacturer's protocol. Both kits are based on the alkaline lysis of *E. coli* and on the subsequent binding of plasmid DNA to DNA-binding columns. The concentration and purity of plasmid DNA preparations was determined photometrically. 200 μ L of a 1:100 to 1:200 dilution of plasmid DNA in ddH₂O were pipetted into a quartz cuvette and the absorption at 260 and 280 nm was measured with an Ultraspec 3300 pro photometer (GE Healthcare). A 260 nm/280 nm absorption ratio of 1.8 indicated a pure DNA preparation. DNA concentration was determined as follows: DNA concentration [μ g/] = absorption at 260 nm x 50 x dilution factor.

2.6.4 DNA sequencing

DNA sequencing was performed in a capillary-based automated sequencer (ABI Prism 3100 Genetic Analyzer, Applied Biosystems) after a cycle-sequence reaction using the BigDye-Terminator v3.1 Cycle Sequencing Kit (Applied Biosystems). Here, the DNA template was amplified linearly by a DNA polymerase using a sequence-specific primer (Zimmermann, 2006). The dNTP mixture is supplemented with dideoxynucleotides (ddNTPs), tagged with four different fluorescence labels referring to the four different bases (A, T, G, C). Upon incorporation of a ddNTP, the extension of the DNA stretch was prohibited, resulting in a DNA fragment with a certain length labeled with a base-specific fluorescence tag. The mixture of labeled DNA fragments generated during the cycle process were separated according to the fragment length using capillary electrophoresis and analyzed for their tag. From these data the DNA sequence can be delineated. 200 ng of plasmid-DNA template were mixed with 2 μ L BigDye Terminator Mix containing the DNA polymerase and the fluorescence-labeled dideoxynucleotides, 0.5 μ L primer (10 pmol/ μ L) and ddH₂O up to an end volume of 10 μ L. Oligonucleotides used as primer for sequencing should have a melting temperature of about 50°C.

The PCR DNA Engine Tetrad Gradient Cycler PTC-225 (MJ Research, BioRad) was used with the following cycling program with 30 cycles from step 2 to 4:

1. 96°C 2 min for first denaturation of the double-stranded DNA template
2. 96°C 30 sec for denaturation of the DNA template
3. 50°C 15 sec for annealing of the primer to the DNA template
4. 60°C 4 min for elongation of the primer catalyzed by the polymerase
5. 60°C 4 min for final elongation

After the cycle-sequence reaction, the DNA was precipitated by adding 8 μ L HPLC-grade H₂O and 32 μ L 95% (v/v) ethanol (p.A.). After 15 min incubation at RT in the dark, the reaction mixtures were centrifuged (15 min, 16000 g, RT). The DNA pellet was then washed in 200 μ L 70% (v/v) ethanol in HPLC-grade H₂O and centrifuged (10 min, 16000 g, RT). The DNA pellet was dried at RT and dissolved in 75 μ L HPLC-grade H₂O. 25 μ L of the dissolved DNA was transferred onto a microtiter plate, which was placed into the automated sequencer. The resulting data were analyzed using ContigExpress in the Vector NTI Suite 9.0 software package (Invitrogen).

2.6.5 Agarose gel electrophoresis

DNA fragments were separated, identified and purified by agarose gel electrophoresis. 1% (w/v) DNA agarose (Biozym, Oldendorf, Germany) in TAE buffer (40 mM Tris-acetate, 1 mM ethylenediaminetetraacetate (EDTA), pH 8.0) was dissolved by boiling in a microwave. The agarose solution supplemented with 0.5 µg/mL of the fluorescent DNA-intercalating ethidium bromide was poured into the gel trays (gel trays for SubCell GT chambers, BioRad) and the combs were inserted. After solidification of the gels, combs were removed and the trays were put into the electrophoresis chamber (SubCell GT chambers, BioRad) and gels were overlaid with TAE buffer. DNA samples were treated with gel loading buffer (6x: 0.25% (w/v) bromophenol blue, 40% (w/v) sucrose) and loaded onto the gel. Electrophoresis was performed with 50-100 V until the bromophenol blue dye front reached the end of the gel. DNA fragments were visualized by an UV transilluminator (Herolab). To determine the size of the DNA fragments a 1 kb and a 100 bp DNA standard (New England Biolabs) were used. For purification, DNA fragments were excised with a scalpel and eluted from the gel plugs by the QIAquick Gel Extraction Kit (Qiagen) according to the manufacturer's protocol.

2.6.6 Polymerase chain reaction (PCR)

PCR was done essentially according to a standard procedure (Saiki et al., 1988). Here, the DNA template is amplified exponentially by a DNA polymerase using two sequence specific primers that bind to the sense and antisense strand of the DNA template, respectively. Oligonucleotides used as primers are described in 1.4.4 (Tables 3 and 4). The reaction mixture (20 µL) contained 50-200 ng cDNA template, 10 µL 5 x Phusion HF buffer (containing 1.5 mM MgCl₂; New England Biolabs), 200 µM dNTPs each, 0.5 µM sense and 0.5 µM antisense oligonucleotide primers and 0.5 µL Phusion DNA polymerase (corresponding to 1 U; New England Biolabs) in ddH₂O. PCR reaction was performed in a thermal cycler (PCR DNA Engine Tetrad Gradient Cycler PTC-225, MJ Research, BioRad) with the following amplification program:

1. 96°C 1 min for first denaturation of the double-stranded DNA template
2. 96°C 30 sec for denaturation of the DNA template
3. (*)°C 30 sec for annealing of the primer to the DNA template
4. 72°C (**)
sec for elongation of the primer catalyzed by the polymerase
5. 72°C 5 min for final elongation

The amplification stage comprised 30 cycles from step 2 to 4. The annealing temperature (*) was set as the mean value of the melting temperatures of sense and antisense primers. Sense

and antisense primers were designed with the Vector NTI Suite 9.0 software so that (i) the melting temperatures of the primer was between 50°C and 65°C, (ii) the difference in the melting temperatures of the chosen primer was below 3°C and (iii) hairpin structures and dimerization were unfavorable. The time required for elongation (***) depended on the length of the desired PCR product. For Phusion DNA polymerase 1 min elongation was sufficient for a 1 kb PCR fragment.

2.6.7 Gateway cloning

The Gateway cloning system (Invitrogen) is based on site-specific recombination mediated by the λ integrase family of recombinases (Hartley et al., 2000). It allows fast and easy cloning of inserts, a prerequisite for the generation of larger numbers of expression vectors. The Gateway system consists of two classes of vectors, the Donor and the Destination Vectors. The Donor Vectors are used for the generation of generic Entry Clones, which contain the coding sequence of proteins of interest. The Entry Clones are recombined with Destination Vectors in order to obtain specific expression constructs (Destination Clones).

In the presented Gateway cloning strategy, the open reading frames of the protein of interest were first amplified by PCR. The PCR primers contain the *attB*1/2 recombination sites in order to allow a recombination with the pDONR201 plasmid for the generation of an Entry Clone in the LR reaction. Since the *attB* sites are quite long (29 bp), a two step PCR strategy is advantageous. In the first PCR, half of the needed *attB* sites are attached to the primers. In the second PCR, generic *attB*1/2 primers for all constructs are used to complete the *attB* sites (see Figure 19 B). The Entry Clones were then recombined with the appropriate destination plasmid; pDEST N-SF-TAP or pDEST C-SF-TAP, to obtain the destination expression clone. An overview of the Gateway cloning strategy is shown in Figure 19A. Note: the Donor Vectors as well as the Destination Vectors contain *ccdB* marker for negative selection to avoid background caused by empty pDONR and pDEST vectors in the BP and LR reactions, respectively. The *ccdB* gene is toxic for E. coli K12 strains like DH5 α . Only strains containing the *ccdB* survival T1^R strain (Invitrogen), can be used for amplification of these plasmids (Gloeckner, in press).

Gene specific primers were designed for the open reading frame of interest flanked by *attB* linker sequences (see Figure 14 B). For N-terminal fusion constructs, the correct open reading frame has to be considered. For C-terminal fusion constructs, an appropriate stop codon has to be inserted into the reverse primer; the forward primer should contain Kozak sequence.

For the first PCR; 5 μ L HF-Reaction Buffer and 0.5 μ L dNTP mix (both provided with the polymerase Kit) were mixed with 1.3 μ L forward/reverse (each) gene specific primer stocks (810 μ M), X μ L template (5-10 ng) and 0.5 μ L Phusion polymerase. The total volume was adjusted with water to a total volume of 25 μ L.

The following program for the thermocycler was used:

1 cycle: 98°C/1 min
10 cycles: 96°C/ 20 sec
55°C/ 40 sec
72°C/ 1 min per kB insert size

For the second PCR; to 10 μ L of the first PCR reaction 10 μ L HF-Reaction Buffer and 0.5 μ L dNTP mix (both provided with the polymerase kit) were added as well as 1.5 μ L of *attB1* and *attB2* primer stocks (10 μ M) and 1 μ L Phusion polymerase. The total volume was adjusted with water to a total volume of 50 μ L.

The following PCR program for the thermocycler was used:

1 cycle: 98°C/1 min
10 cycles: 96°C/ 20 sec
55°C/ 40 sec
72°C/ 1 min per kB insert size
20 cycles: 95°C/ 20 sec
55°C/ 40 sec
72°C/ 1 min per kB insert size

The PCR product was checked by agarose gel electrophoresis (see chapter 2.6.5).

For the BP reaction, 3 μ L PCR product was added to 1 μ L pDONR201 plasmid (90 ng/ μ L) and 1 μ L BP Clonase Mix II (Invitrogen). Following incubation for 1-3h at 25°C, 0.5 μ L Proteinase K was added and the reaction mix was incubated for 10 min at 37°C.

5 μ L of the BP reaction was transformed into DH5 α cells (see chapter 2.6.2) and the cells were plated onto LB kanamycin agar plates. Clones were collected and inoculated with 5 μ L (LB kanamycin). Entry clone plasmids were isolated from overnight cultures (see chapter 2.6.3) and the inserts were verified by sequencing (see chapter 2.6.4).

For the LR reaction, 1 μ L Entry plasmid (90 ng/ μ L) was added to 2 μ L 10 mM Tris-HCL pH 8.0, 1 μ L pDEST/(N-or C-) SF-TAP plasmid (90 ng/ μ L) and 1 μ L LR Clonase Mix II (Invitrogen). Following incubation for 1-3h at 25°C, the reaction was stopped by addition of 0.5 μ L Proteinase K and incubation for 10 min at 37°C

5 μL of the LR reaction was transformed into DH5 α cells (see chapter chapter 2.6.2). The cells were plated onto LB ampicillin agar plates. 5 μL (LB ampicillin) overnight cultures were inoculated with collected clones and plasmids were isolated (see chapter 2.6.3). Inserts were verified by sequencing (see chapter 2.6.4).

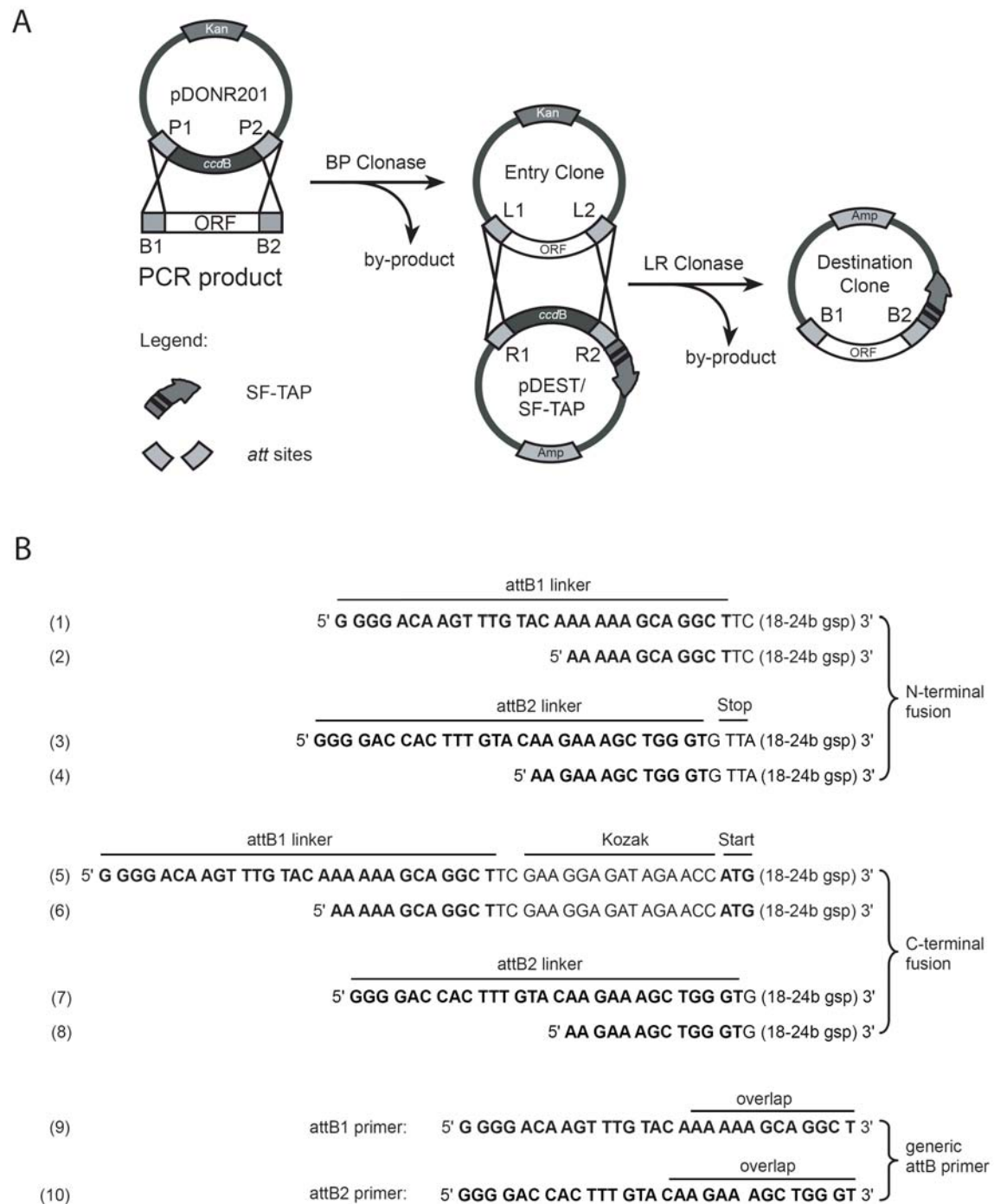


Figure 19: Overview of the Gateway cloning strategy (Gloeckner, in press). **A**) Schematic overview of the BP and LR reaction. BP-reaction: Product of the second PCR (containing *attB1/B2* sites) was recombined with the *attP1/P2* sites of the pDONR201 vector creating Entry clones (containing *attL1/L2* sites) for recombination with the SF-TAP Destination Vectors (containing *attR1/R2* sites) in the LR reaction. **B**) Primers used for the PCR steps preceding the BP reaction. *attB1/B2* linker sequences were attached to the 5' end of gene specific primers (Martin et al.). N-terminal SF-TAP tag fusion products (primers 1)-4): Forward primer 1) and 2): Two nucleotides had been inserted after the *attB1* linker (bold) for in frame cloning. Reverse primer 3) and 4): a stop codon had been introduced. C-terminal SF-TAP tag fusion products (primers 5)-8): Forward primer 5) and 6): a Kozak sequence including a start codon had been introduced after the *attB1* site. Reverse primer 7) and 8): one nucleotide had been inserted after the *attB2* linker (bold) for in frame cloning. A two-step PCR strategy is recommended for efficient PCR amplification. The *attB* sites partially attached to the 5'-end of the gene-specific primers 2)/4) and 6)/8) were used in the first amplification step. The second PCR restores full *attB* sites by generic primers 9)/10) which overlaps with the 5'-overhang of the gene-specific primers. The overlapping sequence is indicated.

2.7 Establishment of an organotypical retinal explant system from murine retina

2.7.1 Culturing of retinal explants

The preparation of a nutrient medium that reflects as closely as possible the *in vivo* chemical milieu of the tissue to be cultured and the creation of culture conditions that supply sufficient anabolites by simple diffusion and remove catabolites from the tissue's immediate environment, are critical steps in the course of *in vitro* studies of organotypical primary cultures. This led to the development of serum-free, chemically-defined growth media capable of long-term culturing of nerve tissues. The use of serum was to be avoided because it contains all kinds of general nutrients, hormones, and growth factors, as well as inhibitory and toxic agents. A second disadvantage in the use of serum is the frequent variation in growth-promoting properties between different serum batches, which makes it impossible to conduct reproducible, quantitative studies. Finally, when using a serum-supplemented medium, it is very difficult to purify and analyze factors synthesized by the cells and released into the nutrient medium. The R16 nutrient medium, which represents the basis for the retinal explant medium, was primarily developed for the growth and differentiation of neonatal rat neocortex tissue (Romijn, 1988), and optimized by Caffè and colleagues for the culturing of retinal explants (Caffè et al., 1989). The complete list of chemicals making up the R16 nutrient media is shown in tables 15, 16 and 17. The R16 Powder Medium was manufactured by Invitrogen. The R16 Powder Medium was used as basis for the preparation of R16 Basal or R16 Complete medium, respectively. The R16 Complete medium is composed of 63 ingredients that can arbitrarily be divided into three groups. Group 1 consists of salts, group 2 includes amino acids except for the potentially neurotoxic amino acids glutamate and aspartate. Group 3 includes sugars and vitamins.

Table 15: Composition of R16 Powder medium (Invitrogen):

Ingredients	mg/Liter	mM
Glucose	3446	19.1
D(+)-Galactose	15	0.83
D(+)-Mannose	10	0.56
L-Alanine	2.01	0.023
L-Arginine	104.12	0.494
L-Asparagine	3.38	0.023
L-Cystine	38.33	0.134
L-Glycine	21.94	0.292
L-Histidine	33.07	0.158
L-Isoleucine	71.63	0.546
L-Leucine	73.70	0.562
L-Lysine	106.90	0.585
L-Methionine	21.25	0.142
L-Phenylalanine	45.67	0.276
L-Proline	7.78	0.068
L-Serine	30.72	0.292
L-Threonine	66.94	0.562
L-Tryptophan	11.26	0.055
L-Tyrosine	49.82	0.275
L-Valine	65.82	0.562
Choline chloride	6.07	0.0435
Purescine	16.11	0.18
L-Carnitine	2.0	0.0124
Sodium phenole red	5.0	
NaHCO ₃	2762.1	0.0329
NaH ₂ PO ₄ x 2 H ₂ O	95.38	0.00061
Na ₂ HPO ₂	31.95	0.00023
ZnSO ₄ x 7 H ₂ O	0.20	0.0007

Table 16: Additives to R16 Powder medium for Basal media:

Ingredients	mg/liter	mM
Ethanolamine	1	0.0164
Biotin (vitamin H)	0.1	0.00041
CuSO ₄ x 5 H ₂ O	0.0025	0.00001
MnCl ₂ x 4 H ₂ O	0.001	0.000005
Na ₂ SeO ₃ x 5 H ₂ O	0.0079	0.00003

Table 17: Additives to R16 Powder medium for Complete media:

Ingredients	mg/liter	mM
Albumin	2600	0.04
Sodium pyruvate	50	0.45
L-Cysteine HCl	7.09	0.045
L-Glutamine	25	0.171
Glutathione	1.0	0.00325
Transferrin	10	0.00013
Retinol (vitamin A)	0.1	0.00035
Retinyl acetate	0.1	0.00030
Thiamine HCl	2.77	0.00821
Vitamin B12	0.31	0.00023
Ascorbic acid (Vitamin C)	100	0.580
DL- α -tocopherol (Vitamin E)	1.0	0.00232
DL- α -tocopheryl acetate	1.0	0.00212
Linoleic acid	1.0	0.00356
Linolenic acid	1.0	0.00359
Thioctic acid	0.045	0.00022
Progesterone	0.0063	0.00002
Triiodothyronine (T3)	0.002	0.000003
Corticosterone	0.02	0.000058
Insuline	2.0	0.00033
CaCl ₂ x 2 H ₂ O	188.74	0.00128
Fe(NO ₃) ₃ x 9 H ₂ O	0.068	0.000017
FeSO ₄ x 7 H ₂ O	0.19	0.00068
KCl	320.34	0.00429
MgSO ₄ x 7 H ₂ O	168.27	0.00068
NaCl	6030	0.103
NaHCO ₃	2762.1	0.0329
NaH ₂ PO ₄ x 2 H ₂ O	95.38	0.00061
Na ₂ HPO ₂	31.95	0.00023
ZnSO ₄ x 7 H ₂ O	0.20	0.0007

For the preparation of R16 Basal medium one vial of the R16 powder media was dissolved in 800 mL ddH₂O and additives for Basal media (see table 16) were added. The media was filtered with a Steritop-GP filter unit (0.22 μ m; Millipore) and the volume was adjusted to 1 L with sterile ddH₂O. For the preparation of Complete media, the Basal media was supplemented with required additives (see table 17) and filtered with a Steritop-GP filter unit. The media was stored for up to 4 weeks at 4°C.

In order to have an accessible model to study changes in the mouse retina due to application of Rho-kinase inhibitors, the organotypical retinal explant system from murine retina was

established in our laboratory (according to (Caffe et al., 1993), (Soderpalm et al., 1994), (Soderpalm et al., 1999), (Soderpalm et al., 2000)).

For preparation of the explant culture, C57/BL6 mice were sacrificed at postnatal day (PN) 7 by decapitation. The heads were wiped clean with a tissue soaked in 70% EtOH. The eyes were enucleated and incubated for 15 min in R16 Basal media containing 1.2% Proteinase K (MP Biomedicals) at 37°C. The Proteinase K activity was inhibited by rinsing the eyes in 10% FCS in R16 Basal media. All preparative steps were performed in a Petri dish with R16 Basal media under a binocular.

All additional tissues, like tendons and muscles, were carefully removed from the eyeball with a small scissor and straight forceps (FST). The anterior segment, the vitreous body and the sclera were removed and the retina together with attached RPE was flat mounted with the photoreceptor side facing down on the culture plate insert (Millipore) (see Figure 20) and the explants were cultured for 8 days in 6-well culture dishes containing 1.5 mL R16 complete media changing the media every 48h.

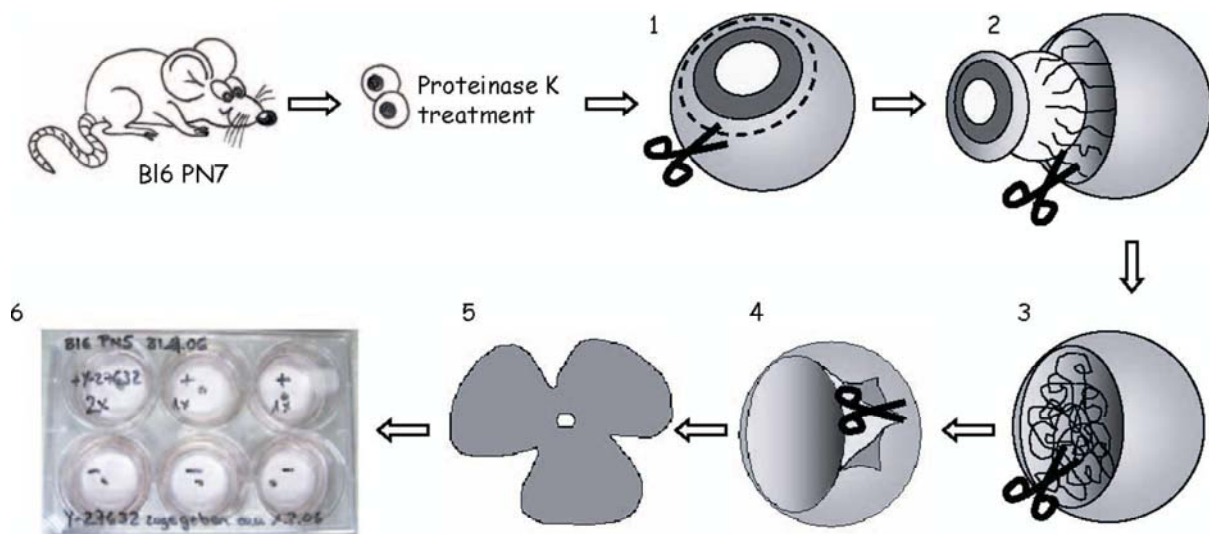


Figure 20: Steps in preparation of an organotypical explant culture from postnatal murine eyes (PN7). 1) After proteinase K treatment of the eyes, an incision around the cornea was made with a small scissor and 2) cornea, lens and vitreous body were removed from the eyeball by carefully cutting all the small blood vessels connected to the vitreous body and the retina. 3) After removal of the vitreous body, the remains of the small blood vessels were removed from inside the eyeball. 4) The sclera was carefully removed from the RPE. 5) The retina together with attached RPE was flat mounted with the photoreceptor side facing down on the culture plate insert. The explants were cultured for 8 days in 6-well culture dishes containing 1.5 R16 Complete medium.

For Rho-Kinase inhibition experiments, Rho-Kinase inhibitor Y-27632 (Calbiochem) was applied to the explant cultures from the first day in culture on, in a concentration of 5 μ M in

Complete media. Media containing the Rho-Kinase inhibitor was changed every 48 h and explants were cultured for 8 days.

In the present study all explants were cultured up to a postnatal age of 15 days, meaning that the PN7 tissue was maintained for 8 days *in vitro* (PN7 + div8).

2.7.2 Analysis of explant cultures

2.7.2.1 Tissue analysis

Explants were immersion-fixed for 15 min at RT in 4% paraformaldehyd in PBS (Gibco). The fixed retina was cryoprotected by consecutive incubation at RT in 5% and 10% sucrose in PBS (1 h each) and at 4°C in 20% sucrose overnight. The part of the filter containing the cryoprotected retina was carefully excised and the retina still attached to the piece of filter, was embedded in tissue freezing media (Polyscience), cut in 12 µm sections and transferred onto glass slides. The sections were incubated in blocking reagent (3% goat serum (PAA Laboratories) in PBST (PBS with 0.1% Tween20) for 30 min and primary antibodies were applied in a humidified chamber overnight at 4°C. The following antibodies were used in concentrations as specified in table 8: anti-arrestin, anti-rhodopsin, anti-syntaxin, anti-RhoA, anti-CRMP2, anti-tubulin, anti-Rock II, anti-GFAP, anti-PKC, anti-GS, anti-tubulin and alexa 568 coupled phalloidin. Alexa-coupled secondary antibodies (see table 9) were applied at RT for 1h in a 1:1000 dilution along with DAPI in a 1:500 dilution. The sections were mounted with FluorSafe (Calbiochem). Images were obtained by fluorescence microscopy using fluorescein isothiocyanate (FITC), Rhodamine, DAPI and Nomarski optical filter sets (40x/0.75, Axioskop 2, AxioCam HRc, AxioVision 4, Zeiss, Göttingen, Germany) and adjusted using the AxioVision 4 software package.

2.7.2.2 Test for apoptosis - TUNEL assay

The T4 terminal deoxynucleotidyl transferase-mediated dUTP nick end labeling (TUNEL) assay was used to visualize DNA fragmentation, a late marker of apoptosis. DNA fragmentation leads to free 3'-OH groups that are recognized by the enzyme T4 terminal deoxynucleotidyl transferase, which attaches fluorescence-labeled dUTPs, resulting in fluorescence-labeled DNA fragments in the nuclei. TUNEL reaction was performed using the *in situ* cell death detection kit (Roche Applied Sciences) and Chromatide Bodipy™ FL-dUTP (Molecular Probes, Invitrogen) as fluorescence-labeled dUTP.

Cryosections of retinal explants (as described in 2.7.2.1) were washed two times in PBS and incubated for 2 min with cold permeabilization solution (0.1% Triton X-100, 0.1% (w/v) sodium citrate, freshly prepared).

After removal of permeabilization solution, cells were washed twice with 50 μ L PBS at RT. TUNEL reaction was induced by adding 30 μ L TUNEL reaction mix (enzyme solution (Roche) and Chromatide BodipyTM FL-dUTP (Molecular Probes) diluted 1:10 and 1:100 with label solution (Roche), respectively) per sample. Following incubation for 1 h at 37°C under humidified conditions, the slides were washed six times with 50 μ L PBST per sample. The slides were embedded in one droplet FluorSave (Calbiochem, VWR) and stored at 4°C overnight. Images were obtained by fluorescence microscopy using a fluorescein isothiocyanate (FITC) and Nomarski optical filter sets (40x/0.75, Axioskop 2, AxioCam HRc, AxioVision 4, Zeiss, Göttingen, Germany) and adjusted using the AxioVision 4 software package. As positive control, cryosections were treated with 50 μ L *DNaseI* (1 mg/mL *DNaseI* in DMEM/0.1 (w/v) BSA) prior to the TUNEL reaction. As negative control, TUNEL reaction was performed without T4 terminal deoxynucleotidyl transferase.

2.8 Production of rat and mouse monoclonal CRMP2 specific antibodies

Animals produce antibodies in response to proteins or other molecules recognized as foreign by their immune system (antigens). The antibodies are secreted into the plasma by B cells that are able to interact with the immunogen. Several factors determine the intensity of the immune response including the size of the antigen, its chemical characteristics, and how foreign it is to the animal. Because the antibody response increases with repeated exposure to the antigen, the production of monoclonal antibodies against a certain protein requires the repeated immunization of an animal with a specific antigen. This antigen can be the whole CRMP2 protein or a CRMP2 specific peptide. Peptide antigens have the advantage that the generated antibodies can be targeted to unique sequence regions of the protein. This is especially useful when proteins like CRMP2 are investigated that belong to families of high sequence homology. A disadvantage of peptide antibodies is that they recognize linear epitopes but it is not certain that they will also recognize the native protein.

To increase the intensity of the immune response, antigens are combined with complex mixtures called adjuvants. The mixtures contain agents like mineral salts, oil emulsions (*e.g.* incomplete Freund's adjuvants (IFA)), and synthetic (*e.g.* synthetic oligodeoxynucleotides containing unmethylated CpG motifs (like CPG 2006)) or microbacterial products that enhance the immune response without generating unwanted antibodies against components of

the adjuvants. Because peptides are small molecules, whose immunogenic strength is weak and mostly elicit a weak immune response, coupling to carrier proteins is important. The most commonly selected carrier is Keyhole limpet hemocyanin (KLH), a respiratory protein found in mollusks. Its large size makes it very immunogenic and its phylogenetic separation between mammals and mollusks increases the immunogenicity and reduces the risk of cross-reactivity between antibodies against the KLH carrier and naturally occurring proteins in mammalian samples. Ovalbumin (OVA) is another useful carrier protein. I was used to couple the peptide antigens to the 96 well target plates in enzyme-linked immunosorbent assay (ELISA) screens to test if the antibodies were specific for the peptide alone and not the carrier.

2.8.1 Peptide selection

Selected peptides for the generation of protein specific antibodies should fulfill following requirements: 1) The selected amino acid sequences should provide soluble peptides under the experimental conditions. 2) Epitopes from solvent-exposed regions on the surface of the protein should be chosen. Here, computer algorithms that predict predominantly hydrophilic and hydrophobic portions of polypeptides, helping to identify solvent-exposed regions of the protein are useful for epitope selection from protein sequences (*e.g.* <http://www.predictprotein.org>). 3) The desired antigen should not share by chance a region of homology or identity with a sequence of a unrelated protein. Searching databases using Web-based protocols such as BLAST (<http://blast.ncbi.nlm.nih.gov/Blast.cgi>) can help to prevent this occurrence. When designing sequence specific antibodies to a member of a protein family, it is necessary to determine a peptide sequence that is unique to the selected family member. Specialized programs (like Vector NTI; Invitrogen) facilitate the alignment of the amino acid sequences of multiple members of a protein family. Sequences of functional domains common or distinct to several related polypeptides can be highlighted. This alignment enables the identification of sequences that are specific to a single member of the family and may be suitable for the development of specific antibodies.

For selection of collapsing response mediator protein 2 (CRMP2) specific peptides for the antibody generation, the human protein sequences of the CRMP-family proteins were aligned (using Vector NTI; Invitrogen) (see Figure 21). Two amino acid sequences from different regions of the protein were chosen (see Figure 21 and Table 18).

Table18: Peptide antigens used for immunization

Name	Antigen/epitope	Antigen-sequence	length
Beer1	aa 486-528; C-terminus	C ⁴⁶⁸ SRLAELRGVPRGLYDGPVCEVSVTPKTVTPASSAKTSPAKQQA ⁵²⁸	42aa
Beer4	aa 147-161; N-terminus	C ¹⁴⁷ GIQEEMEALVKDHGV ¹⁶¹	15aa

All peptides were synthesized and coupled to the carrier proteins KLH or OVA, respectively, by Rackwitz Peptide Specialty Service (Heidelberg). All rat and mouse monoclonal peptide antibodies were produced in cooperation with Dr. Elisabeth Kremmer according to standard procedures. Shortly, rats and mice were immunized with 50 µg peptide-KLH using CPG 2006 and IFA as adjuvants.

When a sufficient antibody titer was reached in the serum, immunized mice and rats were euthanized. The spleen was removed to use as a source of immune cells for fusion with myeloma cells resulting in immortal hybridoma cells. Hybridoma cells were distributed to 96 well plates containing feeder cells and selection medium that allows only fused cells to grow. Hybridoma cell lines that secreted antibodies that reacted strongly with the desired antigen in ELISA screens (using an irrelevant peptide as negative control) and whose CRMP2 specificity was tested in Western blot (see chapter 2.1.7), were selected for stable recloning in cell culture.

Translation of CRMP1_human (1) MADRRRAWNTEDDLVPYLARPGSAAQTPRQKYGGMFAAVEGAYE
 Translation of CRMP2_human (1) -----
 Translation of CRMP3_human (1) -----
 Translation of CRMP4_human (1) -----
 Translation of CRMP5_human (1) -----

Translation of CRMP1_human (45) NKTIDFDAYSVGRRGSARTPRSAGRPDVGLPGPGGSEDTASDV
 Translation of CRMP2_human (1) -----
 Translation of CRMP3_human (1) -----
 Translation of CRMP4_human (1) -----
 Translation of CRMP5_human (1) -----

Translation of CRMP1_human (89) SEPSGSAVSSPGERDERPPTLRIRRPAPRDLPLGRDNGQSDRLL
 Translation of CRMP2_human (1) -----MSYQGKKN-----IPRITSDRLL
 Translation of CRMP3_human (1) -----MSEQGKKS-----IPRITSDRLL
 Translation of CRMP4_human (1) -----MSYQGKKN-----IPRITSDRLL
 Translation of CRMP5_human (1) -----MLANSASVRIIL

Translation of CRMP1_human (133) IKGGRIINDDQSLYADVILEDGLIKQIGENLIVPGGVKTIENG
 Translation of CRMP2_human (19) IKGGKIVNDDQSFYADYIMEDGLIKQIGENLIVPGGVKTIEAHS
 Translation of CRMP3_human (19) IRGGRIVNDDQSFYADVHVEDGLIKQIGENLIVPGGKTIIDAHG
 Translation of CRMP4_human (19) IKGGRIVNDDQSFYADYIMEDGLIKQIGENLIVPGGVKTIENG
 Translation of CRMP5_human (12) IKGGKVVNDDCTHEADVYIENGTIQQVGRELMI PGGAKVIDATG

Translation of CRMP1_human (177) RMVIPGGIDVNTYLQKPSQGMTAADDFQGTAAALVGGTTMIID
 Translation of CRMP2_human (63) RMVIPGGIDVHTRFQMPDQGMTSADDFQGTAAALAGGTTMIID
 Translation of CRMP3_human (63) LMVLPGGVDVHTRLQMPVLGMTPADDFCQGTAAALAGGTTMIID
 Translation of CRMP4_human (63) KMVIPGGIDVHTHFQMPYKGMTTVDDFFQGTAAALAGGTTMIID
 Translation of CRMP5_human (56) -----

Translation of CRMP1_human (221) HVVPEPGSSLLTSFEKWHEAADTKSCCDYSLHVDITSWYDGVRE
 Translation of CRMP2_human (107) HVVPEPGTISLLAEDQWREWADSKSCCDYSLHVDISEWHKGIQE
 Translation of CRMP3_human (107) HVFPDTGVSSLLAAYERWRERADSAACCDYSLHVDITRWHESEIKE
 Translation of CRMP4_human (107) HVVPEPESSLTEAYEKWREWADGKSCCDYALHVDITHWNDLSVKQ
 Translation of CRMP5_human (100) HVLPDKETSLVDAYEKCRGLADPKVCCDYALHVGITWWAPKVKKA

Translation of CRMP1_human (265) ELEVLVQDKGVNSFQVYMAKDVYQMSDSQLYEAFPTFLKGLGAV
 Translation of CRMP2_human (151) EMEALVKDHGVNSFLVYMAEKDREQLTDCQIYEVLSVIRDIGAI
 Translation of CRMP3_human (151) ELEALVKEKGVNSFLVYMAKDRCCSDSQMYEIPFSIIRDLGAL
 Translation of CRMP4_human (151) EVQNLIKDKGVNSFMVYMAKDLVQVSNTELYEIFTCLGELGAI
 Translation of CRMP5_human (144) -----

Translation of CRMP1_human (309) ILVHAENGDLIAQEQRILEMGITGPEGHVLSRPEELEAEAVFR
 Translation of CRMP2_human (195) AQVHAENGDIIEBQQRILDLGITGPEGHVLSRPEEVEAEAVNR
 Translation of CRMP3_human (195) AQVHAENGDIIEBQQRILEMGITGPEGHVLSRPEEVEAEAVYR
 Translation of CRMP4_human (195) AQVHAENGDIIEBQQRILEMGITGPEGHVLSRPEELEAEAVFR
 Translation of CRMP5_human (188) ARVHAENGELVAEGAKEALDLGITGPEGIETSRPEELEAEATHR

Translation of CRMP1_human (353) AITTIAGRINCPVYITKVMSSKSAADIIALARKKGPLVFGPEPIAAS
 Translation of CRMP2_human (239) AITIANQTNCPLYITKVMSSKSSAEVIAQARKKGTVVYGEPIITAS
 Translation of CRMP3_human (239) AVTIAKQANCPLYVTKVMSSKGAADAIQAARRGVVVFGEPIITAS
 Translation of CRMP4_human (239) AITIASQTNCPLYVTKVMSSKSAADLISQARKKGNVVFGEPIITAS
 Translation of CRMP5_human (232) VITIANRTHCPLYLVNVSISISAGDVIAAAKMQGKVLAETTTAH

Translation of CRMP1_human (397) LGTDGTHYWSKNWAKAAAFVTSPPPLSPDPTTPDYLTSLIACGDL
 Translation of CRMP2_human (283) LGTDGSHYWSKNWAKAAAFVTSPPPLSPDPTTPDFLNSLLSCGDL
 Translation of CRMP3_human (283) LGTDGSHYWSKNWAKAAAFVTSPPVNPDPPTTADHLTCLLSSGDL
 Translation of CRMP4_human (283) LGIDGTHYWSKNWAKAAAFVTSPPPLSPDPTTPDYINSLLASGDL
 Translation of CRMP5_human (276) -----

Translation of CRMP1_human (441) QVTGSGHCPYSTAQKAVGKDNFTLIPEGVNGTEERMVTVWVKAV
 Translation of CRMP2_human (327) QVTGSAHCTENTAQKAVGKDNFTLIPEGTNGTEERMSVIVDKAV
 Translation of CRMP3_human (327) QVTGSAHCTFTTAQKAVGKDNFALIPEGTNGTEERMSMVWVKCV
 Translation of CRMP4_human (327) QLSGSAHCTFSTAQKAVGKDNFTAIPEGTNGVEERMSVIVDKAV
 Translation of CRMP5_human (320) -----

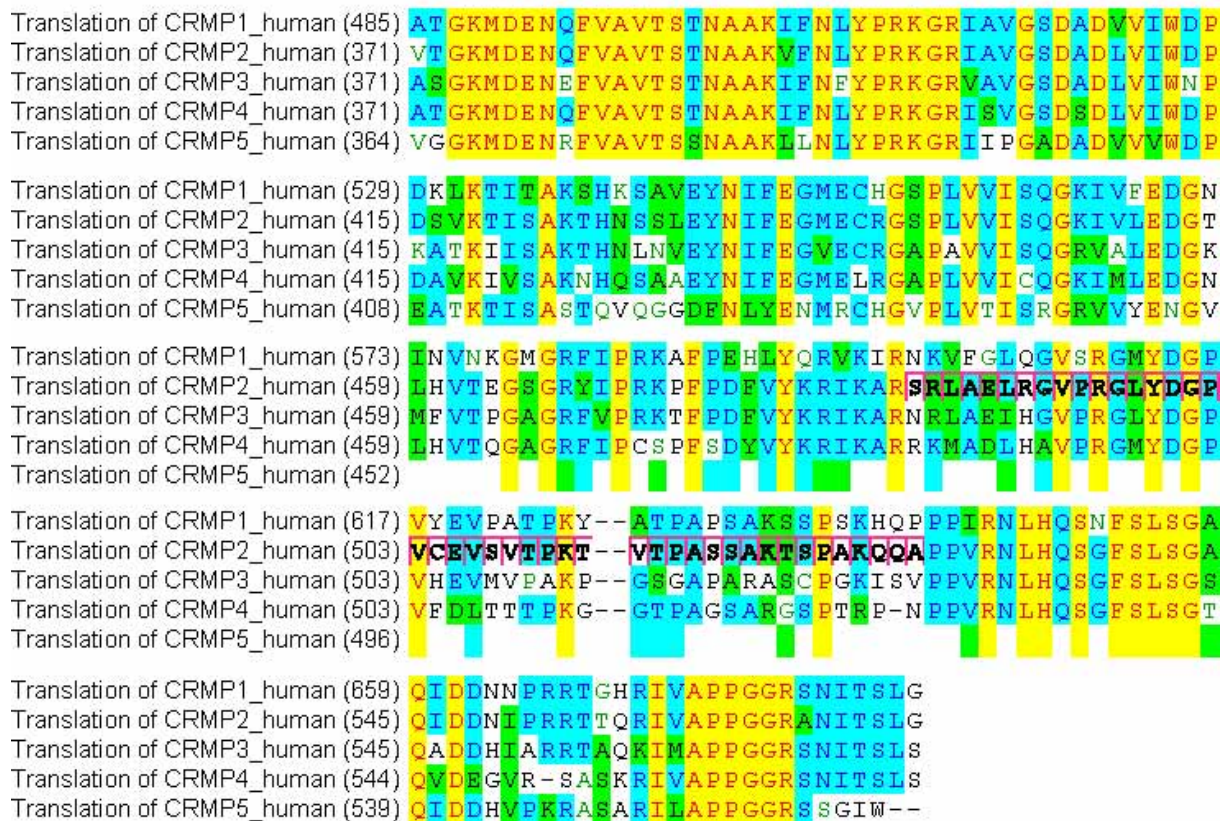


Figure 21: Peptide selection. Alignment of the five human CRMP-family protein sequences (Vector NTI; Invitrogen). The two peptides selected for antibody production are highlighted in bold black letters in a purple square, non-similar amino acids are depicted in thin black letters; dark blue letters on light blue background represent conservative amino acids; black letters on green background indicate similar amino acids, red letters on yellow background displays identical amino acids conserved in all five CRMPs and green letters depict weakly similar amino acids.

2.8.2 Antibody validation by Western blot

The specificity of the obtained antibodies was tested by Western blot analysis on porcine retina lysates (see chapter 2.1.8.1) and HEK293 cell lysates (see chapter 2.1.8.4.2). For Western blot analysis, 12% SDS mini gels (Mini Protean 3, BD) (see chapter 2.1.3) were loaded with 200 µg of retina or HEK293 lysate, respectively. A preparative comb was used. Following electrophoresis and semi-dry blotting (see chapter 2.1.7.1), the membranes were cut into 0.5 cm vertical strips. The single strips were transferred into 15 mL falcon tubes, respectively, were they were blocked with blocking reagent and incubated with antibody diluted 1:10 in blocking reagent (as described in chapter 2.1.7). Following incubation with secondary antibody (see Table 9) in blocking reagent (1 h, RT), immunoreactive signals were visualized (as described in chapter 2.1.7). Antibodies showing a clear immunosignal with low background staining in range of the molecular weight of CRMP2 (572 aa, 62 kDA) were considered as positive and selected for subcloning by limited dilution to obtain a stable monoclonal cell line.

If the obtained WB signal was not satisfactory, Western blot analysis was repeated under different blocking conditions using 1% PVP or 5% BSA as blocking reagent.

2.8.3 Antibody validation by immunohistochemistry (IHC)

The CRMP2 specificity of the stable clones was again tested by Western blot analysis as described in 2.8.2). Suitability of the obtained antibodies for IHC was tested on cryosections of porcine retina as described in chapter 2.7.2.1 with following modifications: A modified blocking reagent was used (1% BSA and 0.25% Triton 100 in PBS); and the antibodies were applied undiluted.

2.8.4 Antibody validation by immunoprecipitation

To obtain antibodies applicable for IP from primary retinal tissues, all WB positive and stably subcloned antibodies were tested for their suitability for IP. One major problem faced here, was the unspecific binding of the secondary antibody to the heavy- and light-chain of immunoglobulin G (IgG) that overlaid the CRMP2 signal. To validate if the antibodies were able to immunoprecipitate CRMP2, IP of recombinant SF-Tap tagged CRMP2 from HEK293 cell lysates was performed (see chapter 2.1.8.4). This not only provides the Tag additional 5 kDa weight to the protein, it also enables the use of an anti-FLAG HRP-conjugated antibody for detection of immunoprecipitated SF-Tap tagged CRMP2 protein. Thereby, the use of a secondary antibody, with its unspecific binding to IgG domains, could be avoided. Antibodies that were able to pull SF-Tap tagged CRMP2 protein from HEK lysate, were further validated by IP of endogenous CRMP2 protein from ROS lysates and subsequent identification of the bait by mass spectrometry (see chapter 2.1.9.4.1).

G. RESULTS

1. ANALYSIS OF RHO GTPASES IN ROD OUTER SEGMENTS (ROS)

At the beginning of this study, this work was based on preceding sucrose-density gradient experiments by Dr. Magdalena Swiatek-deLange that suggested the presence of a rhodopsin/RhoA/Rac1/Rock II/CRMP2/tubulin signaling multiprotein complex in porcine ROS, which had not been validated or further characterized so far. The proteins of this multiprotein complex are all part of signaling networks conserved between different neuronal cell types and are thus likely to play a pivotal role in photoreceptor cell physiology. RhoA and Rac1 were shown to participate in protein transport as well as in structural organisation of cells (reviewed by (Etienne-Manneville and Hall, 2002)), while the CRMP family was described as one of the main regulators of polarity development in neuronal cells (Arimura et al., 2000). One aim of this study was the validation and further characterization of the putative rhodopsin/RhoA/Rac1/Rock II/CRMP2/tubulin multiprotein complex and its components in ROS.

1.1 Identification of the Rac1 interactome in ROS

Although the role of Rho GTPases has been investigated in a wide variety of cells, only few studies have addressed their role in retinal photoreceptors. Rac1, for instance was shown to be involved in the regulation of rhodopsin transport carrier fusion in photoreceptors of *Rana barlandieri* conjointly with phosphoinositides, ezrin/moesin and Rab8 (Deretic et al., 2004). Although Rac1 is believed to play an important role in the regulation of physiological processes in photoreceptors and its activity has been reported to be activated by light ROS ((Petrov et al., 1994), (Wieland et al., 1990), (Balasubramanian and Slepak, 2003)), no function could be assigned so far. The importance of Rac1 for development and maintenance of photoreceptor morphology has been demonstrated by the rescue of rhabdomere morphogenesis after expression of dominant active Drac1 in rhodopsin-null mutants of *Drosophila melanogaster* (Chang and Ready, 2000). In an other study Rac1 was shown to be involved in apoptosis of light-induced photoreceptor degeneration in mice (Belmonte et al., 2006). To further investigate the role of Rac1 in ROS, one aim of this study was the identification of Rac1 interaction partners in porcine ROS. Therefore, Rac1 was immunoprecipitated with a mouse anti-Rac1 antibody from soluble and membranous fractions of ROS. Immunoprecipitates were analysed by 1-DE- or 2-DE-SDS-PAGE and subjected to MALDI-MS/MS analysis.

1.1.1 Establishment of the Rac1 IP from soluble and membranous ROS fractions

For the analysis of the Rac1 interactome in ROS, IP of Rac1 from soluble and membranous fractions of ROS had to be established. For mass spectrometric analysis, the IP conditions had

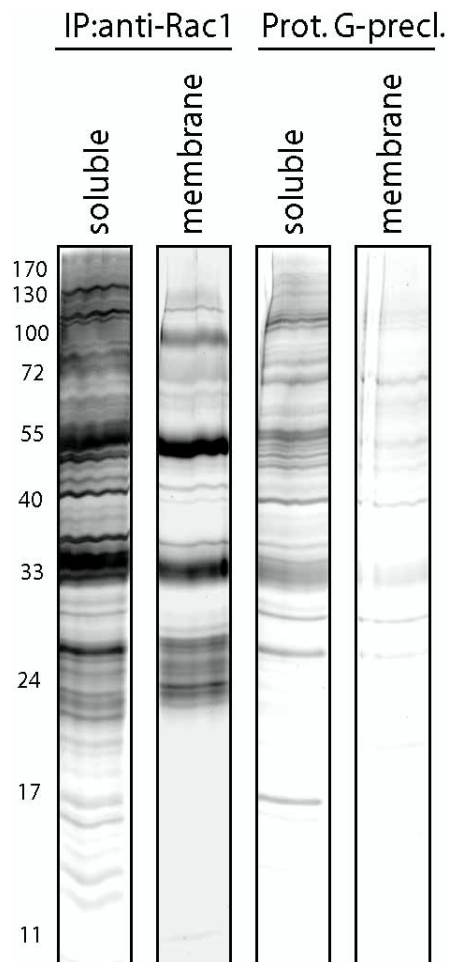


Figure 22: Silver stained 1-DE gels of Rac1-immunoprecipitations from soluble and membranous ROS fractions. left panel: eluate of an anti-Rac1 IP from the soluble and membranous fraction of porcine ROS. Right panel: Eluate of unspecifically bound proteins to protein-G agarose from soluble and membranous ROS fractions. The displayed gels are representative for at least three independent experiments.

to be optimized to reduce the number of unspecifically bound proteins in the immunoprecipitates. Because most unspecifically bound proteins result from an unspecific association with protein-G agarose beads, protein-G agarose beads without anti-Rac1 antibody were used as a negative control (bead control).

Eluates from the Rac1 IPs and from the bead controls were resolved by 1-DE-PAGE and proteins were visualized by silver staining. While in the bead control of the membranous fraction the number of unspecifically bound proteins was rather low, it was considerably higher in the bead control of the soluble fraction (Figure 22, right panels). Only bands from the co-immunoprecipitates of the soluble and membranous fractions (Figure 22, left panels), which differed compared to the bead control, could be considered as Rac1-specific interactions and were subjected to mass spectrometric analysis.

To obtain a higher resolution of the co-immunoprecipitated proteins, the 2-DE-PAGE technique was applied (Figure 23). Additionally, protein-G agarose beads were preincubated with BSA to enhance the specificity of the IP. The Figures 23A and 23B show anti-Rac1 co-immunoprecipitates from soluble ROS fractions resolved by 2-DE-PAGE.

Preincubation of the protein-G agarose beads with BSA (Figure 23B) enhanced the specificity of the IP and resulted in a decreased number of protein spots compared to the IP without BSA preincubated beads (Figure 23A). Figure 23F shows the 2-DE-gel of the protein-G agarose bead control from the soluble fraction with BSA preincubated protein-G agarose beads. Besides several spots in the middle of the gel that are

derived from protein-G, nearly no other protein spots were visible on the silver stained 2-DE-gel, demonstrating that the level of unspecific binding was reduced to a minimum.

The anti-Rac1 co-immunoprecipitates from the membranous ROS fractions resolved by 2-DE PAGE are displayed in Figure 23C (without BSA) and 23D (with BSA). Due to the known problems of membrane proteins with 2-DE-PAGE, only very few proteins were resolved on the gels. Compared to Figure 23E, where the anti-Rac1 antibody alone is resolved by 2-DE-PAGE, only a few additional protein spots were visible on the gels of the membranous fractions. This indicates that the observed protein spots result almost solely from the heavy and light chains of the antibody. Therefore, co-immunoprecipitates of the membranous fractions were later on resolved by 1-DE-PAGE, while immunoprecipitates from the soluble fraction were resolved by 2-DE gels, due to a better resolution by this technique. Co-immunoprecipitated protein bands/spots specific to Rac1 IP were excised from the different gels and subjected to MALDI-MS/MS analysis.

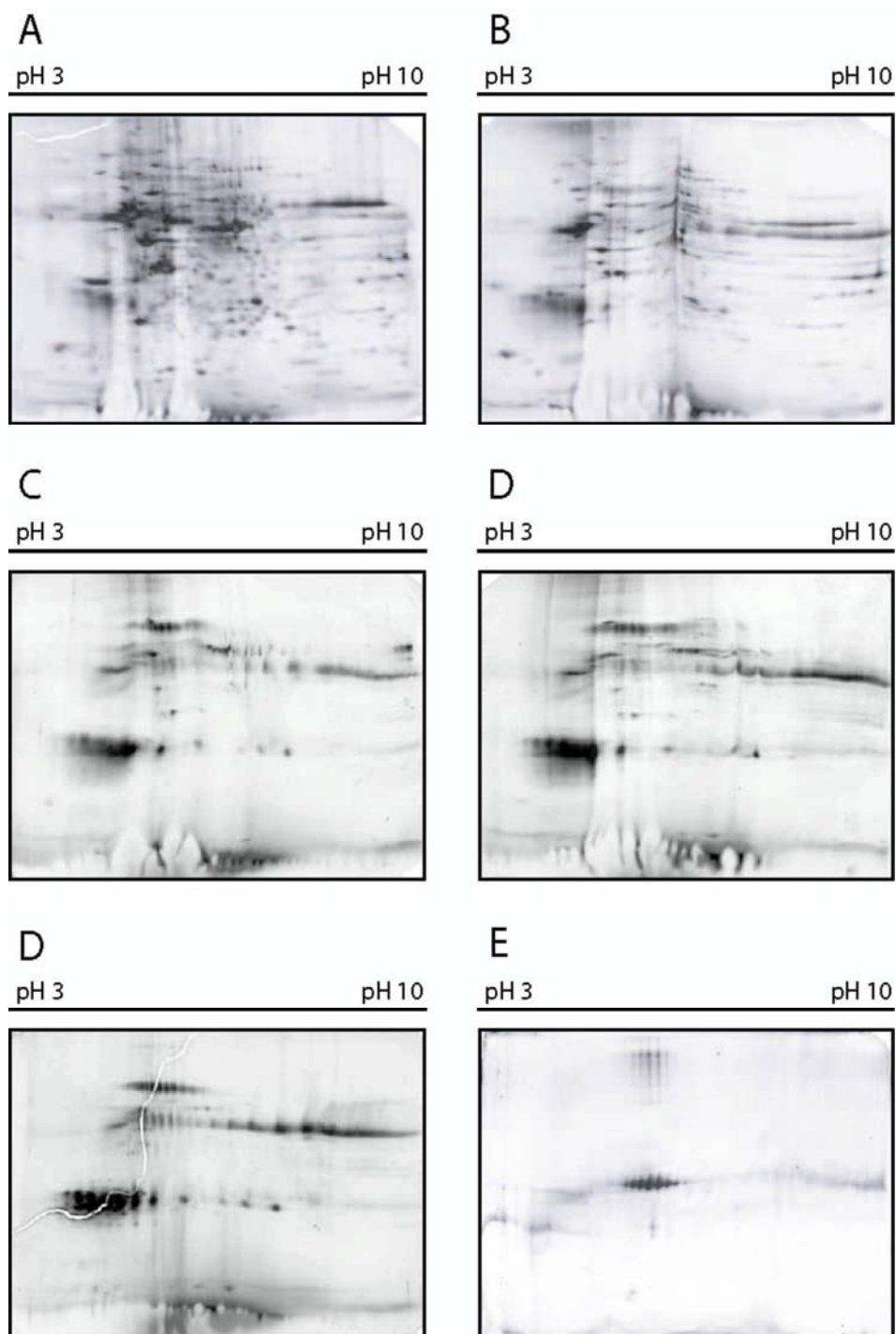


Figure 23: Silver stained 2-DE gels of Rac1-immunoprecipitations from soluble and membranous ROS fractions. **A)** 2-DE gel of a Rac1 IP from the soluble fraction of light-adapted ROS without BSA preincubation of the protein G agarose beads; it shows a higher amount of unspecifically bound proteins than in **B)**, where the same sample was immunoprecipitated with BSA preincubated beads. **C)** Immunoprecipitate from the membranous fraction without BSA preincubated beads resolved by 2-DE PAGE. **D)** Immunoprecipitate from the membranous fraction with BSA preincubated beads resolved by 2-DE PAGE. **E)** 2-DE gel of the anti-Rac1 antibody. **F)** 2-DE gel of the eluate from BSA preincubated protein-G agarose beads without antibody. The displayed gels are representative for at least three independent experiments.

1.1.2 22 Rac1 specific interactors in ROS were identified by mass spectrometry

By MALDI-MS/MS analysis of the purified Rac1 protein complexes, 22 Rac1 interactors were identified (Table 19) in ROS. Many of the identified Rac1 interactors have previously been associated with phototransduction or are components of the cytoskeleton, but only five of the detected Rac1 interactions in this study have been already described in the literature. Amongst these already well-established Rac1 interactors are the cytoskeletal proteins actin α and γ as well as α and β tubulin, strengthening the link of Rac1, which is principally known for its role in regulation of the actin cytoskeleton, with microtubule dynamics. Besides these cytoskeletal proteins another already described interactor, the regulatory protein CRMP2, was identified in ROS. CRMP2 was described as one of the main regulators of polarity development in neuronal cells where it was reported to be involved in the coordinated activation of Rac1 and RhoA, required for neurite outgrowth (Koh, 2006) (see chapter 2.3.1). The detection of CRMP2 by mass spectrometry with a mascot “proteins score” of 48 was at the threshold of the set criteria for protein identification (see chapter 2.1.9.5.1), but was subsequently confirmed by WB analysis (see Figure 24A).

The other 17 identified interactors represent putative new Rac1 interaction partners in ROS. From the phototransduction cascade (see introduction, chapter 1.2.1), the α -chain of 3',5'-cyclic-GMP phosphodiesterase, recoverin, arrestin and the α , β and γ subunits of transducin were identified. Another interesting Rac1 interaction was found with the aryl hydrocarbon receptor-interacting protein like 1 (AIPL1), which is associated with LCA (see introduction, chapter 1.3.2.1) and may be involved in retinal protein trafficking (Sohocki et al., 2000). Additionally, a number of glycolytic enzymes were identified, like glyceraldehyd 3-phosphate dehydrogenase, enolase β and phosphopyruvat hydratase alpha (enolase α). Enolase α is reported to be involved in several autoimmune-diseases, as anti-enolase-apha antibodies are associated with cancer-associated retinopathy and retinal degenerations in humans (Adamus et al., 1998).

Furthermore, with epoxid hydrolase and peroxiredoxin, two enzymes involved in cellular protection against oxidative stress were identified. Also mitochondrial proteins like the ADP/ATP carrier protein T2, a subunit of the mitochondrial f1-ATPase and malate dehydrogenase, were detected that have to be considered as contaminations from the inner segment of the photoreceptor. From the RAS superfamily of GTPases, Rab1 was identified, which is involved in vesicular trafficking (Haas et al., 2007).

Identity	Organism	MW	PI	Pep. Count	Prot. Score	Acc. No.
3',5'-cyclic-GMP phosphodiesterase alpha chain	Bovine	100087	5.33	13	164	P11541
Recoverin	Bovine	23376	8.37	4	65	P21457
S-antigen/Arrestin	Pig	45302	4.70	9	115	P79260
Transducin alpha chain B	Bovine	36581	5.85	4	201	P04696
Transducin beta chain B	Bovine	38020	7.01	12	395	P11017
Transducin source gamma subunit, chain G	Bovine	7764	9.46	3	121	P02698
Actin γ	Bovine	41977	5.31	10	327	P63258
Actin β , chain A	Bovine	41895	5.22	14	358	P60712
Tubulin α	Macaca mulatta	49662	5.32	17	327	Q9GLW6
Tubulin β	Pig	48319	5.58	22	342	P02554
Aryl-hydrocarbon interacting protein-like 1-AIPL-1	Bovine	38847	5.86	7	51	Q95MP1
Glyceraldehyd 3-phosphate dehydrogenase	Pig	35910	8.52	4	110	P00355
Enolase β	Mouse	47206	6.81	9	301	P21550
Phosphopyruvate hydratase alpha (enolase α)	Human	47481	8.52	17	319	P06733
Epoxide hydrolase	Pig	52646	7.25	12	90	P79381
Peroxiredoxin 2	Pig	14272	7.25	5	156	P52552
ADP,ATP carrier protein T2	Bovine	33084	9.82	15	322	Q8SQH5
F1-atpase delta and 1 epsilon subunits, chain F	Bovine	50154	4.98	14	116	1BMF_E
Malate dehydrogenase	Pig	33390	6.81	11	264	P00346
Phosphodiesterase 4B	Mouse	44098	4.98	8	54	Q8VBU5
GTP-binding protein Rab1	Rat	22977	5.95	5	85	Q6NYB7
CRMP-2, dihydropyrimidase-related protein 2	Rat	62638	5.95	4	48	P47942

Table 19: The Rac1 interactome in ROS. Endogenous Rac1 was immunoprecipitated with a mouse anti-Rac1 antibody. Eluates were separated by 1D- or 2D SDS-PAGE. Following silver staining, bands were excised and analysed by MALDI-MS/MS analysis. The main complex consists of several proteins involved in phototransduction, cellular development or are elements of the cytoskeleton.

In this study, the successful establishment and optimization of a Rac1 IP from soluble and membranous fractions of ROS in combination with different resolving techniques, enabled the identification of 22 Rac1 interaction partners in ROS. 17 of them represent putative new interactions. Many of the identified proteins are part of the cytoskeleton or the phototransduction cascade. This links light perception through rhodopsin with signalling networks involved in structural integrity and polarity of photoreceptors and suggests an interdependence of visual perception and proper cellular structure.

1.2 Co-immunoprecipitations reveal a light-dependent dynamic of the Rac1/RhoA/CRMP2/tubulin/Rock II multiprotein complex in ROS

The reported Rac1 activation in ROS by light ((Wieland et al., 1990), (Petrov et al., 1994), (Balasubramanian and Slepak, 2003)) suggested also that interactions of Rac1 with signaling molecules may be regulated by light. Following the identification of the Rac1 interactome in ROS, the effect of light on the signaling network of Rac1 and RhoA in ROS was further investigated. Both proteins were immunoprecipitated from light- and dark-adapted porcine ROS, respectively. Co-immunoprecipitated proteins were investigated by WB analysis for a light-dependence of their interaction. Furthermore, to evaluate if there are proteins that interact only with the GTP-bound, active form of Rac1, PAK-Pull-Downs of GTP-bound Rac1 from light- and dark-adapted ROS were performed.

Co-immunoprecipitation with an anti-Rac1 antibody in combination with WB analysis revealed that interactions of Rac1 with CRMP2, RhoA and tubulin are indeed regulated in a light-dependent manner (Figure 24A).

The highest amount of CRMP2 was co-immunoprecipitated with Rac1 from the light-adapted membranous fraction, while in the dark-adapted membranous fraction no CRMP2 signal was detectable. In the soluble fractions of both light- and dark-adapted ROS, CRMP2 was immunoprecipitated, although the immunosignal in the light-adapted fraction was very weak. RhoA was strongly co-immunoprecipitated with Rac1 in the light-adapted soluble and membranous fractions. In the dark-adapted fraction, only very little RhoA was co-immunoprecipitated from the soluble fraction while it was absent in the membranous fraction. Interaction of Rac1 with tubulin was weak and could only be observed in the soluble fraction of dark-adapted ROS, while an interaction of Rac1 with Rock II was not detected at all.

Immunoprecipitation of RhoA from light- and dark-adapted soluble and membranous ROS fractions with anti-RhoA antibody in combination with WB analysis further confirmed the regulation of the Rac1/RhoA/CRMP2/tubulin/Rock II signaling complex by light (Figure 24B).

CRMP2, Rock II and Tubulin were exclusively co-immunoprecipitated with RhoA in the dark-adapted soluble fraction. While the immunosignal of Rock II and tubulin was very strong, the signal of CRMP2 was rather weak. Interaction of RhoA with Rac1 occurred only in the light-adapted state, with a stronger interaction in the soluble ROS fraction. In the dark-adapted state, no Rac1-specific signal was detected.

Using anti-Rac1 and anti-RhoA immunoprecipitations from light- and dark-adapted soluble and membranous fractions of ROS in combination with WB analysis, the existence of the

Rac1/RhoA/CRMP2/tubulin/Rock II multiprotein complex in ROS was not only validated, but this complex was also demonstrated to be regulated by light.

1.2.1 CRMP2 and tubulin interact with the active, GTP-bound form of Rac1

To determine, if Rac1 is activated by light in porcine ROS, as it was already demonstrated for other species ((Wieland et al., 1990), (Petrov et al., 1994), (Balasubramanian and Slepak, 2003)), and to detect interactions that are specific for the GTP-bound form of Rac1, the GST fusion of the Rac binding domain of PAK1-kinase was used. This domain is able to selectively capture the GTP-bound, active form of Rac1 and was used to pull-down GTP-bound Rac1 from soluble and membranous fractions of light- and dark-adapted ROS. By WB analysis with an anti-Rac1 antibody, it was demonstrated that the largest amount of active Rac1 was pulled-down in the light-adapted membranous fraction. A weaker signal was detected in the soluble fraction of light-adapted ROS. In the dark-adapted soluble and membranous fractions, only very little active Rac1 was present (Figure 24C).

Together with active Rac1, CRMP2 was pulled from the soluble and membranous fractions of light-adapted ROS. Tubulin was shown to co-precipitate with the GTP-bound form of Rac1 in the dark-adapted soluble fraction, although the detected tubulin signal was very weak. Besides CRMP2 and tubulin, RPGR, another candidate to be involved in Rac1 signaling, was investigated for its interaction with active Rac1 in ROS. RPGR was shown to strongly co-precipitate with active Rac1 in the light-adapted fractions, while in the dark-adapted fractions only little RPGR was detected.

Using the GST fusion of the Rac binding domain of PAK1-kinase, it was demonstrated in this study that Rac1 is activated in the light. Furthermore it was shown that components of the Rac1/RhoA/CRMP2/tubulin/Rock II multiprotein complex, CRMP2 and tubulin, specifically interact with the active form of Rac1 in ROS.

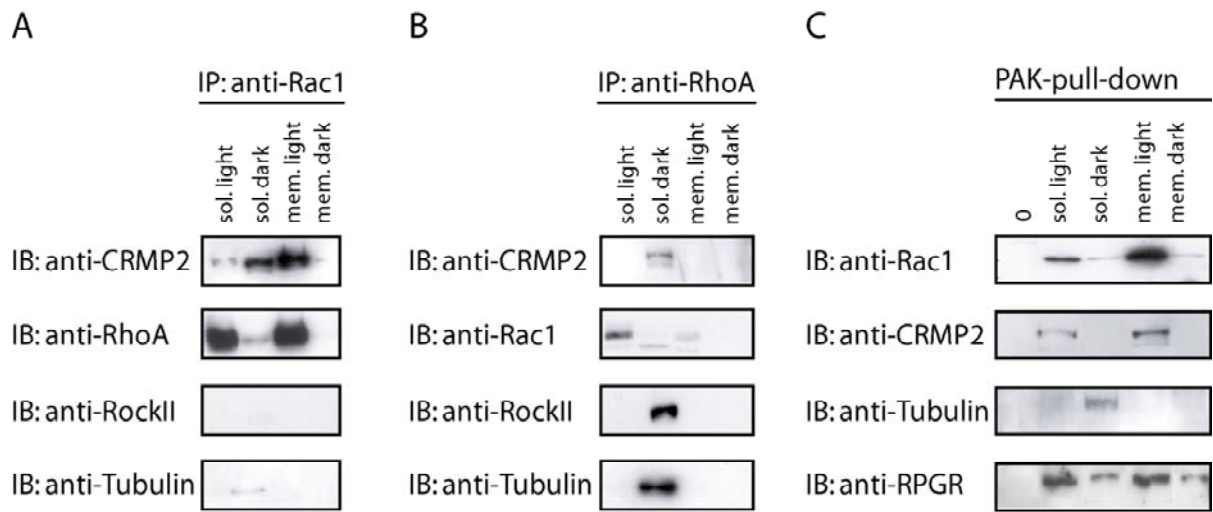


Figure 24: Analysis of light-regulated Rac1- and RhoA-interactions in ROS. **A-B)** equal amounts of protein (500 μ g), divided into soluble and membranous fractions, were immunoprecipitated using anti-Rac1 (**A**) or anti-RhoA antibodies (**B**), respectively. Eluates were analyzed by Western blot with anti-Rac1, anti-RhoA, anti-Rock II, anti-CRMP2 or anti-Tubulin β antibodies. **C)** PAK-pull-down of active, GTP-bound Rac1 from soluble and membranous fractions of light-and dark-adapted ROS, analysed by Western blot with anti-Rac1, anti-CRMP2, anti-tubulin and anti-RPGR antibodies.

2. DEVELOPMENT AND VALIDATION OF CRMP2-SPECIFIC MONOCLONAL ANTIBODIES

In this study CRMP2 was identified as part of the conserved signaling complex Rac1/RhoA/CRMP2/tubulin/Rock II in ROS. Furthermore it was demonstrated that members of this signaling complex display a light-dependent dynamic and that the activity of the Rho GTPase Rac1 is regulated by light. In neuronal cells, CRMP2 has already been described as one of the main regulators of polarity and development and is also discussed as a molecular switch in RhoA- and Rac1-signaling (Arimura et al., 2000). Although this points to CRMP2 as a very important molecule in neuronal cells, no commercially available CRMP2 antibodies existed at the beginning of this study. Because such antibodies are indispensable for a further characterization of the function of CRMP2 in ROS, one aim of this study was the production of monoclonal CRMP2 specific antibodies. For an in depth investigation of the role of CRMP2 in ROS, we aimed at a production of monoclonal CRMP2 antibodies in mice and rats that were suitable for Western blot analysis (Towbin et al.), immunohistochemistry (IHC) as well as for immunoprecipitation (IP).

2.1 Antibody specificity and characterization of rat and mouse monoclonal antibodies against CRMP2

2.1.1 Production of monoclonal anti-CRMP2 antibodies using two different CRMP2-specific peptides

Rats and mice were immunized with two different CRMP2-specific peptides, Beer1 and Beer4. Both peptides were selected according to criteria specified in Material and Methods (chapter 2.8.1). The supernatants of the obtained antibody secreting, but prior to the step of stable subcloning still polyclonal, clones were tested in a differential ELISA against OVA-coupled CRMP2 peptides using an unrelated peptide as negative control. Immunization with the peptide Beer1 resulted in 39 ELISA-positive mouse clones and 60 ELISA positive rat clones (Table 20). Peptide Beer4 only provided three ELISA-positive rat clones (Table 21). The total of 102 clones that were positive in the ELISA assay were further tested for their CRMP2-specificity on WB from porcine retina lysates. Although nearly all ELISA-positive clones provided an immunosignal on WB at the expected molecular weight (62 kDa), many of them also showed strong background staining, or produced additional unspecific bands on WB. The background was independent of the used blocking conditions (5% BSA, 5% milk or 1% PVP in TBST, respectively). Therefore only 31 clones (12 from mouse and 19 from rat) out of 99 obtained clones from Beer1 were considered as CRMP2-specific and selected as

WB-positive (Table 20). From Beer4 only a single clone was selected as WB-positive (Table 21). From all WB-positive clones, the six clones that provided the best results in terms of high signal and low background (see Figure 25A), were selected for the generation of stable antibody-producing monoclonal cells lines (Table 20 and 21). The selected clones showed a strong immunosignal at 62 kDa, corresponding to the molecular weight of CRMP2 (Figure 25A). Lane 1 (Figure 25A) shows CRMP2 detected using an already established monoclonal antibody as positive control (a limited amount of this antibody was obtained as a kind gift from Y. Ihara, University of Tokyo). Besides the CRMP2-specific signal on WB, the antibodies Beer1-4A6, Beer1-2D5 and Beer1-5D6 also showed a weak, unspecific WB signal at 72 kDa. Beer1-3A10 reacted unspecifically with a protein around 7 kDa and Beer4-5E1 showed two unspecific bands around 72 and 38 kDa. The best result was obtained with the antibody Beer1-3B10, showing a strong signal at 62 kDa, low background staining and no unspecific bands.

Table 20: Characterization of rat and mouse monoclonal antibodies against CRMP2 obtained by immunization with peptide Beer1

Raised in	Clone	WB	Stabile clone	WB	IHC	IP
rat	5D6	positive	100%	positive	positive	positive
rat	2D5	positive	100%	positive	positive	negative
rat	4A6	positive	100%	negative	positive	negative
mouse	3B10	positive	100%	positive	negative	negative
mouse	3A10	positive	100%	positive	n.t.	negative
rat	5E7	negative	n. t.	n. t.	n. t.	n. t.
rat	5E11	negative	n. t.	n. t.	n. t.	n. t.
rat	3D9	positive	n. t.	n. t.	n. t.	n. t.
rat	7E12	positive	n. t.	n. t.	n. t.	n. t.
rat	5C9	negative	n. t.	n. t.	n. t.	n. t.
rat	7E10	positive	n. t.	n. t.	n. t.	n. t.
rat	7D12	negative	n. t.	n. t.	n. t.	n. t.
rat	2G6	negative	n. t.	n. t.	n. t.	n. t.
rat	6A12	positive	n. t.	n. t.	n. t.	n. t.
rat	8G4	negative	n. t.	n. t.	n. t.	n. t.
rat	5E6	negative	n. t.	n. t.	n. t.	n. t.
rat	6D10	positive	n. t.	n. t.	n. t.	n. t.
rat	5C1	positive	n. t.	n. t.	n. t.	n. t.
rat	3E8	negative	n. t.	n. t.	n. t.	n. t.
rat	8G2	negative	n. t.	n. t.	n. t.	n. t.
rat	7D11	negative	n. t.	n. t.	n. t.	n. t.
rat	8F2	negative	n. t.	n. t.	n. t.	n. t.
rat	1C11	negative	n. t.	n. t.	n. t.	n. t.
rat	7C10	negative	n. t.	n. t.	n. t.	n. t.
rat	7H11	negative	n. t.	n. t.	n. t.	n. t.

rat	2F8	negative	n. t.	n. t.	n. t.	n. t.
rat	7H1	negative	n. t.	n. t.	n. t.	n. t.
rat	6C4	negative	n. t.	n. t.	n. t.	n. t.
rat	8A5	negative	n. t.	n. t.	n. t.	n. t.
rat	4G3	negative	n. t.	n. t.	n. t.	n. t.
rat	7D3	negative	n. t.	n. t.	n. t.	n. t.
rat	7F2	negative	n. t.	n. t.	n. t.	n. t.
rat	7G6	negative	n. t.	n. t.	n. t.	n. t.
rat	7H4	positive	n. t.	n. t.	n. t.	n. t.
rat	8B2	positive	n. t.	n. t.	n. t.	n. t.
rat	4B11	negative	n. t.	n. t.	n. t.	n. t.
rat	5B7	negative	n. t.	n. t.	n. t.	n. t.
rat	3E10	negative	n. t.	n. t.	n. t.	n. t.
rat	7D5	negative	n. t.	n. t.	n. t.	n. t.
rat	5B11	negative	n. t.	n. t.	n. t.	n. t.
rat	5B2	negative	n. t.	n. t.	n. t.	n. t.
rat	4B6	positive	n. t.	n. t.	n. t.	n. t.
rat	4A6	positive	n. t.	n. t.	n. t.	n. t.
rat	7H5	negative	n. t.	n. t.	n. t.	n. t.
rat	7D2	negative	n. t.	n. t.	n. t.	n. t.
rat	5A6	negative	n. t.	n. t.	n. t.	n. t.
rat	5B9	negative	n. t.	n. t.	n. t.	n. t.
rat	7F1	negative	n. t.	n. t.	n. t.	n. t.
rat	6C7	negative	n. t.	n. t.	n. t.	n. t.
rat	8B4	positive	n. t.	n. t.	n. t.	n. t.
rat	6A5	negative	n. t.	n. t.	n. t.	n. t.
rat	6G3	negative	n. t.	n. t.	n. t.	n. t.
rat	6A2	negative	n. t.	n. t.	n. t.	n. t.
rat	5F10	negative	n. t.	n. t.	n. t.	n. t.
rat	7D8	positive	n. t.	n. t.	n. t.	n. t.
rat	6H11	positive	n. t.	n. t.	n. t.	n. t.
rat	7B9	negative	n. t.	n. t.	n. t.	n. t.
rat	8C5	negative	n. t.	n. t.	n. t.	n. t.
rat	7G10	negative	n. t.	n. t.	n. t.	n. t.
rat	8C4	positive	n. t.	n. t.	n. t.	n. t.
rat	8B3	negative	n. t.	n. t.	n. t.	n. t.
rat	7A6	negative	n. t.	n. t.	n. t.	n. t.
rat	8C9	negative	n. t.	n. t.	n. t.	n. t.
rat	7D6	negative	n. t.	n. t.	n. t.	n. t.
rat	6E6	negative	n. t.	n. t.	n. t.	n. t.
rat	6A3	negative	n. t.	n. t.	n. t.	n. t.
rat	5H2	negative	n. t.	n. t.	n. t.	n. t.
rat	8H4	negative	n. t.	n. t.	n. t.	n. t.
rat	8C12	negative	n. t.	n. t.	n. t.	n. t.
rat	5H10	negative	n. t.	n. t.	n. t.	n. t.
mouse	4B12	negative	n. t.	n. t.	n. t.	n. t.
mouse	1G2	positive	n. t.	n. t.	n. t.	n. t.
mouse	4D5	positive	n. t.	n. t.	n. t.	n. t.
mouse	2E1	negative	n. t.	n. t.	n. t.	n. t.
mouse	1A7	positive	n. t.	n. t.	n. t.	n. t.
mouse	1A6	positive	n. t.	n. t.	n. t.	n. t.

mouse	3F12	positive	n. t.	n. t.	n. t.	n. t.
mouse	4F1	positive	n. t.	n. t.	n. t.	n. t.
mouse	4G7	negative	n. t.	n. t.	n. t.	n. t.
mouse	2E3	negative	n. t.	n. t.	n. t.	n. t.
mouse	2D12	negative	n. t.	n. t.	n. t.	n. t.
mouse	1E3	negative	n. t.	n. t.	n. t.	n. t.
mouse	1B9	negative	n. t.	n. t.	n. t.	n. t.
mouse	2D11	negative	n. t.	n. t.	n. t.	n. t.
mouse	1C5	negative	n. t.	n. t.	n. t.	n. t.
mouse	2C12	negative	n. t.	n. t.	n. t.	n. t.
mouse	3B12	negative	n. t.	n. t.	n. t.	n. t.
mouse	2G9	negative	n. t.	n. t.	n. t.	n. t.
mouse	3E6	negative	n. t.	n. t.	n. t.	n. t.
mouse	2B9	negative	n. t.	n. t.	n. t.	n. t.
mouse	4A3	positive	n. t.	n. t.	n. t.	n. t.
mouse	3B3	negative	n. t.	n. t.	n. t.	n. t.
mouse	3F2	negative	n. t.	n. t.	n. t.	n. t.
mouse	4D4	negative	n. t.	n. t.	n. t.	n. t.
mouse	2G8	positive	n. t.	n. t.	n. t.	n. t.
mouse	4C6	positive	n. t.	n. t.	n. t.	n. t.
mouse	3F2	positive	n. t.	n. t.	n. t.	n. t.
mouse	3E6	positive	n. t.	n. t.	n. t.	n. t.
mouse	3F12	positive	n. t.	n. t.	n. t.	n. t.

n. t.: not tested

Table 21: Characterization of rat monoclonal antibodies against CRMP2 obtained by immunization with peptide Beer4

Raised in	Clone	WB	Stabile clone	WB	IHC	IP
rat	5E1	positive	100%	negative	n. t.	n. t.
rat	5C2	negative	n. t.	n. t.	n. t.	n. t.
rat	7B7	negative	n. t.	n. t.	n. t.	n. t.

n. t.: not tested

2.1.2 Immunization of rats and mice with two different CRMP2 antigens resulted in four CRMP2 specific stable monoclonal cell lines

The supernatants of the stable monoclonal clones were re-evaluated for their CRMP2-specificity on WB from porcine retina lysates. During the process of subcloning by limited dilution in order to obtain stable, monoclonal anti-CRMP2 antibody-producing cell lines, the clones Beer1-4A6 and Beer4-5E1 had lost their CRMP2-specificity. Instead of producing a single band at 62 kDa on WB, consistent with the molecular weight of CRMP2, they only showed a double band around 55kDa (Figure 25B, lane 2 and 7). The stable clones Beer1-2D5, Beer1-5D6, Beer1-3B10 and Beer1-3A10 (Figure 25B, lane 3-6) all showed a strong immunosignal at 62 kDa with very low background staining and high specificity. Only Beer1-2D5 resulted in two additional weak unspecific signals at 90 and 50 kDa. The established

CRMP2-specific antibody (a kind gift from Y. Ihara, University of Tokyo) was used as positive control (Figure 25B, lane 1).

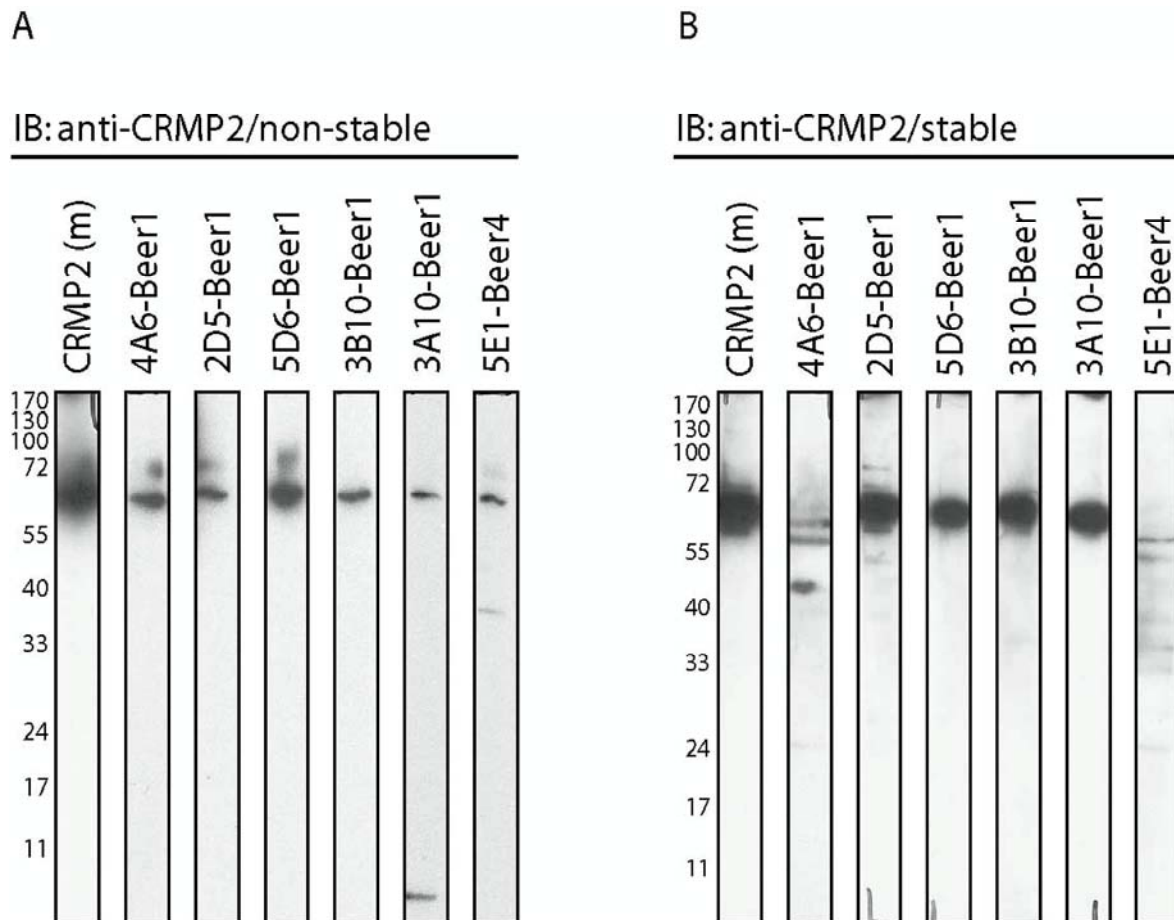


Figure 25: Characterization of CRMP2 specificity of the produced monoclonal antibodies by WB analysis of porcine retina lysate. **A)** Clones selected for stable re-cloning. **B)** Stable clones of monoclonal anti-CRMP2 antibody-producing cell lines

2.1.3 Rat and mouse anti-CRMP2 antibodies recognize CRMP2 on IHC of porcine retina

The suitability of the obtained anti-CRMP2 antibodies from stable monoclonal cell lines for immunohistochemistry was tested on cryosections from porcine retina. The rat anti-CRMP2 antibodies Beer1-5D6 and Beer1-2D5 (Figure 26A) as well as the mouse anti-CRMP2 antibodies Beer1-3A10 and Beer1-3A10 (Figure 26B), revealed a ubiquitously distributed staining throughout the retina. This staining pattern is consistent with the ubiquitous distribution of CRMP2 in the retina demonstrated by Yuasa-Kawada and colleagues (Yuasa-Kawada et al., 2003). A strong CRMP2 immunosignal was detected at the outer limiting membrane as well as at the INL and GCL (Figure 26A and 26B). A similar but weaker staining was observed with the anti-CRMP2 antibody Beer1-4A6 (Figure 26C, left panel),

which did not recognize CRMP2 on WB (see Figure 25B). On the other hand, immunostaining with the anti-CRMP2 antibody Beer4-5E1 showed a completely different staining pattern, reminiscent of Müller-glia cell staining in the retina (Figure 26, right panel). This loss of CRMP2 specificity of the clone Beer4-5E1 is consistent with the WB results (see Figure 25B). There the antibodies from the stable monoclonal cell line Beer4-5E1 had lost their CRMP2 specificity too.

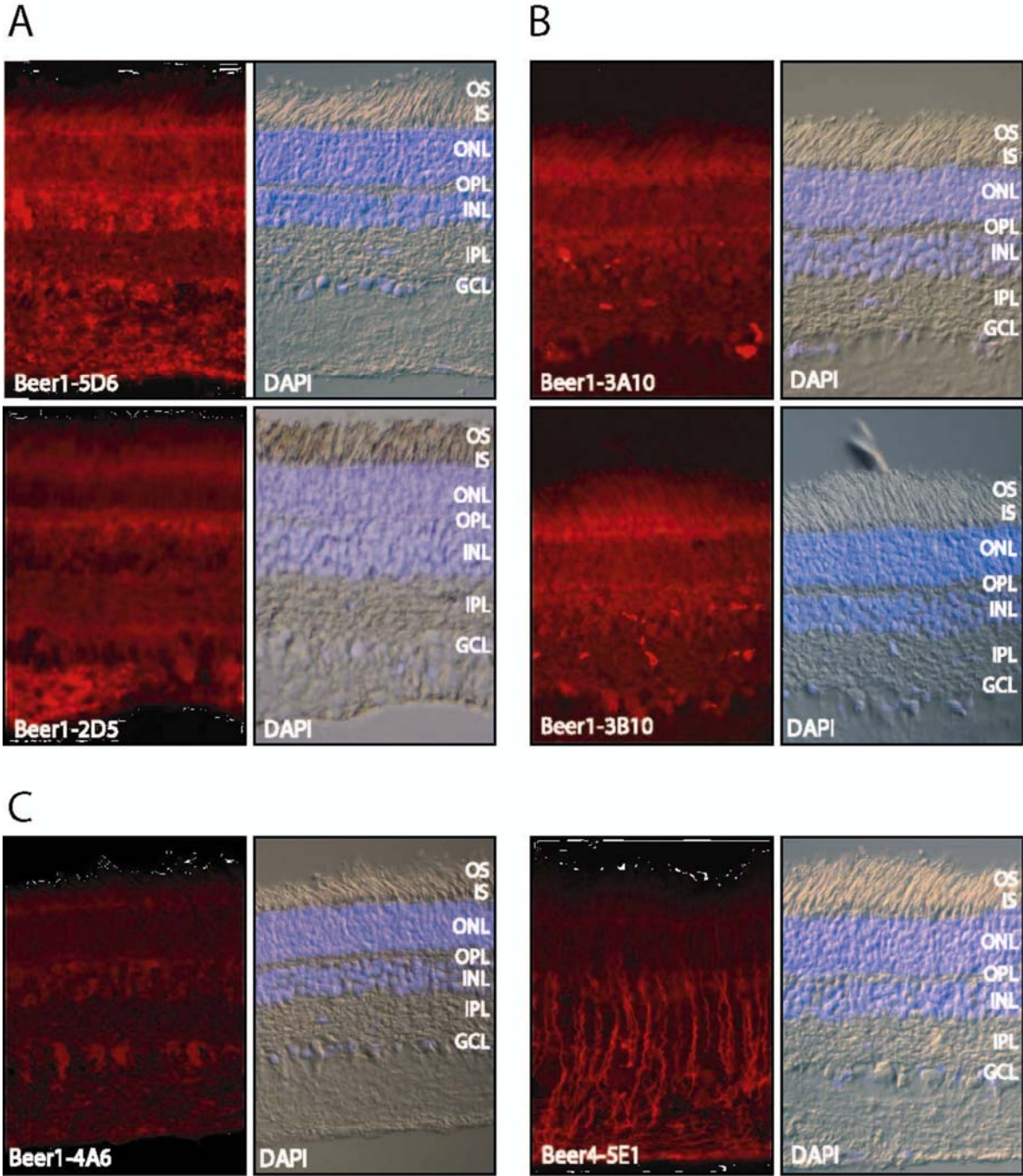


Figure 26: Immunohistochemistry with anti-CRMP2 antibodies from stable monoclonal cell lines on cryosections of porcine retina. **A)** stable monoclonal rat cell lines (Beer1). **B)** stable monoclonal mouse cell lines (Beer1). **C)** stable monoclonal rat cell lines (Beer1, left panel; Beer4 right panel) that produced a CRMP2 unspecific signal on Western blot. Inner segments (IS); outer segments (OS); outer nuclear layer (ONL); outer plexiform layer (Gavin et al.); inner nuclear layer (INL); inner plexiform Layer (IPL); ganglion cell layer (GCL).

2.1.4 Rat anti-CRMP2 antibodies from the stable monoclonal cell line Beer1-5D6 immunoprecipitate endogenous and recombinant CRMP2

Although the CRMP2-specificity of the stable antibody producing clones was already tested by extensive WB analyses, these studies only proved that the produced anti-CRMP2 antibodies are able to recognize the completely SDS-denatured form of the protein. For IP on the other hand, the produced anti-CRMP2 antibodies must recognize the native form of the protein. Therefore, the suitability of the produced CRMP2-specific monoclonal antibodies from stable cell lines to immunoprecipitate native, endogenous CRMP2 was tested on porcine retinal lysate. WB analysis of the immunoprecipitates using an established anti-CRMP2 rabbit antibody (a kind gift from J. Kappler, University of Bonn) revealed bands between 60 and 75 kDa (Figure 27A). Although these signals correspond approximately to the molecular weight of CRMP2 (62 kDa), an unambiguous detection of immunoprecipitated CRMP2 was hindered due to unspecific cross reactivity of the rabbit secondary antibody with mouse and rat IgG heavy and light chains and a high background staining. Unspecific binding of proteins to the protein G-agarose beads was excluded by a negative control without antibody (lane 6, Figure 27A). To circumvent the problem of unspecific binding of the secondary antibody, the antibodies were tested for their IP-suitability by IP of overexpressed recombinant SF-TAP tagged CRMP2 from HEK293 lysate. Here, the successful IP of recombinant SF-TAP tagged CRMP2 with the produced monoclonal anti-CRMP2 antibodies could be detected with a HRP-conjugated anti-FLAG antibody. No secondary antibody was necessary for detection. As shown in Figure 27B, only the stable antibody producing clone Beer1-5D6 immunoprecipitated recombinant CRMP2. The other tested clones were unsuitable for IP. The IP of endogenous CRMP2 with anti-CRMP2 Beer1-5D6 antibody from porcine retina lysate was further validated by identification of the immunoprecipitated protein by mass spectrometry. After resolving the immunoprecipitate by SDS-PAGE, the gel was silver-stained and the band corresponding to the molecular weight of CRMP2 was subjected to analyses by mass spectrometry (Figure 27C). LS-MS/MS analysis revealed the identity of the immunoprecipitated protein as CRMP2, and therefore proved that the stable antibody producing clone Beer-5D6 is also able to immunoprecipitate endogenous CRMP2.

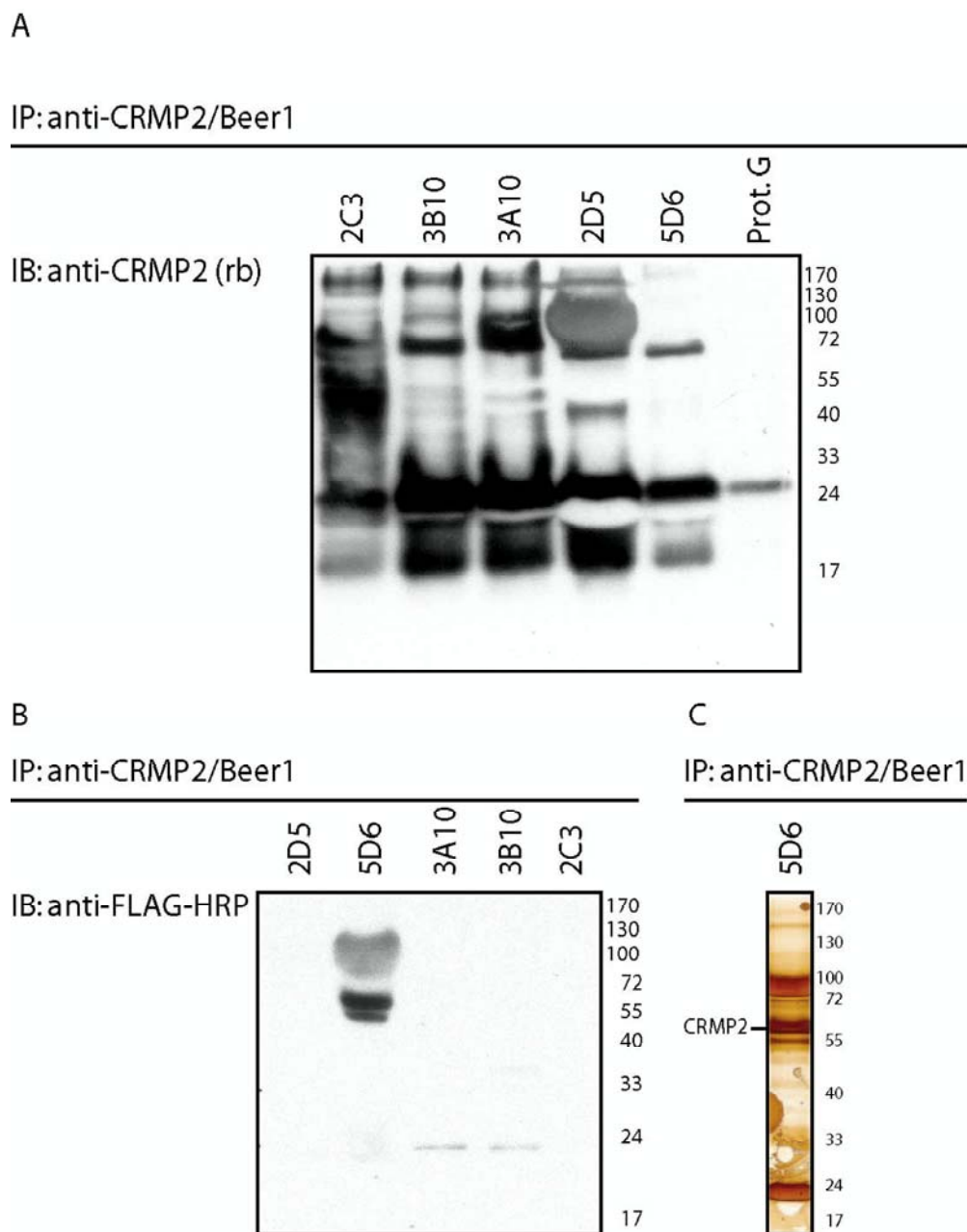


Figure 27: Validation of the CRMP2 specific monoclonal antibodies from stable hybridoma cell lines for IP. **A)** Anti-CRMP2 IP from porcine retinal lysate. Detection of immunoprecipitated CRMP2 with the established polyclonal rabbit CRMP2 antibody (a kind gift from J. Kappler, University of Bonn) was hindered due to unspecific cross reactivity of the rabbit secondary antibody with mouse and rat IgG heavy and light chains. **B)** IP of recombinant SF-TAP tagged CRMP2 from HEK293 lysate. Successful IP of SF-tagged recombinant CRMP2 with the produced monoclonal anti-CRMP2 antibodies was detected with a HRP-conjugated anti-FLAG antibody. By the use of this directly coupled antibody for CRMP2 detection, unspecific cross reactivity by the secondary antibody was circumvented. Immunoprecipitation of recombinant CRMP2 was only accomplished with the stable antibody producing clone Beer-5D6. **C)** Silver stained gel of the anti-CRMP2 Beer1-5D6 immunoprecipitate from porcine retina lysate. The identity of the band at 62 kDa as CRMP2 was confirmed by LC-MS7MS mass spectrometry.

In this study, the successful production and characterization of four stable lines of rat and mouse monoclonal CRMP2 specific antibodies is reported. The obtained antibodies recognized specifically CRMP2 on WB and were also suitable for immunohistochemical analysis. The antibody Beer1-5D6 was also shown to successfully immunoprecipitate CRMP2 from HEK293 and porcine retinal lysate.

3. MOUSE RETINAL EXPLANTS: AN ORGANOTYPICAL CULTURE SYSTEM FOR THE INVESTIGATION OF RETINAL DEVELOPMENT AND MAINTENANCE

To study the physiological function of Rac1 and RhoA signaling in the retina, a model system was necessary that highly resembles the *in vivo* situation and enables the application of pharmacological agents for the specific blocking of GTPase and Rock II signaling without unnecessary animal testing.

Caffe and colleagues were able to show that a postnatal mouse retina could be cultured as a long-term organotypic retinal explant in serum-free medium for more than four weeks (Caffe et al., 2001). Morphological and molecular analyses of the retina demonstrated that *in vitro* most of the histotypic and neurochemical characteristics of the retinal tissue develop comparable to the *in vivo* littermates. Rod and cone photoreceptors develop under organotypic culture conditions with normal morphological and histochemical properties. Rods were reported to form stacks of discs membranes (Soderpalm et al., 1994) and display an expression of the photoreceptor specific proteins, rhodopsin and arrestin, exactly as *in vivo*. This suggests that photoreceptor metabolic processes in the explants *in vitro* are apparently normal. Explants therefore provide a suitable system for the investigation of retinal and photoreceptor development and maintenance. Growth factors and specific inhibitors can easily be applied and due to the culturing in serum-free medium observed effects can be attributed directly to the applied reagents. We therefore chose the retinal explant system to study the role of the Rho GTPases Rac1 and RhoA and their associated signaling pathways in mammalian photoreceptors.

Postnatal day (PN) 7 C57BL/6 mouse retinas were grown with attached retinal pigment epithelium (RPE). Retinas were cultured for eight days and after fixation of the tissue, cryosections of the explants were examined for morphologic development and apoptotic cell death using cell-specific immunohistochemical markers and the terminal deoxynucleotidyl transferase-mediated dUTP nick end labeling (TUNEL) assay.

3.1 Establishment of an organotypical retinal explant culture system

3.1.1 Retinal explants at div8 show limited apoptotic cell death

TUNEL assays of retinal explants at div8 revealed only a few apoptotic cells in the ONL (red arrows), indicating that apoptosis in the retinal explants at div8 occurred in photoreceptors, but at a rather low level (Figure 28A). In the negative control without T4 terminal deoxynucleotidyl transferase, no TUNEL-positive cells were observed (Figure 28B). As positive control, retinal explants were treated with *DNaseI* to induce DNA fragmentation. Staining of the DNA-fragments with fluorescein-labeled dUTPs in the TUNEL reaction showed that nearly all cell bodies were TUNEL-positive (Figure 28C).

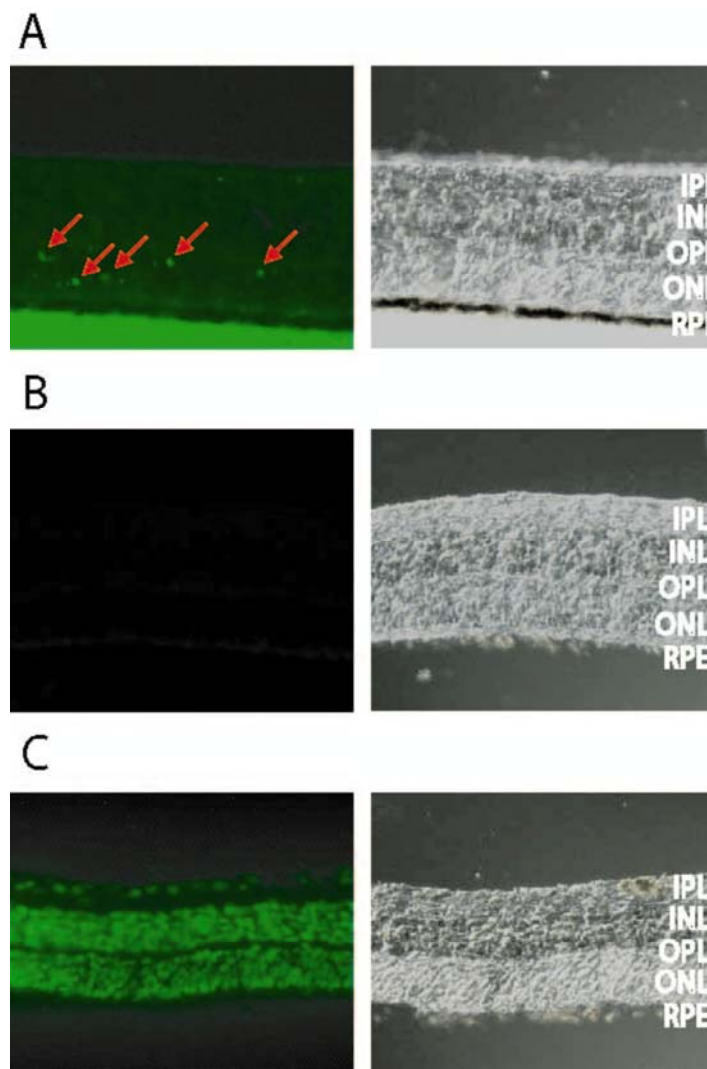


Figure 28: TUNEL assay of retinal explants (div8). **A)** TUNEL assay revealed only few apoptotic cells in the ONL. **B)** negative control without T4 terminal deoxynucleotidyl transferase. **C)** positive control with *DNaseI*-treated retina sections. IPL: Inner plexiform layer; INL: inner nuclear layer; OPL: outer plexiform layer; ONL: outer nuclear layer; RPE: retinal pigment epithelium.

3.1.2 Validation of the correct cytoarchitecture of div8 retinal explants by immunohistochemistry (IHC) with celltype-specific markers

The cytoarchitecture of the retinal explants was investigated at div8 with several celltype-specific antibodies by IHC. As rod-specific markers arrestin and rhodopsin were used. Consistent with the literature (Caffe et al., 2001), arrestin labeling was observed in the outer and inner segments of photoreceptors as well as in photoreceptor cell bodies at the ONL. Furthermore, a punctuate labeling in the OPL, corresponding to photoreceptor synapses, was observed (Figure 29A). Rhodopsin showed a strong labeling of the outer segments of rod photoreceptors and a weak staining of the rod cell bodies in the ONL (Figure 29B). Rhodopsin labeling was also observed at the cells of the RPE, but this was due to a preparational artifact during cryosectioning where the RPE, still attached to the culturing filter, was detached with parts of the ROS from the rest of the retina. Immunolabeling of syntaxin, a specific marker for amacrine cells in the retina, showed weak staining of amacrine cell bodies in the INL and intense immunoreactivity of their dendrites in the IPL as well as a faint labeling in the OPL (Figure 29C).

Staining of rod bipolar cells with a PKC α antibody showed strong immunoreactivity of their cell bodies at the outer margin of the INL and weaker immunoreactivity of descending bipolar cell axons and their axon terminals in the IPL. Additional staining in the photoreceptor layer corresponded to the labeled S-cones (Figure 29D). Staining of retinal glia cells with GS- or GFAP antibodies (Figure 29E-F) revealed immunoreactivity on radial fibers of MC throughout the entire thickness of the retina and astrocytes in the GCL. GS immunoreactivity was also detected in cell bodies of MC in the INL.

Analysis of the established organotypical retinal explants at div8 by TUNEL analysis and IHC demonstrated that the explants are viable with only a few apoptotic cells present, and that the cytoarchitecture of the retina shows a normal development. Therefore the established explant system successfully operates in our lab as described by Caffe and colleagues (Caffe, Ahuja et al. 2001) and can be used to study the physiological function of Rac1 and RhoA signaling in the retina by application of a Rock II-specific inhibitor on the explants.

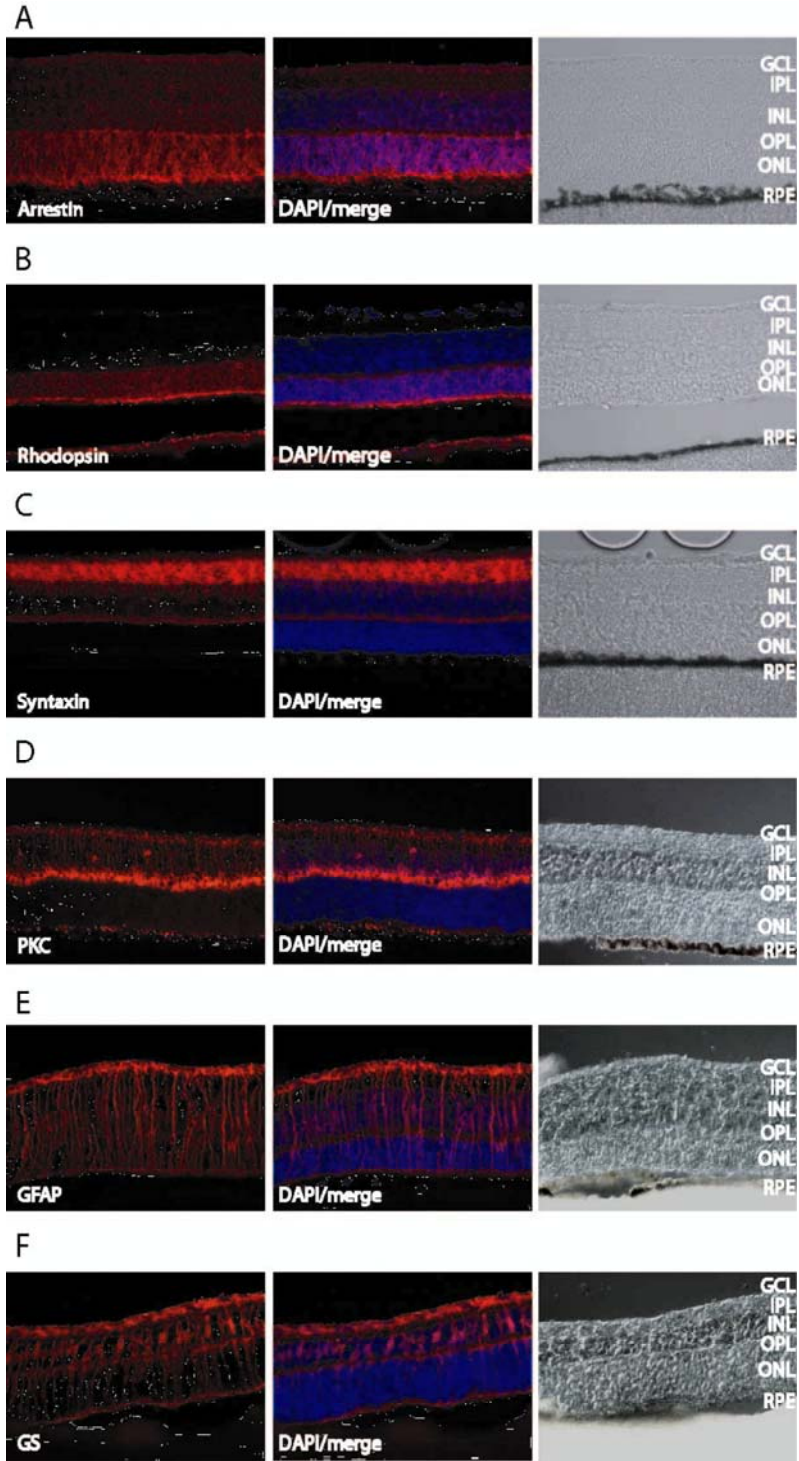


Figure 29: Immunohistochemical analysis of retinal explants (div8). Cryosections were stained with cell type-specific antibodies: **A)** anti-visual arrestin (rods). **B)** anti-rhodopsin (rods). **C)** anti-syntaxin (amacrine cells). **D)** anti-PKC α (rod bipolar cells). **E)** anti-GFAP (glia cells). **F)** anti-GS (glia cells). GCL: Ganglion cell layer; IPL: Inner plexiform layer; INL: inner nuclear layer; OPL: outer plexiform layer; ONL: outer nuclear layer; RPE: retinal pigment epithelium.

3.1.3 Application of a Rock II-specific inhibitor on retinal explants affects distribution of RhoA in photoreceptors

Arimura and colleagues (Arimura et al., 2005) demonstrated that CRMP2 is a prominent Rock II substrate in the brain. In DRG neurons, CRMP2 is phosphorylated at Thr-555 by Rock II, which is activated by GTP-bound RhoA in response to lysophosphatidic acid (LPA) signaling. Phosphorylation of CRMP2 by Rock II deactivated the ability of CRMP2 to promote microtubule assembly during growth cone collapse (Arimura et al., 2005). Because RhoA and Rac1 are regulators of the cytoskeleton and are also involved in proteins transport, it may be possible that our identified Rac1/RhoA/CRMP2/Rock II signaling complex in ROS may be involved in disc morphogenesis or protein transport via the connecting cilium. To investigate if photoreceptor morphology or protein distribution is affected by a disturbance of the Rac1- and RhoA-associated protein complexes, organotypical murine retinal explants were cultivated for eight days with and without application of the Rock II specific inhibitor Y-27632 to the culture medium.

The effect of Rock II inhibition and the consequent inhibition of Rock II-dependent CRMP2 phosphorylation (Arimura et al., 2005), on morphology, development, protein expression and localization on retinal explants was investigated.

While morphology and development of the retinas treated with Rock II inhibitor appeared normal, IHC analyses revealed several alterations on the protein level compared to the untreated control retinas.

The most prominent differences between the retinas cultured in presence or absence of the Rock II inhibitor Y-27632, were observed on sections that were co-immunolabeled with antibodies against RhoA and rhodopsin. While the labeling pattern of rhodopsin in rod photoreceptor outer segments did not differ between the treated and untreated retinas, immunoreactivity of RhoA was clearly enhanced in OS of explants treated with Y-27632 compared to control retinas (Figure 30A). Y-27632 treatment led to an increased colocalization of RhoA with rhodopsin, suggesting that the inhibition of Rock II provoked a translocation of RhoA to the OS of photoreceptors.

Co-staining of f-actin (filamentous actin) and Rac1 (Figure 30B) also revealed differences between the retinal explants cultured in presence of Y-27632 and the untreated controls. Actin filaments were labeled with fluorochrome-coupled phalloidin. Phalloidin is a fungal alkaloid from *Amanita phalloides* that binds specifically to f-actin. The labeling of f-actin in the retina cultured with Rock II inhibitor was enhanced at the outer limiting membrane, the outer plexiform layer (Gavin et al.) as well as in the IPL compared to untreated controls (Figure

30B). Immunostaining of Rac1 revealed a ubiquitous distribution of Rac1 immunoreactivity throughout the entire retina in Y-27632-treated explants and controls, but the Rac1 signal was also increased in presence of Rock II inhibitor. F-actin and Rac1 colocalized in treated and untreated retinas at the outer limiting membrane, the OPL and in the IPL.

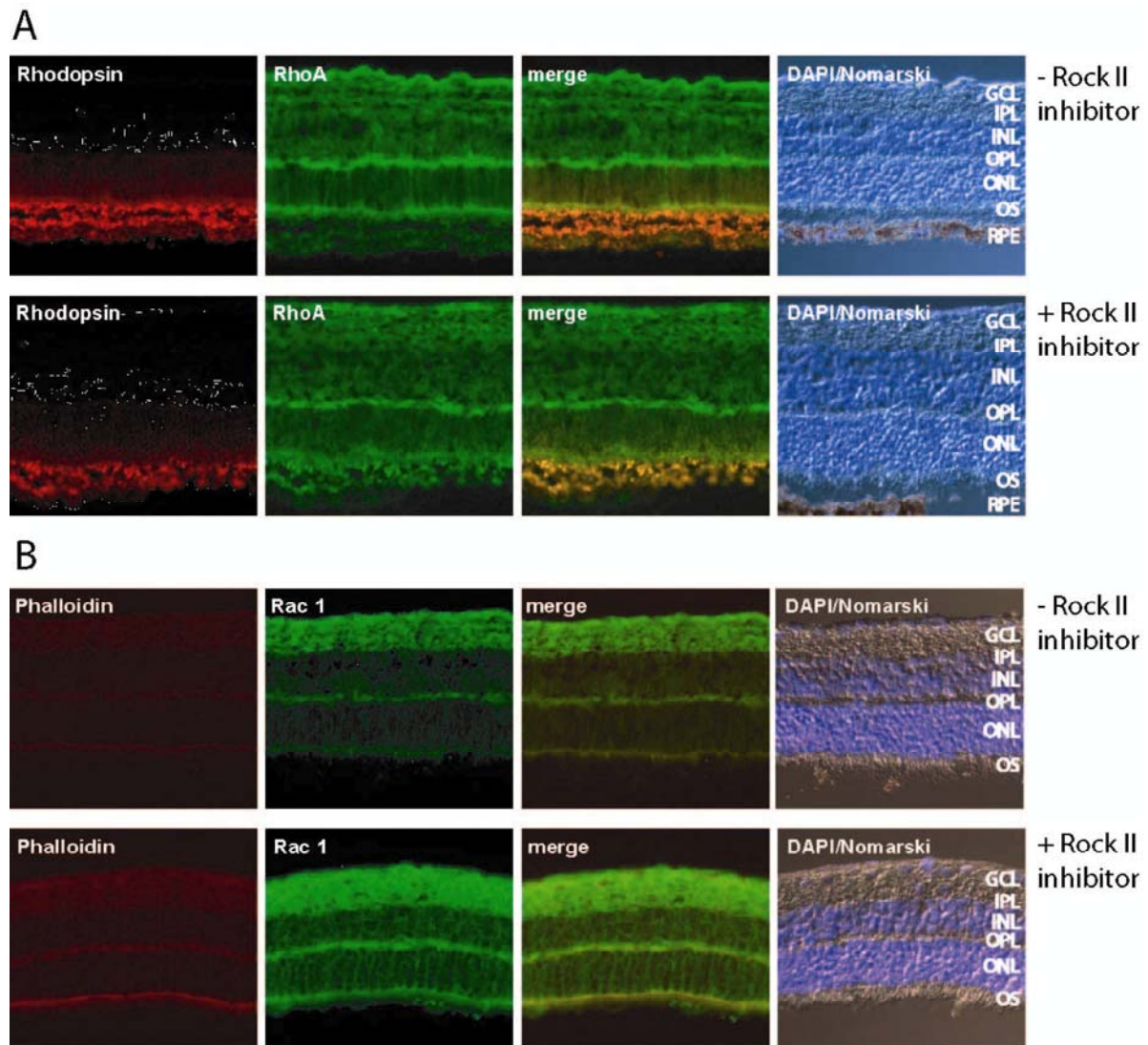


Figure 30: Immunohistochemical analysis of retinal explants (div8) that were cultured in the absence or presence of the Rock II specific inhibitor Y-27632. Co-staining was performed with the following antibodies or reagents: **A)** anti-rhodopsin (red) and anti-RhoA (green); **B)** phalloidin-alexa (red) and anti-Rac1 (green).

No differences were observed between retinas cultured with or without Rock II inhibitor, co-stained for CRMP2 and tubulin. CRMP2 immunoreactivity was detected throughout the retina (Figure 30C, left panels) but was most intense at the outer limiting membrane, as well as in the inner nuclear layer (INL) and inner plexiform layer (IPL). Tubulin immunoreactivity was also present ubiquitously distributed throughout the retina (Figure 30C, second panels

from the left). An overlay of both stainings showed that CRMP2 and tubulin colocalize throughout the retina, in Y-27632-treated as well as untreated explants.

Co-staining for Rock II and tubulin revealed a similar staining pattern. No differences in immunoreactivity were observed between of the retinas cultured in presence or absence of the Rock II inhibitor Y-27632. Rock II as well as tubulin showed a ubiquitous distribution and were colocalized throughout the retina.

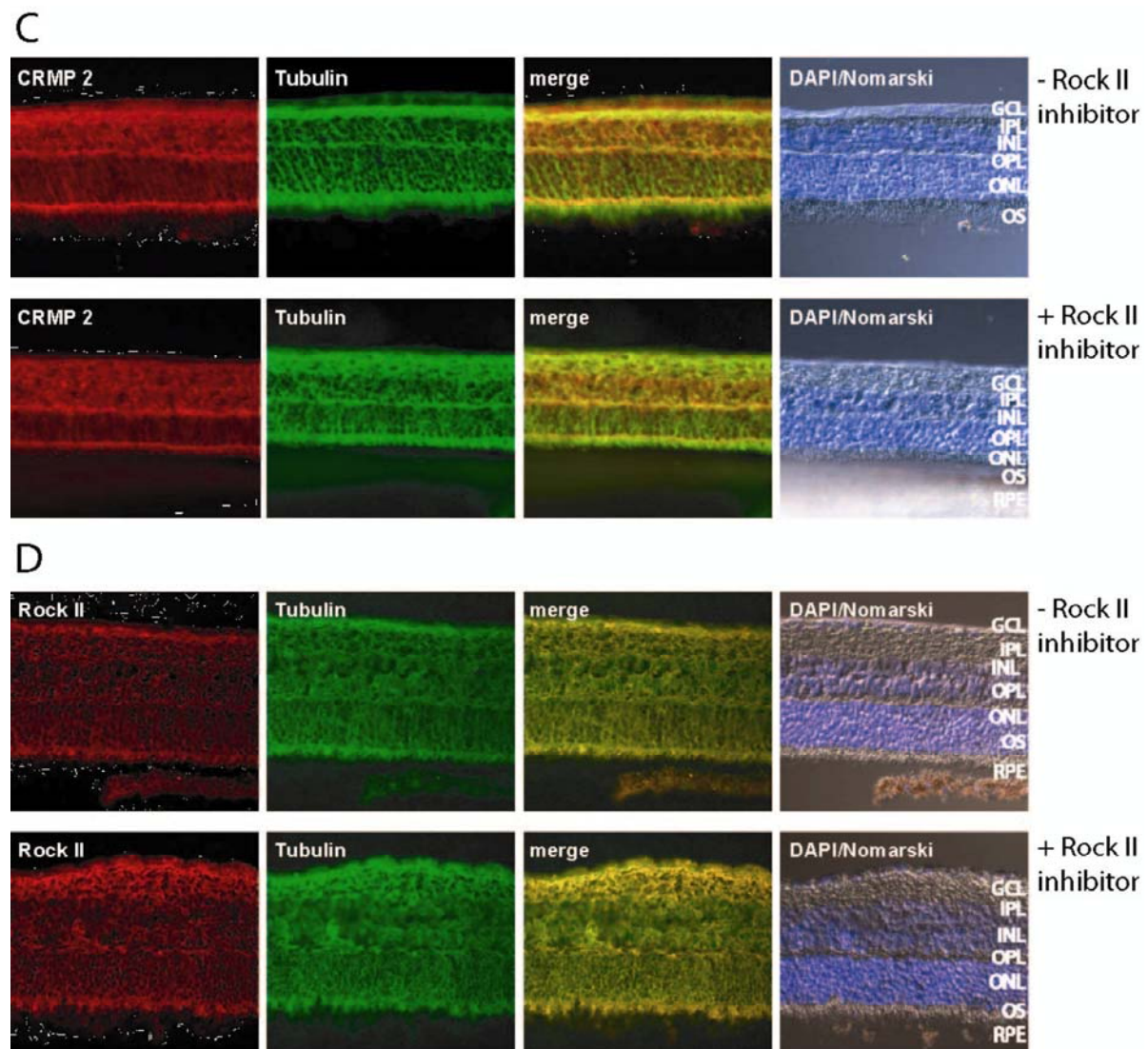


Figure 30: Immunohistochemical analysis of retinal explants (div8) that were cultured in the absence or presence of the Rock II specific inhibitor Y-27632. Co-staining was performed with the following antibodies or reagents: **C)** anti-CRMP2 (red) and anti-tubulin (green); **D)** anti-rock II (red) and anti-tubulin (green).

Altogether, the establishment of the organotypical retinal explant culture system provided an appropriate system for the investigation of the effect of Rock II inhibition on morphology, development and protein levels of the retina.

Although the functional analysis of retinal explants, grown with and without the Rock II specific inhibitor Y-27632, revealed no apparent effect on morphology and development of the retinas, several alterations on the protein level were observed. Rock II inhibition demonstrated a translocation of RhoA to the ROS membranes, while f-actin staining was shown to be enhanced in the treated retinas compared to the untreated controls, probably indicating the existence of a higher amount of f-actin.

4. OPTIMIZATION OF BN-PAGE FOR ISOLATION OF NATIVE PROTEIN COMPLEXES FROM ROS

Among IP and pull-down assays, BN-PAGE is an excellent method for the isolation and analysis of native multiprotein complexes. BN-PAGE was developed by Schägger and colleagues for the separation of mitochondrial membrane protein complexes ((Schagger et al., 1994), (Schagger, 2001)) and it is based on the solubilization of native membrane protein complexes with comparatively mild non-ionic detergent that can then be separated by native electrophoretic methods. In BN-PAGE, the isolation of native membrane protein complexes is the most critical step. Because the same detergent can extract lipids from different membranes differentially, which in turn may affect protein stability, the conditions for solubilization and electrophoresis of native proteins complexes from ROS had to be optimized systematically.

In a first step two non-ionic detergents, digitonin (6g/g protein) and β -dodecylmaltoside (DM) (7g/g Protein), were compared for their suitability to solubilize native membrane protein complexes from ROS (see Figure 31A) in a common Bis-Tris-buffered BN-PAGE setup according to Schägger (Schagger and von Jagow 1991). Prior to solubilization of the protein complexes, ROS were divided by freeze-thaw fractionation into a soluble and a membranous fraction. Solubilization of the protein complexes from the membranous fraction, with its huge amount of the highly hydrophobic seven transmembrane protein rhodopsin, revealed the best results when DM was used as detergent. The use of the milder detergent digitonin on the other hand resulted in a rather poor solubilization of ROS protein complexes, apparent by only few bands in BN-PAGE (see Figure 31A, right lane of the left panel). Solubilization with DM provided a much better solubilization and resulted in a higher number of distinct protein bands in BN-PAGE (see Figure 31A, right lane of the right panel). We therefore chose DM over digitonin for all further experiments.

The next step for the optimization of native protein complex isolation from ROS was to choose the right buffer system for BN-PAGE. Two different buffer systems described by Schägger were compared: the Bis-Tris system (Figure 31A, left panel) (Schagger and von Jagow 1991) and the imidazole system (Figure 31B, right panel) (Schagger, 2001). Although both buffer systems were nearly equal in their separation capacity, the imidazole system provided a better reproducibility and less streaking. It was therefore chosen for all further experiments.

Solubilization of the ROS membranes is increased at higher detergent concentrations, but if the detergent concentration becomes too high it reaches a critical level and detergent micelles charged with Coomassie are formed perturbing the separation of protein complexes in the gel.

Such detergent micelles started to appear if ROS membranes were solubilized with a higher DM concentration than 11g/g protein (see Figure 31C, right lane). Since no differences in the number of bands separated by the other detergent concentrations were observed, the lowest amount of detergent concentration (7g/g protein) was chosen for the following experiments.

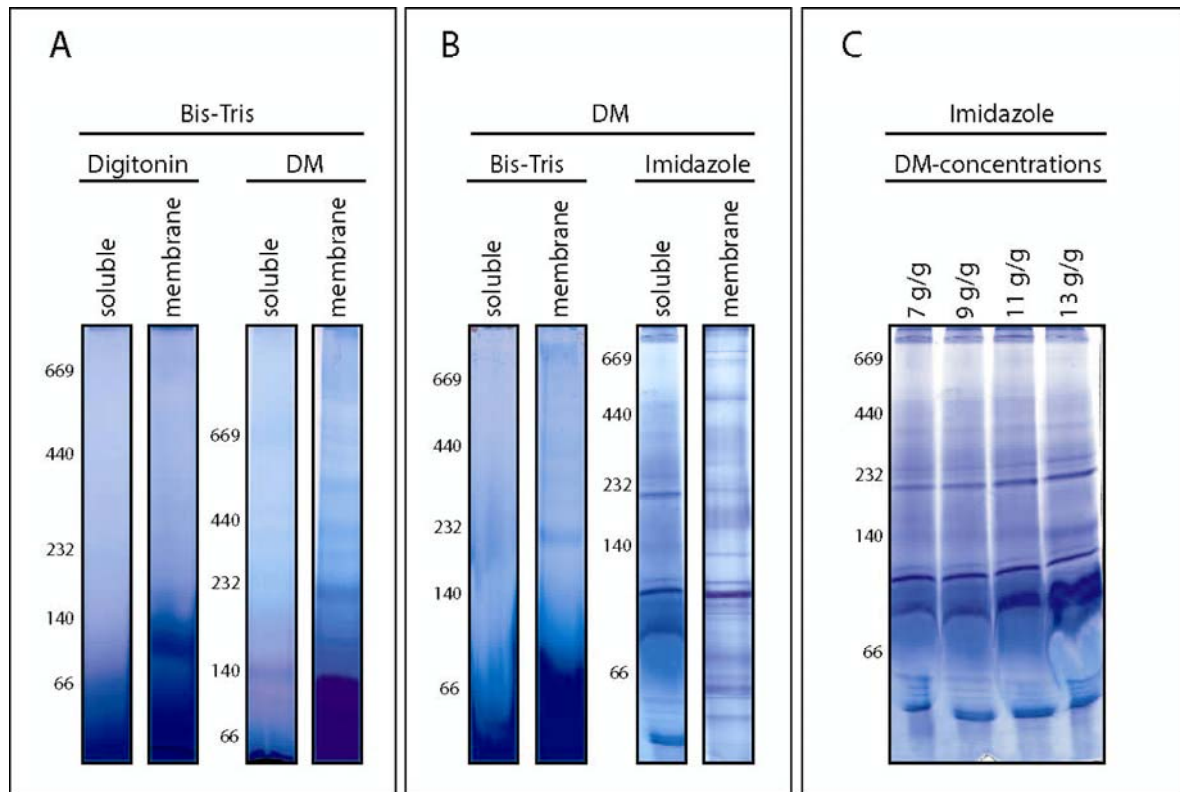


Figure 31: Solubilization and separation of native protein complexes from ROS by BN-PAGE. **A)** Optimization of the used detergent for protein complex solubilization from ROS using a Bis-tris buffered BN-PAGE. Left panel: ROS membranes (left lane) solubilized with Digitonin (6g/g protein); Right panel: ROS membranes solubilized with DM (7g/g protein). **B)** Proteins were solubilized with DM (7g/g protein) and the different buffer systems for BN-PAGE were compared: Bis-tris and imidazole. Left panel: first dimension of a BN-PAGE with a Bis-Tris buffered system. First lane: ROS light-adapted soluble fraction; second lane: ROS light-adapted membrane fraction. Right panel: first dimension of a Coomassie-stained BN-PAGE with an imidazole buffered system. First lane: ROS light-adapted soluble fraction; second lane: ROS light-adapted membrane fraction. **C)** The DM concentration was optimized for the requirements of protein complex solubilization from ROS membranes. Different DM concentrations were tested using an imidazole buffer system for BN-PAGE. The BN gel was Coomassie-stained for a better visualization of the separated protein complexes.

5. PDE δ - A GDI FOR RAC1 IN PORCINE ROS?

Rho GTPases are monomeric enzymes cycling between an active, membrane-associated GTP-bound and an inactive, soluble GDP-bound form. They function as molecular switches, regulating a variety of cellular processes, including gene expression, development of cell morphology, cell migration and cell growth (reviewed by (Etienne-Manneville and Hall, 2002)). Three classes of specific factors regulate the activity of Rho GTPases: GEFs, GAPs and GDIs (see introduction chapter 2.2.5). GDIs inhibit the dissociation of bound guanine nucleotides, GDP or GTP, from their partner GTPases, by controlling their interaction with GEFs or GAPs, respectively. Besides this function, another characteristic feature of GDIs is their ability to modulate the cycling of Rho GTPases between cytosol and membranes. By binding of the membrane-targeting prenyl moiety at the C-terminus of Rho GTPases in their hydrophobic binding pocket, GDIs solubilize Rho GTPases from membranes (reviewed by (DerMardirossian and Bokoch, 2005)).

Despite a number of studies ((Chang and Ready, 2000), (Deretic et al., 2004), (Belmonte et al., 2006)) that showed that Rac1 was an essential molecule for photoreceptor function, only limited knowledge is available to date on the regulation of Rac1 activity in photoreceptors. And, the absence of RhoGDI, one of the key regulators of Rac1 GTPase function, though present in the inner segments of photoreceptors (Deretic et al., 2004) not detected in ROS (Balasubramanian and Slepak, 2003), leads to the assumption that another molecule must assume GDI function for Rac1 in ROS. A possible candidate may be the delta subunit of retinal rod cGMP phosphodiesterase 6 (PDE δ). The 17 kDa protein PDE δ was formerly considered to be a regulatory subunit of PDE6, a key enzyme in vertebrate phototransduction (Polans et al., 1996), but in the course of the studies on PDE δ , numerous proteins were identified as PDE δ -interacting proteins. This, together with the broad expression pattern of PDE δ that is expressed in all mammalian tissues analyzed to date ((Florio et al., 1996), (Marzesco et al., 1998)), suggested that PDE δ may be a protein with various cellular functions.

As most of the identified PDE δ -interacting proteins are prenylated, PDE δ was termed prenyl-binding protein (PrBP/ δ) (Zhang et al., 2006), but PDE δ was also shown to interact with several proteins in a prenylation-independent manner (see introduction chapter 3.2). One of the most interesting properties of PDE δ is its ability to extract prenylated proteins from cellular membranes ((Florio et al., 1996), (Marzesco et al., 1998), (Nancy et al., 2002)), reminiscent of the well characterized action of RhoGDI on Rho family GTPases.

Interestingly, PDE δ also exhibits striking structural similarities with the established structure of RhoGDI ((Hoffman et al., 2000),(Nancy et al., 2002)). Both proteins have a hydrophobic pocket designed to bind prenylated proteins, but the pocket within PDE δ is shallower than the corresponding pocket in RhoGDI (Hoffman et al., 2000) (see introduction chapter 3.2.2). This properties and the fact that PDE δ is expressed at highest levels in the retina (Florio et al., 1996), (Marzesco et al., 1998) compared to all tissues analyzed to date, led us to the hypothesis, which was investigated in this study, that PDE δ may be a possible candidate to function as GDI for Rac1 in ROS.

5.1 Localization and expression of PDE δ and Rac1 in porcine retina

5.1.1 Colocalization of PDE δ and Rac1 in the retina

If PDE δ functions as GDI for Rac1 in ROS, both proteins should be present and colocalize in this substructure of the porcine retina. Since in photoreceptors interactions/colocalization of proteins can be light-regulated (Calvert et al., 2006), we performed immunohistochemistry of sections from light- and dark-adapted porcine retinas (Figure 32A and 32B). In the outer retina, immunoreactivity of Rac1 and PDE δ was detected throughout the IS and OS of photoreceptor cells in both light- and dark-adapted retinas, as well as in the outer plexiform layer and in the ONL. No apparent difference between Rac1 and PDE δ in light- or dark-adapted retinas was observed. Under both conditions, Rac1 and PDE δ colocalize in the OS and IS as well as in the OPL and ONL. Colocalization of both proteins was also observed in the inner retina (data not shown). Western blot analysis of total lysates from light- and dark-adapted ROS revealed that the amount of Rac1 and PDE δ remained unaltered in light- compared to dark-adapted ROS (Figure 33A).

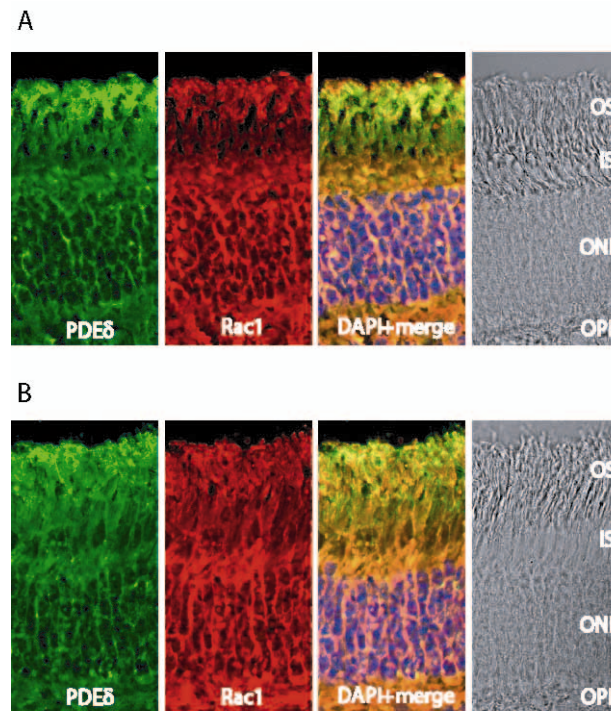


Figure 32: Colocalization of Rac1 and PDE δ in light- and dark-adapted porcine retina. Immunohistochemistry of light- **A**) or dark-adapted **B**) porcine retinal cryosections with anti-Rac1 and anti-PDE δ antibodies. Rac1 and PDE δ colocalized in the *OS* and *IS* as well as in the *OPL* and *ONL* with no significant differences between the light- or dark-adapted states. Sections incubated in the absence of primary antibody showed no staining (data not shown). *OS*, outer segment; *IS*, inner segment; *ONL*, outer nuclear layer; *OPL*, outer plexiform layer.

5.1.2 PDE δ is enriched in the membranes of dark-adapted porcine ROS

Since Rho GTPases are regulated via their membrane association (DerMardirossian and Bokoch, 2005), we investigated the distribution of Rac1 and PDE δ in soluble and membranous fractions of light- and dark-adapted ROS. PDE δ was present in a soluble and a membrane bound form. In the light-adapted state, the main fraction of PDE δ was in the soluble fraction and only a minor fraction of PDE δ was membrane bound (Figure 33A). In the dark-adapted state, PDE δ was also present in the soluble and membranous state, but compared to the light-adapted state, PDE δ was enriched in the membranes of dark-adapted ROS (Figure 33A). Rac1 on the other hand was predominantly membrane-associated, as already shown in bovine ROS (Balasubramanian et al. 2003), but very low amounts of Rac1 were also present in the soluble fractions. In contrast to PDE δ a light-dependent distribution was not detected (Figure 33A). Western blot analysis of light- and dark-adapted ROS therefore showed that PDE δ is enriched in membranes of dark-adapted ROS, demonstrating a light-dependent translocation of PDE δ .

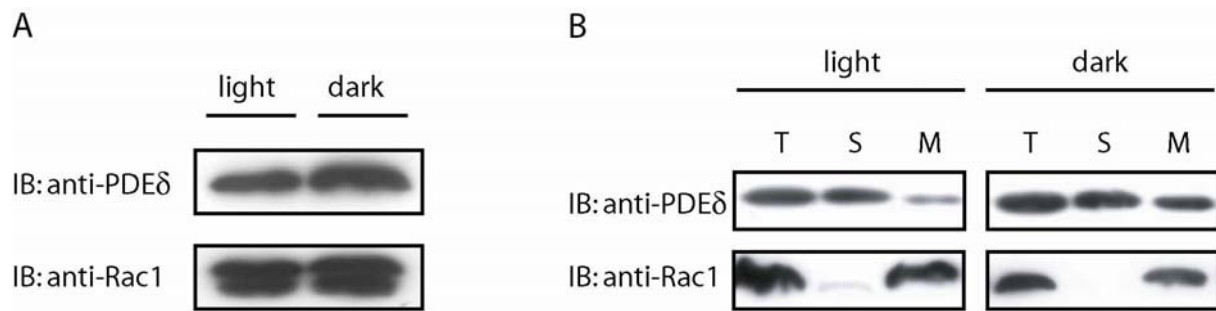


Figure 33: Localization of Rac1 and PDE δ in light- and dark-adapted porcine retina. **A)** Western blots of total lysates from light- and dark-adapted ROS (15 μ g) incubated with anti-Rac1 and anti-PDE δ antibodies. No significant difference in reactivity with these antibodies was detected, indicating that the amount of Rac1 and PDE δ remained unaltered in light- and dark-adapted ROS. **B)** light- and dark-adapted ROS corresponding to 15 μ g of protein (T) were lysed and fractionated into a soluble (S) and a membranous (M) fraction and separated by SDS-PAGE. Immunoblots with anti-Rac1 antibodies show that Rac1, primarily present in the membranous fractions, exhibited no significant differences in the distribution between the light- and dark-adapted states. Immunoblots with anti-PDE δ antibodies show that PDE δ was mainly detected in the soluble fractions, but was enriched in the membranes of dark adapted ROS. Western blot panels are representative of at least three independent experiments that gave the same result.

5.2 Interaction of PDE δ and Rac1 in ROS

5.2.1 PDE δ co-immunoprecipitates with Rac1 in ROS

To investigate if PDE δ and Rac1 interact in ROS, PDE δ and Rac1 co-immunoprecipitation assays from light- and dark-adapted ROS were performed. Light- and dark-adapted total ROS were solubilized with β -dodecylmaltoside. Rac1 was immunoprecipitated with anti-Rac1 antibodies, and the immunoprecipitates were subjected to Western blot analysis. As shown in Figure 34A, PDE δ co-immunoprecipitates with Rac1 in light- and dark-adapted ROS. More PDE δ in dark-adapted ROS indicates a stronger association of PDE δ with Rac1 in the dark-adapted state.

For further characterization of the light-regulated interaction of Rac1 and PDE δ both proteins were immunoprecipitated from the soluble and membranous fractions of light- and dark-adapted ROS. Immunoprecipitation of Rac1 from light- and dark-adapted soluble and membranous ROS fractions with anti-Rac1 revealed that consistent with the distribution of Rac1 in ROS (Figure 33A), the highest amount of Rac1 was immunoprecipitated from the membranous fractions (Figure 34B). In the soluble fractions less Rac1 was immunoprecipitated, also reflecting the situation in ROS as shown in Figure 33A. In all four fractions PDE δ was co-immunoprecipitated with Rac1, but in the soluble and membranous fractions of light-adapted ROS less PDE δ was co-immunoprecipitated. In the dark-adapted

fractions more PDE δ was found in Rac1 immunoprecipitates, underlining that both proteins exhibit a stronger association in dark-adapted ROS (Figure 34B). In the dark-adapted soluble fraction of ROS the largest part of Rac1 was complexed with PDE δ . Here only a rather small amount of Rac1 is immunoprecipitated, nevertheless, compared to the amount of Rac1, the co-immunoprecipitated amount of PDE δ is very high. To confirm these result, we co-immunoprecipitated Rac1 from light- and dark-adapted soluble and membranous ROS fractions with anti-PDE δ antibodies (Figure 34C). The immunoprecipitation of PDE δ from light- and dark-adapted soluble and membranous ROS fractions also reflected the distribution of PDE δ in light- and dark-adapted ROS (Figure 33A), showing high amount of PDE δ in the soluble fractions of light- and dark-adapted ROS. PDE δ was enriched in the dark-adapted membranous fraction compared to the light-adapted membranous fraction, where PDE δ was present only in a very low amount. Co-immunoprecipitation of Rac1 occurred in the membranous fractions. In the light-adapted membranous fraction only very little Rac1 was detectable, whereas a higher amount of Rac1 co-immunoprecipitated with PDE δ in the dark-adapted membranous fraction (Figure 34C). These data support the notion that PDE δ and Rac1 exhibit a stronger association in dark-adapted ROS, and are there preferentially in the membranous fractions.

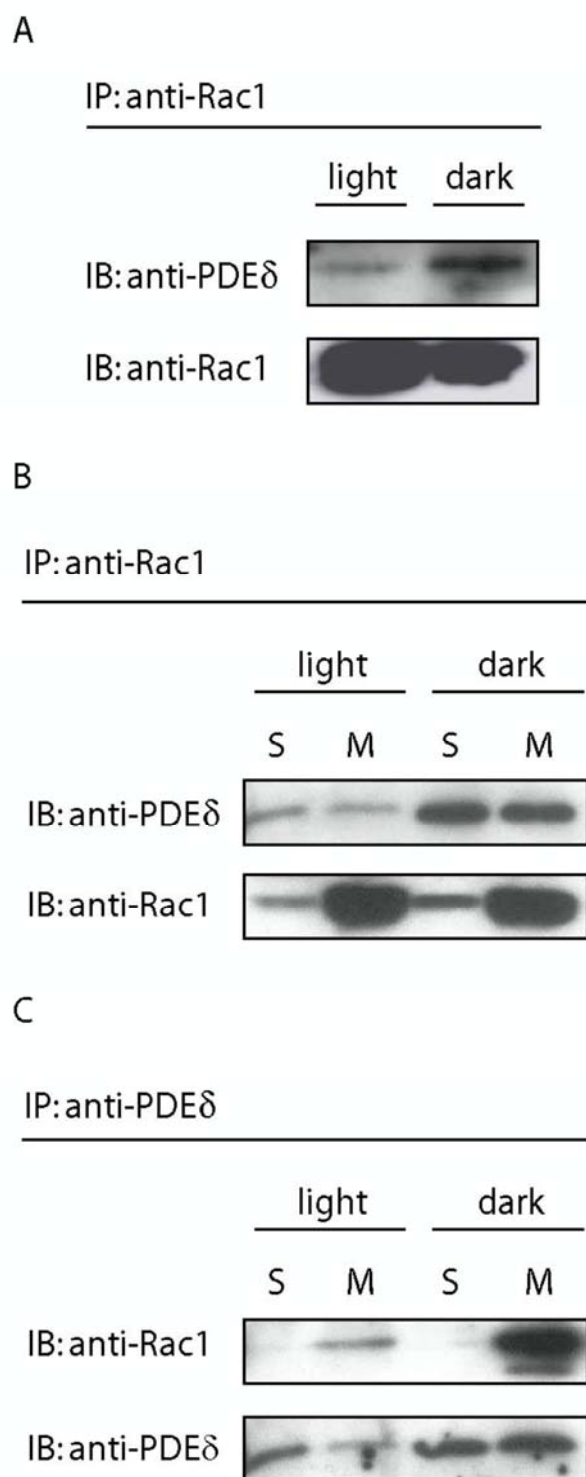


Figure 34: Light-dependent association of Rac1 and PDE δ in ROS.

A) IPs from total lysates of light- and dark-adapted ROS (500 μ g) using anti-Rac1 antibodies. Immunoprecipitated proteins were eluted with Laemi-buffer and the eluates were probed on Western blots with either anti-Rac1 or anti-PDE δ antibodies. As shown in **A**, more PDE δ coprecipitated with Rac1 in the dark-adapted state, indicating a stronger association of both proteins in the dark. **B-C**, equal amounts of protein (500 μ g), divided into soluble and membranous fractions, were immunoprecipitated using anti-Rac1 (**B**) or anti-PDE δ antibodies (**C**), respectively. Eluates were probed on Western blots with anti-Rac1 or anti-PDE δ . IP with anti-Rac1 antibodies showed that the highest amount of Rac1 was immunoprecipitated from the membranous fractions. In all four fractions PDE δ was co-immunoprecipitated with Rac1 but the highest amount of PDE δ was co-immunoprecipitated in the dark adapted fractions, indicating a stronger association of both proteins in dark-adapted ROS. Immunoprecipitates with anti-PDE δ antibodies showed the highest reactivity for PDE δ in the light- and dark-adapted soluble fractions and in the dark-adapted membranous fractions. Rac1 was immunoprecipitated in the light- and dark-adapted membranous fractions, but the strongest immunosignal for Rac1 was obtained in the dark adapted membranous fraction, again indicating a stronger association of both proteins in the dark. Immunosignals were absent from immunoprecipitates with normal mouse IgG (data not shown).

5.2.2 Isolation and analysis of native protein complexes from ROS by BN-PAGE

To further validate that PDE δ and Rac1 colocalize in ROS in native protein complexes, a two-dimensional approach, with native BN-PAGE as first dimension and denaturing SDS-PAGE as second dimension was applied (BN/SDS-PAGE). The use of non-ionic detergents allows the solubilization of native membrane protein complexes that can then be separated by

native electrophoretic methods ((Schagger et al., 1994), (Wittig and Schagger, 2005)). In the first dimension, solubilized native multiprotein complexes are separated according to their molecular masses. The second dimension resolves all individual components of the multiprotein complexes under denaturing conditions. All protein subunits released from one protein complex, are separated along the electric field gradient and are positioned in a straight line, one below the other, according to their molecular masses.

5.2.2.1 PDE δ and Rac1 colocalize in ROS in native protein complexes

Western blot analysis of the first dimension of BN-PAGE of soluble and membranous fractions of light- and dark-adapted ROS showed that PDE δ and Rac1 colocalize in dark-adapted ROS in the soluble and membranous fraction in a complex of app. 200 kDa (Figure 35, right panel). Because protein transfer from the first dimension onto blotting membranes is rather difficult and often inefficient, we also performed Western blot analysis of the second dimension of BN-PAGE of soluble and membranous fractions of light- and dark-adapted ROS.

Western blot analysis of the second dimension not only revealed that PDE δ and Rac1 colocalize in ROS but were found in diverse protein complexes depending on the light- (Figure 36A) or dark-adapted state (Figure 36B) of the retina. Colocalization of PDE δ and Rac1 was stronger in dark-adapted ROS, where both proteins colocalized in the soluble as well as in the membranous fraction. In dark-adapted ROS, PDE δ was part of distinct complexes ranging from high molecular weight complexes of 660 kDa to smaller complexes of around 90 kDa but the colocalization of PDE δ and Rac1 in the soluble and membranous fraction occurred in each case in different complexes (Figure 36B). In light-adapted ROS, no colocalization of PDE δ and Rac1 was detected in the soluble fraction. In the membranous fraction of light-adapted ROS, PDE δ and Rac1 colocalized in a single complex of approximately 300 kDa.

BN-PAGE revealed that PDE δ and Rac1 colocalize in light-and dark-adapted ROS and the stronger colocalization of both proteins in dark-adapted ROS support the data obtained from the co-immunoprecipitations (see Figure 34A-C), where both proteins also showed a stronger association in dark-adapted ROS.

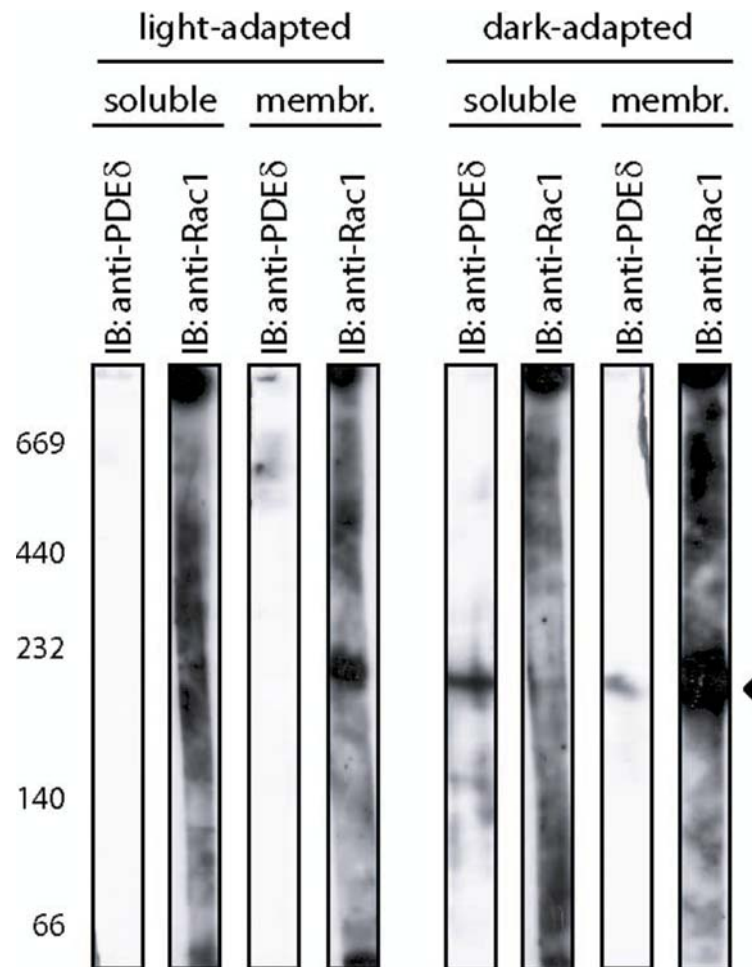


Figure 35: Western blot of a first dimension of a BN-PAGE from light- and dark-adapted ROS, soluble and membranous fractions. The BN lanes were excised from the gel and blotted onto PVDF membranes. Prior to electrotransfer using the semi-dry blotting method, the gel strips were incubated in a denaturing solution (1% SDS and 1% β -mercaptoethanol). After electrotransfer, the membrane strips were cut in the middle and one half was incubated with anti-Rac1 antibody and the other with anti-PDE δ antibody.

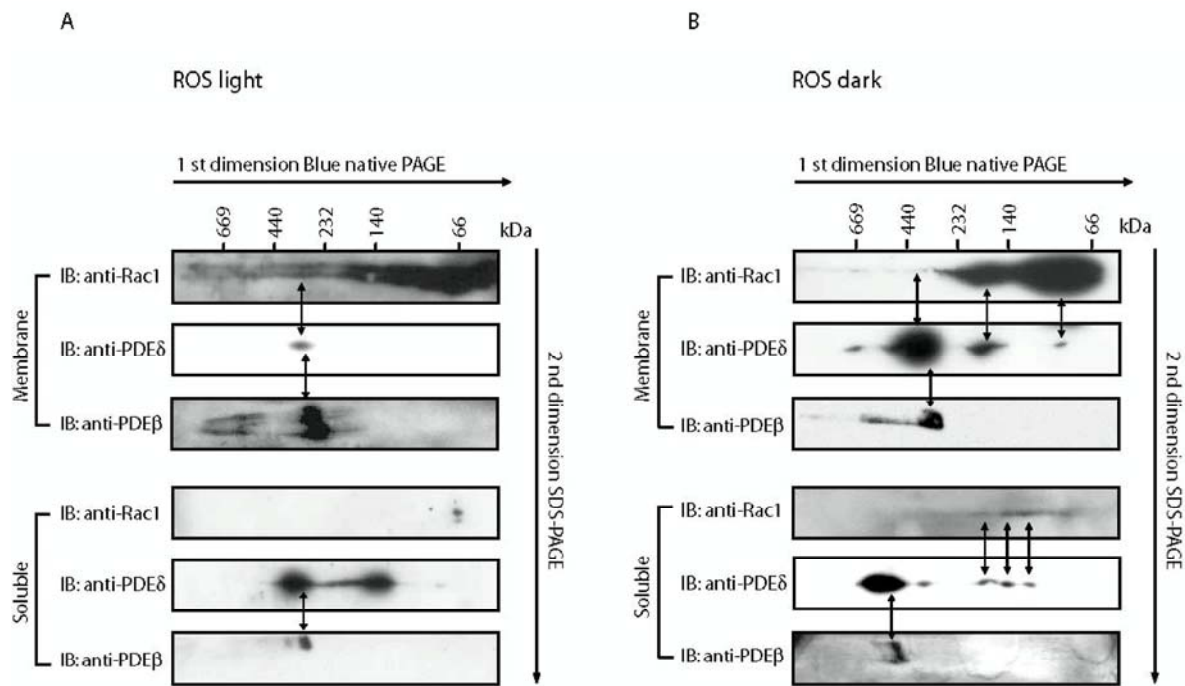


Figure 36: PDE δ and Rac1 colocalize in ROS in native protein complexes. Following solubilization with β -dodecylmaltoside, native ROS protein complexes from soluble and membranous fractions of light- and dark-adapted ROS were separated by BN-PAGE. In a subsequent denaturing second dimension, components of the native protein complexes were separated by SDS-PAGE. Western blots with anti-Rac1 and anti-PDE δ antibodies showed that, depending on the light- **A**) or dark-adapted **B**) state of the retina, PDE δ and Rac1 colocalized but were part of different complexes in ROS. Colocalization of PDE δ and Rac1 seemed to be stronger in the dark-adapted state, where both proteins colocalized in the soluble and membranous fractions. In light-adapted ROS, colocalization of PDE δ and Rac1 was only detectable in the membranous fraction but not in the soluble fraction.

5.3 Light-dependent carboxyl-methylation of Rac1 in ROS

GTPases like Rac1, containing a Cys-A-A-Leu (A = aliphatic amino acid) structure in its C-terminal region, are post-translationally processed by 1) geranylgeranylation of the cysteine residue; 2) removal of the A-A-Leu portion by peptidase cleavage and 3) carboxyl-methylation of the exposed cysteine residue (Didsbury et al., 1989) by an S-adenosyl-L-methionine-dependent methyltransferase. The carboxyl-methylation of Rac1 was shown to regulate the association of Rac1 with RhoGDI in mouse embryonic fibroblasts (Papaharalambus et al., 2005). Since the S-adenosyl-L-methionine-dependent methyltransferase is present in ROS (Perez-Sala et al., 1991) and the carboxyl-methylation is the only step in this modification pathway that is reversible under physiological conditions, and has been shown to be involved in the regulation of protein/protein interactions (Cook et al., 2000) and the activity control of prenylated proteins (Perez-Sala et al., 1991), we investigated whether Rac1 is carboxyl-methylated in ROS in a light-dependent manner.

Incubation of isolated light- and dark-adapted ROS membranous or soluble fractions with [methyl-³H]-SAM resulted in the radioactive labelling of several proteins with apparent molecular masses of about 98 and 60 kDa in the soluble fractions and with 98, 60 and a doublet at about 24 and 21 kDa in the membranous fractions (Figure 37B). The proteins at 21 and 24 kDa in the membranous fractions showed a light-dependent methylation, while the methylation of the other proteins was not altered in light- and dark-adapted ROS. For identification of the methylated proteins, the tritiated bands were cut out and subjected to MALDI-TOF/TOF-MS/MS analysis. The 98 kDa tritiated protein band was identified as PDE α and β (see Table 22). The methylation of the PDE α and PDE β in bovine retina has already been reported earlier (Cook et al., 2000). The methylation of the lower molecular weight proteins has also been reported in bovine ROS and it has been postulated that these proteins belong to a family of G-proteins (Perez-Sala et al., 1991) but until now the identity of these methylated proteins remains unknown. By mass spectrometrical analysis we identified the proteins around 24 kDa as Ras-family proteins, namely several Rab proteins (see Table 24). To verify that the light-dependent methylated 21 kDa (Figure 37B; arrowhead) protein is Rac1, we immunoprecipitated tritiated Rac1 from light-adapted membranous and soluble ROS fractions (Figure 37C). From the membranous fraction a single tritiated protein around 21 kDa was immunoprecipitated (Figure 37C, arrowhead) demonstrating that this tritiated protein indeed corresponds to Rac1. From the soluble fraction no tritiated protein was precipitated (data not shown). The 21 kDa protein band from the immunoprecipitation was excised and identified as Rac1 by mass-spectrometry (Table 23). The results revealed that Rac1 is methylated in ROS in a light-dependent manner, and that this methylation occurs in the membranous light-adapted fraction.

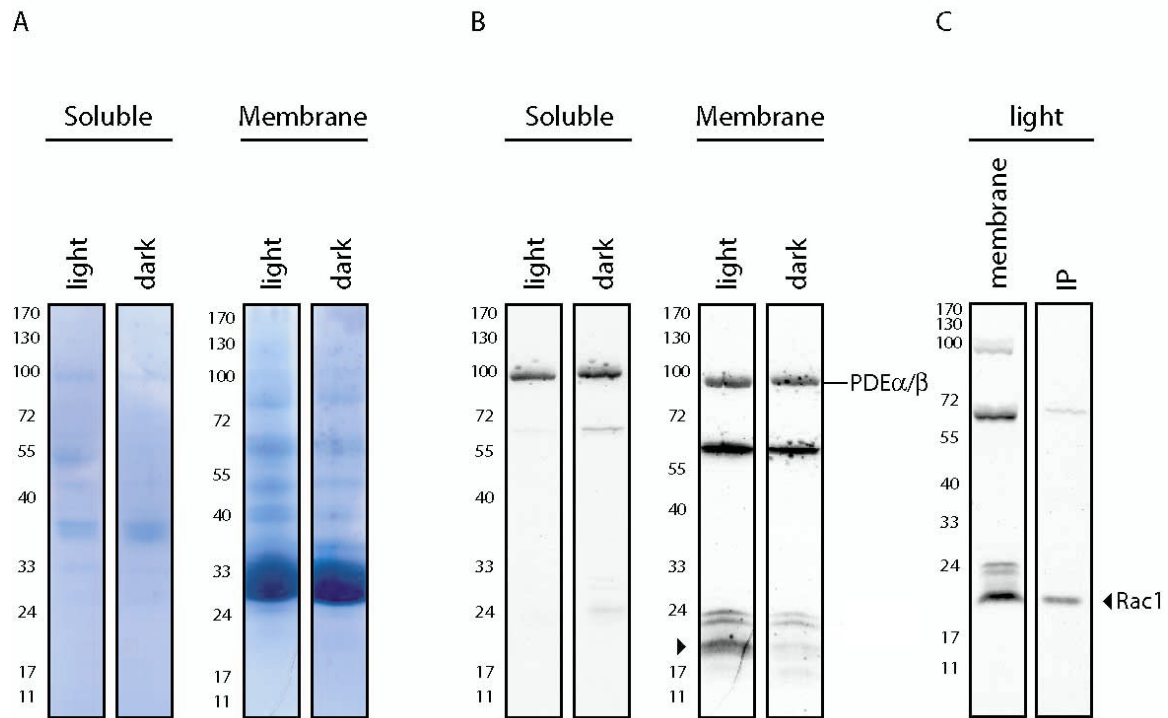


Figure 37: Light dependent carboxyl-methylation of Rac1 in ROS. *In vitro* methylation of light- or dark-adapted ROS was carried out as described in Material and Methods, chapter 2.6. After 1h of *in vitro* methylation, light- and dark-adapted ROS were divided into soluble and membranous fractions, submitted to SDS-PAGE, stained with Coomassie blue **A**) and incubated with Amplify. For fluorography, gels were dried and exposed to film at -80°C for 7 days **B**) In Figure 37A the Coomassie stained gels of the methylation assays are shown and in Figure 37B the corresponding autoradiography is pictured. Light-dependent methylation is detectable in four different bands around 24 and 21 kDa, while two other bands around 60 and 96 kDa are equally methylated in light- and dark-adapted ROS. **C**) To proof that the 21 kDa band (arrow) corresponds to Rac1, we immunoprecipitated tritiated Rac1 from light-adapted membranous fractions of ROS (see Material and Methods, chapter 2.6.1). Immunoprecipitated proteins were eluted with Laemi-buffer and subjected to SDS-PAGE. Coomassie stained gels were soaked in Amplify and bands were analyzed for methylation by fluorography. The immunoprecipitation of Rac1 shows a single tritiated protein around 21 kDa (arrow). To confirm that this band is indeed Rac1, we excised the band and analyzed it by mass spectrometry.

Table 22: LC-MS/MS analysis of the radiolabelled 98 kDa band

Protein name	Protein accession numbers	Protein molecular weight (Da)	Protein identification probability	Number of unique peptides	Number of unique spectra	Number of total spectra	Percentage of total spectra	Percentage sequence coverage
Rod cGMP-specific 3',5'-cyclic phosphodiesterase subunit alpha - Bos taurus (Bovine)	PDE6A BOVIN	99.325.4	100.00%	18	23	32	1.21%	21.00%
Rod cGMP-specific 3',5'-cyclic phosphodiesterase subunit beta precursor - Bos taurus (Bovine)	PDE6B BOVIN	98.314.7	100.00%	8	8	8	0.30%	12.70%

Table 23: LC-MS/MS analysis of immunoprecipitated, radiolabelled Rac1

Protein name	Protein accession numbers	Protein molecular weight (Da)	Protein identification probability	Number of unique peptides	Number of unique spectra	Number of total spectra	Percentage of total spectra	Percentage sequence coverage
Ras-related C3 botulinum toxin substrate 1 precursor - Bos taurus (Bovine)	RAC1 BOVIN	21.432.6	99.00%	2	2	2	0.29%	7.81%

Table 24: LC-MS/MS analysis of the radiolabelled bands around 24 kDa

Protein name	Protein accession numbers	Protein molecular weight (Da)	Protein identification probability	Number of unique peptides	Number of unique spectra	Number of total spectra	Percentage of total spectra	Percentage sequence coverage
Ras-related protein Rab-21 - Bos taurus (Bovine)	RAB21 BOVIN	24.128.6	99.00%	2	2	2	0.12%	12.20%
Ras-related protein Rab-4A - Bos taurus (Bovine)	RAB4A BOVIN	23.856.8	99.90%	2	2	2	0.12%	11.30%
Ras-related protein Rab-5B - Gallus.gallus (Chicken)	RAB5B CHICK	23.596.8	99.90%	3	3	3	0.19%	18.60%
Ras-related protein Rab-5A - Bos taurus (Bovine)	RAB5A BOVIN	23.670.9	99.90%	3	4	5	0.31%	17.20%
Ras-related protein Rab-7a - Bos taurus (Bovine)	RAB7A BOVIN	23.526.1	99.00%	2	2	2	0.14%	11.10%
Ras-related protein Rab-14 - Gallus.gallus (Chicken)	RAB14 CHICK	23.879.6	100.00%	8	9	9	0.62%	46.50%
Ras-related protein Rab-5C - Bos taurus (Bovine)	RAB5C BOVIN	23.448.7	99.90%	3	3	3	0.21%	17.60%
Ras-related protein Rab-11A - Bos taurus (Bovine)	RB11A BOVIN	24.452.0	100.00%	4	6	7	0.49%	20.80%
Ras-related protein Rab-35 - Homo sapiens (Human)	RAB35 HUMAN	23.007.2	100.00%	5	5	5	0.35%	21.40%
Ras-related protein Rab-1A - Canis familiaris (Dog)	RAB1A CANFA	22.660.4	100.00%	3	4	7	0.49%	20.50%
Ras-related protein Rab-8A - Bos taurus (Bovine)	RAB8A BOVIN	23.667.6	100.00%	4	4	4	0.28%	20.30%
Ras-related protein Rab-4B - Canis familiaris (Dog)	RAB4B CANFA	23.569.2	99.00%	2	2	2	0.14%	7.51%
Ras-related protein Rab-3A - Bos taurus (Bovine)	RAB3A BOVIN	24.936.3	100.00%	5	5	6	0.42%	27.30%
Ras-related protein Rab-2B - Homo sapiens (Human)	RAB2B HUMAN	24.197.1	99.00%	2	4	4	0.28%	7.87%
Ras-related protein Rab-2A - Canis familiaris (Dog)	RAB2A CANFA	23.528.2	100.00%	6	7	7	0.56%	36.80%
Ras-related protein Rab-18 - Bos taurus (Bovine)	RAB18 BOVIN	22.973.5	100.00%	6	6	6	0.48%	27.20%

5.4 PDE δ dissociates Rac1 from ROS membranes in vitro

Bovine PDE δ has been shown to solubilize the membrane-bound α and β subunits of PDE6 from isolated ROS membranes (Florio et al., 1996). Marzesco and colleagues (Marzesco et al., 1998) were able to show that recombinant human PDE δ was able to dissociate the small GTPase Rab13 from cellular membranes. The solubilization properties of PDE δ resemble, to some extent, that of known GDIs, such as RabGDI or RhoGDI. Therefore we tested whether purified recombinant human PDE δ (rhPDE δ) had the property to dissociate Rac1 from ROS membranes. ROS membranes were incubated with increasing amounts of rhPDE δ and centrifuged to retrieve the solubilized fraction of Rac1. The supernatant as well as the pellets were then analyzed by Western blot. As shown in Figure 38, addition of rhPDE δ resulted in the solubilization of Rac1 from ROS membranes. The solubilization occurred in a dose-dependent manner with increasing amounts of rhPDE δ . As a positive control, the ability of PDE δ to solubilize PDE β from ROS membranes (Florio et al., 1996) was tested. As expected, PDE δ solubilizes PDE β in a dose-dependent manner from the membranes (Figure 38). This demonstrated that PDE δ can solubilize Rac1 from ROS membranes, a feature characteristic for GDIs.

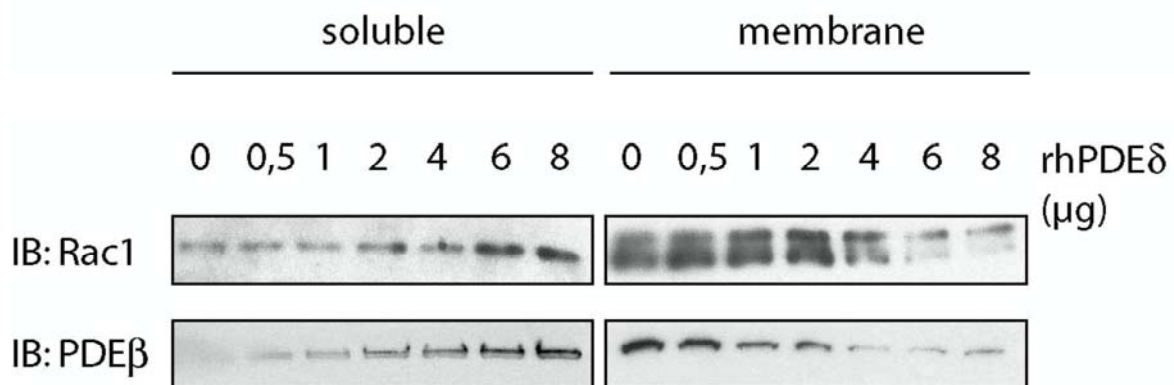


Figure 38: In vitro solubilization of Rac1 GTPase from light- and dark-adapted ROS membranes. Membranes were prepared from light- and dark-adapted ROS. The isolated membranes were incubated for 1h at 37 °C with different amounts of recombinant human PDE δ (rhPDE δ) or buffer alone and unsolubilized material was recovered by ultracentrifugation. Immunoblots with anti-Rac1 or anti-PDE β antibodies showed that PDE δ solubilizes Rac1 from ROS membranes in a dose dependent manner. The already demonstrated ability of PDE δ to solubilize PDE β from ROS membranes in a dose dependent manner (Florio et al., 1996), was used here to demonstrate the functional activity of the rhPDE δ protein.

6. IDENTIFICATION OF THE LEBERCILIN INTERACTOME

Leber congenital amaurosis (LCA) causes blindness or severe visual impairment at or within a few month of birth. By homozygosity mapping, the *LCA5* gene on chromosome 6q14 was identified, which encodes the novel ciliary protein lebercilin. Homozygous nonsense and frameshift mutations were detected in five LCA families, in the sixth family the *LCA5* transcript was completely absent (den Hollander, Koenekoop et al. 2007). Although lebercilin shows a wide expression pattern throughout development, the phenotype in patients with *LCA5* mutations is limited to the eye. Lebercilin localizes to the connecting cilia of photoreceptors and to the microtubules, centrioles and primary cilia of cultured mammalian cells. In order to characterize the function of this novel ciliary protein, tandem affinity purification (Gloeckner et al., 2007a) of N- or C-terminally tagged lebercilin fusion protein variants was used to identify lebercilin interactors from human embryonic kidney 293 (HEK293) cells. By SF-TAP and LC/MS/MS analysis, 24 lebercilin interactors were identified by Karsten Boldt in our lab (see Table 25 and (den Hollander et al., 2007)), many of which have previously been associated with microtubules and/or have important centrosomal or ciliary functions.

Swissprot ID	Human protein	Description	Identified in x of 2 analyses ^a	
			Lebercilin-NTAPe	Lebercilin-CTAPe
Q86VQ0	CF152	Lebercilin	2	2
Adaptor proteins				
P62258	1433E	14-3-3c	2	2
P31946	1433B	14-3-3β/α	2	2
P61981	1433G	14-3-3γ	2	2
P63104	1433Z	14-3-3ζ/δ	2	2
P27348	1433T	14-3-3θ	2	2
Q04917	1433F	14-3-3η	1	1
Cytoskeletal and associated proteins				
P06748	NPM	Nucleophosmin	1	1
P19338	NUCL	Nucleolin	2	2
P63167	DYL1	Dynein light chain 1	1	1
Q96FJ2	DYL2	Dynein light chain 2, cytoplasmic	1	
Cellular signaling proteins				
P67870	CSK2B	Casein kinase II subunit β	2	2
P68400	CSK21	Casein kinase II subunit α	2	2
P19784	CSK22	Casein kinase II subunit α'	2	1
Q01105	SET	Phosphatase 2A inhibitor I2PP2A	2	
Chaperones and co-chaperones				
P08107	HSP71	Heat shock 70-kDa protein 1	2	2
P11142	HSP7C	Heat shock cognate 71-kDa protein	2	2
P11021	GRP78	78-kDa glucose-related protein	2	2
P34931	HS70L	Heat shock 70-kDa protein 1L	1	
P38646	GRP75	Stress-70 protein	2	2
Miscellaneous				
Q96S59	RANB9	Ran-binding protein 9	2	1
P55209	NP1L1	Nucleosome assembly protein 1-like 1	2	
Q14241	ELOA1	Transcription elongation factor B polypeptide 3	2	
Q93008	USP9X	Ubiquitin thioesterase FAF-X	1	
Q07021	C1QBPF	Glycoprotein gC1qBP	1	1

Table 25: TAP and LC-MS/MS analysis of the lebercilin interactome in HEK293 cells. ^a N- and C-terminally tagged lebercilin was purified via SF-TAP purification. Eluates were precipitated and subjected to tryptic digestion before direct analysis by LC-MS/MS

6.1 The lebercilin multiprotein complex in the retina

6.1.1 A lebercilin specific antibody immunoprecipitates lebercilin from porcine retina lysate

In this study, the presence of the identified lebercilin interactome in the retina was demonstrated by co-immunoprecipitation of lebercilin with anti-lebercilin antibody from porcine retinal lysates in combination with Western blot analysis (see Figure 40 and (den Hollander et al., 2007).

A rabbit polyclonal antibody directed against lebercilin (obtained from C. F. Inglehearn, Leeds) was used detecting a 100 kDa signal corresponding to lebercilin in porcine retinal lysate (Figure 39 left panel), human retinal homogenates and SK-N-SH cells (a human neuroblastoma cell line) transfected with recombinant Myc-lebercilin. In lysates from untransfected cells, no signal was observed (den Hollander et al., 2007). Different amounts of anti-lebercilin antibody (4, 8 and 12 μg) were used for immunoprecipitation of lebercilin from porcine retina lysate (Figure 39). The amount of precipitated lebercilin increased with higher amounts of used antibody (Figure 39), but due to the limited availability of the anti-lebercilin antibody, we decided to use 8 μg of antibody for further immunoprecipitations.

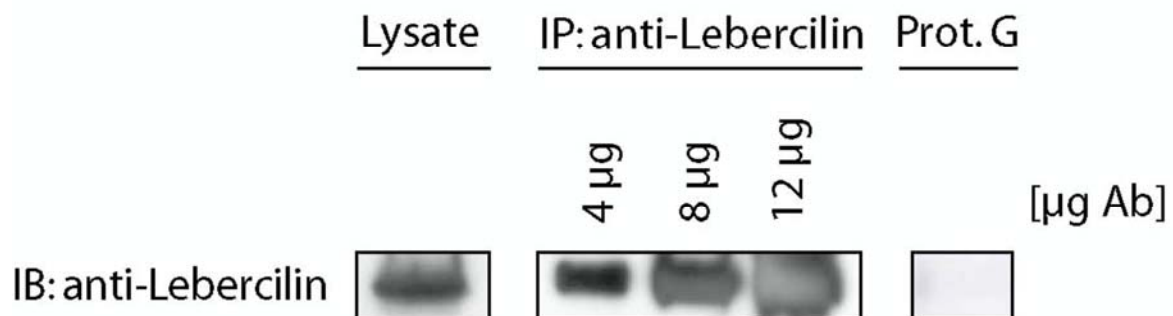


Figure 39: Immunoprecipitation of lebercilin by the anti-lebercilin antibody. The indicated amounts of antibody were used for immunoprecipitation (IP) from porcine retinal lysates (500 μg). As a control, 25 μg of retinal lysates was loaded onto SDS-gel (left lane). As a negative control, protein-G agarose beads were loaded (right lane) to demonstrate the specificity of the immunoprecipitation.

6.1.2 Analysis of the lebercilin interactome in the retina

In this study, we wanted to demonstrate that the lebercilin interactome, identified in HEK293 cells, is also present in the retina. Therefore we employed anti-lebercilin antibodies to immunoprecipitate the lebercilin-associated protein complex from porcine retinal extracts. Using specific antibodies against several members of the interactome, Western blot analysis of the anti-lebercilin immunoprecipitate was conducted. We were able to correlate the TAP

findings to the retinal context (Figure 40). Nucleophosmin, nucleolin, the dynein-binding dynactin subunits p50-dynamitin and p150-glued, 14-3-3 ϵ , and HSP70 were all found to be part of the lebercilin complex in the porcine retina. Weak unspecific binding to protein-G-agarose beads (Figure 40, right panel) was observed for nucleophosmin, nucleolin, p150-glued and HSP70. β -Actin was included as a negative control to demonstrate the specificity of the immunoprecipitation.

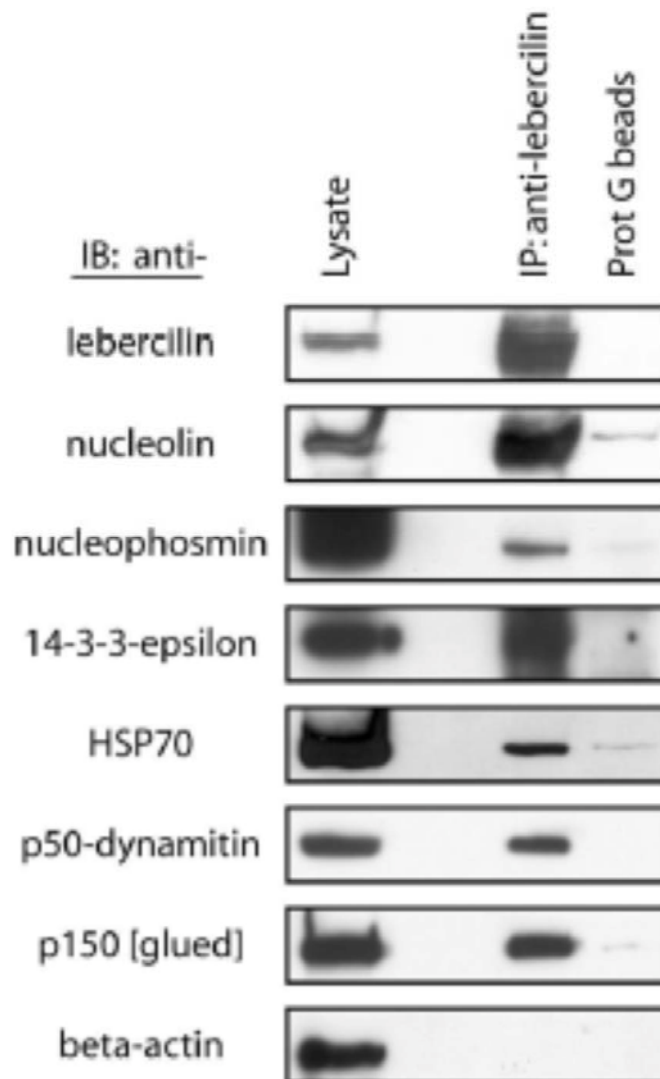


Figure 40: Lebercilin interactome. Lebercilin was immunoprecipitated with the anti-lebercilin antibody from 500 μ g of porcine retinal lysate. The purified protein complex was separated by SDS-PAGE and analysed by Western blot analysis with specific antibodies against proteins identified by mass-spectrometry after SF-TAP complex purification (see Table 22 (den Hollander et al., 2007)).

Many of the found lebercilin interactors have previously been associated with microtubules, and/or have important centrosomal or ciliary functions. The presence of cytoplasmic dynein in the TAP complexes (Table 25) was further confirmed by co-immunoprecipitation from retinal lysate through the dynein-binding dynactin subunits p50-dynamitin and p150-glued (Figure 40). It points to a link of lebercilin with microtubule dynamics and suggests an involvement in minus end-directed microtubule transport. Another interactor, nucleophosmin (Table 25 and Figure 40), has recently been shown to localize to centrosomes (Shinmura et al., 2005) where it is involved in the regulation of centrosome duplication by interaction with Rho kinase (RockII) (Ma et al., 2006). Nucleophosmin also serves as a substrate of polo-like kinase (Plk1), a key regulator of centrosome function (Zhang et al., 2004b), and binds RPGR, which is involved in X-linked retinal dystrophies (Shu et al., 2005). Nucleolin, also present in the lebercilin complex (Table 25 and Figure 40), is, like nucleophosmin, a mainly nuclear multifunctional protein involved in nucleocytoplasmic shuttling (Ginisty et al., 1999). Nucleolin has been shown to bind to casein kinase 2 (CK2) in photoreceptors ((Li et al., 1996), (Hollander et al., 1999)). CK2 is also present in the lebercilin interactome (Table 25). It regulates microtubule dynamics (Lim et al., 2004), localizes to the centrosome (Faust et al., 2002) and regulates localization of several proteins to cilia via phosphorylation ((Schermer et al., 2005), (Hu et al., 2006)). Finally, lebercilin interacts with 14-3-3 scaffold proteins (Table 25 and Figure 40), which bind and regulate the function of many phosphorylated proteins (Mhaweck, 2005) and are associated with centrosomal protein complexes ((Pietromonaco et al., 1996), (Chen et al., 2006a)).

This study confirmed the lebercilin interactome obtained from the TAP analysis and identified a lebercilin multiprotein complex in the retina. The identified interactors implicate lebercilin as a ciliary and microtubule associated protein in the retina and strengthens the relevance of the interactome in the retinal disease mechanism of LCA. Our findings emphasize the major role of disrupted ciliary processes in the molecular pathogenesis of this devastating blinding disease and the identified interactors may represent potential candidate genes for LCA and other ciliopathies.

H. DISCUSSION

1. RAC1 IN ROS: A LINK BETWEEN PHOTOTRANSDUCTION AND THE CYTOSKELETON?

Most, if not all proteins require binding to other proteins to function in a regulated manner. These regulatory and functional interactions result in the formation of various multiprotein complexes, which exhibit spatial and temporal changes, and their disruption, or alterations in their composition, leads to most profound consequences.

A large group of genetically inherited blinding diseases is associated with mutations in genes expressed in photoreceptors. Such mutations not only result in the impairment of the mutated protein, but also in a disruption of functional downstream protein networks, leading to alterations in the compositions of multiprotein complexes and in protein localization, with most severe physiological consequences. In the light-perceiving molecule rhodopsin alone, more than a hundred different mutations are described that may cause the retinal degenerative disease *retinitis pigmentosa* (<http://www.sph.uth.tmc.edu/RetNet/>).

A link between rhodopsin induced photoreceptor degeneration and the regulation of the cytoskeleton via Rac1 was established by the observation of Chang and colleagues (Chang and Ready, 2000), who demonstrated that expression of dominant active Drac1 in rhodopsin-null mutants of *Drosophila* rescued rhabdomere morphogenesis. Rac1, which belongs to the family of Rho GTPases, acts as a molecular switch in cell signaling. It cycles between an inactive, primarily cytosolic, GDP-bound state and an active GTP-bound state, usually associated with membranes, and transduces signals from membrane receptors to downstream effectors. They can modify actin- and tubulin-associated proteins and thereby regulate cytoskeletal architecture and dynamics.

The role of Rho GTPases has been investigated in a huge variety of cells, but since the functions of Rho GTPases have been shown to be cell type and stimulus specific ((Wu et al., 2006), (Cappello et al., 2006), (Chen et al., 2006b)), it has become increasingly clear that the signaling role of a Rho GTPase in a specific cell type cannot be necessarily predict its function and signaling mechanism in another type of cell. Therefore, also the knowledge about function and signaling of Rac1, one of the best studied Rho GTPases, is limited in photoreceptors, because to date, only very few studies have addressed the role of Rac1 these cells. In this study, the role of Rac1 in porcine ROS was investigated. By affinity purification of Rac1 associated protein complexes from ROS in combination with MALDI-MS/MS analysis, the Rac1 interactome in ROS was analyzed and 22 Rac1 interactors were identified. Only five of the identified Rac1 interactors have already been described in the literature,

while the other 17 interacting proteins represent putative new Rac1 interaction partners. Among the five already well established Rac1 interactors are the cytoskeletal proteins actin α and γ , as well as α and β tubulin. This strengthens the link of Rac1, which is principally known for its role in regulation of the actin cytoskeleton, with microtubule dynamics. Another identified and already well described Rac1 interactor, which links Rac1 with the microtubule cytoskeleton, is CRMP2. The tubulin interacting protein CRMP2 was described as one of the main regulators of polarity development in neuronal cells, where it was reported to be involved in the coordinated activation of Rac1 and RhoA, required for neurite outgrowth (Koh, 2006).

Elements of the phototransduction cascade, which have been identified in this study as Rac1 interactors, were the α subunit of 3',5'-cyclic-GMP phosphodiesterase, recoverin, arrestin and the α , β and γ subunits of transducin (see chapter 1.2.1). Transducin α and arrestin are direct interactors of rhodopsin, establishing a link between the light-sensing molecule rhodopsin and Rac1. G-proteins coupled membrane receptors, including rhodopsin family members, have already been shown to regulate the Rho family of GTPases (Mitchell et al., 1998), raising the possibility that rhodopsin contributes to photoreceptor morphogenesis through Rho family GTPases. Photoreceptors lacking rhodopsin have been shown to degenerate in humans, mice, and *Drosophila* ((Humphries et al., 1997), (Chang and Ready, 2000)). In *Drosophila* photoreceptors, the importance of Rac1 was demonstrated by transgenic expression of dominant active *Drosophila* Drac1 that rescued photoreceptor morphogenesis in rhodopsin-null mutants. Expression of dominant-negative Drac1 on the other hand resulted in a phenotype similar to that observed in rhodopsin-null mutant flies. Expression of a constitutively active variant of RhoA did not rescue rhodopsin-null morphogenesis, demonstrating a rescue specificity among Rho GTPases for Drac1. Thus, rhodopsin appears to organize the actin cytoskeleton through Drac1, contributing to a structural support essential for photoreceptor morphogenesis. Given the several parallels between vertebrate and *Drosophila* retinal development, it is possible that vertebrate rhodopsin may also regulate the photoreceptor cytoskeleton through Rac1. Figure 41 represents a putative, Rac1 centered, interaction network, where data obtained by IP in combination with mass spectrometry and/or WB analysis. Data from literature as well as data demonstrating PDE δ as a Rac1 interacting molecule with GDI function for Rac1 (see Discussion, chapter 2), were integrated into the network. It demonstrates that Rac1 may link rhodopsin with elements of the cytoskeleton.

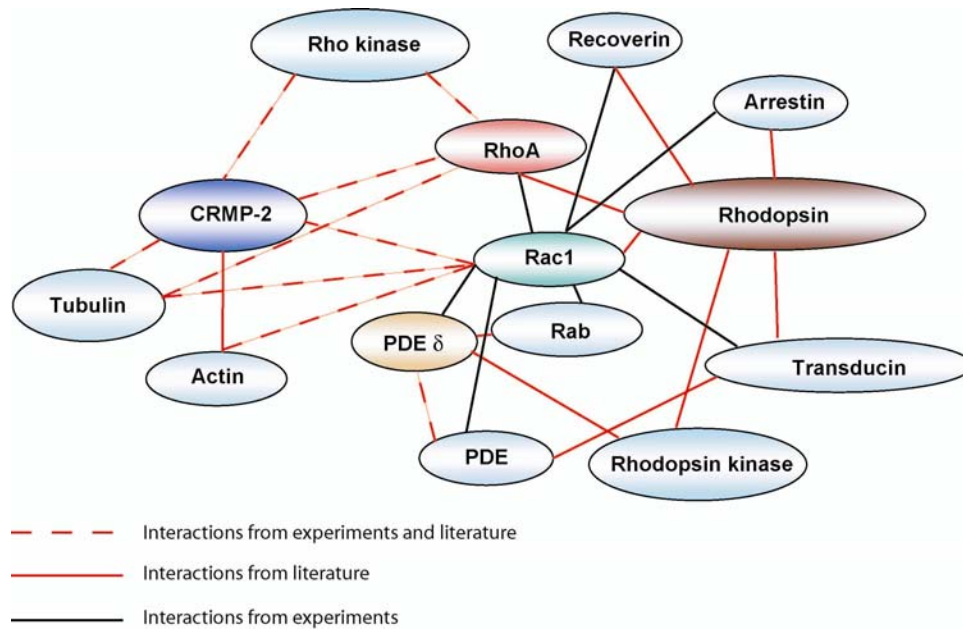


Figure 41: Rac1 interaction network. Possible Rac1 interaction network as obtained from IP data (WB and mass spectrometry), pull-down assay and literature. The interaction of Rac1 with PDE δ was added due to data, demonstrating GDI function of PDE δ for Rac1

Another important observation, linking Rho GTPase with rhodopsin signaling in photoreceptors, was that Rac1 interacts with photoexcited rhodopsin in squid and bovine photoreceptors and that Rac1 is activated by light ((Petrov et al., 1994), (Balasubramanian and Slepak, 2003)). In line with these data, a light-dependent activation of Rac1 in porcine ROS was demonstrated in this study. It was shown that Rac1 is activated in the light where it is predominantly associated with membranes. In dark-adapted ROS, only very little active Rac1 was present. Furthermore it was demonstrated in this study that CRMP2 and tubulin interact with the GTP-bound active form of Rac1. CRMPs were initially identified as signal mediators in semaphoring-induced growth cone collapse (Goshima et al., 1995). However, their ubiquitous expression in and outside the developing nervous system suggests that CRMPs are not only essential components for growth cone signaling, but are also involved in many other cellular processes ((Kamata et al., 1998), (Kato et al., 1998)). CRMP2 was identified as a tubulin interacting protein in rat CNS. It was shown to bind to tubulin heterodimers and to promote microtubule assembly and axonal elongation (Fukata et al., 2002). Nevertheless, in ROS, the interaction of Rac1 with tubulin does not seem to be provided via CRMP2. In the light-adapted soluble and membranous fractions, where CRMP2 was co-precipitated with active Rac1, no tubulin was detected and in the dark-adapted soluble fraction, where tubulin was co-precipitated with active Rac1, no CRMP2 was present. Arimura and colleagues (Arimura et al., 2005) demonstrated that phosphorylation of CRMP2 by Rock II prevents the

association of CRMP2 with tubulin heterodimers. This regulation of CRMP2-activity may result in a reduction in microtubule assembly, followed by the collapse of growth cone morphology. Several groups have demonstrated that the GTP-bound active form of RhoA is able to activate Rock II ((Matsui et al., 1996), (Ishizaki et al., 1996), (Amano et al., 1997), (Arimura et al., 2000)), which in turn can phosphorylate CRMP2 ((Shamah et al., 2001), (Knoll and Drescher, 2004), (Sahin et al., 2005)). Therefore, it may be possible that activated Rac1 is able to activate a CRMP2-specific kinase, which in turn phosphorylates CRMP2 and that this phosphorylation hinders an interaction with tubulin. The identity of this putative kinase has still to be determined, because no interaction of Rac1 with one possible kinase candidate, namely Rock II, was observed by co-immunoprecipitation assays from ROS with anti-Rac1 antibodies. Consistent with the data from the active PAK-pull down assay, CRMP2 was co-immunoprecipitated in the light-adapted fractions of ROS, where Rac1 was shown to be activated, but also in the dark-adapted soluble fraction, where it seems to interact with an inactive form of Rac1. An interaction with Tubulin was observed in the dark-adapted soluble fraction, and here the interaction with Rac1 may be provided via the tubulin-binding protein CRMP2.

Co-Immunoprecipitation of RhoA further confirmed that the Rac1/RhoA/CRMP2/tubulin/Rock II signaling complex shows a light-dependent dynamic. CRMP2, Rock II and Tubulin were exclusively co-immunoprecipitated with RhoA in the dark-adapted soluble fraction. In contrast to the Rac1 co-immunoprecipitation, RhoA colocalized with CRMP2 exclusively in the dark-adapted soluble fraction of ROS, where also tubulin and Rock II were found to be co-precipitating. This suggests that the signaling pathways of Rac1 and RhoA may be connected via CRMP2, which forms a complex in the dark-adapted soluble fraction with Rac1 and RhoA, while Rock II is only part of the RhoA signaling complex. Arimura and colleagues (Arimura et al., 2000) demonstrated that CRMP2 is phosphorylated at Thr-555 by Rock II in response to LPA in dorsal root ganglion neurons indicating a role of phosphorylated CRMP2 in LPA induced growth cone collapse. However, mutation of CRMP2 at Thr-555 (Arimura et al., 2000) or application of Rock II specific inhibitors (Wahl et al., 2000) lead only to a partial inhibition of growth cone collapse, which could result from a balance between Rac1- and RhoA-driven morphological effects regulated by CRMP2. Arimura and colleagues also demonstrated (Arimura et al., 2000) that CRMP2, in combination with either active RhoA or Rac1, and pivotally regulated by Rock II, can switch GTPase signaling, which has implications for the dynamics of neuronal growth cone guidance. It is possible that CRMP2 represents in ROS a physiological switch that coordinates

the balance between Rac1- and RhoA driven morphological effects, as already suggested by Arimura and colleagues (Arimura et al., 2000).

RhoA and Rac1 participate in protein transport as well as structural organization of cells and Rac1 is able to rescue photoreceptor degeneration in a Rhodopsin-null mutant of *Drosophila* (Chang and Ready, 2000), while the CRMP family is one of main regulators of polarity development in neuronal cells (Arimura et al., 2000). Figure 42 shows a schematic representation of the possible involvement of CRMP2 in signal transduction pathways in ROS.

ROS and its discs are renewed daily in a process in which nascent discs are formed by evagination of the plasma membrane base of the connecting cilium and are shed at the tip of the ROS ((Young, 1967), (Young and Bok, 1969), (Steinberg et al., 1980)). The process of disc morphogenesis depends on an f-actin network located at the distal end of the connecting cilium (Chaitin et al., 1984). Interference with actin filament polymerization by cytochalasin D inhibits initiation of membrane evagination and new disc formation ((Williams et al., 1988), (Vaughan and Fisher, 1989)). Because RhoA and Rac1 are regulators of the cytoskeleton and are also involved in proteins transport, it may be possible that the Rac1 and RhoA signaling complexes in ROS may be involved in disc morphogenesis or protein transport via the connecting cilium. To investigate, if the photoreceptor morphology of the protein distribution is affected by a disturbance of the Rac1 and RhoA associated protein complexes, organotypical murine retinal explants were cultivated with or without the Rock II specific inhibitor Y-27632. Although the morphology of the treated retina was unaltered compared to the untreated control, RhoA was shown to translocate upon Rock II inhibition to the ROS membranes. Rho GTPases are activated at cellular membranes, where GEFs reside (Etienne-Manneville and Hall, 2002). Because activation of Rock II by active RhoA ((Matsui et al., 1996), (Amano et al., 1997), (Ishizaki et al., 1996)) is blocked by the Rock II inhibitor Y-27632; translocation of RhoA to the ROS membrane may be an attempt of the cell to enhance the amount of active RhoA in order to try to compensate for the inhibition of Rock II.

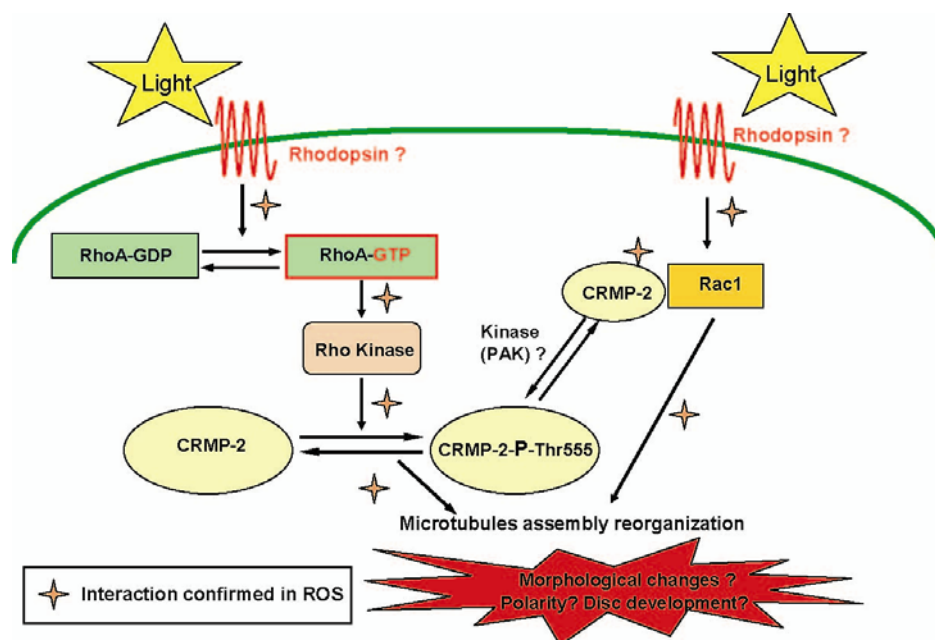


Figure 42: Possible involvement of CRMP2 in signal transduction pathways in ROS (inspired by the work of Arimura and colleagues (Arimura et al., 2000)). Interactions confirmed in ROS by literature and/or experimental data from IPs are labelled with a orange star.

In this work, the successful production and characterization of four stable lines of monoclonal antibodies directed against the C-terminus of CRMP2 is reported. As shown by Western blot analysis against retina lysate, the four monoclonal antibodies recognized specifically CRMP2, which migrates at 62kDa. Out of the four CRMP2 specific antibodies, all were suitable for immunohistochemical analysis, while only one was able to react with the native form of CRMP2 and was successfully immunoprecipitation from porcine retinal lysate. This antibody therefore represents an excellent tool for a further characterization of the CRMP2 in ROS.

In this study 22 Rac1 interactors were identified. While five of these interactors have already been described for Rac1 in the literature, the other 17 interacting proteins represent putative new Rac1 interaction partners.

Many of the identified Rac1 interactors in ROS are proteins associated with phototransduction or are components of the cytoskeleton, underlining that Rac1 may link both elements. The demonstrated light-regulation of Rac1 links these protein complexes to rhodopsin, and the identified Rac1 and RhoA associated protein complexes revealed a light and dark regulated dynamic. RhoA and Rac1 participate in protein transport as well as structural organisation of cells and Rac1 is able to rescue photoreceptor degeneration in a Rhodopsin-null mutant of *Drosophila* (Chang and Ready, 2000), and CRMP2 is one of main regulators of polarity development in neuronal cells (Arimura et al., 2000). This links light perception through rhodopsin with signaling networks involved in structural integrity and polarity of

photoreceptors and suggests an interdependence of visual perception and proper cellular structure.

2. PDE δ EXERTS GUANINE NUCLEOTIDE DISSOCIATION INHIBITOR FUNCTION FOR RAC1 IN PORCINE ROD OUTER SEGMENTS

Rac1 is important to maintain photoreceptor morphology in flies (Chang and Ready, 2000). Besides the reported light-regulation of Rac1 activity in ROS ((Petrov et al., 1994), (Wieland et al., 1990), (Balasubramanian and Slepak, 2003)), only sparse information is available concerning Rac1 function and regulation in ROS. Moreover, one of the key regulators of Rac1, RhoGDI, was not detected in ROS (Balasubramanian and Slepak, 2003), therefore it is most likely that another molecule assumes this function in this cellular compartment.

The δ subunit of PDE6 (PDE δ) exhibits striking structural and functional similarities to RhoGDI ((Florio et al., 1996), (Marzesco et al., 1998), (Hoffman et al., 2000), (Nancy et al., 2002)). In this study it was shown that PDE δ binds to Rac1 in ROS in a light-dependent manner and that this interaction correlates with a light-dependent carboxyl-methylation of Rac1. It was further demonstrated that PDE δ solubilizes, similar to a GDI, Rac1 from ROS membranes. Therefore, it was shown in this study that PDE δ exerts GDI function for Rac1 in ROS.

2.1 Localization of PDE δ and Rac1 in ROS

By immunofluorescence staining it was shown that PDE δ and Rac1 colocalize in light- and dark-adapted ROS. Moreover, a light-dependent translocation of PDE δ in the dark to ROS membranes, where Rac1 was shown to be primarily localized, was demonstrated by Western blot analysis. Although no such light-dependent translocation was reported in the literature for PDE δ or RhoGDI so far, DerMardirossian and colleagues (DerMardirossian et al., 2006) demonstrated a similar translocation of RhoGDI to the plasma membranes of HeLa cells upon phosphorylation by Src-kinase.

2.2 Light-dependent interaction of PDE δ and Rac1 in ROS

Besides the light-dependent association of PDE δ with ROS membranes, a light-dependence of the Rac1/PDE δ interaction, which is stronger in dark-adapted ROS, was also demonstrated in this study. This demonstrates that the Rac1-PDE δ protein complex is favoured in the dark-adapted state, where Rac1 predominantly exists in the GDP-bound state (Balasubramanian and Slepak, 2003). While PDE δ and Rac1 in the light only interact at ROS membranes, both proteins are associated in the soluble and membranous fractions of dark-adapted ROS.

The association of the Rac1-PDE δ complex with ROS membranes is of particular interest in the current debate, concerning the localization and the mechanism of the dissociation of Rho GTPase-RhoGDI complexes, which is still poorly understood (Ugolev et al., 2006). Our data argues for the movement of an intact Rho GTPase-RhoGDI complex to the membrane, where dissociation is to take place. This would also fit a model by Lian and colleagues (Lian et al., 2000), which demonstrated that Rac1 and RhoGDI can interact even when Rac1 is bound to the membrane. RhoGDIs were reported to be negative regulators of Rho GTPase activity by inhibition of GDP (and GTP) dissociation, inhibition of intrinsic and GAP-induced GTP hydrolysis, and by controlling the partitioning of Rho GTPases between cytosol and plasma membranes ((Zalcman et al., 1999), (Dransart et al., 2005)). Structural and biochemical studies depicted that GEFs cannot act on Rho GTPases when they are bound to RhoGDI ((Snyder et al., 2002), (Robbe et al., 2003)). The association of PDE δ with Rac1 at the membranes of dark-adapted ROS may therefore control the association of Rac1 with GEFs, keeping the GTPase in the inactive state.

Despite these negative roles attributed to RhoGDIs, GDIs are more and more discussed to act as positive regulators, necessary for the correct targeting and regulation of Rho GTPases by conferring cues for spatial restriction, guidance and availability to effector molecules. The fact that RhoGDI binding does not involve engagement of all the effector-binding regions on the GTPases (Dvorsky and Ahmadian, 2004), permits the formation of higher order complexes, as observed in our study by BN-PAGE from light- and dark-adapted ROS. We showed that PDE δ and Rac1 form different complexes in the soluble and membranous fractions of dark-adapted ROS with probably different interacting molecules. One example of a functional higher order complex was shown by Grizot and colleagues (Grizot et al., 2001). The authors demonstrated that the Rac1(GDP)-RhoGDI complex was able to interact with and activate NADPH oxidase, although its efficiency was lower than that of free Rac1(GTP).

2.3 In the manner of a GDI, PDE δ dissociates Rac1 from ROS membranes

By application of purified rhPDE δ it was shown that the interaction of PDE δ with Rac1 leads to a dose-dependent solubilization of Rac1 from purified ROS membranes *in vitro*, a trait that was already shown to be characteristic for RhoGDI, which exerts such activity on Rho family GTPases (DerMardirossian and Bokoch, 2005).

Besides this observed characteristic GDI function of PDE δ , the hypothesis that PDE δ exerts such a function is further supported by its reported structural similarity with RhoGDI. Data provided by recent crystallography of PDE δ revealed an immunoglobulin-like β -fold

structure, similar to the structure of RhoGDI. Two β -sheet propellers form a hydrophobic pocket that provides the structural basis for the binding between PDE δ and prenyl chains (Hanzal-Bayer et al., 2002), although the pocket identified within PDE δ was shown to be shallower than the corresponding pocket in RhoGDI (Hoffman et al., 2000). While RhoGDI function depends on interaction with prenyl groups ((Hoffman et al., 2000), (Di-Poi et al., 2001)), PDE δ , however, exerts binding in a prenylation-dependent as well as in a prenylation-independent fashion. Interaction with the non-prenylated N-terminus of the retinal protein RPGR ((Linari et al., 1999b)), which is homologous to the guanine nucleotide exchange factor (GEF) RCC1, and with the prenylated GTPase Arl1 ((Linari et al., 1999a), was shown to occur in a prenylation-independent manner. For the interaction of PDE δ with the catalytic subunits of PDE6 on the other hand, prenylation of the subunits was shown to be essential (Florio et al., 1996). It is also likely that the interaction of PDE δ with Rac1 is mediated with participation of the prenylated C-terminus of Rac1.

As most Rho GTPases, Rac1 is synthesized as soluble protein in the cytosol but is able to associate with membranes via a posttranslational prenyl-modification at its C-terminus, a geranylgeranyl tail, that is inserted into the lipid bilayer of cellular membranes (Clarke, 1992). GDIs are able to solubilize the Rho GTPases by transfer of the prenyl tail from the lipid bilayer into their prenyl binding pocket, resulting in dissociation of the GDI-GTPase complex from the membrane (Nomanbhoy et al., 1999). The ability of PDE δ to solubilize Rac1 from ROS membranes suggests a similar mechanism.

2.4 Light-dependent carboxyl-methylation of Rac1 in ROS

The C-terminal cystein of Rac1 is posttranslationally not only modified by prenylation, but also by carboxyl-methylation (Didsbury et al., 1989). The responsible S-adenosyl-L-methionine-dependent methyltransferase (ICMT) was found in ROS, where it is associated with membranes (Perez-Sala et al., 1991). In contrast to prenylation, carboxyl-methylation is a posttranslational modification that is reversible under physiological conditions. Because carboxyl-methylation is supposed to be involved in the regulation of protein/protein interactions (Cook et al., 2000) and the controlling of the activity of prenylated proteins (Perez-Sala et al., 1991), the methylation pattern of Rac1 in light- and dark-adapted ROS by *in vitro* methylation using [methyl-³H]-SAM was investigated. A light-dependent methylation of membrane-bound Rac1 in light-adapted ROS that correlates with the reported light-dependent interaction of Rac1 with PDE δ was demonstrated. The observed stronger

association of both proteins in dark-adapted ROS, suggests a stronger interaction of PDE δ with unmethylated Rac1.

This correlates well with data from Papaharalambus et al. (Papaharalambus et al., 2005), who investigated the effect of ICMT inhibition on the interaction of Rac1 with its inhibitor RhoGDI. The authors showed that the association of non-methylated Rac1 with RhoGDI was dramatically increased in the *Icmt*-deficient *versus* wild-type mouse embryonic fibroblasts. These results suggested that ICMT regulates Rac1 activity by controlling the interaction of Rac1 and its GDI, probably by regulating the release of Rac1 from the GDI complex (Papaharalambus et al., 2005). Besides the light-dependent carboxyl-methylation of Rac1 described in this study, Rac1 was also shown to be activated in response to light ((Petrov et al., 1994), (Wieland et al., 1990), (Balasubramanian and Slepak, 2003)). In membranes of light-adapted ROS, Rac1 exists predominantly in the active, GTP-bound state (Balasubramanian and Slepak, 2003). If the light-dependent methylation of Rac1 in ROS is due to a light-dependent activation of ICMT or if the carboxyl-methylation is modulated by GTP binding, as suggested by Backlund and Aksamit (Backlund and Aksamit, 1988), remains to be elucidated.

The data presented in this study demonstrates that Rac1 and PDE δ interact in ROS in a light-dependent manner and that PDE δ exerts GDI function for Rac1. Both proteins have been supposed to play a role in protein transport (Deretic et al., 2004), (Zhang et al., 2004a), (Zhang et al., 2006), (Zhang et al., 2007). Protein trafficking is particularly important for photoreceptors where high turnover of outer segments, housing the phototransduction machinery, requires unusually active protein transport (Zhang et al., 2004a). PDE δ is likely to act as a soluble transport factor for prenylated proteins in photoreceptors, thereby associated with Arl proteins ((Zhang et al., 2004a), (Zhang et al., 2006), (Zhang et al., 2007)). Data from transgenic mice lacking PDE δ expression in the retina due to targeted mutation (Zhang et al., 2007) display an impaired transport of prenylated proteins, particularly GRK1 and PDE6, to rod and cone outer segments. An altered photoreceptor physiology and a phenotype of a slowly progressing rod/cone dystrophy was also observed (Zhang et al., 2007). Rac1 was shown to be involved in the regulation of rhodopsin transport carrier fusion in photoreceptors of *Rana barlandieri* conjointly with phosphoinositides, ezrin/moesin and Rab8 (Deretic et al., 2004). Although no clear function for Rac1 in photoreceptors could be assigned so far, it was shown to be very important for the development and maintenance of photoreceptor morphology as demonstrated by the rescue of the rhabdomere morphogenesis by expression of dominant active Drac1 in rhodopsin-null *Drosophila* mutants (Chang and Ready, 2000).

For a better understanding of Rac1 function in photoreceptors, a better understanding of its regulation is a prerequisite. This study demonstrates a light-dependent regulation of Rac1 via methylation as well as by PDE δ , a protein providing GDI function for Rac1 in ROS. This will hopefully help to elucidate the role of Rac1 and PDE δ for photoreceptor function.

I. PERSPECTIVE

This study demonstrated that the Rac1/RhoA/CRMP2/Rock II/tubulin signaling complex in ROS shows a light-dependent dynamic. This suggests that CRMP2 functions in ROS as a physiological switch that coordinates the balance between Rac1- and RhoA driven signaling, as already suggested by Arimura and colleagues for CRMP2 signaling in neurons (Arimura et al., 2000). In this study the successful production and characterization of four stable lines of monoclonal antibodies, directed against the C-terminus of CRMP2, was reported. While all four antibodies were suitable for WB and immunohistochemical analysis, one antibody was also able to precipitate the native CRMP2 protein from porcine retinal lysate, and therefore represents an excellent tool for a further characterization of CRMP2 function in ROS.

Objective 1: Identification of the CRMP2 interactome in ROS.

Co-immunoprecipitation of CRMP2 interacting proteins ROS in combination with mass spectrometry may enable the identification of the CRMP2 interactome in ROS.

Objective 2: Quantification of light- and dark-dependent CRMP2 interactions in ROS.

Quantitative labelling methods, like ICPL, may shed light on the possible regulatory function of CRMP2 of light-regulated signaling pathways in ROS. Labelling of light- and dark-adapted ROS and subsequent co-immunoprecipitation of CRMP2 interacting proteins may enable a quantification of light- and dark-dependent interactions in ROS.

Objective 3: Identification of light- and dark-dependent CRMP2 phosphorylation sites

Immunoprecipitation of CRMP2 from light- and dark-adapted ROS in combination with subsequent mass spectrometric analysis and phosphopeptide-enrichment (*e.g.* TiO₂) may enable an identification of the phosphorylation status of CRMP2 in light- and dark-adapted ROS. Although this study already suggested Rock II as a possible kinase for CRMP2 in ROS, it was already shown in several studies that CRMP2 is regulated by several kinases in response to extracellular stimulation ((Arimura et al., 2000), (Cole et al., 2004), (Brown et al., 2004), (Yoshimura et al., 2005)). Therefore Rock II may not be the only kinase phosphorylating CRMP2 in ROS and the existence of several different phosphorylation states of CRMP2 is likely.

This study also demonstrated by BN-PAGE analysis that PDE δ and Rac1 colocalize in ROS in native protein complexes, revealing a light-dependent dynamic. The size of the identified

Rac1 and PDE δ associated protein demonstrates a formation of higher order complexes and suggests an involvement of other, yet unidentified proteins. For Rac1 in complex with RhoGDI one example of a functional higher order complex was already shown by Grizot and colleagues (Grizot et al., 2001). The authors demonstrated that the Rac1(GDP)-RhoGDI complex was able to interact with and activate NADPH oxidase, although its efficiency was lower than that of free Rac1(GTP).

Objective 4: Identification of the Rac1 and PDE δ associated protein complexes composition by BN-PAGE in combination with mass spectrometry.

J. REFERENCES

- Adamus, G., Amundson, D., Seigel, G.M. and Machnicki, M. Anti-enolase-alpha autoantibodies in cancer-associated retinopathy: epitope mapping and cytotoxicity on retinal cells. *J Autoimmun* **11** (1998), pp. 671-7.
- Adra, C.N., Manor, D., Ko, J.L., Zhu, S., Horiuchi, T., Van Aelst, L., Cerione, R.A. and Lim, B. RhoGDIgamma: a GDP-dissociation inhibitor for Rho proteins with preferential expression in brain and pancreas. *Proc Natl Acad Sci U S A* **94** (1997), pp. 4279-84.
- Allen, W.E., Zicha, D., Ridley, A.J. and Jones, G.E. A role for Cdc42 in macrophage chemotaxis. *J Cell Biol* **141** (1998), pp. 1147-57.
- Amano, M., Chihara, K., Kimura, K., Fukata, Y., Nakamura, N., Matsuura, Y. and Kaibuchi, K. Formation of actin stress fibers and focal adhesions enhanced by Rho-kinase. *Science* **275** (1997), pp. 1308-11.
- Anant, J.S., Ong, O.C., Xie, H.Y., Clarke, S., O'Brien, P.J. and Fung, B.K. In vivo differential prenylation of retinal cyclic GMP phosphodiesterase catalytic subunits. *J Biol Chem* **267** (1992), pp. 687-90.
- Arimura, N., Inagaki, N., Chihara, K., Menager, C., Nakamura, N., Amano, M., Iwamatsu, A., Goshima, Y. and Kaibuchi, K. Phosphorylation of collapsin response mediator protein-2 by Rho-kinase. Evidence for two separate signaling pathways for growth cone collapse. *J Biol Chem* **275** (2000), pp. 23973-80.
- Arimura, N., Menager, C., Kawano, Y., Yoshimura, T., Kawabata, S., Hattori, A., Fukata, Y., Amano, M., Goshima, Y., Inagaki, M., Morone, N., Usukura, J. and Kaibuchi, K. Phosphorylation by Rho kinase regulates CRMP-2 activity in growth cones. *Mol Cell Biol* **25** (2005), pp. 9973-84.
- Artemyev, N.O., Surendran, R., Lee, J.C. and Hamm, H.E. Subunit structure of rod cGMP-phosphodiesterase. *J Biol Chem* **271** (1996), pp. 25382-8.
- Backlund, P.S., Jr. and Aksamit, R.R. Guanine nucleotide-dependent carboxyl methylation of mammalian membrane proteins. *J Biol Chem* **263** (1988), pp. 15864-7.
- Baehr, W.L., P., Visual Cascade, Article A225 ed. Nature Publishing Group (2001).
- Balasubramanian, N. and Slepak, V.Z. Light-mediated activation of Rac-1 in photoreceptor outer segments. *Curr Biol* **13** (2003), pp. 1306-10.
- Batten, M.L., Imanishi, Y., Maeda, T., Tu, D.C., Moise, A.R., Bronson, D., Possin, D., Van Gelder, R.N., Baehr, W. and Palczewski, K. Lecithin-retinol acyltransferase is essential for accumulation of all-trans-retinyl esters in the eye and in the liver. *J Biol Chem* **279** (2004), pp. 10422-32.
- Beales, P.L. Lifting the lid on Pandora's box: the Bardet-Biedl syndrome. *Curr Opin Genet Dev* **15** (2005), pp. 315-23.

- Beales, P.L., Elcioglu, N., Woolf, A.S., Parker, D. and Flinter, F.A. New criteria for improved diagnosis of Bardet-Biedl syndrome: results of a population survey. *J Med Genet* **36** (1999), pp. 437-46.
- Beavo, J.A., Conti, M. and Heaslip, R.J. Multiple cyclic nucleotide phosphodiesterases. *Mol Pharmacol* **46** (1994), pp. 399-405.
- Belmonte, M.A., Santos, M.F., Kihara, A.H., Yan, C.Y. and Hamassaki, D.E. Light-Induced photoreceptor degeneration in the mouse involves activation of the small GTPase Rac1. *Invest Ophthalmol Vis Sci* **47** (2006), pp. 1193-200.
- Berson, E.L. Retinitis pigmentosa. The Friedenwald Lecture. *Invest Ophthalmol Vis Sci* **34** (1993), pp. 1659-76.
- Bibb, L.C., Holt, J.K., Tarttelin, E.E., Hodges, M.D., Gregory-Evans, K., Rutherford, A., Lucas, R.J., Sowden, J.C. and Gregory-Evans, C.Y. Temporal and spatial expression patterns of the CRX transcription factor and its downstream targets. Critical differences during human and mouse eye development. *Hum Mol Genet* **10** (2001), pp. 1571-9.
- Bjarnadottir, T.K., Gloriam, D.E., Hellstrand, S.H., Kristiansson, H., Fredriksson, R. and Schioth, H.B. Comprehensive repertoire and phylogenetic analysis of the G protein-coupled receptors in human and mouse. *Genomics* **88** (2006), pp. 263-73.
- Blacque, O.E. and Leroux, M.R. Bardet-Biedl syndrome: an emerging pathomechanism of intracellular transport. *Cell Mol Life Sci* **63** (2006), pp. 2145-61.
- Bowes, C., Li, T., Danciger, M., Baxter, L.C., Applebury, M.L. and Farber, D.B. Retinal degeneration in the rd mouse is caused by a defect in the beta subunit of rod cGMP-phosphodiesterase. *Nature* **347** (1990), pp. 677-80.
- Boylan, J.P. and Wright, A.F. Identification of a novel protein interacting with RPGR. *Hum Mol Genet* **9** (2000), pp. 2085-93.
- Bradford, M.M. A rapid and sensitive method for the quantitation of microgram quantities of protein utilizing the principle of protein-dye binding. *Anal Biochem* **72** (1976), pp. 248-54.
- Brann, M.R. and Cohen, L.V. Diurnal expression of transducin mRNA and translocation of transducin in rods of rat retina. *Science* **235** (1987), pp. 585-7.
- Braun, R.J., Kinkl, N., Beer, M. and Ueffing, M. Two-dimensional electrophoresis of membrane proteins. *Anal Bioanal Chem* **389** (2007), pp. 1033-45.
- Brew, H. and Attwell, D. Electrogenic glutamate uptake is a major current carrier in the membrane of axolotl retinal glial cells. *Nature* **327** (1987), pp. 707-9.
- Broekhuysse, R.M., Tolhuizen, E.F., Janssen, A.P. and Winkens, H.J. Light induced shift and binding of S-antigen in retinal rods. *Curr Eye Res* **4** (1985), pp. 613-8.
- Brown, M., Jacobs, T., Eickholt, B., Ferrari, G., Teo, M., Monfries, C., Qi, R.Z., Leung, T., Lim, L. and Hall, C. Alpha2-chimaerin, cyclin-dependent Kinase 5/p35, and its target

- collapsin response mediator protein-2 are essential components in semaphorin 3A-induced growth-cone collapse. *J Neurosci* **24** (2004), pp. 8994-9004.
- Bussow, H. The astrocytes in the retina and optic nerve head of mammals: a special glia for the ganglion cell axons. *Cell Tissue Res* **206** (1980), pp. 367-78.
- Caffe, A.R., Ahuja, P., Holmqvist, B., Azadi, S., Forsell, J., Holmqvist, I., Soderpalm, A.K. and van Veen, T. Mouse retina explants after long-term culture in serum free medium. *J Chem Neuroanat* **22** (2001), pp. 263-73.
- Caffe, A.R., Soderpalm, A. and van Veen, T. Photoreceptor-specific protein expression of mouse retina in organ culture and retardation of rd degeneration in vitro by a combination of basic fibroblast and nerve growth factors. *Curr Eye Res* **12** (1993), pp. 719-26.
- Caffe, A.R., Visser, H., Jansen, H.G. and Sanyal, S. Histotypic differentiation of neonatal mouse retina in organ culture. *Curr Eye Res* **8** (1989), pp. 1083-92.
- Calvert, P.D., Strissel, K.J., Schiesser, W.E., Pugh, E.N., Jr. and Arshavsky, V.Y. Light-driven translocation of signaling proteins in vertebrate photoreceptors. *Trends Cell Biol* **16** (2006), pp. 560-8.
- Cappello, S., Attardo, A., Wu, X., Iwasato, T., Itohara, S., Wilsch-Brauninger, M., Eilken, H.M., Rieger, M.A., Schroeder, T.T., Huttner, W.B., Brakebusch, C. and Gotz, M. The Rho-GTPase cdc42 regulates neural progenitor fate at the apical surface. *Nat Neurosci* **9** (2006), pp. 1099-107.
- Caron, E. and Hall, A. Identification of two distinct mechanisms of phagocytosis controlled by different Rho GTPases. *Science* **282** (1998), pp. 1717-21.
- Cepko, C. Lineage versus environment in the embryonic retina. *Trends Neurosci* **16** (1993), pp. 96-7; author reply 98.
- Chaitin, M.H., Schneider, B.G., Hall, M.O. and Papermaster, D.S. Actin in the photoreceptor connecting cilium: immunocytochemical localization to the site of outer segment disk formation. *J Cell Biol* **99** (1984), pp. 239-47.
- Chan-Ling, T. and Stone, J. Factors determining the migration of astrocytes into the developing retina: migration does not depend on intact axons or patent vessels. *J Comp Neurol* **303** (1991), pp. 375-86.
- Chang, H.Y. and Ready, D.F. Rescue of photoreceptor degeneration in rhodopsin-null *Drosophila* mutants by activated Rac1. *Science* **290** (2000), pp. 1978-80.
- Chen, C.Y., Olayioye, M.A., Lindeman, G.J. and Tang, T.K. CPAP interacts with 14-3-3 in a cell cycle-dependent manner. *Biochem Biophys Res Commun* **342** (2006a), pp. 1203-10.
- Chen, J., Halls, S.C., Alfaro, J.F., Zhou, Z. and Hu, M. Potential beneficial metabolic interactions between tamoxifen and isoflavones via cytochrome P450-mediated pathways in female rat liver microsomes. *Pharm Res* **21** (2004), pp. 2095-104.

- Chen, L., Liao, G., Yang, L., Campbell, K., Nakafuku, M., Kuan, C.Y. and Zheng, Y. Cdc42 deficiency causes Sonic hedgehog-independent holoprosencephaly. *Proc Natl Acad Sci U S A* **103** (2006b), pp. 16520-5.
- Chuang, T.H., Xu, X., Knaus, U.G., Hart, M.J. and Bokoch, G.M. GDP dissociation inhibitor prevents intrinsic and GTPase activating protein-stimulated GTP hydrolysis by the Rac GTP-binding protein. *J Biol Chem* **268** (1993), pp. 775-8.
- Clarke, S. Protein isoprenylation and methylation at carboxyl-terminal cysteine residues. *Annu Rev Biochem* **61** (1992), pp. 355-86.
- Cole, A.R., Knebel, A., Morrice, N.A., Robertson, L.A., Irving, A.J., Connolly, C.N. and Sutherland, C. GSK-3 phosphorylation of the Alzheimer epitope within collapsin response mediator proteins regulates axon elongation in primary neurons. *J Biol Chem* **279** (2004), pp. 50176-80.
- Coleman, J.E. and Semple-Rowland, S.L. GC1 deletion prevents light-dependent arrestin translocation in mouse cone photoreceptor cells. *Invest Ophthalmol Vis Sci* **46** (2005), pp. 12-6.
- Conti, M. and Jin, S.L. The molecular biology of cyclic nucleotide phosphodiesterases. *Prog Nucleic Acid Res Mol Biol* **63** (1999), pp. 1-38.
- Cook, T.A., Ghomashchi, F., Gelb, M.H., Florio, S.K. and Beavo, J.A. Binding of the delta subunit to rod phosphodiesterase catalytic subunits requires methylated, prenylated C-termini of the catalytic subunits. *Biochemistry* **39** (2000), pp. 13516-23.
- Cottrell, J.S. Protein identification by peptide mass fingerprinting. *Pept Res* **7** (1994), pp. 115-24.
- Curcio, C.A., Sloan, K.R., Kalina, R.E. and Hendrickson, A.E. Human photoreceptor topography. *J Comp Neurol* **292** (1990), pp. 497-523.
- den Hollander, A.I., Heckenlively, J.R., van den Born, L.I., de Kok, Y.J., van der Velde-Visser, S.D., Kellner, U., Jurklies, B., van Schooneveld, M.J., Blankenagel, A., Rohrschneider, K., Wissinger, B., Cruysberg, J.R., Deutman, A.F., Brunner, H.G., Apfelstedt-Sylla, E., Hoyng, C.B. and Cremers, F.P. Leber congenital amaurosis and retinitis pigmentosa with Coats-like exudative vasculopathy are associated with mutations in the crumbs homologue 1 (CRB1) gene. *Am J Hum Genet* **69** (2001), pp. 198-203.
- den Hollander, A.I., Koenekoop, R.K., Mohamed, M.D., Arts, H.H., Boldt, K., Towns, K.V., Sedmak, T., Beer, M., Nagel-Wolfrum, K., McKibbin, M., Dharmaraj, S., Lopez, I., Ivings, L., Williams, G.A., Springell, K., Woods, C.G., Jafri, H., Rashid, Y., Strom, T.M., van der Zwaag, B., Gosens, I., Kersten, F.F., van Wijk, E., Veltman, J.A., Zonneveld, M.N., van Beersum, S.E., Maumenee, I.H., Wolfrum, U., Cheetham, M.E., Ueffing, M., Cremers, F.P., Inglehearn, C.F. and Roepman, R. Mutations in LCA5, encoding the ciliary protein lebercilin, cause Leber congenital amaurosis. *Nat Genet* **39** (2007), pp. 889-95.
- Dent, E.W. and Gertler, F.B. Cytoskeletal dynamics and transport in growth cone motility and axon guidance. *Neuron* **40** (2003), pp. 209-27.

- Deretic, D., From the golgi to the rod outer segment: formation, movement, docking and fusion of rhodopsin transport carriers. Worl Scientific Publishing Co. Pte. Ltd., Singapore (2004).
- Deretic, D., Traverso, V., Parkins, N., Jackson, F., Rodriguez de Turco, E.B. and Ransom, N. Phosphoinositides, ezrin/moesin, and rac1 regulate fusion of rhodopsin transport carriers in retinal photoreceptors. *Mol Biol Cell* **15** (2004), pp. 359-70.
- DerMardirossian, C. and Bokoch, G.M. GDIs: central regulatory molecules in Rho GTPase activation. *Trends Cell Biol* **15** (2005), pp. 356-63.
- DerMardirossian, C., Rocklin, G., Seo, J.Y. and Bokoch, G.M. Phosphorylation of RhoGDI by Src regulates Rho GTPase binding and cytosol-membrane cycling. *Mol Biol Cell* **17** (2006), pp. 4760-8.
- Dharmaraj, S., Li, Y., Robitaille, J.M., Silva, E., Zhu, D., Mitchell, T.N., Maltby, L.P., Baffoe-Bonnie, A.B. and Maumenee, I.H. A novel locus for Leber congenital amaurosis maps to chromosome 6q. *Am J Hum Genet* **66** (2000), pp. 319-26.
- Di-Poi, N., Faure, J., Grizot, S., Molnar, G., Pick, E. and Dagher, M.C. Mechanism of NADPH oxidase activation by the Rac/Rho-GDI complex. *Biochemistry* **40** (2001), pp. 10014-22.
- Didsbury, J., Weber, R.F., Bokoch, G.M., Evans, T. and Snyderman, R. rac, a novel ras-related family of proteins that are botulinum toxin substrates. *J Biol Chem* **264** (1989), pp. 16378-82.
- Dransart, E., Olofsson, B. and Cherfilis, J. RhoGDIs revisited: novel roles in Rho regulation. *Traffic* **6** (2005), pp. 957-66.
- Dryja, T.P., Adams, S.M., Grimsby, J.L., McGee, T.L., Hong, D.H., Li, T., Andreasson, S. and Berson, E.L. Null RPGRIP1 alleles in patients with Leber congenital amaurosis. *Am J Hum Genet* **68** (2001), pp. 1295-8.
- Dryja, T.P., McGee, T.L., Reichel, E., Hahn, L.B., Cowley, G.S., Yandell, D.W., Sandberg, M.A. and Berson, E.L. A point mutation of the rhodopsin gene in one form of retinitis pigmentosa. *Nature* **343** (1990), pp. 364-6.
- Dvorsky, R. and Ahmadian, M.R. Always look on the bright site of Rho: structural implications for a conserved intermolecular interface. *EMBO Rep* **5** (2004), pp. 1130-6.
- Elias, R.V., Sezate, S.S., Cao, W. and McGinnis, J.F. Temporal kinetics of the light/dark translocation and compartmentation of arrestin and alpha-transducin in mouse photoreceptor cells. *Mol Vis* **10** (2004), pp. 672-81.
- Ershova, G., Derre, J., Chetelin, S., Nancy, V., Berger, R., Kaplan, J., Munnich, A. and de Gunzburg, J. cDNA sequence, genomic organization and mapping of PDE6D, the human gene encoding the delta subunit of the cGMP phosphodiesterase of retinal rod cells to chromosome 2q36. *Cytogenet Cell Genet* **79** (1997), pp. 139-41.
- Essayan, D.M. Cyclic nucleotide phosphodiesterases. *J Allergy Clin Immunol* **108** (2001), pp. 671-80.

- Etienne-Manneville, S. and Hall, A. Rho GTPases in cell biology. *Nature* **420** (2002), pp. 629-35.
- Fanning, A.S. and Anderson, J.M. Protein-protein interactions: PDZ domain networks. *Curr Biol* **6** (1996), pp. 1385-8.
- Fanto, M., Weber, U., Strutt, D.I. and Mlodzik, M. Nuclear signaling by Rac and Rho GTPases is required in the establishment of epithelial planar polarity in the Drosophila eye. *Curr Biol* **10** (2000), pp. 979-88.
- Faust, M., Gunther, J., Morgenstern, E., Montenarh, M. and Gotz, C. Specific localization of the catalytic subunits of protein kinase CK2 at the centrosomes. *Cell Mol Life Sci* **59** (2002), pp. 2155-64.
- Feig, L.A. Ral-GTPases: approaching their 15 minutes of fame. *Trends Cell Biol* **13** (2003), pp. 419-25.
- Fenn, J.B., Mann, M., Meng, C.K., Wong, S.F. and Whitehouse, C.M. Electrospray ionization for mass spectrometry of large biomolecules. *Science* **246** (1989), pp. 64-71.
- Florio, S.K., Prusti, R.K. and Beavo, J.A. Solubilization of membrane-bound rod phosphodiesterase by the rod phosphodiesterase recombinant delta subunit. *J Biol Chem* **271** (1996), pp. 24036-47.
- Foxman, S.G., Heckenlively, J.R., Bateman, J.B. and Wirtschafter, J.D. Classification of congenital and early onset retinitis pigmentosa. *Arch Ophthalmol* **103** (1985), pp. 1502-6.
- Francis, S.H., Turko, I.V. and Corbin, J.D. Cyclic nucleotide phosphodiesterases: relating structure and function. *Prog Nucleic Acid Res Mol Biol* **65** (2001), pp. 1-52.
- Fransson, A., Ruusala, A. and Aspenstrom, P. Atypical Rho GTPases have roles in mitochondrial homeostasis and apoptosis. *J Biol Chem* **278** (2003), pp. 6495-502.
- Frederick, J.M., Krasnoperova, N.V., Hoffmann, K., Church-Kopish, J., Ruther, K., Howes, K., Lem, J. and Baehr, W. Mutant rhodopsin transgene expression on a null background. *Invest Ophthalmol Vis Sci* **42** (2001), pp. 826-33.
- Freund, C.L., Wang, Q.L., Chen, S., Muskat, B.L., Wiles, C.D., Sheffield, V.C., Jacobson, S.G., McInnes, R.R., Zack, D.J. and Stone, E.M. De novo mutations in the CRX homeobox gene associated with Leber congenital amaurosis. *Nat Genet* **18** (1998), pp. 311-2.
- Friedman, J.S., Chang, B., Kannabiran, C., Chakarova, C., Singh, H.P., Jalali, S., Hawes, N.L., Branham, K., Othman, M., Filippova, E., Thompson, D.A., Webster, A.R., Andreasson, S., Jacobson, S.G., Bhattacharya, S.S., Heckenlively, J.R. and Swaroop, A. Premature truncation of a novel protein, RD3, exhibiting subnuclear localization is associated with retinal degeneration. *Am J Hum Genet* **79** (2006), pp. 1059-70.
- Fukada, M., Watakabe, I., Yuasa-Kawada, J., Kawachi, H., Kuroiwa, A., Matsuda, Y. and Noda, M. Molecular characterization of CRMP5, a novel member of the collapsin response mediator protein family. *J Biol Chem* **275** (2000), pp. 37957-65.

- Fukata, Y., Itoh, T.J., Kimura, T., Menager, C., Nishimura, T., Shiromizu, T., Watanabe, H., Inagaki, N., Iwamatsu, A., Hotani, H. and Kaibuchi, K. CRMP-2 binds to tubulin heterodimers to promote microtubule assembly. *Nat Cell Biol* **4** (2002), pp. 583-91.
- Fukumoto, Y., Kaibuchi, K., Hori, Y., Fujioka, H., Araki, S., Ueda, T., Kikuchi, A. and Takai, Y. Molecular cloning and characterization of a novel type of regulatory protein (GDI) for the rho proteins, ras p21-like small GTP-binding proteins. *Oncogene* **5** (1990), pp. 1321-8.
- Furukawa, T., Morrow, E.M., Li, T., Davis, F.C. and Cepko, C.L. Retinopathy and attenuated circadian entrainment in Crx-deficient mice. *Nat Genet* **23** (1999), pp. 466-70.
- Gavin, A.C., Bosche, M., Krause, R., Grandi, P., Marzioch, M., Bauer, A., Schultz, J., Rick, J.M., Michon, A.M., Cruciat, C.M., Remor, M., Hofert, C., Schelder, M., Brajenovic, M., Ruffner, H., Merino, A., Klein, K., Hudak, M., Dickson, D., Rudi, T., Gnau, V., Bauch, A., Bastuck, S., Huhse, B., Leutwein, C., Heurtier, M.A., Copley, R.R., Edelmann, A., Querfurth, E., Rybin, V., Drewes, G., Raida, M., Bouwmeester, T., Bork, P., Seraphin, B., Kuster, B., Neubauer, G. and Superti-Furga, G. Functional organization of the yeast proteome by systematic analysis of protein complexes. *Nature* **415** (2002), pp. 141-7.
- Gerber, S., Bonneau, D., Gilbert, B., Munnich, A., Dufier, J.L., Rozet, J.M. and Kaplan, J. USH1A: chronicle of a slow death. *Am J Hum Genet* **78** (2006), pp. 357-9.
- Gharahdaghi, F., Weinberg, C.R., Meagher, D.A., Imai, B.S. and Mische, S.M. Mass spectrometric identification of proteins from silver-stained polyacrylamide gel: a method for the removal of silver ions to enhance sensitivity. *Electrophoresis* **20** (1999), pp. 601-5.
- Giessler, A., Pulvermuller, A., Trojan, P., Park, J.H., Choe, H.W., Ernst, O.P., Hofmann, K.P. and Wolfrum, U. Differential expression and interaction with the visual G-protein transducin of centrin isoforms in mammalian photoreceptor cells. *J Biol Chem* **279** (2004), pp. 51472-81.
- Ginisty, H., Sicard, H., Roger, B. and Bouvet, P. Structure and functions of nucleolin. *J Cell Sci* **112 (Pt 6)** (1999), pp. 761-72.
- Gloeckner, C.J., Boldt, K., Schumacher, A., Roepman, R. and Ueffing, M. A novel tandem affinity purification strategy for the efficient isolation and characterisation of native protein complexes. *Proteomics* **7** (2007a), pp. 4228-34.
- Gloeckner, C.J., Boldt, K., Schumacher, A. and Ueffing, M. , Tandem affinity purification of protein complexes from mammalian cells by the Strep/FLAG (SF)-TAP tag (in press).
- Gloeckner, J., Boldt, K., Schumacher, A., Roepman, R. and Ueffing, M. A novel tandem affinity purification strategy for the efficient isolation and characterization of native protein complexes. *Proteomics* **7** (2007b), p. in press.
- Görg, A., Postel, W. and Gunther, S. The current state of two-dimensional electrophoresis with immobilized pH gradients. *Electrophoresis* **9** (1988), pp. 531-46.

- Goshima, Y., Nakamura, F., Strittmatter, P. and Strittmatter, S.M. Collapsin-induced growth cone collapse mediated by an intracellular protein related to UNC-33. *Nature* **376** (1995), pp. 509-14.
- Gosser, Y.Q., Nomanbhoy, T.K., Aghazadeh, B., Manor, D., Combs, C., Cerione, R.A. and Rosen, M.K. C-terminal binding domain of Rho GDP-dissociation inhibitor directs N-terminal inhibitory peptide to GTPases. *Nature* **387** (1997), pp. 814-9.
- Grady, W.M. and Markowitz, S.D. Genetic and epigenetic alterations in colon cancer. *Annu Rev Genomics Hum Genet* **3** (2002), pp. 101-28.
- Granvogl, B., Reisinger, V. and Eichacker, L.A. Mapping the proteome of thylakoid membranes by de novo sequencing of intermembrane peptide domains. *Proteomics* **6** (2006), pp. 3681-95.
- Green, J.S., Parfrey, P.S., Harnett, J.D., Farid, N.R., Cramer, B.C., Johnson, G., Heath, O., McManamon, P.J., O'Leary, E. and Pryse-Phillips, W. The cardinal manifestations of Bardet-Biedl syndrome, a form of Laurence-Moon-Biedl syndrome. *N Engl J Med* **321** (1989), pp. 1002-9.
- Grizot, S., Faure, J., Fieschi, F., Vignais, P.V., Dagher, M.C. and Pebay-Peyroula, E. Crystal structure of the Rac1-RhoGDI complex involved in nadph oxidase activation. *Biochemistry* **40** (2001), pp. 10007-13.
- Haas, A.K., Yoshimura, S., Stephens, D.J., Preisinger, C., Fuchs, E. and Barr, F.A. Analysis of GTPase-activating proteins: Rab1 and Rab43 are key Rabs required to maintain a functional Golgi complex in human cells. *J Cell Sci* **120** (2007), pp. 2997-3010.
- Hall, C., Brown, M., Jacobs, T., Ferrari, G., Cann, N., Teo, M., Monfries, C. and Lim, L. Collapsin response mediator protein switches RhoA and Rac1 morphology in N1E-115 neuroblastoma cells and is regulated by Rho kinase. *J Biol Chem* **276** (2001), pp. 43482-6.
- Hamilton, S.E., Prusti, R.K., Bentley, J.K., Beavo, J.A. and Hurley, J.B. Affinities of bovine photoreceptor cGMP phosphodiesterases for rod and cone inhibitory subunits. *FEBS Lett* **318** (1993), pp. 157-61.
- Hanzal-Bayer, M., Renault, L., Roversi, P., Wittinghofer, A. and Hillig, R.C. The complex of Arl2-GTP and PDE delta: from structure to function. *EMBO J* **21** (2002), pp. 2095-106.
- Hartley, J.L., Temple, G.F. and Brasch, M.A., DNA cloning using in vitro site-specific recombination, 2000/11/15 ed (2000).
- Heckenlively, J.R., Yoser, S.L., Friedman, L.H. and Oversier, J.J. Clinical findings and common symptoms in retinitis pigmentosa. *Am J Ophthalmol* **105** (1988), pp. 504-11.
- Hendrickson, A. and Hicks, D. Distribution and density of medium- and short-wavelength selective cones in the domestic pig retina. *Exp Eye Res* **74** (2002), pp. 435-44.
- Heo, W.D. and Meyer, T. Switch-of-function mutants based on morphology classification of Ras superfamily small GTPases. *Cell* **113** (2003), pp. 315-28.

- Hillenkamp, F., Karas, M., Beavis, R.C. and Chait, B.T. Matrix-assisted laser desorption/ionization mass spectrometry of biopolymers. *Anal Chem* **63** (1991), pp. 1193A-1203A.
- Ho, T.C., Yang, Y.C., Cheng, H.C., Wu, A.C., Chen, S.L., Chen, H.K. and Tsao, Y.P. Activation of mitogen-activated protein kinases is essential for hydrogen peroxide - induced apoptosis in retinal pigment epithelial cells. *Apoptosis* **11** (2006), pp. 1899-908.
- Hoffman, G.R., Nassar, N. and Cerione, R.A. Structure of the Rho family GTP-binding protein Cdc42 in complex with the multifunctional regulator RhoGDI. *Cell* **100** (2000), pp. 345-56.
- Hollander, B.A., Liang, M.Y. and Besharse, J.C. Linkage of a nucleolin-related protein and casein kinase II with the detergent-stable photoreceptor cytoskeleton. *Cell Motil Cytoskeleton* **43** (1999), pp. 114-27.
- Hong, D.H., Pawlyk, B.S., Adamian, M. and Li, T. Dominant, gain-of-function mutant produced by truncation of RPGR. *Invest Ophthalmol Vis Sci* **45** (2004), pp. 36-41.
- Hong, D.H., Yue, G., Adamian, M. and Li, T. Retinitis pigmentosa GTPase regulator (RPGR)-interacting protein is stably associated with the photoreceptor ciliary axoneme and anchors RPGR to the connecting cilium. *J Biol Chem* **276** (2001), pp. 12091-9.
- Hopkins, A.L. and Groom, C.R. The druggable genome. *Nat Rev Drug Discov* **1** (2002), pp. 727-30.
- Horst, C.J., Johnson, L.V. and Besharse, J.C. Transmembrane assemblage of the photoreceptor connecting cilium and motile cilium transition zone contain a common immunologic epitope. *Cell Motil Cytoskeleton* **17** (1990), pp. 329-44.
- Hu, J., Bae, Y.K., Knobel, K.M. and Barr, M.M. Casein kinase II and calcineurin modulate TRPP function and ciliary localization. *Mol Biol Cell* **17** (2006), pp. 2200-11.
- Hubbell, H.R., Rothblum, L.I. and Hsu, T.C. Identification of a silver binding protein associated with the cytological silver staining of actively transcribing nucleolar regions. *Cell Biol Int Rep* **3** (1979), pp. 615-22.
- Humphries, M.M., Rancourt, D., Farrar, G.J., Kenna, P., Hazel, M., Bush, R.A., Sieving, P.A., Sheils, D.M., McNally, N., Creighton, P., Erven, A., Boros, A., Gulya, K., Capecchi, M.R. and Humphries, P. Retinopathy induced in mice by targeted disruption of the rhodopsin gene. *Nat Genet* **15** (1997), pp. 216-9.
- Hurwitz, R.L., Bunt-Milam, A.H., Chang, M.L. and Beavo, J.A. cGMP phosphodiesterase in rod and cone outer segments of the retina. *J Biol Chem* **260** (1985), pp. 568-73.
- Ishizaki, T., Maekawa, M., Fujisawa, K., Okawa, K., Iwamatsu, A., Fujita, A., Watanabe, N., Saito, Y., Kakizuka, A., Morii, N. and Narumiya, S. The small GTP-binding protein Rho binds to and activates a 160 kDa Ser/Thr protein kinase homologous to myotonic dystrophy kinase. *EMBO J* **15** (1996), pp. 1885-93.

- Jacinto, A., Martinez-Arias, A. and Martin, P. Mechanisms of epithelial fusion and repair. *Nat Cell Biol* **3** (2001), pp. E117-23.
- Jacobs, G.H. Photopigments and seeing--lessons from natural experiments: the Proctor lecture. *Invest Ophthalmol Vis Sci* **39** (1998), pp. 2204-16.
- Jacobs, G.H., Neitz, J. and Deegan, J.F., 2nd Retinal receptors in rodents maximally sensitive to ultraviolet light. *Nature* **353** (1991), pp. 655-6.
- Jaffee, E.M., Hruban, R.H., Canto, M. and Kern, S.E. Focus on pancreas cancer. *Cancer Cell* **2** (2002), pp. 25-8.
- Jeon, C.J., Strettoi, E. and Masland, R.H. The major cell populations of the mouse retina. *J Neurosci* **18** (1998), pp. 8936-46.
- Jiang, M.H., Hoog, A., Ma, K.C., Nie, X.J., Olsson, Y. and Zhang, W.W. Endothelin-1-like immunoreactivity is expressed in human reactive astrocytes. *Neuroreport* **4** (1993), pp. 935-7.
- Jin, S., Cornwall, M.C. and Oprian, D.D. Opsin activation as a cause of congenital night blindness. *Nat Neurosci* **6** (2003), pp. 731-5.
- Jin, Z. and Strittmatter, S.M. Rac1 mediates collapsin-1-induced growth cone collapse. *J Neurosci* **17** (1997), pp. 6256-63.
- Kamata, T., Daar, I.O., Subleski, M., Copeland, T., Kung, H.F. and Xu, R.H. Xenopus CRMP-2 is an early response gene to neural induction. *Brain Res Mol Brain Res* **57** (1998), pp. 201-10.
- Kaplan, J., Bonneau, D., Frezal, J., Munnich, A. and Dufier, J.L. Clinical and genetic heterogeneity in retinitis pigmentosa. *Hum Genet* **85** (1990), pp. 635-42.
- Kaplan, M.W., Iwata, R.T. and Sears, R.C. Lengths of immunolabeled ciliary microtubules in frog photoreceptor outer segments. *Exp Eye Res* **44** (1987), pp. 623-32.
- Kato, Y., Hamajima, N., Inagaki, H., Okamura, N., Koji, T., Sasaki, M. and Nonaka, M. Post-meiotic expression of the mouse dihydropyrimidinase-related protein 3 (DRP-3) gene during spermiogenesis. *Mol Reprod Dev* **51** (1998), pp. 105-11.
- Keller, A., Nesvizhskii, A.I., Kolker, E. and Aebersold, R. Empirical statistical model to estimate the accuracy of peptide identifications made by MS/MS and database search. *Anal Chem* **74** (2002), pp. 5383-92.
- Kennedy, M.J., Dunn, F.A. and Hurley, J.B. Visual pigment phosphorylation but not transducin translocation can contribute to light adaptation in zebrafish cones. *Neuron* **41** (2004), pp. 915-28.
- Khanna, H., Hurd, T.W., Lillo, C., Shu, X., Parapuram, S.K., He, S., Akimoto, M., Wright, A.F., Margolis, B., Williams, D.S. and Swaroop, A. RPGR-ORF15, which is mutated in retinitis pigmentosa, associates with SMC1, SMC3, and microtubule transport proteins. *J Biol Chem* **280** (2005), pp. 33580-7.

- Kimura, K., Kawamoto, K., Teranishi, S. and Nishida, T. Role of Rac1 in fibronectin-induced adhesion and motility of human corneal epithelial cells. *Invest Ophthalmol Vis Sci* **47** (2006), pp. 4323-9.
- Kimura, T., Watanabe, H., Iwamatsu, A. and Kaibuchi, K. Tubulin and CRMP-2 complex is transported via Kinesin-1. *J Neurochem* **93** (2005), pp. 1371-82.
- Kjoller, L. and Hall, A. Signaling to Rho GTPases. *Exp Cell Res* **253** (1999), pp. 166-79.
- Knoll, B. and Drescher, U. Src family kinases are involved in EphA receptor-mediated retinal axon guidance. *J Neurosci* **24** (2004), pp. 6248-57.
- Koh, C.G. Rho GTPases and their regulators in neuronal functions and development. *Neurosignals* **15** (2006), pp. 228-37.
- Kohno, K., Normington, K., Sambrook, J., Gething, M.J. and Mori, K. The promoter region of the yeast KAR2 (BiP) gene contains a regulatory domain that responds to the presence of unfolded proteins in the endoplasmic reticulum. *Mol Cell Biol* **13** (1993), pp. 877-90.
- Kornau, H.C., Schenker, L.T., Kennedy, M.B. and Seeburg, P.H. Domain interaction between NMDA receptor subunits and the postsynaptic density protein PSD-95. *Science* **269** (1995), pp. 1737-40.
- Kraynov, V.S., Chamberlain, C., Bokoch, G.M., Schwartz, M.A., Slabaugh, S. and Hahn, K.M. Localized Rac activation dynamics visualized in living cells. *Science* **290** (2000), pp. 333-7.
- Kyhse-Andersen, J. Electroblothing of multiple gels: a simple apparatus without buffer tank for rapid transfer of proteins from polyacrylamide to nitrocellulose. *J Biochem Biophys Methods* **10** (1984), pp. 203-9.
- Laemmli, U.K. Cleavage of structural proteins during the assembly of the head of bacteriophage T4. *Nature* **227** (1970), pp. 680-5.
- le Maire, M., Champeil, P. and Moller, J.V. Interaction of membrane proteins and lipids with solubilizing detergents. *Biochim Biophys Acta* **1508** (2000), pp. 86-111.
- Leber, T., Über Retinitis pigmentosa und angeborene Amaurose. Archiv für Ophthalmologie, Berlin (1869).
- Lee, T., Winter, C., Marticke, S.S., Lee, A. and Luo, L. Essential roles of Drosophila RhoA in the regulation of neuroblast proliferation and dendritic but not axonal morphogenesis. *Neuron* **25** (2000), pp. 307-16.
- Lem, J. and Fain, G.L. Constitutive opsin signaling: night blindness or retinal degeneration? *Trends Mol Med* **10** (2004), pp. 150-7.
- Li, D., Dobrowolska, G. and Krebs, E.G. The physical association of casein kinase 2 with nucleolin. *J Biol Chem* **271** (1996), pp. 15662-8.
- Li, J., Edwards, P.C., Burghammer, M., Villa, C. and Schertler, G.F. Structure of bovine rhodopsin in a trigonal crystal form. *J Mol Biol* **343** (2004), pp. 1409-38.

- Li, W., Herman, R.K. and Shaw, J.E. Analysis of the *Caenorhabditis elegans* axonal guidance and outgrowth gene *unc-33*. *Genetics* **132** (1992), pp. 675-89.
- Li, Z., Van Aelst, L. and Cline, H.T. Rho GTPases regulate distinct aspects of dendritic arbor growth in *Xenopus* central neurons in vivo. *Nat Neurosci* **3** (2000), pp. 217-25.
- Li, Z.Y., Wong, F., Chang, J.H., Possin, D.E., Hao, Y., Petters, R.M. and Milam, A.H. Rhodopsin transgenic pigs as a model for human retinitis pigmentosa. *Invest Ophthalmol Vis Sci* **39** (1998), pp. 808-19.
- Lian, L.Y., Barsukov, I., Golovanov, A.P., Hawkins, D.I., Badii, R., Sze, K.H., Keep, N.H., Bokoch, G.M. and Roberts, G.C. Mapping the binding site for the GTP-binding protein Rac-1 on its inhibitor RhoGDI-1. *Structure* **8** (2000), pp. 47-55.
- Liang, Y., Fotiadis, D., Filipek, S., Saperstein, D.A., Palczewski, K. and Engel, A. Organization of the G protein-coupled receptors rhodopsin and opsin in native membranes. *J Biol Chem* **278** (2003), pp. 21655-62.
- Lim, A.C., Tiu, S.Y., Li, Q. and Qi, R.Z. Direct regulation of microtubule dynamics by protein kinase CK2. *J Biol Chem* **279** (2004), pp. 4433-9.
- Linari, M., Hanzal-Bayer, M. and Becker, J. The delta subunit of rod specific cyclic GMP phosphodiesterase, PDE delta, interacts with the Arf-like protein Arl3 in a GTP specific manner. *FEBS Lett* **458** (1999a), pp. 55-9.
- Linari, M., Ueffing, M., Manson, F., Wright, A., Meitinger, T. and Becker, J. The retinitis pigmentosa GTPase regulator, RPGR, interacts with the delta subunit of rod cyclic GMP phosphodiesterase. *Proc Natl Acad Sci U S A* **96** (1999b), pp. 1315-20.
- Liu, B.P. and Strittmatter, S.M. Semaphorin-mediated axonal guidance via Rho-related G proteins. *Curr Opin Cell Biol* **13** (2001), pp. 619-26.
- Liu, Q., Zhou, J., Daiger, S.P., Farber, D.B., Heckenlively, J.R., Smith, J.E., Sullivan, L.S., Zuo, J., Milam, A.H. and Pierce, E.A. Identification and subcellular localization of the RP1 protein in human and mouse photoreceptors. *Invest Ophthalmol Vis Sci* **43** (2002), pp. 22-32.
- Lorenz, B., Migliaccio, C., Lichtner, P., Meyer, C., Strom, T.M., D'Urso, M., Becker, J., Ciccodicola, A. and Meitinger, T. Cloning and gene structure of the rod cGMP phosphodiesterase delta subunit gene (PDED) in man and mouse. *Eur J Hum Genet* **6** (1998), pp. 283-90.
- Lotery, A.J., Jacobson, S.G., Fishman, G.A., Weleber, R.G., Fulton, A.B., Namperumalsamy, P., Heon, E., Levin, A.V., Grover, S., Rosenow, J.R., Kopp, K.K., Sheffield, V.C. and Stone, E.M. Mutations in the *CRB1* gene cause Leber congenital amaurosis. *Arch Ophthalmol* **119** (2001), pp. 415-20.
- Lottspeich, F., Bioanalytik. Spectrum Akademischer Verlag, 8203750 Heidelberg (1998).
- Lugnier, C. Cyclic nucleotide phosphodiesterase (PDE) superfamily: a new target for the development of specific therapeutic agents. *Pharmacol Ther* **109** (2006), pp. 366-98.
- Luo, L. Rho GTPases in neuronal morphogenesis. *Nat Rev Neurosci* **1** (2000), pp. 173-80.

- Lyons, J., Landis, C.A., Harsh, G., Vallar, L., Grunewald, K., Feichtinger, H., Duh, Q.Y., Clark, O.H., Kawasaki, E., Bourne, H.R. and et al. Two G protein oncogenes in human endocrine tumors. *Science* **249** (1990), pp. 655-9.
- Ma, Z., Kanai, M., Kawamura, K., Kaibuchi, K., Ye, K. and Fukasawa, K. Interaction between ROCK II and nucleophosmin/B23 in the regulation of centrosome duplication. *Mol Cell Biol* **26** (2006), pp. 9016-34.
- Maeda, A., Maeda, T., Imanishi, Y., Kuksa, V., Alekseev, A., Bronson, J.D., Zhang, H., Zhu, L., Sun, W., Saperstein, D.A., Rieke, F., Baehr, W. and Palczewski, K. Role of photoreceptor-specific retinol dehydrogenase in the retinoid cycle in vivo. *J Biol Chem* **280** (2005), pp. 18822-32.
- Malchow, R.P., Qian, H.H. and Ripps, H. gamma-Aminobutyric acid (GABA)-induced currents of skate Muller (glial) cells are mediated by neuronal-like GABA_A receptors. *Proc Natl Acad Sci U S A* **86** (1989), pp. 4326-30.
- Marlhens, F., Bareil, C., Griffoin, J.M., Zrenner, E., Amalric, P., Eliaou, C., Liu, S.Y., Harris, E., Redmond, T.M., Arnaud, B., Claustres, M. and Hamel, C.P. Mutations in RPE65 cause Leber's congenital amaurosis. *Nat Genet* **17** (1997), pp. 139-41.
- Martin, S.J., Reutelingsperger, C.P., McGahon, A.J., Rader, J.A., van Schie, R.C., LaFace, D.M. and Green, D.R. Early redistribution of plasma membrane phosphatidylserine is a general feature of apoptosis regardless of the initiating stimulus: inhibition by overexpression of Bcl-2 and Abl. *J Exp Med* **182** (1995), pp. 1545-56.
- Marzesco, A.M., Galli, T., Louvard, D. and Zahraoui, A. The rod cGMP phosphodiesterase delta subunit dissociates the small GTPase Rab13 from membranes. *J Biol Chem* **273** (1998), pp. 22340-5.
- Masland, R.H. The fundamental plan of the retina. *Nat Neurosci* **4** (2001), pp. 877-86.
- Matsui, T., Amano, M., Yamamoto, T., Chihara, K., Nakafuku, M., Ito, M., Nakano, T., Okawa, K., Iwamatsu, A. and Kaibuchi, K. Rho-associated kinase, a novel serine/threonine kinase, as a putative target for small GTP binding protein Rho. *EMBO J* **15** (1996), pp. 2208-16.
- Meindl, A., Dry, K., Herrmann, K., Manson, F., Ciccodicola, A., Edgar, A., Carvalho, M.R., Achatz, H., Hellebrand, H., Lennon, A., Migliaccio, C., Porter, K., Zrenner, E., Bird, A., Jay, M., Lorenz, B., Wittwer, B., D'Urso, M., Meitinger, T. and Wright, A. A gene (RPGR) with homology to the RCC1 guanine nucleotide exchange factor is mutated in X-linked retinitis pigmentosa (RP3). *Nat Genet* **13** (1996), pp. 35-42.
- Menon, S.T., Han, M. and Sakmar, T.P. Rhodopsin: structural basis of molecular physiology. *Physiol Rev* **81** (2001), pp. 1659-88.
- Mhawech, P. 14-3-3 proteins--an update. *Cell Res* **15** (2005), pp. 228-36.
- Miller, R.F. and Dowling, J.E. Intracellular responses of the Muller (glial) cells of mudpuppy retina: their relation to b-wave of the electroretinogram. *J Neurophysiol* **33** (1970), pp. 323-41.

- Miller, S.S. and Steinberg, R.H. Potassium modulation of taurine transport across the frog retinal pigment epithelium. *J Gen Physiol* **74** (1979), pp. 237-59.
- Mirshahi, M., Thillaye, B., Tarraf, M., de Kozak, Y. and Faure, J.P. Light-induced changes in S-antigen (arrestin) localization in retinal photoreceptors: differences between rods and cones and defective process in RCS rat retinal dystrophy. *Eur J Cell Biol* **63** (1994), pp. 61-7.
- Mitchell, D.C., Bryan, B.A., Liu, J.P., Liu, W.B., Zhang, L., Qu, J., Zhou, X., Liu, M. and Li, D.W. Developmental expression of three small GTPases in the mouse eye. *Mol Vis* **13** (2007), pp. 1144-53.
- Mitchell, R., McCulloch, D., Lutz, E., Johnson, M., MacKenzie, C., Fennell, M., Fink, G., Zhou, W. and Sealfon, S.C. Rhodopsin-family receptors associate with small G proteins to activate phospholipase D. *Nature* **392** (1998), pp. 411-4.
- Mitsuuchi, Y. and Testa, J.R. Cytogenetics and molecular genetics of lung cancer. *Am J Med Genet* **115** (2002), pp. 183-8.
- Mohamed, M.D., Topping, N.C., Jafri, H., Raashed, Y., McKibbin, M.A. and Inglehearn, C.F. Progression of phenotype in Leber's congenital amaurosis with a mutation at the LCA5 locus. *Br J Ophthalmol* **87** (2003), pp. 473-5.
- Molday, R.S. and Molday, L.L. Differences in the protein composition of bovine retinal rod outer segment disk and plasma membranes isolated by a ricin-gold-dextran density perturbation method. *J Cell Biol* **105** (1987), pp. 2589-601.
- Moore, S.J., Green, J.S., Fan, Y., Bhogal, A.K., Dicks, E., Fernandez, B.A., Stefanelli, M., Murphy, C., Cramer, B.C., Dean, J.C., Beales, P.L., Katsanis, N., Bassett, A.S., Davidson, W.S. and Parfrey, P.S. Clinical and genetic epidemiology of Bardet-Biedl syndrome in Newfoundland: a 22-year prospective, population-based, cohort study. *Am J Med Genet A* **132** (2005), pp. 352-60.
- Nancy, V., Callebaut, I., El Marjou, A. and de Gunzburg, J. The delta subunit of retinal rod cGMP phosphodiesterase regulates the membrane association of Ras and Rap GTPases. *J Biol Chem* **277** (2002), pp. 15076-84.
- Nancy, V., Wolthuis, R.M., de Tand, M.F., Janoueix-Lerosey, I., Bos, J.L. and de Gunzburg, J. Identification and characterization of potential effector molecules of the Ras-related GTPase Rap2. *J Biol Chem* **274** (1999), pp. 8737-45.
- Nathans, J. and Hogness, D.S. Isolation, sequence analysis, and intron-exon arrangement of the gene encoding bovine rhodopsin. *Cell* **34** (1983), pp. 807-14.
- Nathans, J., Thomas, D. and Hogness, D.S. Molecular genetics of human color vision: the genes encoding blue, green, and red pigments. *Science* **232** (1986), pp. 193-202.
- Nawy, S. and Jahr, C.E. cGMP-gated conductance in retinal bipolar cells is suppressed by the photoreceptor transmitter. *Neuron* **7** (1991), pp. 677-83.
- Nesvizhskii, A.I., Keller, A., Kolker, E. and Aebersold, R. A statistical model for identifying proteins by tandem mass spectrometry. *Anal Chem* **75** (2003), pp. 4646-58.

- Neves, S.R., Ram, P.T. and Iyengar, R. G protein pathways. *Science* **296** (2002), pp. 1636-9.
- Newman, E.A. Membrane physiology of retinal glial (Muller) cells. *J Neurosci* **5** (1985), pp. 2225-39.
- Newman, E.A. Regulation of potassium levels by Muller cells in the vertebrate retina. *Can J Physiol Pharmacol* **65** (1987), pp. 1028-32.
- Nomanbhoy, T.K., Erickson, J.W. and Cerione, R.A. Kinetics of Cdc42 membrane extraction by Rho-GDI monitored by real-time fluorescence resonance energy transfer. *Biochemistry* **38** (1999), pp. 1744-50.
- Nomanbhoy, T.K., Leonard, D.A., Manor, D. and Cerione, R.A. Investigation of the GTP-binding/GTPase cycle of Cdc42Hs using extrinsic reporter group fluorescence. *Biochemistry* **35** (1996), pp. 4602-8.
- Nonaka, S., Tanaka, Y., Okada, Y., Takeda, S., Harada, A., Kanai, Y., Kido, M. and Hirokawa, N. Randomization of left-right asymmetry due to loss of nodal cilia generating leftward flow of extraembryonic fluid in mice lacking KIF3B motor protein. *Cell* **95** (1998), pp. 829-37.
- Norton, A.W., D'Amours, M.R., Grazio, H.J., Hebert, T.L. and Cote, R.H. Mechanism of transducin activation of frog rod photoreceptor phosphodiesterase. Allosteric interaction between the inhibitory gamma subunit and the noncatalytic cGMP-binding sites. *J Biol Chem* **275** (2000), pp. 38611-9.
- Norton, A.W., Hosier, S., Terew, J.M., Li, N., Dhingra, A., Vardi, N., Baehr, W. and Cote, R.H. Evaluation of the 17-kDa prenyl-binding protein as a regulatory protein for phototransduction in retinal photoreceptors. *J Biol Chem* **280** (2005), pp. 1248-56.
- Obata, S. and Usukura, J. Morphogenesis of the photoreceptor outer segment during postnatal development in the mouse (BALB/c) retina. *Cell Tissue Res* **269** (1992), pp. 39-48.
- Okada, T., Sugihara, M., Bondar, A.N., Elstner, M., Entel, P. and Buss, V. The retinal conformation and its environment in rhodopsin in light of a new 2.2 Å crystal structure. *J Mol Biol* **342** (2004), pp. 571-83.
- Oldham, W.M. and Hamm, H.E. Heterotrimeric G protein activation by G-protein-coupled receptors. *Nat Rev Mol Cell Biol* **9** (2008), pp. 60-71.
- Olsen, J.V., Ong, S.E. and Mann, M. Trypsin cleaves exclusively C-terminal to arginine and lysine residues. *Mol Cell Proteomics* **3** (2004), pp. 608-14.
- Olson, M.F., Ashworth, A. and Hall, A. An essential role for Rho, Rac, and Cdc42 GTPases in cell cycle progression through G1. *Science* **269** (1995), pp. 1270-2.
- Ozdinler, P.H. and Erzurumlu, R.S. Regulation of neurotrophin-induced axonal responses via Rho GTPases. *J Comp Neurol* **438** (2001), pp. 377-87.
- Palczewski, K. G protein-coupled receptor rhodopsin. *Annu Rev Biochem* **75** (2006), pp. 743-67.

- Palczewski, K., Kumasaka, T., Hori, T., Behnke, C.A., Motoshima, H., Fox, B.A., Le Trong, I., Teller, D.C., Okada, T., Stenkamp, R.E., Yamamoto, M. and Miyano, M. Crystal structure of rhodopsin: A G protein-coupled receptor. *Science* **289** (2000), pp. 739-45.
- Pan, J., Wang, Q. and Snell, W.J. Cilium-generated signaling and cilia-related disorders. *Lab Invest* **85** (2005), pp. 452-63.
- Papaharalambus, C., Sajjad, W., Syed, A., Zhang, C., Bergo, M.O., Alexander, R.W. and Ahmad, M. Tumor necrosis factor alpha stimulation of Rac1 activity. Role of isoprenylcysteine carboxylmethyltransferase. *J Biol Chem* **280** (2005), pp. 18790-6.
- Papermaster, D.S. The birth and death of photoreceptors: the Friedenwald Lecture. *Invest Ophthalmol Vis Sci* **43** (2002), pp. 1300-9.
- Papermaster, D.S., Schneider, B.G. and Besharse, J.C. Vesicular transport of newly synthesized opsin from the Golgi apparatus toward the rod outer segment. Ultrastructural immunocytochemical and autoradiographic evidence in *Xenopus* retinas. *Invest Ophthalmol Vis Sci* **26** (1985), pp. 1386-404.
- Pappin, D.J. Peptide mass fingerprinting using MALDI-TOF mass spectrometry. *Methods Mol Biol* **64** (1997), pp. 165-73.
- Pellikka, M., Tanentzapf, G., Pinto, M., Smith, C., McGlade, C.J., Ready, D.F. and Tepass, U. Crumbs, the *Drosophila* homologue of human CRB1/RP12, is essential for photoreceptor morphogenesis. *Nature* **416** (2002), pp. 143-9.
- Pereira-Leal, J.B. and Seabra, M.C. Evolution of the Rab family of small GTP-binding proteins. *J Mol Biol* **313** (2001), pp. 889-901.
- Perez-Sala, D., Tan, E.W., Canada, F.J. and Rando, R.R. Methylation and demethylation reactions of guanine nucleotide-binding proteins of retinal rod outer segments. *Proc Natl Acad Sci U S A* **88** (1991), pp. 3043-6.
- Perrault, I., Hanein, S., Gerber, S., Barbet, F., Ducroq, D., Dollfus, H., Hamel, C., Dufier, J.L., Munnich, A., Kaplan, J. and Rozet, J.M. Retinal dehydrogenase 12 (RDH12) mutations in leber congenital amaurosis. *Am J Hum Genet* **75** (2004), pp. 639-46.
- Perrault, I., Rozet, J.M., Calvas, P., Gerber, S., Camuzat, A., Dollfus, H., Chatelin, S., Souied, E., Ghazi, I., Leowski, C., Bonnemaïson, M., Le Paslier, D., Frezal, J., Dufier, J.L., Pittler, S., Munnich, A. and Kaplan, J. Retinal-specific guanylate cyclase gene mutations in Leber's congenital amaurosis. *Nat Genet* **14** (1996), pp. 461-4.
- Perrault, I., Rozet, J.M., Gerber, S., Ghazi, I., Leowski, C., Ducroq, D., Souied, E., Dufier, J.L., Munnich, A. and Kaplan, J. Leber congenital amaurosis. *Mol Genet Metab* **68** (1999), pp. 200-8.
- Petrov, V.M., Artamonov, I.D. and Lipkin, V.M. Small GTP-binding proteins of squid photoreceptor. Interaction with photoactivated rhodopsin. *FEBS Lett* **337** (1994), pp. 274-6.
- Philp, N.J., Chang, W. and Long, K. Light-stimulated protein movement in rod photoreceptor cells of the rat retina. *FEBS Lett* **225** (1987), pp. 127-32.

- Pietromonaco, S.F., Seluja, G.A., Aitken, A. and Elias, L. Association of 14-3-3 proteins with centrosomes. *Blood Cells Mol Dis* **22** (1996), pp. 225-37.
- Pinter, M., Jekely, G., Szepesi, R.J., Farkas, A., Theopold, U., Meyer, H.E., Lindholm, D., Nassel, D.R., Hultmark, D. and Friedrich, P. TER94, a Drosophila homolog of the membrane fusion protein CDC48/p97, is accumulated in nonproliferating cells: in the reproductive organs and in the brain of the imago. *Insect Biochem Mol Biol* **28** (1998), pp. 91-8.
- Polans, A., Baehr, W. and Palczewski, K. Turned on by Ca²⁺! The physiology and pathology of Ca(2+)-binding proteins in the retina. *Trends Neurosci* **19** (1996), pp. 547-54.
- Praetorius, H.A., Praetorius, J., Nielsen, S., Frokiaer, J. and Spring, K.R. Beta1-integrins in the primary cilium of MDCK cells potentiate fibronectin-induced Ca²⁺ signaling. *Am J Physiol Renal Physiol* **287** (2004), pp. F969-78.
- Pruyne, D. and Bretscher, A. Polarization of cell growth in yeast. I. Establishment and maintenance of polarity states. *J Cell Sci* **113** (Pt 3) (2000), pp. 365-75.
- Pulvermuller, A., Giessl, A., Heck, M., Wottrich, R., Schmitt, A., Ernst, O.P., Choe, H.W., Hofmann, K.P. and Wolfrum, U. Calcium-dependent assembly of centrin-G-protein complex in photoreceptor cells. *Mol Cell Biol* **22** (2002), pp. 2194-203.
- Qin, N., Pittler, S.J. and Baehr, W. In vitro isoprenylation and membrane association of mouse rod photoreceptor cGMP phosphodiesterase alpha and beta subunits expressed in bacteria. *J Biol Chem* **267** (1992), pp. 8458-63.
- Rabilloud, T., Adessi, C., Giraudel, A. and Lunardi, J. Improvement of the solubilization of proteins in two-dimensional electrophoresis with immobilized pH gradients. *Electrophoresis* **18** (1997), pp. 307-16.
- Raich, W.B., Agbunag, C. and Hardin, J. Rapid epithelial-sheet sealing in the Caenorhabditis elegans embryo requires cadherin-dependent filopodial priming. *Curr Biol* **9** (1999), pp. 1139-46.
- Rakic Lj, M., Rusic, M. and Levental, M. [Biochemical structure of myelin in the central nervous system]. *Glas Srp Akad Nauka [Med]* (1981), pp. 173-91.
- Randazzo, P.A., Nie, Z., Miura, K. and Hsu, V.W. Molecular aspects of the cellular activities of ADP-ribosylation factors. *Sci STKE* **2000** (2000), p. RE1.
- Raymond, S.M. and Jackson, I.J. The retinal pigmented epithelium is required for development and maintenance of the mouse neural retina. *Curr Biol* **5** (1995), pp. 1286-95.
- Redmond, T.M. and Hamel, C.P. Genetic analysis of RPE65: from human disease to mouse model. *Methods Enzymol* **316** (2000), pp. 705-24.
- Redmond, T.M., Yu, S., Lee, E., Bok, D., Hamasaki, D., Chen, N., Goletz, P., Ma, J.X., Crouch, R.K. and Pfeifer, K. Rpe65 is necessary for production of 11-cis-vitamin A in the retinal visual cycle. *Nat Genet* **20** (1998), pp. 344-51.

- Reifschneider, N.H., Goto, S., Nakamoto, H., Takahashi, R., Sugawa, M., Dencher, N.A. and Krause, F. Defining the mitochondrial proteomes from five rat organs in a physiologically significant context using 2D blue-native/SDS-PAGE. *J Proteome Res* **5** (2006), pp. 1117-32.
- Reiners, J., Nagel-Wolfrum, K., Jurgens, K., Marker, T. and Wolfrum, U. Molecular basis of human Usher syndrome: deciphering the meshes of the Usher protein network provides insights into the pathomechanisms of the Usher disease. *Exp Eye Res* **83** (2006), pp. 97-119.
- Reisinger, V. and Eichacker, L.A. Analysis of Membrane Protein Complexes by Blue Native PAGE. *Proteomics* **6 Suppl 2** (2006), pp. 6-15.
- Ridge, K.D., Abdulaev, N.G., Sousa, M. and Palczewski, K. Phototransduction: crystal clear. *Trends Biochem Sci* **28** (2003), pp. 479-87.
- Rieder, C.L., Faruki, S. and Khodjakov, A. The centrosome in vertebrates: more than a microtubule-organizing center. *Trends Cell Biol* **11** (2001), pp. 413-9.
- Rigaut, G., Shevchenko, A., Rutz, B., Wilm, M., Mann, M. and Seraphin, B. A generic protein purification method for protein complex characterization and proteome exploration. *Nat Biotechnol* **17** (1999), pp. 1030-2.
- Robbe, K., Otto-Bruc, A., Chardin, P. and Antonny, B. Dissociation of GDP dissociation inhibitor and membrane translocation are required for efficient activation of Rac by the Dbl homology-pleckstrin homology region of Tiam. *J Biol Chem* **278** (2003), pp. 4756-62.
- Roepman, R., Bauer, D., Rosenberg, T., van Duijnhoven, G., van de Vosse, E., Platzer, M., Rosenthal, A., Ropers, H.H., Cremers, F.P. and Berger, W. Identification of a gene disrupted by a microdeletion in a patient with X-linked retinitis pigmentosa (XLRP). *Hum Mol Genet* **5** (1996a), pp. 827-33.
- Roepman, R., Bernoud-Hubac, N., Schick, D.E., Maugeri, A., Berger, W., Ropers, H.H., Cremers, F.P. and Ferreira, P.A. The retinitis pigmentosa GTPase regulator (RPGR) interacts with novel transport-like proteins in the outer segments of rod photoreceptors. *Hum Mol Genet* **9** (2000a), pp. 2095-105.
- Roepman, R., Schick, D. and Ferreira, P.A. Isolation of retinal proteins that interact with retinitis pigmentosa GTPase regulator by interaction trap screen in yeast. *Methods Enzymol* **316** (2000b), pp. 688-704.
- Roepman, R., van Duijnhoven, G., Rosenberg, T., Pinckers, A.J., Bleeker-Wagemakers, L.M., Bergen, A.A., Post, J., Beck, A., Reinhardt, R., Ropers, H.H., Cremers, F.P. and Berger, W. Positional cloning of the gene for X-linked retinitis pigmentosa 3: homology with the guanine-nucleotide-exchange factor RCC1. *Hum Mol Genet* **5** (1996b), pp. 1035-41.
- Rohlich, P. The sensory cilium of retinal rods is analogous to the transitional zone of motile cilia. *Cell Tissue Res* **161** (1975), pp. 421-30.
- Romijn, H.J. Development and advantages of serum-free, chemically defined nutrient media for culturing of nerve tissue. *Biol Cell* **63** (1988), pp. 263-8.

- Ruchhoeft, M.L., Ohnuma, S., McNeill, L., Holt, C.E. and Harris, W.A. The neuronal architecture of *Xenopus* retinal ganglion cells is sculpted by rho-family GTPases in vivo. *J Neurosci* **19** (1999), pp. 8454-63.
- Sah, V.P., Seasholtz, T.M., Sagi, S.A. and Brown, J.H. The role of Rho in G protein-coupled receptor signal transduction. *Annu Rev Pharmacol Toxicol* **40** (2000), pp. 459-89.
- Sahai, E. and Marshall, C.J. RHO-GTPases and cancer. *Nat Rev Cancer* **2** (2002), pp. 133-42.
- Sahin, M., Greer, P.L., Lin, M.Z., Poucher, H., Eberhart, J., Schmidt, S., Wright, T.M., Shamah, S.M., O'Connell, S., Cowan, C.W., Hu, L., Goldberg, J.L., Debant, A., Corfas, G., Krull, C.E. and Greenberg, M.E. Eph-dependent tyrosine phosphorylation of ephexin1 modulates growth cone collapse. *Neuron* **46** (2005), pp. 191-204.
- Saiki, R.K., Gelfand, D.H., Stoffel, S., Scharf, S.J., Higuchi, R., Horn, G.T., Mullis, K.B. and Erlich, H.A. Primer-directed enzymatic amplification of DNA with a thermostable DNA polymerase. *Science* **239** (1988), pp. 487-91.
- Sakmar, T.P. Structure of rhodopsin and the superfamily of seven-helical receptors: the same and not the same. *Curr Opin Cell Biol* **14** (2002), pp. 189-95.
- Sarthy, P.V. and Bunt, A.H. The ultrastructure of isolated glial (Muller) cells from the turtle retina. *Anat Rec* **202** (1982), pp. 275-83.
- Sasaki, T., Kato, M. and Takai, Y. Consequences of weak interaction of rho GDI with the GTP-bound forms of rho p21 and rac p21. *J Biol Chem* **268** (1993), pp. 23959-63.
- Schadel, S.A., Heck, M., Marezki, D., Filipek, S., Teller, D.C., Palczewski, K. and Hofmann, K.P. Ligand channeling within a G-protein-coupled receptor. The entry and exit of retinals in native opsin. *J Biol Chem* **278** (2003), pp. 24896-903.
- Schagger, H. Blue-native gels to isolate protein complexes from mitochondria. *Methods Cell Biol* **65** (2001), pp. 231-44.
- Schagger, H., Cramer, W.A. and von Jagow, G. Analysis of molecular masses and oligomeric states of protein complexes by blue native electrophoresis and isolation of membrane protein complexes by two-dimensional native electrophoresis. *Anal Biochem* **217** (1994), pp. 220-30.
- Schagger, H. and von Jagow, G. Blue native electrophoresis for isolation of membrane protein complexes in enzymatically active form. *Anal Biochem* **199** (1991), pp. 223-31.
- Scheffzek, K., Stephan, I., Jensen, O.N., Illenberger, D. and Gierschik, P. The Rac-RhoGDI complex and the structural basis for the regulation of Rho proteins by RhoGDI. *Nat Struct Biol* **7** (2000), pp. 122-6.
- Scherle, P., Behrens, T. and Staudt, L.M. Ly-GDI, a GDP-dissociation inhibitor of the RhoA GTP-binding protein, is expressed preferentially in lymphocytes. *Proc Natl Acad Sci U S A* **90** (1993), pp. 7568-72.
- Schermer, B., Hopker, K., Omran, H., Ghenoiu, C., Fliegau, M., Fekete, A., Horvath, J., Kottgen, M., Hackl, M., Zschiedrich, S., Huber, T.B., Kramer-Zucker, A., Zentgraf,

- H., Blaukat, A., Walz, G. and Benzing, T. Phosphorylation by casein kinase 2 induces PACS-1 binding of nephrocystin and targeting to cilia. *EMBO J* **24** (2005), pp. 4415-24.
- Schmitt, A. and Wolfrum, U. Identification of novel molecular components of the photoreceptor connecting cilium by immunoscreens. *Exp Eye Res* **73** (2001), pp. 837-49.
- Seddon, A.M., Curnow, P. and Booth, P.J. Membrane proteins, lipids and detergents: not just a soap opera. *Biochim Biophys Acta* **1666** (2004), pp. 105-17.
- Shamah, S.M., Lin, M.Z., Goldberg, J.L., Estrach, S., Sahin, M., Hu, L., Bazalakova, M., Neve, R.L., Corfas, G., Debant, A. and Greenberg, M.E. EphA receptors regulate growth cone dynamics through the novel guanine nucleotide exchange factor ephexin. *Cell* **105** (2001), pp. 233-44.
- Shevchenko, A., Wilm, M., Vorm, O. and Mann, M. Mass spectrometric sequencing of proteins silver-stained polyacrylamide gels. *Anal Chem* **68** (1996), pp. 850-8.
- Shih, J.Y., Yang, S.C., Hong, T.M., Yuan, A., Chen, J.J., Yu, C.J., Chang, Y.L., Lee, Y.C., Peck, K., Wu, C.W. and Yang, P.C. Collapsin response mediator protein-1 and the invasion and metastasis of cancer cells. *J Natl Cancer Inst* **93** (2001), pp. 1392-400.
- Shinmura, K., Tarapore, P., Tokuyama, Y., George, K.R. and Fukasawa, K. Characterization of centrosomal association of nucleophosmin/B23 linked to Crm1 activity. *FEBS Lett* **579** (2005), pp. 6621-34.
- Shinohara, N., Ogiso, Y., Tanaka, M., Sazawa, A., Harabayashi, T. and Koyanagi, T. The significance of Ras guanine nucleotide exchange factor, son of sevenless protein, in renal cell carcinoma cell lines. *J Urol* **158** (1997), pp. 908-11.
- Shu, X., Fry, A.M., Tulloch, B., Manson, F.D., Crabb, J.W., Khanna, H., Faragher, A.J., Lennon, A., He, S., Trojan, P., Giessl, A., Wolfrum, U., Vervoort, R., Swaroop, A. and Wright, A.F. RPGR ORF15 isoform co-localizes with RPGRIP1 at centrioles and basal bodies and interacts with nucleophosmin. *Hum Mol Genet* **14** (2005), pp. 1183-97.
- Skerra, A. and Schmidt, T.G. Use of the Strep-Tag and streptavidin for detection and purification of recombinant proteins. *Methods Enzymol* **326** (2000), pp. 271-304.
- Snyder, J.T., Worthylake, D.K., Rossman, K.L., Betts, L., Pruitt, W.M., Siderovski, D.P., Der, C.J. and Sondek, J. Structural basis for the selective activation of Rho GTPases by Dbl exchange factors. *Nat Struct Biol* **9** (2002), pp. 468-75.
- Soderling, S.H. and Beavo, J.A. Regulation of cAMP and cGMP signaling: new phosphodiesterases and new functions. *Curr Opin Cell Biol* **12** (2000), pp. 174-9.
- Soderpalm, A., Szel, A., Caffè, A.R. and van Veen, T. Selective development of one cone photoreceptor type in retinal organ culture. *Invest Ophthalmol Vis Sci* **35** (1994), pp. 3910-21.

- Soderpalm, A.K., Fox, D.A., Karlsson, J.O. and van Veen, T. Retinoic acid produces rod photoreceptor selective apoptosis in developing mammalian retina. *Invest Ophthalmol Vis Sci* **41** (2000), pp. 937-47.
- Soderpalm, A.K., Karlsson, J., Caffè, A.R. and vanVeen, T. 9-cis-retinoic acid in combination with retinal pigment epithelium induces apoptosis in cultured retinal explants only during early postnatal development. *Brain Res Dev Brain Res* **118** (1999), pp. 169-76.
- Sohocki, M.M., Bowne, S.J., Sullivan, L.S., Blackshaw, S., Cepko, C.L., Payne, A.M., Bhattacharya, S.S., Khaliq, S., Qasim Mehdi, S., Birch, D.G., Harrison, W.R., Elder, F.F., Heckenlively, J.R. and Daiger, S.P. Mutations in a new photoreceptor-pineal gene on 17p cause Leber congenital amaurosis. *Nat Genet* **24** (2000), pp. 79-83.
- Sohocki, M.M., Sullivan, L.S., Mintz-Hittner, H.A., Birch, D., Heckenlively, J.R., Freund, C.L., McInnes, R.R. and Daiger, S.P. A range of clinical phenotypes associated with mutations in CRX, a photoreceptor transcription-factor gene. *Am J Hum Genet* **63** (1998), pp. 1307-15.
- Sokolov, M., Lyubarsky, A.L., Strissel, K.J., Savchenko, A.B., Govardovskii, V.I., Pugh, E.N., Jr. and Arshavsky, V.Y. Massive light-driven translocation of transducin between the two major compartments of rod cells: a novel mechanism of light adaptation. *Neuron* **34** (2002), pp. 95-106.
- Spira, A.W. and Milman, G.E. The structure and distribution of the cross-striated fibril and associated membranes in guinea pig photoreceptors. *Am J Anat* **155** (1979), pp. 319-37.
- Steinberg, R.H., Fisher, S.K. and Anderson, D.H. Disc morphogenesis in vertebrate photoreceptors. *J Comp Neurol* **190** (1980), pp. 501-8.
- Stenmark, H. and Olkkonen, V.M. The Rab GTPase family. *Genome Biol* **2** (2001), p. REVIEWS3007.
- Stone, J. and Dreher, Z. Relationship between astrocytes, ganglion cells and vasculature of the retina. *J Comp Neurol* **255** (1987), pp. 35-49.
- Strissel, K.J., Lishko, P.V., Trieu, L.H., Kennedy, M.J., Hurley, J.B. and Arshavsky, V.Y. Recoverin undergoes light-dependent intracellular translocation in rod photoreceptors. *J Biol Chem* **280** (2005), pp. 29250-5.
- Strissel, K.J., Sokolov, M., Trieu, L.H. and Arshavsky, V.Y. Arrestin translocation is induced at a critical threshold of visual signaling and is superstoichiometric to bleached rhodopsin. *J Neurosci* **26** (2006), pp. 1146-53.
- Suber, M.L., Pittler, S.J., Qin, N., Wright, G.C., Holcombe, V., Lee, R.H., Craft, C.M., Lolley, R.N., Baehr, W. and Hurwitz, R.L. Irish setter dogs affected with rod/cone dysplasia contain a nonsense mutation in the rod cGMP phosphodiesterase beta-subunit gene. *Proc Natl Acad Sci U S A* **90** (1993), pp. 3968-72.
- Suda, K., Filipek, S., Palczewski, K., Engel, A. and Fotiadis, D. The supramolecular structure of the GPCR rhodopsin in solution and native disc membranes. *Mol Membr Biol* **21** (2004), pp. 435-46.

- Sung, C.H., Makino, C., Baylor, D. and Nathans, J. A rhodopsin gene mutation responsible for autosomal dominant retinitis pigmentosa results in a protein that is defective in localization to the photoreceptor outer segment. *J Neurosci* **14** (1994), pp. 5818-33.
- Takahashi, K., Sasaki, T., Mammoto, A., Takaishi, K., Kameyama, T., Tsukita, S. and Takai, Y. Direct interaction of the Rho GDP dissociation inhibitor with ezrin/radixin/moesin initiates the activation of the Rho small G protein. *J Biol Chem* **272** (1997), pp. 23371-5.
- Tam, B.M., Moritz, O.L., Hurd, L.B. and Papermaster, D.S. Identification of an outer segment targeting signal in the COOH terminus of rhodopsin using transgenic *Xenopus laevis*. *J Cell Biol* **151** (2000), pp. 1369-80.
- Teller, D.C., Okada, T., Behnke, C.A., Palczewski, K. and Stenkamp, R.E. Advances in determination of a high-resolution three-dimensional structure of rhodopsin, a model of G-protein-coupled receptors (GPCRs). *Biochemistry* **40** (2001), pp. 7761-72.
- Towbin, H., Staehelin, T. and Gordon, J. Electrophoretic transfer of proteins from polyacrylamide gels to nitrocellulose sheets: procedure and some applications. *Proc Natl Acad Sci U S A* **76** (1979), pp. 4350-4.
- Travis, G.H., Brennan, M.B., Danielson, P.E., Kozak, C.A. and Sutcliffe, J.G. Identification of a photoreceptor-specific mRNA encoded by the gene responsible for retinal degeneration slow (rds). *Nature* **338** (1989), pp. 70-3.
- Tso, M.O., Li, W.W., Zhang, C., Lam, T.T., Hao, Y., Petters, R.M. and Wong, F. A pathologic study of degeneration of the rod and cone populations of the rhodopsin Pro347Leu transgenic pigs. *Trans Am Ophthalmol Soc* **95** (1997), pp. 467-79; discussion 479-83.
- Uchida, Y., Ohshima, T., Sasaki, Y., Suzuki, H., Yanai, S., Yamashita, N., Nakamura, F., Takei, K., Ihara, Y., Mikoshiba, K., Kolattukudy, P., Honnorat, J. and Goshima, Y. Semaphorin3A signalling is mediated via sequential Cdk5 and GSK3beta phosphorylation of CRMP2: implication of common phosphorylating mechanism underlying axon guidance and Alzheimer's disease. *Genes Cells* **10** (2005), pp. 165-79.
- Ueda, T., Kikuchi, A., Ohga, N., Yamamoto, J. and Takai, Y. Purification and characterization from bovine brain cytosol of a novel regulatory protein inhibiting the dissociation of GDP from and the subsequent binding of GTP to rhoB p20, a ras p21-like GTP-binding protein. *J Biol Chem* **265** (1990), pp. 9373-80.
- Ugolev, Y., Molshanski-Mor, S., Weinbaum, C. and Pick, E. Liposomes comprising anionic but not neutral phospholipids cause dissociation of Rac(1 or 2) x RhoGDI complexes and support amphiphile-independent NADPH oxidase activation by such complexes. *J Biol Chem* **281** (2006), pp. 19204-19.
- Vageli, D., Kiaris, H., Delakas, D., Anezinis, P., Cranidis, A. and Spandidos, D.A. Transcriptional activation of H-ras, K-ras and N-ras proto-oncogenes in human bladder tumors. *Cancer Lett* **107** (1996), pp. 241-7.
- Vasioukhin, V., Bauer, C., Yin, M. and Fuchs, E. Directed actin polymerization is the driving force for epithelial cell-cell adhesion. *Cell* **100** (2000), pp. 209-19.

- Vastrik, I., Eickholt, B.J., Walsh, F.S., Ridley, A. and Doherty, P. Sema3A-induced growth-cone collapse is mediated by Rac1 amino acids 17-32. *Curr Biol* **9** (1999), pp. 991-8.
- Vaughan, D.K. and Fisher, S.K. Cytochalasin D disrupts outer segment disc morphogenesis in situ in rabbit retina. *Invest Ophthalmol Vis Sci* **30** (1989), pp. 339-42.
- von Lintig, F.C., Dreilinger, A.D., Varki, N.M., Wallace, A.M., Casteel, D.E. and Boss, G.R. Ras activation in human breast cancer. *Breast Cancer Res Treat* **62** (2000), pp. 51-62.
- Wahl, S., Barth, H., Ciossek, T., Aktories, K. and Mueller, B.K. Ephrin-A5 induces collapse of growth cones by activating Rho and Rho kinase. *J Cell Biol* **149** (2000), pp. 263-70.
- Watanabe, T. and Raff, M.C. Retinal astrocytes are immigrants from the optic nerve. *Nature* **332** (1988), pp. 834-7.
- Weis, K. Regulating access to the genome: nucleocytoplasmic transport throughout the cell cycle. *Cell* **112** (2003), pp. 441-51.
- Wennerberg, K. and Der, C.J. Rho-family GTPases: it's not only Rac and Rho (and I like it). *J Cell Sci* **117** (2004), pp. 1301-12.
- Wessel, D. and Flügge, U.I. A method for the quantitative recovery of protein in dilute solution in the presence of detergents and lipids. *Anal Biochem* **138** (1984), pp. 141-3.
- Wheatley, D.N. Primary cilia in normal and pathological tissues. *Pathobiology* **63** (1995), pp. 222-38.
- Wheatley, D.N., Wang, A.M. and Strugnell, G.E. Expression of primary cilia in mammalian cells. *Cell Biol Int* **20** (1996), pp. 73-81.
- Whelan, J.P. and McGinnis, J.F. Light-dependent subcellular movement of photoreceptor proteins. *J Neurosci Res* **20** (1988), pp. 263-70.
- Wieland, T., Ulibarri, I., Aktories, K., Gierschik, P. and Jakobs, K.H. Interaction of small G proteins with photoexcited rhodopsin. *FEBS Lett* **263** (1990), pp. 195-8.
- Williams, D.S., Linberg, K.A., Vaughan, D.K., Fariss, R.N. and Fisher, S.K. Disruption of microfilament organization and deregulation of disk membrane morphogenesis by cytochalasin D in rod and cone photoreceptors. *J Comp Neurol* **272** (1988), pp. 161-76.
- Wilson, S.J. and Smyth, E.M. Internalization and recycling of the human prostacyclin receptor is modulated through its isoprenylation-dependent interaction with the delta subunit of cGMP phosphodiesterase 6. *J Biol Chem* **281** (2006), pp. 11780-6.
- Wittig, I., Carrozzo, R., Santorelli, F.M. and Schagger, H. Supercomplexes and subcomplexes of mitochondrial oxidative phosphorylation. *Biochim Biophys Acta* **1757** (2006), pp. 1066-72.
- Wittig, I. and Schagger, H. Advantages and limitations of clear-native PAGE. *Proteomics* **5** (2005), pp. 4338-46.

- Wittmann, T. and Waterman-Storer, C.M. Cell motility: can Rho GTPases and microtubules point the way? *J Cell Sci* **114** (2001), pp. 3795-803.
- Wong, W.T., Faulkner-Jones, B.E., Sanes, J.R. and Wong, R.O. Rapid dendritic remodeling in the developing retina: dependence on neurotransmission and reciprocal regulation by Rac and Rho. *J Neurosci* **20** (2000), pp. 5024-36.
- Woodruff, M.L., Wang, Z., Chung, H.Y., Redmond, T.M., Fain, G.L. and Lem, J. Spontaneous activity of opsin apoprotein is a cause of Leber congenital amaurosis. *Nat Genet* **35** (2003), pp. 158-64.
- Wu, X., Quondamatteo, F., Lefever, T., Czuchra, A., Meyer, H., Chrostek, A., Paus, R., Langbein, L. and Brakebusch, C. Cdc42 controls progenitor cell differentiation and beta-catenin turnover in skin. *Genes Dev* **20** (2006), pp. 571-85.
- Xu, G.F., O'Connell, P., Viskochil, D., Cawthon, R., Robertson, M., Culver, M., Dunn, D., Stevens, J., Gesteland, R., White, R. and et al. The neurofibromatosis type 1 gene encodes a protein related to GAP. *Cell* **62** (1990), pp. 599-608.
- Yang, J. and Li, T. Focus on molecules: rootletin. *Exp Eye Res* **83** (2006), pp. 1-2.
- Yoshimura, T., Kawano, Y., Arimura, N., Kawabata, S., Kikuchi, A. and Kaibuchi, K. GSK-3beta regulates phosphorylation of CRMP-2 and neuronal polarity. *Cell* **120** (2005), pp. 137-49.
- Young, R.W. The renewal of photoreceptor cell outer segments. *J Cell Biol* **33** (1967), pp. 61-72.
- Young, R.W. The daily rhythm of shedding and degradation of rod and cone outer segment membranes in the chick retina. *Invest Ophthalmol Vis Sci* **17** (1978), pp. 105-16.
- Young, R.W. and Bok, D. Participation of the retinal pigment epithelium in the rod outer segment renewal process. *J Cell Biol* **42** (1969), pp. 392-403.
- Yuasa-Kawada, J., Suzuki, R., Kano, F., Ohkawara, T., Murata, M. and Noda, M. Axonal morphogenesis controlled by antagonistic roles of two CRMP subtypes in microtubule organization. *Eur J Neurosci* **17** (2003), pp. 2329-43.
- Zalcman, G., Closson, V., Camonis, J., Honore, N., Rousseau-Merck, M.F., Tavitian, A. and Olofsson, B. RhoGDI-3 is a new GDP dissociation inhibitor (GDI). Identification of a non-cytosolic GDI protein interacting with the small GTP-binding proteins RhoB and RhoG. *J Biol Chem* **271** (1996), pp. 30366-74.
- Zalcman, G., Dorseuil, O., Garcia-Ranea, J.A., Gacon, G. and Camonis, J. RhoGAPs and RhoGDIs, (His)stories of two families. *Prog Mol Subcell Biol* **22** (1999), pp. 85-113.
- Zhang, F.L. and Casey, P.J. Protein prenylation: molecular mechanisms and functional consequences. *Annu Rev Biochem* **65** (1996), pp. 241-69.
- Zhang, H., Cuenca, N., Ivanova, T., Church-Kopish, J., Frederick, J.M., MacLeish, P.R. and Baehr, W. Identification and light-dependent translocation of a cone-specific antigen, cone arrestin, recognized by monoclonal antibody 7G6. *Invest Ophthalmol Vis Sci* **44** (2003), pp. 2858-67.

- Zhang, H., Frederick, J.M. and Baehr, W. Functional study of photoreceptor PDEdelta. *Adv Exp Med Biol* **572** (2006), pp. 485-90.
- Zhang, H., Li, S., Doan, T., Rieke, F., Detwiler, P.B., Frederick, J.M. and Baehr, W. Deletion of PrBP/delta impedes transport of GRK1 and PDE6 catalytic subunits to photoreceptor outer segments. *Proc Natl Acad Sci U S A* **104** (2007), pp. 8857-62.
- Zhang, H., Liu, X.H., Zhang, K., Chen, C.K., Frederick, J.M., Prestwich, G.D. and Baehr, W. Photoreceptor cGMP phosphodiesterase delta subunit (PDEdelta) functions as a prenyl-binding protein. *J Biol Chem* **279** (2004a), pp. 407-13.
- Zhang, H., Shi, X., Paddon, H., Hampong, M., Dai, W. and Pelech, S. B23/nucleophosmin serine 4 phosphorylation mediates mitotic functions of polo-like kinase 1. *J Biol Chem* **279** (2004b), pp. 35726-34.
- Zhang, K., DeClue, J.E., Vass, W.C., Papageorge, A.G., McCormick, F. and Lowy, D.R. Suppression of c-ras transformation by GTPase-activating protein. *Nature* **346** (1990), pp. 754-6.
- Zhu, X., Li, A., Brown, B., Weiss, E.R., Osawa, S. and Craft, C.M. Mouse cone arrestin expression pattern: light induced translocation in cone photoreceptors. *Mol Vis* **8** (2002), pp. 462-71.
- Zimmermann, J.: DNA-Sequenzierung. In: Lottspeich, F. and Engels, J.W. (Lottspeich, F. and Engels, J.W.(Lottspeich, F. and Engels, J.W.s), *Bioanalytik*. Spektrum Akademischer Verlag, München (2006), pp. 777-803.

K. ANNEX

1. FIGURE INDEX

Figure	Title	Page
1	Section of the human eye	13
2	Vertebrate photoreceptors	15
3	Rhodopsin	20
4	Model of rod phototransduction	22
5	Diagram illustration of a rod photoreceptor and its ciliary apparatus	25
6	Morphology and polarity	34
7	The Rho GTPase cycle	38
8	Schematic representation of signal transduction pathways involved in growth cone collapse	42
9	The hydrophobic pocket in PDE δ	48
10	Alignment of PDE δ , RhoGDI and UNC119/RG4 proteins	50
11	2-DE electrophoresis of native protein complexes	67
12	Separation principle of 2-DE gel electrophoresis	69
13	The most important steps during Western blotting	73
14	Diagram of a horizontal graphite blotter for semi dry blotting	74
15	Overview of the SF-TAP procedure	78
16	The MALDI principle	80
17	Fragmentation of peptides	81
18	ROS isolation	86
19	Overview of the Gateway cloning strategy	96
20	Steps in preparation of an organotypical explant culture from postnatal murine eyes	100
21	Peptide selection. Alignment of the five human CRMP-family protein sequences	106
22	Silver stained 1-DE gels of Rac1-immunoprecipitations from soluble and membranous ROS fractions.	109
23	Silver stained 2-DE gels of Rac1-immunoprecipitations from soluble and membranous ROS fractions	111
24	Analysis of light-regulated Rac1- and RhoA-interactions in ROS	116
25	Characterization of CRMP2 specificity of the produced monoclonal antibodies by WB analysis of porcine retina lysate	121
26	Immunohistochemistry with anti-CRMP2 antibodies from stable monoclonal cell lines on cryosections of porcine retina	123
27	Validation of the CRMP2 specific monoclonal antibodies from stable hybridoma cell lines for IP	125
28	TUNEL assay of retinal explants (div8)	128
29	Immunohistochemical analysis of retinal explants (div8)	130
30	Immunohistochemical analysis of retinal explants (div8) that were cultured in the absence or presence of the Rock II specific inhibitor Y-27632	132/133
31	Solubilization and separation of native protein complexes from ROS by BN-PAGE	136
32	Colocalization of Rac1 and PDE δ in light- and dark-adapted porcine retina	139
33	Localization of Rac1 and PDE δ in light- and dark-adapted porcine retina	140
34	Light-dependent association of Rac1 and PDE δ in ROS	142
35	Western blot of a first dimension of a BN-PAGE from light-and dark-adapted	144

	ROS, soluble and membranous fractions	
36	PDE δ and Rac1 colocalize in ROS in native protein complexes	145
37	Light dependent carboxyl-methylation of Rac1 in ROS.	147
38	In vitro solubilization of Rac1 GTPase from light- and dark-adapted ROS membranes.	149
39	Immunoprecipitation of lebercilin by the anti-lebercilin antibody	151
40	Lebercilin interactome	152
41	Rac1 interaction network	156
42	Possible involvement of CRMP2 in signal transduction pathways in ROS	159

2. TABLE INDEX

Table	Title	Page
1	Cilia-related disorders	27
2	Human cyclic nucleotide phosphodiesterase isozymes	44
3	Primer for Gateway-Cloning	56
4	Sequencing and PDR primer	56
5	Plasmids	57
6	Constructs	57
7	Mamalian cell lines	58
8	Antibodies against mammalian proteins	58
9	Secondary antibodies	60
10	Gel solution for SDS separating gel (30)	64
11	Gel solution for SDS stacking gel (10)	64
12	Gel solution for SDS gradient separating gel (30)	65
13	Gel solutions for BN-PAGE separating gel (10.5)	68
14	Gel solutions for BN-PAGE stacking gel (20)	68
15	Composition of R16 Powder medium	98
16	Additives to R16 Powder medium for Basal media	98
17	Additives to R16 Powder medium for Complete media	99
18	Peptide antigens used for immunization	104
19	The Rac1 interactome in ROS	113
20	Characterization of rat and mouse monoclonal antibodies against CRMP2 obtained by immunization with peptide Beer1	118
21	Characterization of rat monoclonal antibodies against CRMP2 obtained by immunization with peptide Beer4	120
22	LC-MS/MS analysis of the radiolabelled 98 kDa band	148
23	LC-MS/MS analysis of immunoprecipitated, radiolabelled Rac1	148
24	LC-MS/MS analysis of the radiolabelled bands around 24 kDa	148
25	TAP and LC-MS/MS analysis of the lebercilin interactome in HEK293 cells	150

3. PUBLICATIONS AND PRESENTATIONS

3.1. Journals

den Hollander, A. I., Koenekoop, R. K., Mohamed, M. D., Arts, H. H., Boldt, K., Towns, K. V., Sedmak, T., Beer, M., Nagel-Wolfrum, K., McKibbin, M., Dharmaraj, S., Lopez, I., Ivings, L., Williams, G. A., Springell, K., Woods, C.G., Jafri, H., Rashid, Y., Strom, T. M., van der Zwaag, B., Gosens, I., Kersten, F.F., van Wijk, E., Veltman, J. A., Zonneveld, M. N., van Beersum, S. E., Maumenee, I. H., Wolfrum, U., Cheetham, M. E., Ueffing, M., Cremers, F. P., Inglehearn, C. F., Roepman, R. (2007). Mutations in LCA5, encoding the ciliary protein lebercilin, cause Leber congenital amaurosis. *Nat Genet.* 39: 889-95.

Braun, R. J., Kinkl, N., Beer, M., Ueffing, M. (2007). Two-dimensional electrophoresis of membrane proteins. *Anal Bioanal Chem.* 389:1033-45.

Beer, M. V., Swiatek-de Lange, M., Kinkl, N. and Ueffing, M. Phosphodiesterase delta exerts guanine nucleotide dissociation inhibitor function for Rac1 in porcine rod outer segments. (submitted).

Ueffing, M., Chatr-aryamontri, A., Vogt, A., Campagna, A., Swiatek-de Lange, M., Beer, M. V., Cesareni, G., Serrano, L. and Kiel, C. Structural and functional protein network analysis predicts novel systemic functions for the G-Protein coupled receptor rhodopsin. (In prep.).

3.2 Poster presentations

M. Beer, M. Swiatek-de Lange and M. Ueffing. Analysis of light-dependent dynamics of protein complexes in the retina. 4th Annual World Congress of HUPO, Munich, Germany, August 2005

M. Swiatek-de Lange, M. Beer, A. Chatr-aryamontri, G. Cesareni and M. Ueffing. Analysis of light-dependent dynamics of protein complexes in the retina. 2006 ARVO Annual Meeting, April 2006, Florida.

M. Swiatek-de Lange, A. Chatr-aryamontri, M. Beer, G. Cesareni and M. Ueffing. A protein interaction network linked to the mammalian GPCR rhodopsin. Pro Retina Research-Colloquium, Potsdam, Germany, April 2006.

M. Swiatek-de Lange, M. Beer, and M. Ueffing. Analysis of multicomponent protein networks in the retina. Pro Retina Research-Colloquium, Potsdam, Germany, April 2005.

4. ACKNOWLEDGMENTS

Diese Arbeit wurde in der Arbeitsgruppe Dr. Marius Ueffing, dem Department of Protein Science am Helmholtz Zentrum München, durchgeführt. Die Betreuung und Vertretung dieser Arbeit an der Ludwig Maximilians Universität München erfolgte durch Prof. Lutz Eichacker. Die Vorarbeiten zur vorliegenden Arbeit wurden von Dr. Magdalena Swiatek-DeLange in der Arbeitsgruppe Dr. Marius Ueffing durchgeführt.

Bei Marius möchte ich mich dafür bedanken, dass ich als Doktorandin in seiner Arbeitsgruppe das Thema meiner Doktorarbeit erfolgreich bearbeiten konnte und dass er mir einen Laboraustausch an die Universität von Lund ermöglichte.

Bei Prof. Dr. Lutz Eichacker möchte ich mich herzlich für die Betreuung, für Hilfestellungen bei der BN-PAGE sowie für seinen großen Einsatz als externer Doktorvater bedanken. Für seine neu angetretene Professur in Norwegen wünsche ich ihm alles Gute.

Bei Dr. Magdalena Swiatek-DeLange möchte ich mich für die Betreuung während des ersten Jahres meiner Doktorarbeit, ihre lebensfrohe Art, lustige Videoabende sowie viele wissenschaftliche und nicht-wissenschaftliche Diskussionen bedanken.

Bei Steffi Hauck möchte ich mich herzlich für das Einspringen als Betreuerin nach dem Weggang von Magda bedanken. Bei Probleme mit Experimenten hatte sie immer ein offenes Ohr.

Bei Dr. Norbert Kinkl möchte ich mich ganz besonders dafür bedanken, dass er die Betreuung meiner Doktorarbeit übernommen hat, sowie für sein unermüdliches Korrekturlesen dieser Arbeit und des Papers. Ganz herzlich möchte ich mich bei ihm auch für die vielen wissenschaftlichen und nicht-wissenschaftlichen Diskussionen (besonders zu Zeiten der tour de France) und die unermüdliche Unterstützung bedanken.

Bei Annette Schumacher möchte ich mich dafür bedanke, dass sie in der ganzen Zeit meiner Doktorarbeit eine prima Schreibplatznachbarin war und bei Fragen im Labor immer jederzeit gerne geholfen hat. In ihrer neuen Arbeitstelle wünsche ich ihr alles Gute.

Bei Dr. Johannes Glöckner möchte ich mich für seine immer gern gegebene Unterstützung (vor allem mit Computern und in der Molekularbiologie) bedanken.

Bei Andrea Meixner möchte ich mich für ihre hilfsbereite, nette Art bedanken und dass sie auf allen Retreats immer gerne ein Zimmer mit mir geteilt hat.

Bei Karsten Boldt bedanke ich mich ganz herzlich für seine Hilfe mit der Masse und dass er auch immer gerne mal einen netten Abend mit der „Nationalplatte“ organisiert hat.

Auch bei Dr. Hakan Sarioglu bedanke ich mich ganz herzlich bei seiner Hilfe mit der Masse, sowie dafür, dass er mir für die Zeit des Zusammenschreibens einen ruhigen Arbeitsplatz im „Kabuff“ bereitgestellt hat.

Bei Steffi Schöffmann, Silke Becker, Ralf Braun, Saskia Hanf, Matteo Gorza, Patricia delRio, Gaby Dütsch, Sandra Helm, Dr. Elod Körtvely, Ana Griciuc, Dr. Giovanni Piccoli und Dr. Andreas Vogt bedanke ich mich sehr herzlich, dass sie eine sehr angenehme Arbeitsatmosphäre in der Arbeitsgruppe geschaffen haben und immer hilfsbereit waren.

Bei Mr. Roger Smith möchte ich mich ganz herzlich dafür bedanken, dass er in seinem Urlaub in Deutschland diese Arbeit korrekturgelesen hat.

Bei meinen Eltern und Geschwistern bedanke ich mich für all die Unterstützung im Laufe der Jahre.

Vor allem aber danke ich meinem Mann Tommy, dass er den ganzen Stress der Doktorarbeit mit mir ertragen hat. Ohne ihn wäre ich oft wahnsinning geworden.

5. CURRICULUM VITAE

Lebenslauf

Monika Viktoria Beer, Geb. Wimmer

*24. 12. 1977 in Fürstenfeldbruck/Bayern

Ausbildung

- 09/2005 Laboraustausch an der Univerität von Lund in der Gruppe von Prof. Dr. Theo van Veen.
- Seit 09/2004 Doktorarbeit in der Arbeitsgruppe Dr. Marius Ueffing am Institut für Humangenetik, Department of Protein Science, Helmholtz Zentrum München - Deutsches Forschungszentrum für Gesundheit und Umwelt (GmbH). Thema: „Analysis of Multiprotein Complexes in the Mammalian Retina“.
- 09/2004 Abschluss mit erstem Staatsexamen des Studiums der Biologie und Chemie für Lehramt an Gymnasien an der Ludwig-Maximilians-Universität München.
- 09/2002-02/2003 Werkstudentin bei der Münchner Rückversicherung in München im Casualty Risk Consultment/Bereich Biotechnology bei Dr. Manuela Zweimüller.
- 10/1999-09/2004 Hauptstudium in den Studienfächern Biologie und Chemie für Lehramt an Gymnasien an der Ludwig-Maximilians-Universität München. Zulassungsarbeit am Lehrstuhl von Prof. Dr. Herrmann unter Betreuung von PD Dr. Rainer Maier am Department Biologie I, Bereich Botanik der Ludwig-Maximilians-Universität München. Thema: Allotope Transformation zur Expression der plastidären Genen *petB* und *petD* im Zellkern von *Nicotiana tabacum*.
- 09/1997-09/1999 Grundstudium in den Studienfächern Biologie und Chemie für Lehramt an Gymnasien an der Ludwig-Maximilians-Universität München.
- 1988-06/1997 Graf-Rasso Gymnasium Fürstenfeldbruck/Bayern
Abschluss: Allgemeine Hochschulreife
Gesamtnote: 1,7.
- 1984-1988 Philip-Weiss Grundschule in Fürstenfeldbruck.